Neurological University Hospital Tübingen
Department of Neurology and Epileptology

- WE ARE HUMAN AFTER ALL -
Model systems to study human neuronal function

Thesis submitted as requirement to fulfill the degree
“Doctor of Philosophy” in Experimental Medicine (PhD)

at the
Faculty of Medicine
Eberhard Karls University
Tübingen

by
Niklas Schwarz

2023

Dean: Professor Dr. B. Pichler

1. Reviewer: Professor Dr. H. Lerche
2. Reviewer: Professor Dr. P. M. Loskill
3. Reviewer: Professorin Dr. H. Potschka

Date of oral examination: 04.04.2023

Table of content

1 Introduction 1

1.1 Neurological disorders 1

1.2 Malignant brain tumor diseases 2

1.3 Epilepsy and developmental and epileptic encephalopathy 3

1.4 Voltage-gated ion channels 5

1.5 Voltage-gated potassium channel $K_V1.2$ 7

1.6 Model systems in neuroscience 8

1.7 Induced pluripotent stem cells and their neuronal differentiation 10

1.8 Organotypic brain slice cultures 13

1.9 Aim of this work 15

2 Results 17

2.1 Chapter 1: Reprogramming of fibroblasts with *KCNA2* p.R297Q variant to induced pluripotent stem cells 17

2.2 Chapter 2: Reprogramming of fibroblasts with *KCNA2* p.L328V variant to induced pluripotent stem cells 23

2.3 Chapter 3: Electrophysiological analysis of iPS cell-derived neurons 28

2.3.1 Methods 28

2.3.2 Generation of stable and inducible NGN2-iPS cell lines 28

2.3.3 Production of lentiviruses for neuronal differentiation 29

2.3.4 Generation of stable NGN2-iPS cell lines 29

2.3.5 Preparation and cultivation of mouse astrocytes 30

2.3.6 Differentiation of NGN2-iPS cell lines into neurons 30

2.3.7 Immunohistochemistry 31

2.3.8 Electrophysiology 32

2.3.9 Data and statistical analysis 33

2.3.10 Results 33

2.3.11 Immunocytochemical confirmation of iPS cell-derived neurons 33

2.3.12 Electrophysiological analysis of iPS cell-derived neurons 36

2.3.13 Currents evoked in iPS cell-derived neurons 36
2.3.14 Passive electrical properties of control and patient iPS cell-derived neurons 37
2.3.15 Firing properties of control and patient iPS cell-derived neurons .. 39
2.3.16 Summary 41
2.4 Chapter 4: Establishment of human neocortical organotypic brain slice cultures 42
2.5 Chapter 5: Detailed characterization and genetic manipulation of long-term adult human brain slice cultures . 56
2.6 Chapter 6: A first application example: Virotherapy using oncolytic viruses in human organotypic brain slice cultures. 88
3 Discussion 100
3.1 Reprogramming to induced pluripotent stem cells 101
3.2 Electrophysiological analysis of iPS cell-derived neurons . 103
3.3 Human organotypic brain slice cultures..... 109
3.4 Effects of irradiation and virotherapy on brain tumor initiating cells in human organotypic brain slice cultures 114
3.5 Outlook..... 115
4 Summary 119
5 German summary 121
6 List of references 123

Index of abbreviations

AIS	Axon initial segment
AP	Action potential
AA	Amino acid
BFNS	Benign familial neonatal seizures
BP	Base pair
BSA	Bovine serum albumin
cDNA	Complementary deoxyribonucleic acid
CNS	Central nervous system
CO_2	Carbon dioxide
DEE	Developmental and epileptic encephalopathy
DNA	Deoxyribonucleic acid
EA	Episodic ataxia
E. coli	Escherichia coli
EGFP	Enhanced Green Fluorescent Protein
GBM	Glioblastoma multiforme
GEFS+	Generalized epilepsy with febrile seizures plus
H_2O	Water
hCSF	human cerebrospinal fluid
IGE	Idiopathic generalized epilepsy
ILAE	International League against Epilepsy

IPS cells	Induced pluripotent stem cells
KCNA2	Potassium voltage-gated channel subfamily A member 2
kDa	Kilodalton
mRNA	Messenger ribonucleic acid
NaCl	Sodium chloride
NGN2	Neurogenin-2
Ω	Ohm
PBS	Phosphate Buffered Saline
PCR	Polymerase chain reaction
p.R297Q	Replacement of the amino acid arginine by glutamine in the *KCNA2* gene at position 297
p.L328V	Replacement of the amino acid leucine by valine in the *KCNA2* gene at position 328
RT	Room temperature
SEM	Standard error of the mean
V	Voltage
WT	Wild type

1 Introduction

1.1 Neurological disorders

Neurological disorders encompass abnormalities that affect the structure or function in the central nervous system, the peripheral nervous system or neuromuscular functions. The associated consequences represent a large burden on worldwide health (Patel et al., 2016). The reasons for neurological diseases are as multifarious as their clinical symptoms and can include genetic disorders, head trauma, metabolic disorders, infections or environmental health problems (Nathan & Scobell, 2012). Apoplectic insults, Alzheimer's and other dementias, Parkinson's disease, multiple sclerosis, epilepsy, headache disorders and malignant brain tumors represent three percent of the worldwide burden of disease (Carroll, 2019; Murray et al., 2012). The overall burden of disease is rated using the disability-adjusted life year (DALY), a time-based measure that combines years lost due to premature death, but also the years lived with illness or disability until recovery or death (Gold et al., 2002).

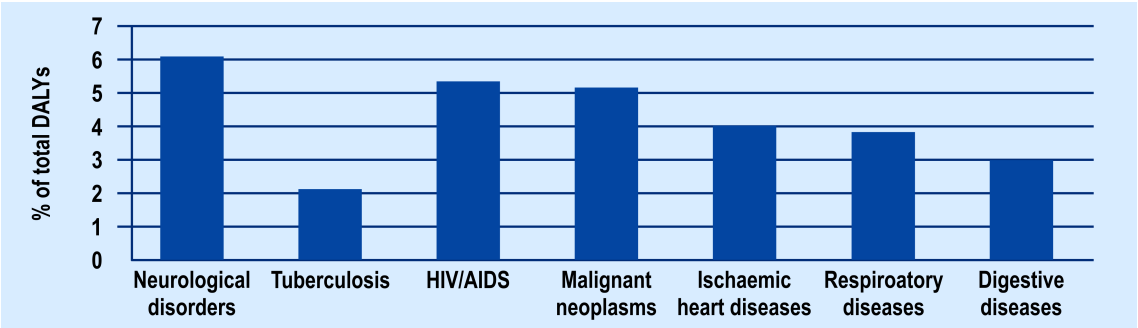


Figure 1: Percentage of total DALYs for neurological disorders and selected diseases

Neurological disorders represent a significant challenge to health care systems and it requires further studies to develop better therapeutic options (modified from WHO 2017).

A better understanding of neurological diseases and better therapy options derived from this knowledge therefore not only have a direct impact on patient health situation, but there is also a great socio-economic interest. Malignant brain tumor diseases and epilepsy play an important role among all these neurological diseases. For a better understanding of the objectives of the present doctoral thesis, these two diseases are explained in more detail below.

1.2 Malignant brain tumor diseases

Brain tumors, particularly glioblastoma multiforme, belong to the most aggressive and difficult-to-treat of all forms of malignancies (Rich & Bigner, 2004). These tumors are able to resist almost all conventional and novel treatments which relates, in part, to the unique cell-intrinsic and micro-environmental properties of brain tissue (Aldape et al., 2019). Brain tumors can cause either generalized or focal neurologic symptoms. Generalized symptoms are caused by increased intracranial pressure and consist of headache, nausea and vomiting. Focal symptoms and signs, such as hemiparesis and aphasia, are correlated to the intracranial location of the tumor. The frequency, severity and duration of symptoms vary with the type of tumor (DeAngelis, 2001). One way of systematizing brain tumors is to differentiate them in terms of cellular origin, cell composition and growth behavior. These aspects underlie the World Health Organization's classification, the current version of which dates from 2016 (Louis et al., 2016). It distinguishes four basic degrees of tumor:

- WHO Grade I (benign) tumors are slow-growing, nonmalignant, and most often with long-term survival (e.g. Pilocytic astrocytoma).
- WHO Grade II (semi-benign) tumors are relatively slow-growing but can recur sometimes as higher grade tumors (e.g. Oligodendroglioma).
- WHO Grade III (semi-malign) tumors are malignant and often recur as higher grade tumors (e.g. Anaplastic astrocytoma).
- WHO Grade IV (malign) tumors reproduce rapidly and very aggressive (e.g. Glioblastoma multiforme).

Primary brain tumors, developing from brain cells or the cells of the meninges, are located behind the blood–brain barrier (BBB), a system of endothelial cells, astrocytes, tight junctions and transport proteins that protect sensitive brain tissue from exposure to factors in the general circulation. The BBB is also impeding exposure to most systemic chemotherapy, which is one reason for the inadequate treatment options to date (Arvanitis et al., 2020; Gerstner & Fine, 2007). New therapy options are therefore urgently needed to reduce the mortality rate of these malignant brain tumor diseases.

1.3 Epilepsy and developmental and epileptic encephalopathy

Epilepsy is one of the most common neurological disorders and affects about 0.5%–1% of the world's population. Approximately 5% of the total population experience at least one epileptic seizure during their lifetime, without developing epilepsy (Allen Hauser & Annegers, 1996; Fiest et al., 2016). Epilepsy is traceable like no other disease in human history. The oldest evidence can be found in ancient Egyptian hieroglyphics in the Ebers Papyrus, which can be dated to the beginning of the New Kingdom (ca.1650-1570 BC) (Dawson & Ebbell, 1938). Similar pre-Christian records can be found in numerous other historical documents such as the "Corpus hippocraticum", a collection of 70 writings, of which the least are likely to originate to Hippocrates. In these documents, epilepsy (Greek: epilambanein = to be taken, to be overwhelmed) is described as a "holy disease" (med. Richard Kapferer & Dr. Georg Stider, 1938). An epileptic seizure is characterized by paroxysmal, synchronous electrical discharges of cerebral neurons in the brain. This can lead to impaired consciousness or to stereotypical behavior or movement of the affected person. The distinction between an occasional epileptic convulsion, which occurs only onetime and is caused by a suitable trigger, such as severe sleep deprivation, hypoglycemia or alcohol withdrawal, and the clinical picture of epilepsy, for which recurring seizures or one seizure plus high risk factors of recurrence are required, not only has therapeutically different consequences, but often significant psychological and social effects. The possible causes of epileptic seizures are so numerous and diverse as their clinical appearance (Hedrich et al., 2013).

According to the new guidelines from the ILAE (International League Against Epilepsy) commission from 2017, seizure types are divided in focal, generalized and unknown seizures (Fisher et al., 2017). On a second level epilepsy types are divided into focal, generalized, combined generalized & focal and unknown types. On a third level an epilepsy syndrome can be diagnosed. At each stage, etiology has to be considered (Scheffer et al., 2017).

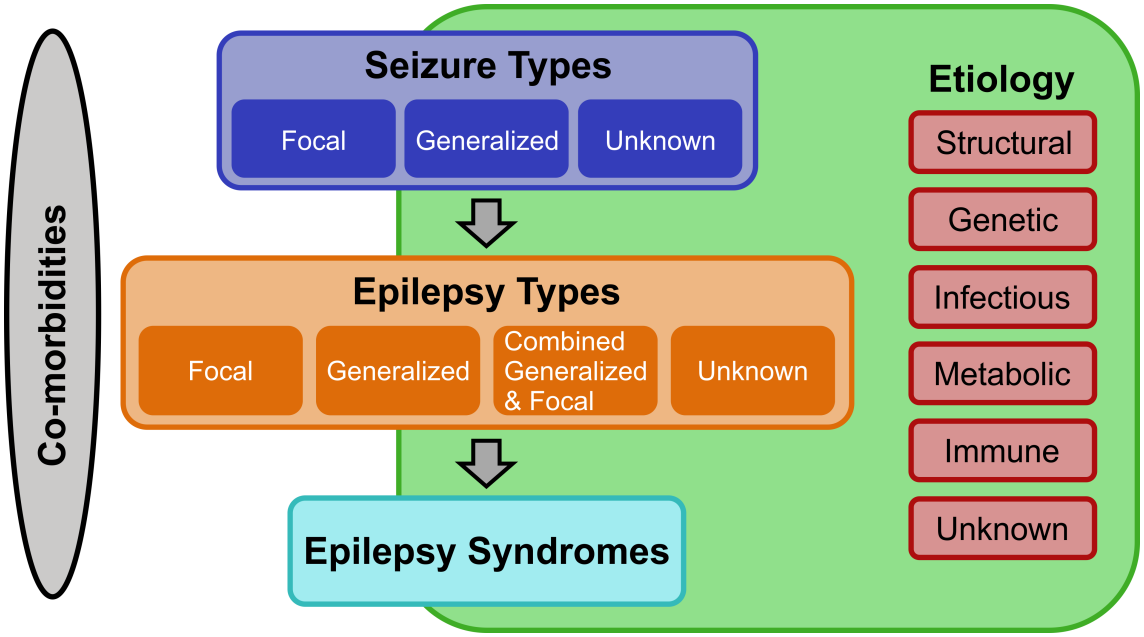


Figure 2: Framework for classification of seizure and epilepsy types

Six etiological subgroups are specified, with emphasis of their potential therapeutic consequences (modified from Scheffer et al., 2017).

Developmental and epileptic encephalopathies (DEEs) are a phenotypically heterogeneous group of severe brain disorders of early age (Guerrini & Pellock, 2012; McTague et al., 2016) characterized by mostly severe, pharmacoresistant epilepsies with intellectual disability, autism, ataxia, movement disorders and other symptoms (Capovilla et al., 2013; El Kosseifi et al., 2019). While DEEs can occur as a result of identifiable lesions in the CNS such as malformations, a causative factor cannot be identified in the majority of cases (S. Khan & Al Baradie, 2012). With the advent of high-throughput next-generation sequencing technologies, a genetic basis could be identified for some of the classic epileptic encephalopathies including Infantile Spasms (IS) and the Lennox-Gastaut syndrome (LGS) (Hamdan et al., 2017). Other examples of DEEs include early myoclonic encephalopathy, Ohtahara, West, Landau-Kleffner and Dravet syndromes. Since ion channels play a crucial role in many of these syndromes, further details of these are discussed in the following section.

1.4 Voltage-gated ion channels

Voltage-gated ion channels are a class of pore-forming transmembrane proteins that allow ions to cross lipid biomembranes. The influx takes place through the membrane along the existing electrochemical gradient. These channels contain charged amino acids, which can be shifted by changes of the electrical field across the membrane and thereby lead to a change in the conformation of the protein, causing the pore to open or close. Together with other ion-translocating enzymes the voltage-gated sodium, calcium and potassium channels are collectively responsible for the establishment of the resting membrane potential and the generation and shape of conducted electrical signals in neurons and other excitable cells (Catterall, 1988). The different channels are precisely located in neurons that affect the processing and the response of the neuron to electrical activity (Trimmer & Rhodes, 2004).

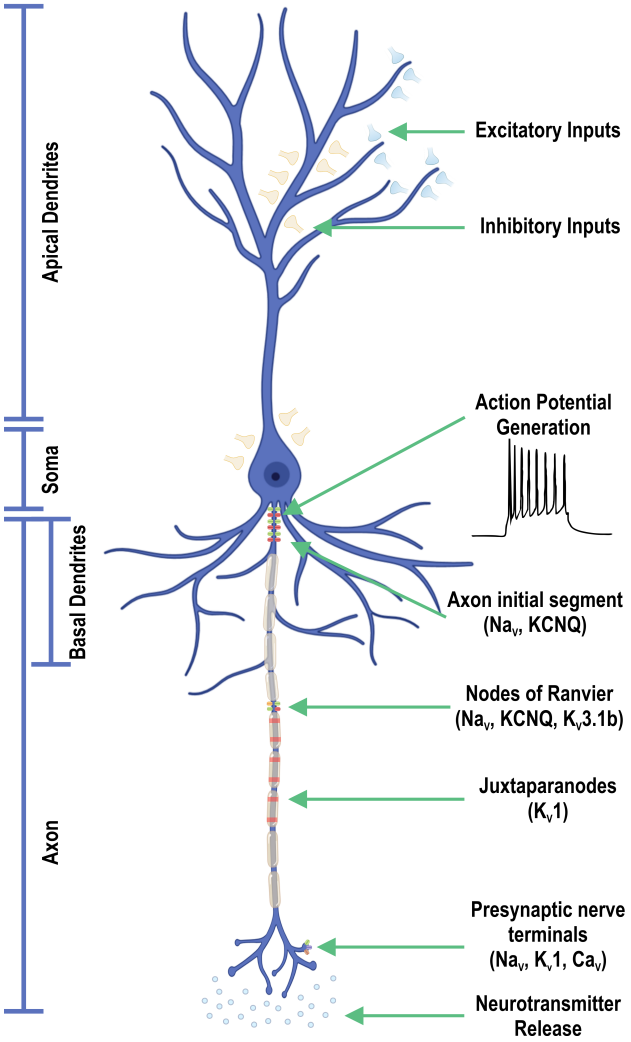


Figure 3: Localization and distribution of voltage-gated ion channels in a neuron

In general, different subtypes of K_V channels are found at diverse regions of a neuron from dendrites, over juxta-paranodes in myelinated axons to presynaptic terminals. Also Na_V channels are found in axon initial segments, dendrites, nodes of Ranvier and presynaptic terminals. The different compositions of channels at specific subcellular compartments have roles in distinct neuronal events, as outlined in the text (modified from Lai and Jan 2006).

Neurons contain different functional somatodendritic and axonal compartments, each with a specific composition of voltage-gated ion channels. The various excitatory and inhibitory inputs are propagated to the cell soma via the dendritic tree, summed up and processed, which triggers an action potential (AP) at the axon initial segment when the cell-specific threshold is exceeded (Child & Benarroch, 2014). Here, the composition of the channels plays a decisive role in the formation and propagation of excitation along the axons. Propagated APs lead to activation of voltage-gated calcium channels at the axon terminals, initiating the vesicular release of the neurotransmitters. The great variability and specificity of the channels is also evident from the fact that there are ten different genes that code for voltage-gated sodium channels ($Na_V1.1$ to $Na_V1.9$ and an atypical sodium channel Na_VX)(Catterall, 2000). Of these, the α-subunits of the subtypes $Na_V1.1$, $Na_V1.2$, and $Na_V1.3$ are expressed in the central nervous system (CNS). $Na_V1.6$ is additionally expressed in the peripheral nervous system (PNS). $Na_V1.7$, Nav1.8, and $Na_V1.9$ are mainly found in the PNS. $Na_V1.4$ and $Na_V1.5$ channels are expressed in skeletal and cardiac muscles, respectively (De Lera Ruiz & Kraus, 2015). The electrophysiological properties can also be modulated by four different ß-subunits (Isom, 2001). The most extensive family, however, are the twelve classes of voltage-gated potassium channels, which are encoded by over 80 known genes (Gutman et al., 2005). The possibility of forming both homo- and heterotetramers results in an even higher channel diversity. Voltage-gated potassium channels play an important role in the regulation of neuronal excitability (Child & Benarroch, 2014). One of these voltage-gated potassium channels is $K_V1.2$, which is encoded by the gene *KCNA2*. Pathological variants in this gene were recently identified as a new causative reason for developmental and epileptic encephalopathies (Masnada et al., 2017; Pena & Coimbra, 2015; Syrbe et al., 2015). Since both patients, of whom iPS cells were generated in this work carry pathological variants in this channel, $K_V1.2$ will be briefly explained in the following.

1.5 Voltage-gated potassium channel $K_V1.2$

The first K_V1 sequence was found in *Drosophila melanogaster* (Fruit fly) and became known as Shaker channel (Salkoff & Wyman, 1981; Tempel et al., 1987). Several vertebrate potassium channels with comparable amino acid sequences were found in mammalians and constitute the K_V1 family ($K_V1.1$, $K_V1.2$, $K_V1.3$, $K_V1.4$, $K_V1.5$ and $K_V1.6$). The expression of $K_V1.2$ subunits can be found in both white and grey matter of the brain, more precisely in different neurons in the neocortex, hippocampus, main olfactory bulb (MOB) and cerebellum (Lorincz & Nusser, 2008). The $K_V1.2$ protein shows a very complex differential subcellular distribution in e.g. cortical pyramidal cells, hippocampal and Purkinje cells. In cerebellar basket cells $K_V1.2$ is concentrated in dendrites, while in other neuronal types, $K_V1.2$ is localized to certain axon tracts and to nerve terminals (Sheng et al., 1994). The channel contains six membrane-spanning domains and belongs to the delayed rectifier class, playing an essential role in efficient repolarization following an action potential (Russell et al., 1994). $K_V1.2$ subunits have been also identified in heterotetrameric complexes with $K_V1.1$ subunits in the juxtaparanodal regions and axon terminals at which they partially control neurotransmitter release (Lambe & Aghajanian, 2001). Furthermore, the complexes facilitate the action potential propagation along the axon (Debanne et al., 1997).

Participation in all these different tasks shows the extremely complex interaction of the individual subunits with one another and their impact on the neuronal firing behavior. Modified functioning of even one subunit in heterotetrameric complexes can therefore bring the finely adjusted equilibrium out of balance and can have far-reaching effects on the functioning of the neuronal network. Of course, not only genetic changes in ion channels have an impact on the proper firing behavior of the neurons, but also pathological variants of proteins that are involved in vesicle release or inadequate myelination are factors that restrict or prevent correct electrophysiological information processing.

The vast majority of these findings were not obtained directly on humans, but with the help of model systems, on which the molecular processes and pathological

variants could be simulated, examined and analyzed. Therefore, in the next section, the requirements for model systems will be briefly outlined, and two model systems will be presented, which are described in more detail in this work and were established in the laboratory. The first is the utilization of induced pluripotent stem (iPS) cells and the neurons differentiated from them. The second is the model of human organotypic brain slice cultures.

1.6 Model systems in neuroscience

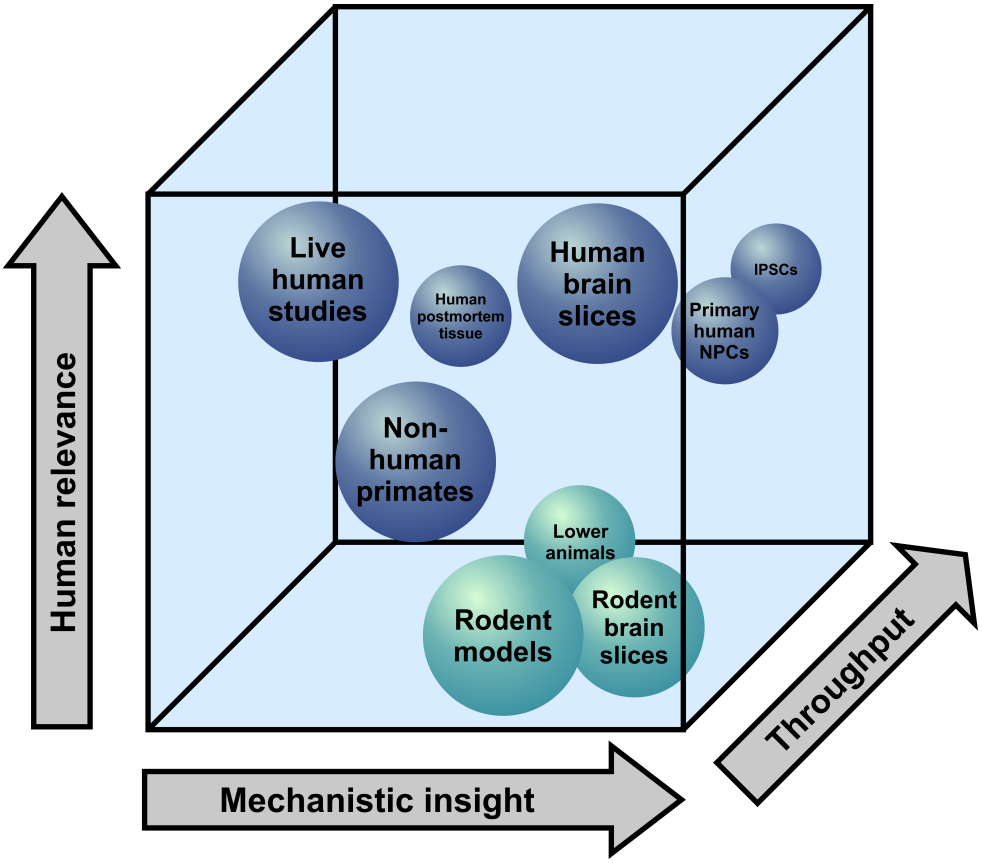


Figure 4: Complementary experimental approaches

In order to get a complete picture of all underlying factors for the human system and possible new therapeutic options, a combination of different complementary model systems is essential. The three axes show: increasing molecular and mechanistic insight (X), increasing human relevance (Y) and increasing throughput (Z). Bubbles in blue depict the primate (most humanoid) systems whereas the other vertebrate models are shown in turquoise. For example, studies in living persons contribute higher relevance for humans than mouse models, but lower molecular and mechanistic insights. The achievement of human induced pluripotent stem cells bring both, with optional automated high-throughput. Human organotypic brain slice cultures could provide an even higher level of human relevance and molecular and mechanistic insights specifically in the field of neuroscience (modified from Dolmetsch and Geschwind 2011).

There are two major goals in human life sciences. First, gaining a more detailed and comprehensive understanding of human physiology and of the origin and development of diseases on a molecular and systemic level and, second, generating improved, more effective and personalized therapies for well-defined diseases. Animal models have been mostly used for this purpose. Fundamental physiological findings about the generation of action potentials were carried out, for example, on the giant axons of squids (Hodgkin & Huxley, 1952). Other examples are the use of frogs to study synaptic transmission (del Castillo & Katz, 1954) or crabs to study the mechanisms of lateral inhibition in the retina (Lange et al., 1966). Animal models also play a key role in researching and understanding diseases. For example, they have been genetically engineered to mimic certain human diseases, such as age-related neurodegenerative diseases, which are largely restricted to humans and rarely occur spontaneously in animals (Jucker, 2010) or how mutations in ion channels can lead to neuronal hyperactivity and thus cause epilepsy (Lerche et al., 2013). To what extent, however, results from such studies can be transferred exactly to the human system remains questionable. These differences between systems are certainly one of the reasons why many newly developed drugs and therapies that have been developed and tested in animals show little or no effect when they are transferred from preclinical research to human trials and test phases.

Neurodevelopmental disorders, neurodegenerative diseases and psychiatric disorders are particularly difficult to simulate and study in the laboratory, since they belong to the most complex human diseases and affect the most sophisticated human organ. Designing effective *in vitro* models are one of the big challenges in neuroscience these days. One of the main problems is the lack of good predictive pre-clinical models to develop new therapies that will reliably show their benefits to the patient. Animal models only help to a limited degree here, even if they make an important contribution to the elucidation of disease mechanisms and help with the discovery of the functional role of specific genes (Dragunow, 2008). To study human cortical cells, postmortem tissue (Braak et al., 2003; Verwer, Hermens, et al., 2002), acute slices (Beck et al., 2000) or *in vivo* measurements in humans (Mormann et al., 2003) were long time the only

possibilities, but there are certain limitations of these measurements regarding molecular pathomechanisms and disease progression. The generation of induced pluripotent stem cell-derived human cortical cells and the establishment of adult human organotypic brain slice cultures are therefore a big step toward learning additional information about pathophysiology and closing the gap, at least in part.

1.7 Induced pluripotent stem cells and their neuronal differentiation

In 2006 Takahashi and Yamanaka showed for the first time that embryonic and adult fibroblast from mouse could be reprogrammed to induced pluripotent stem (iPS) cells by the introduction of four specific genes encoding for the transcription factors Oct3/4, Sox2, c-Myc and Klf4 (Takahashi & Yamanaka, 2006). Human fibroblasts were reprogrammed to iPS cells shortly afterwards by two independent research groups (Takahashi et al., 2007; Yu et al., 2007). Pluripotent stem cells can proliferate indefinitely and differentiate to all somatic cells of the three germ layers of a human body. Like embryonic stem cells iPS cells can be differentiated into cortical neurons and glial cells by addition of different growth factors, defined culture conditions or by overexpression of transcription factors. A variety of different methods and protocols have been described so far. The possibility to investigate diseases of the human brain *in vitro* and study disease-relevant phenotypes largely depends on the ability to differentiate neuronal cultures and networks of defined cellular composition. One strategy is the simulation of cortical development by formation of embryoid bodies (EBs) and neurospheres, which generate cortical projection neurons forming via synaptogenesis mature neural, electrophysiologically active, circuits (Shi, Kirwan, & Livesey, 2012). Another well-established method to obtain neural progenitor cells is dual SMAD inhibition by BMP inhibitor Noggin and TGFβ pathway inhibitor SB431542 (Chambers et al., 2009). The fast generation of pure homogeneous networks of glutamatergic neurons can be achieved by the forced overexpression of Neurogenin-2 (NGN2) (Busskamp et al., 2014; Y. Zhang et al., 2013).The latest

development is three-dimensional neural cultures to produced cerebral organoids (Y. H. Kim et al., 2015; Lancaster et al., 2013; Pasca et al., 2015).

What all these protocols have in common is that for the first time, it is possible to investigate cortical cells, which were previously inaccessible, from patients carrying genetic diversity or specific mutations for neurodevelopmental or neurodegenerative disorders or neuropsychiatric diseases. In addition, they provide a possible source for regenerative medicine and prospective cell therapy applications (Nagoshi & Okano, 2018) as well as an *in vitro* model system for pharmacological and toxicological screenings for neuroactive compounds (Avior et al., 2016; Sison-Young et al., 2012).

Initial studies with iPS cell-differentiated neurons from patients with epileptic encephalopathies were from patients with Dravet syndrome with a mutation in the gene *SCN1A*, which codes for the voltage-gated sodium channel $Na_V1.1$. Higurashi et al. reprogrammed somatic cells to iPS cells from a Dravet-patient with a mutation which leads to a premature stop codon (p.Arg1645*) using a GABAergic (> 50%) differentiation protocol. In comparative electrophysiological measurements with generated control neurons, a functional decrease in the formation of action potentials in GABAergic neurons was observed (Higurashi et al., 2013). In another study fibroblasts of a Dravet-patient (p.Phe1415Ile) and a GEFS+ (generalized epilepsy with febrile seizures plus) patient (p.Gln1923Arg) were generated and then differentiated to iPS cell-derived glutamatergic neurons. Comparison of the generated patient neurons with generated neurons from control iPS cells revealed hyperexcitability of the generated patient neurons (Jiao et al., 2013). All of these different approaches of patient iPS cell-differentiated neurons can be used for preclinical drug testing or other experimental therapy options on human neurons, which previously was only possible with other, more distant model systems. An example of this is shown in Tidball et al., who studied missense variants in the *SCN8A* voltage-gated sodium channel gene which are related to early-infantile epileptic encephalopathy type 13. They differentiated iPS cell-derived neurons from patients who had either elevated persistent current or increased resurgent current compared to controls. Morphologically, all iPS cell-

derived neurons also showed shorter axon initial segment lengths compared to controls. They were able to measure a normalization of the currents after administration of riluzole, an FDA-approved drug and also observed initial success in patients (Tidball et al., 2020).

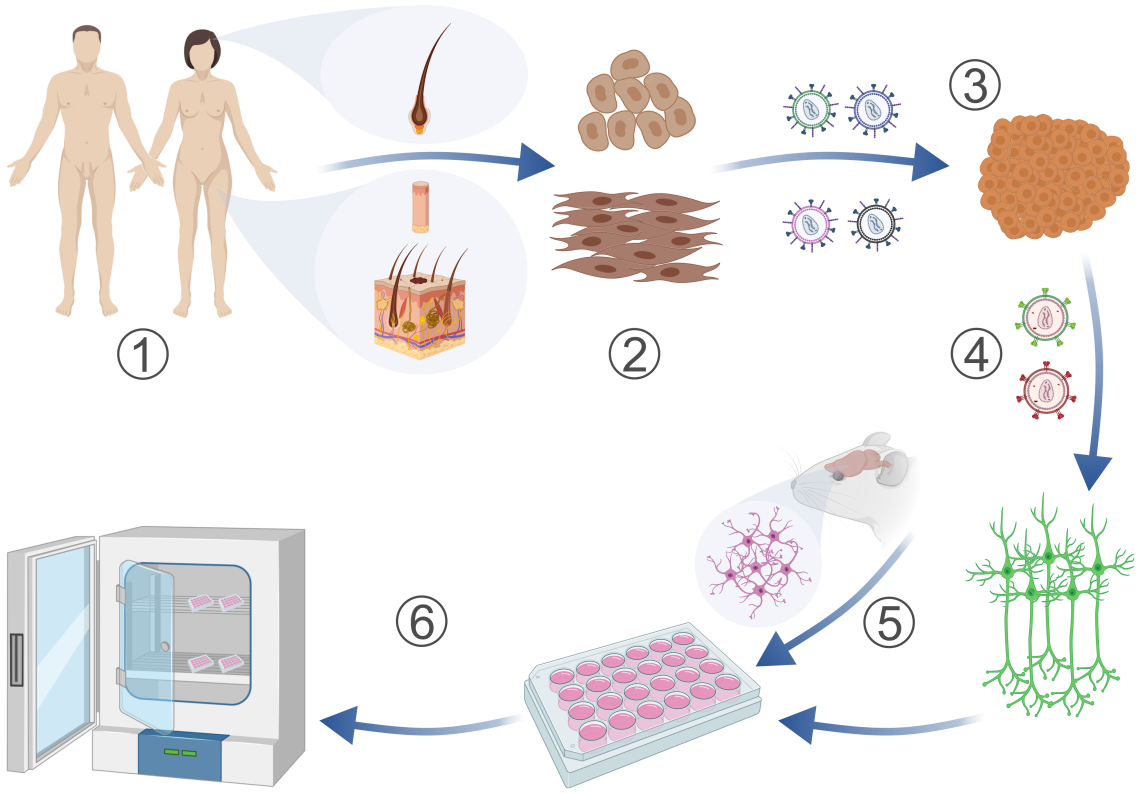


Figure 5: Reprogramming of primary cells to iPS cells and their neuronal differentiation

1. To generate patient-specific primary cells, either a small skin biopsy was taken from the patient or a small amount of hair with the entire hair root was removed. Fibroblasts from the skin biopsy or keratinocytes from the hair roots have then grown out for several weeks. These cells were retrovirally reprogrammed with the four reprogramming factors (*OCT4, SOX2, KLF4, c-MYC*) to induced pluripotent stem (iPS) cells. 3. The clones of these stem cells were expanded and characterized before they were used for further procedures. 4. Neuronal differentiation was induced by the overexpression of the neuronal transcription factor Neurogenin-2 (NGN2). 5. The obtained neurons were co-cultivated together with murine astrocytes for better maturation. 6. For electrophysiological experiments, the neurons were cultivated for several weeks.

1.8 Organotypic brain slice cultures

The use of ethically questionable embryonic stem cells (Kriks et al., 2011) or the previously described induced pluripotent stem (iPS) cell technology, allow human-like neurons to grow *in vitro* (Shi, Kirwan, Smith, et al., 2012; Y. Zhang et al., 2013). These cell cultures are an important tool for studying the function of cells in a controlled environment and to get an insight into pathophysiological mechanisms of human neurodegenerative and other central nervous system (CNS)-related diseases. On the one hand, these approaches are doubtless a huge step towards understanding the mechanisms in the human brain, on the other hand, there are continuing discussions about the maturity and purity, as well as the subtype-identity of the generated human-like neurons (Tao & Zhang, 2016). Another important aspect is the fact that these cultures represent just two-dimensional cell populations whereas there is a clear need to investigate these brain cells in a three-dimensional system where they can develop physiologically and form or preserve their natural architecture. One big advantage of organotypic brain slice cultures is that the cultures hold their three-dimensional organization over time and represent partially the area of the brain of which they are derived (Croft et al., 2019).

The first reports about organotypic brain tissue described cultivation conditions of adult rat hypophysis (Bousquet & Meunier, 1962) and the development of organotypic bioelectric activities in culture (Crain, 1966). A considerable degree of intrinsic self-differentiation of the cells could be observed in these slice cultures. Furthermore, evoked potentials in cultures similar to those of measurements in the cerebral cortex *in situ* could be recorded, as well as a characteristic sensitivity to certain neuropharmacological drugs. This was followed by a detailed description of cultured mouse slices from cerebellum (Wolf, 1970), identifying previously unknown granule cell neurons and their migration *in vitro*.

Therefore, the establishment of human organotypic brain slice cultures have been an important step towards providing a tool that reflects the entire complex human CNS tissue and conserves aspects of synaptic and structural organization

of the original brain tissue. The cortical brain slices include the entire cortical layering and columnar organization, which allows insights into the microcircuitry of the brain (Andersson et al. 2016; Eugène et al. 2014; Schwarz et al. 2017; Schwarz et al. 2019; Ting et al. 2018). These slices may serve in future as bridging technology between cell culture and *in vivo* experiments.

For organotypic brain slice cultures CNS-tissue is sliced into sections of 150–400 µm in thickness with a vibratome. In the most commonly used method, the slices are placed at the air-medium interface between a humidified atmosphere and the culture medium on a semi porous membrane (Stoppini et al., 1991). The supply takes place via oxygen from above and medium from below, whereby the slices are always covered by a thin film of medium. The slices receive nutrition from the medium through small pores in the membrane via capillary forces (Gähwiler et al., 1997).

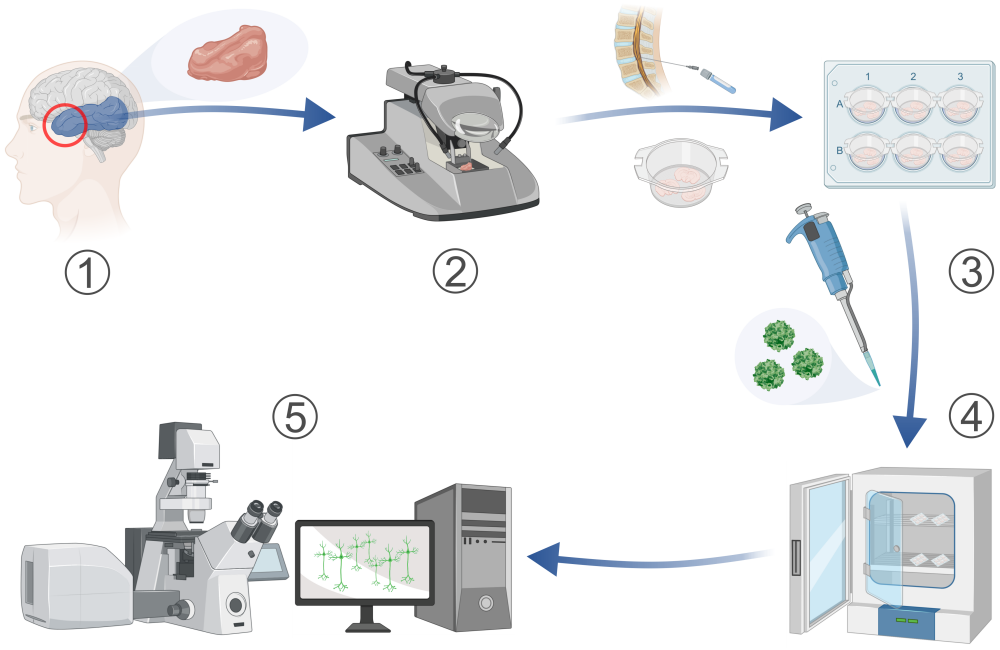


Figure 6: Generation of human organotypic brain slice cultures

1. The pole from the temporal lobe as access tissue was obtained from patients who had undergone resective brain surgery. 2. The tissue was cut using a vibratome to 250µm thick sections. The sections were transferred to a semi porous membrane for further cultivation. 3. Human cerebrospinal fluid (hCSF) was used to cultivate the sections, in which the sections survived for several weeks. 4. At the beginning of the cultivation period, the sections can be treated with various viruses for further examinations. 5. The further analyzes include various microscopic techniques, but also electrophysiological measurements in order to be able to assess the state of health of the sections.

1.9 Aim of this work

The aim of the present work was to find suitable *in vitro* models, that reflect physiological conditions as genuine as possible to simulate and analyze neurological issues, to acquire a more detailed and accurate understanding of how human CNS disease models can be developed and finally used for finding new treatment options. To achieve this goal, the project was divided into the following sub-goals:

Chapter 2.1-2: Reprogramming of fibroblasts to induced pluripotent stem cells:

Fibroblasts were isolated from two patients suffering from developmental and epileptic encephalopathies and reprogrammed to induced pluripotent stem cells. The disease-causing variants were located in the *KCNA2* gene. Pluripotency state of the cells was verified by the expression of several pluripotency markers on RNA and protein level and the capability to differentiate into all three germ layers

Chapter 2.3: Electrophysiological analysis of iPS cell-derived neurons:

For electrophysiological analysis, both patient-derived and in addition already established control iPS cell lines were differentiated into neurons. For a fast and reproductive maturation, a protocol based on the overexpression of the transcription factor Neurogenin-2 (NGN2) was used. Neuronal cells were co-cultured on mouse astrocytes until they were analyzed via the whole-cell patch-clamp technique.

Chapter 4: Establishment of human neocortical organotypic brain slice cultures:

As a new *in vitro* model, human organotypic brain slice cultures from access tissue of resective epilepsy surgery were generated. A systematic comparison of different artificial culturing media versus human cerbrospinal fluid (hCSF) obtained from patients with normal pressure hydrocephalus (NPH) was performed. The presented data demonstrate a robust cortical neuronal survival with network activity and synaptic connectivity and also typical cellular electrophysiological properties, such as robust action potential generation.

Immunocytochemistry confirmed, that hCSF significantly enhances neuron viability in contrast to artificial culturing media.

Chapter 5: Detailed Characterization and genetic manipulation of long-term adult human brain slice cultures

The maintenance of the complex neuronal cytoarchitecture and an electrophysiological stability of human pyramidal neurons in long-term brain slice cultures was described. In addition, an efficient and widespread viral transduction by adeno-associated virus could be achieved. Under defined and controllable conditions, this enables genetic manipulation of the cortical cells while maintaining the normal firing properties of the neurons. No general differences were found when a comparison of the dendritic and spine morphology of pyramidal neurons filled with biocytin or virally GFP-labeled was accomplished. Furthermore, interneurons in cultured human brain slices and interneurons in acute slices were electrophysiologically investigated.

Chapter 6: A first application example: Virotherapy using oncolytic viruses in human organotypic brain slice cultures

Glioblastoma multiforme is the most aggressive type of brain tumor in humans with a median survival of less than 20 months. Virotherapy with adenoviruses is an upcoming therapy option for this type of cancer. As a preclinical experimental set-up glioma spheres were implanted in living human organotypic brain slices to mimic the situation *in vivo*. The spheres showed a significantly delayed growth rate when the tissue was pre-irradiated prior to oncolytic virus infection in comparison to the single treatment methods.

2 Results

2.1 Chapter 1: Reprogramming of fibroblasts with *KCNA2* p.R297Q variant to induced pluripotent stem cells

EBERHARD KARLS
UNIVERSITÄT
TÜBINGEN

Medizinische Fakultät

Declaration of contributions:

Herewith I, Niklas Schwarz declare, that I have contributed to the mayor part of the following publication:

Schwarz N, Uysal B, Rosa, F, Löffler H, Mau-Holzmann UA, Liebau S, Lerche H, Establishment of a human induced pluripotent stem cell (iPSC) line (HIHDNEi002-A) from a patient with developmental and epileptic encephalopathy carrying a KCNA2 (p.Arg297Gln) mutation. Stem Cell Res. 2019 May;37:101445. doi: 10.1016/j.scr.2019.101445. Epub 2019 Apr 19.

The authors contributed to the publications as indicated in the following table (indicated in %):

Contribution	Niklas Schwarz	Betül Uysal	Filip Rosa	Heidi Löffler	Ulrike A. Mau-Holzmann	Stefan Liebau	Holger Lerche
Research concept	90%					5%	5%
Project administration	90%						10%
Funding acquisition	50%						50%
Selection of methods	100%						
Recruitment of patients	80%			10%			10%
Data acquisition	90%			5%	5%		
Data analysis	90%	5%			5%		
Visualization	95%				5%		
Interpretation of results	85%	5%	5%		5%		
Preparation of Manuscript	90%	3%			4%	3%	

Signature of the doctoral candidate: [redacted]

As supervisor, I agree with the declarations by the candidate:

As corresponding author, agree with the declarations by the candidate:

As co-authors, we agree to the declarations above:

[redacted]

[Betül Uysal] [Filip Rosa] [Heidi Löffler]

[redacted]

[Ulrike A. Mau-Holzmann] [Stefan Liebau] [Holger Lerche]

Stem Cell Research 37 (2019) 101445

Contents lists available at ScienceDirect

Stem Cell Research

journal homepage: www.elsevier.com/locate/scr

Lab resource: Stem Cell Line

Establishment of a human induced pluripotent stem cell (iPSC) line (HIHDNEi002-A) from a patient with developmental and epileptic encephalopathy carrying a *KCNA2* (p.Arg297Gln) mutation

Niklas Schwarz[a,*], Betül Uysal[a], Filip Rosa[a], Heidi Löffler[a], Ulrike A. Mau-Holzmann[b], Stefan Liebau[c], Holger Lerche[a]

[a] Department of Neurology and Epileptology, Hertie Institute for Clinical Brain Research, University of Tuebingen, Germany
[b] Department of Medical Genetics and Applied Genomics, University of Tuebingen, Germany
[c] Institute of Neuroanatomy & Developmental Biology, University of Tuebingen, Germany

A B S T R A C T

Developmental and epileptic encephalopathies (DEE) can be caused by mutations in the *KCNA2* gene, coding for the voltage-gated K+ channel $K_v1.2$. This ion channel belongs to the delayed rectifier class of potassium channels and plays a role during the repolarization phase of an action potential. In this study we reprogrammed fibroblasts from a 30-year-old male patient with DDE carrying a point mutation (c.890G > A, p.Arg297Gln) in *KCNA2* to induced pluripotent stem cells. Pluripotency state of the cells was verified by the capability to differentiate into all three germ layers and the expression of several pluripotency markers on RNA and protein levels.

Resource table

Unique stem cell line identifier	HIHDNEi002-A
Alternative name(s) of stem cell line	iPSC-*KCNA2*-P4
Institution	Department of Neurology and Epileptology, Hertie Institute for Clinical Brain Research, University of Tuebingen, Germany
Contact information of distributor	Niklas Schwarz, niklas.schwarz@uni-tuebingen.de
Type of cell line	iPSC
Origin	Human
Additional origin info	Age: 30 years Sex: male Ethnicity: German
Cell Source	Fibroblasts
Clonality	Clonal
Method of reprogramming	Retrovirus
Genetic Modification	YES
Type of Modification	Spontaneous
Associated disease	Developmental and epileptic encephalopathy
Gene/locus	Gene: *KCNA2*, c.890G > A, p.Arg297Gln (heterozygous) Locus: 1p13.3 (GRCh38.p12, Chr1: 110,593,580-110,631,536)
Method of modification	N/A
Name of transgene or resistance	N/A
Inducible/constitutive system	N/A
Date archived/stock date	December 2015
Cell line repository/bank	https://hpscreg.eu/cell-line/HIHDNEi002-A
Ethical approval	Institutional Review Board of the Medical Faculty, University of Tuebingen - Approval Number: 303/2011BO1

Resource utility

This iPSC line is derived from fibroblasts of a patient with developmental and epileptic encephalopathy and will be useful for disease modelling and help to understand the pathophysiology and development of new treatments, since there is still a lack of effective therapies.

Resource details

The term developmental and epileptic encephalopathies includes a phenotypically and genetically heterogeneous group of severe neurological disorders. They are characterized by an early onset in life and by severe and pharmacoresistant epilepsy, cognitive dysfunction and other neurological deficits (Scheffer et al., 2016). Pathological variants in the *KCNA2* gene, which encodes for the voltage-gated K^+ channel $K_v1.2$, were recently identified as a causative reason for developmental and

* Corresponding author.
E-mail address: niklas.schwarz@uni-tuebingen.de (N. Schwarz).

https://doi.org/10.1016/j.scr.2019.101445
Received 22 March 2019; Received in revised form 12 April 2019; Accepted 18 April 2019
Available online 19 April 2019
1873-5061/ © 2019 Published by Elsevier B.V. This is an open access article under the CC BY-NC-ND license (http://creativecommons.org/licenses/BY-NC-ND/4.0/).

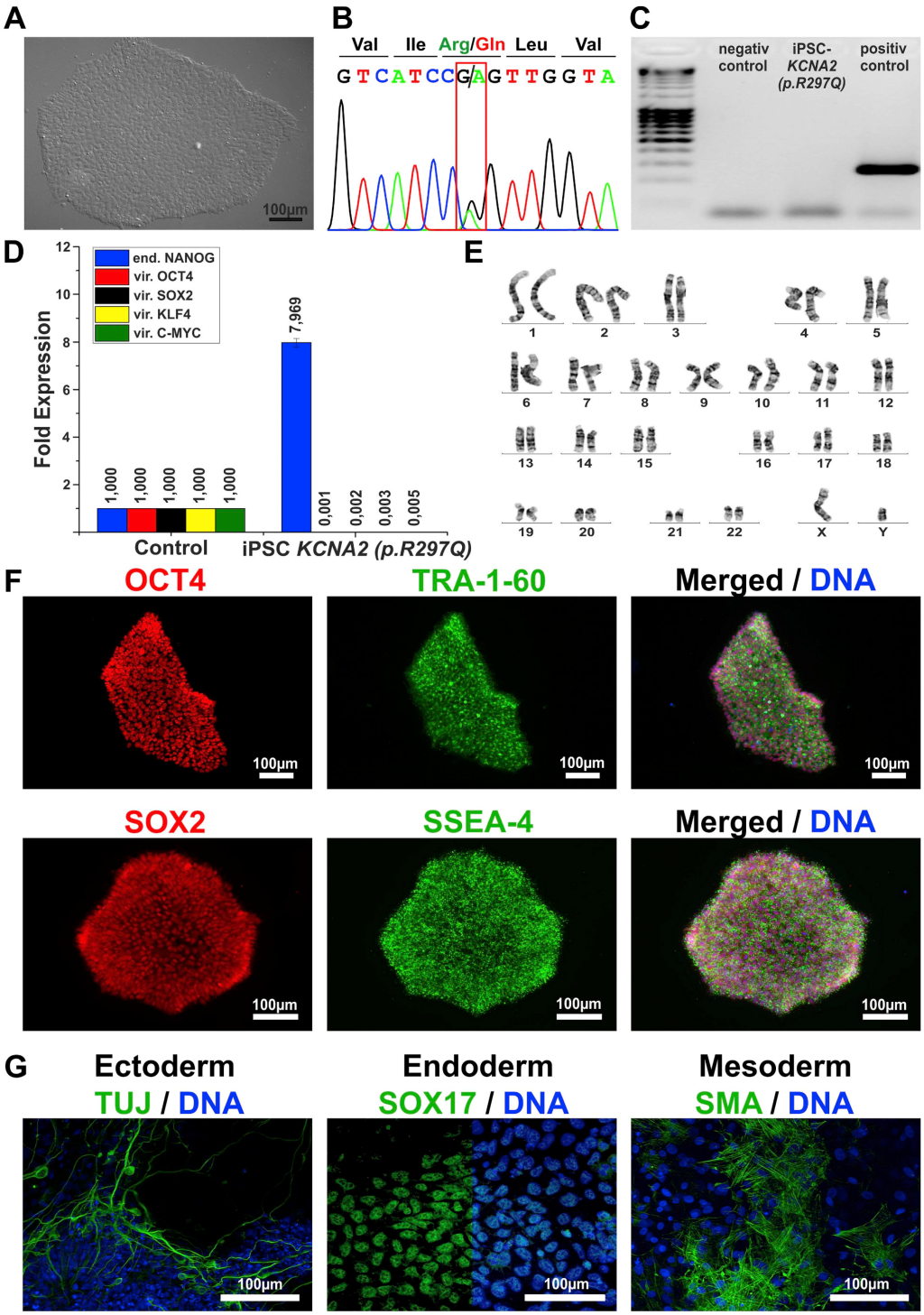


Fig. 1. Characterization and validation of HIHDNEi002-A.

Table 1
Characterization and validation.

Classification	Test	Result	Data
Morphology	Photography	normal	Fig. 1 panel A
Phenotype	Qualitative analysis (Immunocytochemistry)	Staining/expression of pluripotency markers: OCT4, TRA-1-60, SOX2 and SSEA-4	Fig. 1 panel F
	Quantitative analysis (RT-qPCR)	Upregulation of end-NANOG, Downregulation of vir-OCT4, vir-SOX2, vir-KLF4, vir-C-MYC	Fig. 1 panel D
Genotype	Karyotype (G-banding) and resolution	46,XY Resolution 300–400	Fig. 1 panel E
Identity	Microsatellite PCR (mPCR)	N/A	N/A
	STR analysis (PowerPlex®21)	21 sites tested, all matched	Available with the authors
Mutation analysis	Sequencing	Heterozygous point mutation, c.890G > A	Fig. 1 panel B
	Southern Blot OR WGS	N/A	N/A
Microbiology and virology	Mycoplasma	Mycoplasma testing by Ready-to-use PCR Mycoplasma Test Kit Mix from Applichem (#A3744), negative	Fig. 1 panel C
Differentiation potential	Directed differentiation	Expression of Neuron-specific class III beta-tubulin (TUJ1 - ectoderm), SRY-related HMG-box 17 protein (SOX17 - endoderm) and smooth muscle actin (SMA - mesoderm).	Fig. 1 panel G
Donor screening	HIV 1 + 2 Hepatitis B, Hepatitis C	N/A	N/A
Genotype additional info	Blood group genotyping	N/A	N/A
	HLA tissue typing	N/A	N/A

epileptic encephalopathies (Masnada et al., 2017; Syrbe et al., 2015). The fibroblasts of the patient were isolated and reprogrammed with four Yamanaka-factors (OCT4, SOX2, KLF4, C-MYC) from a 30-year-old male patient carrying a heterozygous mutation (c.890G > A, p.Arg297Gln) in *KCNA2*. The morphology of the obtained induced pluripotent stem cell line HIHDNEi002-A (Fig. 1A) was comparable to embryonic stem cells. The full characterization of this stem cell line was achieved after manual picking and clonal expansion on mouse embryonic fibroblasts (MEFs) for at least ten passages. The expected point mutation was confirmed by Sanger sequencing (Fig. 1B). Congruence to the original fibroblasts was affirmed by STR analysis. The iPSC line was found negative for mycoplasma with a Mycoplasma Detection Test Kit Mix from Applichem (Fig. 1C). qRT-PCR verified the silencing of viral pluripotency factors (vir.-OCT4, vir.-SOX2, vir.-KLF4, vir.-C-MYC) to less than 0.01 fold level and the upregulation of the endogenous pluripotency factor NANOG by eight-fold (Fig. 1D). Ordinary genomic integrity was evaluated after ten passages via karyotyping and showed an unsuspicious karyotype (Fig. 1E). Expression of pluripotent markers OCT3/4, TRA-1-60, SOX2 and SSEA-4 was confirmed by immunofluorescence stainings (Fig. 1F). Pluripotency of HIHDNEi002-A was further validated after differentiation of iPSCs from embryoid-bodies into cells of all three embryonic germ layers. Layer specific markers were demonstrated by immunofluorescence stainings (neuron-specific class III beta-tubulin (TUJ, ectoderm), SRY-related HMG-box 17 (SOX17, endoderm) and smooth muscle actin (SMA, mesoderm)) (Fig. 1G). Scale bars in all images are 100 µm.

Materials and methods

Culturing and reprogramming of fibroblast to iPSCs

The consent form for cell biopsy from patient was approved by the Ethics Committee of the Medical Faculty of the University of Tübingen. The dermal fibroblasts from patient skin biopsy were cultured in fibroblast culture medium (DMEM high glucose (Life Technologies) + 10% FCS (Pan BioTech)) at 37 °C, 5% CO_2 with medium change every two to three days. For reprogramming of the fibroblasts four retroviral vectors were used, expressing OCT4, SOX2, KLF4 and C-MYC (all plasmids were a gift from Shinya Yamanaka: pMXs-hOCT3/4 (Addgene plasmid # 17217), pMXs-hSOX2 (Addgene plasmid # 17218), pMXs-hKLF4 (Addgene plasmid # 17219), pMXs-hc-MYC (Addgene plasmid # 17220)) (Takahashi et al., 2007). After ten days, fibroblasts were seeded on a mouse embryonic fibroblast (MEF) feeder-layer cultured in hES medium (Knockout DMEM (Life Technologies), 20% Knockout Serum Replacement (KOSR) (Life Technologies), 0.1 mM beta-mercaptoethanol (Sigma Aldrich), 1% glutamine (Biochrom)m 1% nonessential amino acids (NEAA) (Biochrom) and 5 ng/ml human basic Fibroblast Growth Factor 2 (FGF2) (PeproTech)). After two additional weeks, clonal selection was performed manually by picking individual clones and transferring them to separate wells. For the next ten passages, hES medium was used and clones were transferred manually once a week with the ratio 1:10. For further characterization, colonies were manually transferred onto Matrigel-coated (BD Bioscience) 6-well plates and cultivated feeder-free in mTeSR (StemCell Technologies) Table 1.

Sequencing of mutation site

The heterozygous mutation c.890 T > G, p.Arg297Gln in *KCNA2* was confirmed via Sanger sequencing (GATC, Konstanz, Germany) using primers flanking the mutation (Table 2). The mutation was analyzed with CLC Sequence Viewer 8 (QUIAGEN Bioinformatics).

Mycoplasma detection

For the detection of mycoplasma PCR Mycoplasma Test Kit (Product-No. A3744) from Applichem was used according to the manufacturer's instructions.

qRT-PCR

Silencing of the viral expression of pluripotency factors and the upregulation of NANOG as an endogenous pluripotency marker was confirmed by qRT-PCR with primers specific for viral pluripotency genes or endogenous NANOG (Table 2): RNA of iPSCs was isolated with ISOLATE II RNA mini Kit (Bioline) and following reverse-transcribed to cDNA (Bioline - SensiFAST™ SYBR® Lo-ROX One-Step Kit). For qRT-PCR (ABI7000 lightcycler from Applied Biosystems) QuantiTect SYBR Green Kit (Qiagen) was used. Expression of the genes was normalized to GAPDH and compared to their expression in fibroblasts treated with reprogramming viruses for 8 days (Reinhardt et al., 2013).

Karyotyping and STR analysis

iPSCs were karyotyped according to a standard protocols. G-banding showed a normal karyotype in 22 metaphases. Cell line identity of fibroblasts and iPSCs were confirmed by STR analysis, which revealed that genomic DNA extracted from iPSCs and patient fibroblasts

Table 2
Reagents details.

Antibodies used for immunocytochemistry/flow-citometry			
	Antibody	Dilution	Company Cat # and RRID
Pluripotency markers	Anti-Oct4 rb antibody	1:1000	Abcam (ab19857), RRID: AB_445175
	Anti-SOX2 rb antibody	1:500	Abcam (ab97959), RRID: AB_2341193
	Anti-SSEA4 ms antibody [MC813]	1:500	Abcam (ab16287), RRID: AB_778073
	Anti-TRA-1-60 (R) ms antibody [TRA-1-60]	1:500	Abcam (ab16288), RRID: AB_778563
In vitro differentiation	Anti-TUJ1 rb antibody	1:500	Covance (MRB-435P), RRID: AB_663339
	Anti-SOX17 ms antibody	1:250	R&D Systems (MAB19241-SP), RRID: AB_10920934
	Anti-SMA ms antibody	1:100	Dako (AB_2223500), RRID: AB_2223500
Secondary antibodies	Alexa Fluor 488 Goat anti-Mouse IgG	1:500	Life Technologies (A-11001), RRID: AB_2534069
	Alexa Fluor 568 Goat anti-Rabbit IgG	1:500	Life Technologies (A-11011), RRID: AB_143157

Primers		
	Target	Forward/Reverse primer (5′-3′)
Viral factors (qRT-PCR)	Vir-OCT4	CCCCAGGGCCCCATTTTGGTACC / TTATCGTCGACCACTGTGCTGCTG
	Vir-SOX2	GGCACCCCTGGCATGGCTCTTGGCTC / TTATCGTCGACCACTGTGCTGCTG
	Vir-KLF4	ACGATCGTGGCCCCGGAAAAGGACC / TTATCGTCGACCACTGTGCTGCTG
	Vir-C-MYC	CAACAACCGAAAATGCACCAGCCCCAG / TTATCGTCGACCACTGTGCTGCTG
Pluripotency Markers (qRT-PCR)	End-NANOG	CCTGTATTTGTGGGCCTG / GACAGTCTCCGTGTGAGGCAT
House-Keeping Gene (qRT-PCR)	GAPDH	CTGGTAAAGTGGATATTGTTGCCAT / TGGAATCATATTGGAACATGTAAACC
Targeted mutation sequencing	Mutation *KCNA2* c.890G > A	GTTCTCCTTTGAATTCTTGG / CTCATTACTGTTATTTACAC

matched on all 21 loci tested (Epicentre - QuickExtract™ DNA Extraction Solution). Analyses were performed by the Medical Genetics and Applied Genomics Department of the University of Tübingen.

Immunocytochemical staining

iPSCs were grown on Matrigel-coated coverslips in 24-well plates and fixed with 4% paraformaldehyde solution for 20 min and then washed 3 times with PBS at room temperature (RT). Blocking and permeabilization was accomplished by incubation in blocking buffer (PBS without $CaCl_2$/$MgCl_2$, 10% normal goat serum (NGS), 0.2% Triton X-100) for 60 min (RT). Cells were incubated over two nights at 4 °C with the primary antibody (see Table 2). After 3 times washing with PBS, the secondary antibody (see Table 2) was added and cells were incubated in the dark for 1 h (RT). Primary and secondary antibodies were diluted in PBS without CaCl2/MgCl2, 1% normal goat serum (NGS) and 0.2% Triton X-100. After 3 further washing steps in PBS −/−, DAPI (1,5000) was used for nuclear staining by incubation for 2 min (RT). Cells were mounted using Fluoromount-G (Southern Biotech). Images were captured with an Axio Imager Z1 with ApoTome (Zeiss).

In vitro differentiation potential

To test pluripotency, the ectodermal and mesodermal differentiation was initiated by seeding iPSCs on AggreWell 800 plates (Stemcell Technologies) for Embryoid Body (EB) formation. EB-medium (80% DMEM/F12, 20% KOSR, 1× NEAA, 2 mM L-Alanyl-L-Glutamine (Merck) and 0.1 mM beta-mercaptoethanol) was changed at day 2. At day 4, EBs were collected and plated on 0.1% gelatine-covered (Sigma-Aldrich) coverslips for mesodermal differentiation (Meso-Diff medium: DMEM high glucose (Life Technologies), 20% FCS, 1× NEAA, 1.5 mM beta-mercaptoethanol, 0.5 µM a-Thioglycerol (Sigma-Aldrich)) and on Matrigel-coated coverslips for ectodermal differentiation (Ecto-Diff medium: 48% DMEM/F-12, 48% Neurobasal, 1× N-2 (Capricorn Scientific), 1× B-27 (Capricorn Scientific), 1× Glutamax (Life Technologies), 1× NEAA). Differentiation medium was exchanged every other day and cells were cultivated for additional 2–3 weeks. For endodermal differentiation iPSCs were passaged in single cells on Matrigel-coated coverslips and endodermal differentiation medium was changed every day for 5 days RPMI1640 (Merck) supplemented with 1× B27 (Life Technologies), 0.2% FCS, 2 µM CHIR-99021 (Abcam) and 50 ng/ml Activin A (Stemcell Technologies).

Acknowledgements

N.S. was in part supported from the intramural research funding program of the Faculty of Medicine Tübingen (Fortüne 2381-0-0). This work has been supported by the Federal Ministry of Education and Research program for rare diseases (Treat-ION, grant 01GM1907A).

References

Masnada, S., Hedrich, U.B.S., Gardella, E., Schubert, J., Kaiwar, C., Klee, E.W., ... Rubboli, G., 2017. Clinical spectrum and genotype-phenotype associations of KCNA2-related encephalopathies. Brain 140 (9), 2337–2354. https://doi.org/10.1093/brain/awx184.

Reinhardt, P., Schmid, B., Burbulla, L.F., Schondorf, D.C., Wagner, L., Glatza, M., ... Sterneckert, J., 2013. Genetic correction of a LRRK2 mutation in human iPSCs links parkinsonian neurodegeneration to ERK-dependent changes in gene expression. Cell Stem Cell 12 (3), 354–367. https://doi.org/10.1016/j.stem.2013.01.008.

Scheffer, I.E., French, J., Hirsch, E., Jain, S., Mathern, G.W., Moshe, S.L., ... Zuberi, S.M., 2016. Classification of the epilepsies: new concepts for discussion and debate-special report of the ILAE classification task force of the commission for classification and terminology. Epilepsia Open 1 (1–2), 37–44. https://doi.org/10.1002/epi4.5.

Syrbe, S., Hedrich, U.B.S., Riesch, E., Djemie, T., Muller, S., Moller, R.S., ... Lemke, J.R., 2015. De novo loss- or gain-of-function mutations in KCNA2 cause epileptic encephalopathy. Nat. Genet. 47 (4), 393–399. https://doi.org/10.1038/ng.3239.

Takahashi, K., Tanabe, K., Ohnuki, M., Narita, M., Ichisaka, T., Tomoda, K., Yamanaka, S., 2007. Induction of pluripotent stem cells from adult human fibroblasts by defined factors. Cell 131 (5), 861–872. https://doi.org/10.1016/j.cell.2007.11.019.

2.2 Chapter 2: Reprogramming of fibroblasts with *KCNA2* p.L328V variant to induced pluripotent stem cells

EBERHARD KARLS
UNIVERSITÄT
TÜBINGEN

Medizinische Fakultät

Declaration of contributions:

Herewith I, Niklas Schwarz declare, that I have contributed to the mayor part of the following publication:

Schwarz N, Uysal B, Rosa, F, Löffler H, Mau-Holzmann UA, Liebau S, Lerche H, Generation of an induced pluripotent stem cell (iPSC) line from a patient with developmental and epileptic encephalopathy carrying a *KCNA2* (p.Leu328Val) mutation. Stem Cell Res. 2018 Dec;33:6-9. doi: 10.1016/j.scr.2018.08.019. Epub 2018 Aug 31.

The authors contributed to the publications as indicated in the following table (indicated in %):

Contribution	Niklas Schwarz	Betül Uysal	Filip Rosa	Heidi Löffler	Ulrike A. Mau-Holzmann	Stefan Liebau	Holger Lerche
Research concept	90%					5%	5%
Project administration	90%						10%
Funding acquisition	50%						50%
Selection of methods	100%						
Recruitment of patients	80%			10%			10%
Data acquisition	90%			5%	5%		
Data analysis	90%	5%			5%		
Visualization	95%				5%		
Interpretation of results	85%	5%	5%		5%		
Preparation of Manuscript	90%	3%			4%	3%	

Signature of the doctoral candidate:



As supervisor, I agree with the declarations by the candidate:

As corresponding author, agree with the declarations by the candidate:

As co-authors, we agree to the declarations above:



[Betül Uysal] [Filip Rosa] [Heidi Löffler]



[Ulrike A. Mau-Holzmann] [Stefan Liebau] [Holger Lerche]

Stem Cell Research 33 (2018) 6–9

Contents lists available at ScienceDirect

Stem Cell Research

journal homepage: www.elsevier.com/locate/scr

Lab Resource: Single Cell Line

Generation of an induced pluripotent stem cell (iPSC) line from a patient with developmental and epileptic encephalopathy carrying a *KCNA2* (p.Leu328Val) mutation

Niklas Schwarz[a,*], Betül Uysal[a], Filip Rosa[a], Heidi Löffler[a], Ulrike A. Mau-Holzmann[b], Stefan Liebau[c], Holger Lerche[a]

[a] Department of Neurology and Epileptology, Hertie Institute for Clinical Brain Research, University of Tuebingen, Germany
[b] Department of Medical Genetics and Applied Genomics, University of Tuebingen, Germany
[c] Institute of Neuroanatomy & Developmental Biology, University of Tuebingen, Germany

A B S T R A C T

Mutations in the *KCNA2* gene, coding for the voltage-gated K^+ channel $K_v1.2$, can cause developmental and epileptic encephalopathies. $K_v1.2$ channels play an important role in the repolarization phase of an action potential in nerve cells. Here, we reprogrammed human skin fibroblasts from a 13-year-old male patient with developmental and epileptic encephalopathy carrying a point mutation (c.982T > G, p.Leu328Val) in *KCNA2* to human induced pluripotent stem cells (iPSCs) (HIHDNEi001-A). The cells maintained a normal karyotype and their pluripotency state was verified by the expression and staining of several pluripotency markers and capability to differentiate into all three germ layers.

Resource table.

Unique stem cell line identifier	HIHDNEi001-A
Alternative name(s) of stem cell line	iPSC-*KCNA2*-P3
Institution	Department of Neurology and Epileptology, Hertie Institute for Clinical Brain Research, University of Tuebingen, Germany
Contact information of distributor	Niklas Schwarz, niklas.schwarz@uni-tuebingen.de
Type of cell line	iPSC
Origin	Human
Additional origin info	Age: 13 years Sex: male Ethnicity: German
Cell Source	Fibroblasts
Clonality	Clonal
Method of reprogramming	Retrovirus
Genetic modification	NO
Type of modification	N/A
Associated disease	Developmental and epileptic encephalopathy
Gene/locus	Gene: *KCNA2*, c.982T > G, p.Leu328Val (heterozygous) Locus: 1p13.3 (GRCh38.p12, Chr1: 110,593,580-110,631,536)
Method of modification	N/A
Name of transgene or resistance	N/A
Inducible/constitutive system	N/A
Date archived/stock date	October 2015
Cell line repository/ bank	N/A
Ethical approval	Institutional Review Board of the Medical Faculty, University of Tuebingen - Approval Number: 303/2011BO1

Resource utility

This cell line is derived from fibroblasts of a patient with developmental and epileptic encephalopathy. Since effective therapies are still insufficient, this iPSC line will be useful for disease modelling to better

* Corresponding author.
E-mail address: niklas.schwarz@uni-tuebingen.de (N. Schwarz).

https://doi.org/10.1016/j.scr.2018.08.019
Received 6 July 2018; Received in revised form 13 August 2018; Accepted 23 August 2018
Available online 31 August 2018
1873-5061/ © 2018 The Authors. Published by Elsevier B.V. This is an open access article under the CC BY-NC-ND license (http://creativecommons.org/licenses/BY-NC-ND/4.0/).

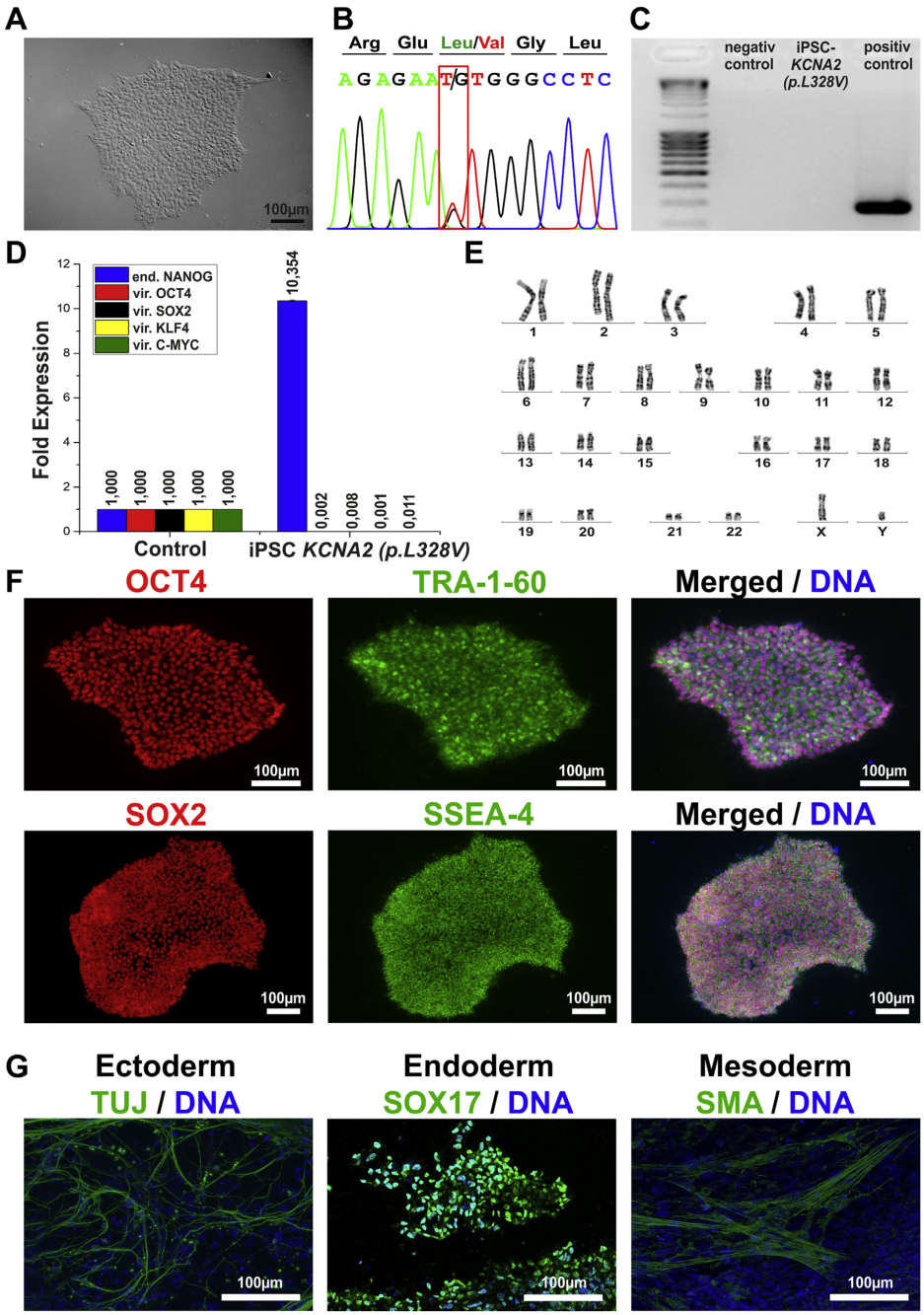


Fig. 1. Characterization and validation of HIHDNEi001-A.

understand the pathophysiology and develop new treatments.

Resource details

Developmental and epileptic encephalopathies comprise a phenotypically and genetically heterogeneous group of severe neurological disorders that occur early in life and are characterized by severe and pharmacoresistant epilepsy, cognitive dysfunction and other neurological deficits (Scheffer et al., 2016). Mutations in the voltage-gated K^+ channel $K_v1.2$, encoded by the gene *KCNA2*, were recently

identified as a new molecular entity within the developmental and epileptic encephalopathies (Masnada et al., 2017; Syrbe et al., 2015). Patient's fibroblasts in this study were isolated and reprogrammed with four Yamanaka factors (OCT4, SOX2, KLF4, C-MYC) from a 13-year-old male patient carrying a heterozygous mutation (c.982T > G, p.Leu328Val) in *KCNA2*. The obtained induced pluripotent stem cell line HIHDNEi001-A (Fig. 1A) displayed a morphology similar to embryonic stem cells. Full characterization was accomplished after manual picking and expansion on mouse embryonic fibroblasts for at least ten passages. Sanger sequencing of the mutation site in iPSCs confirmed the expected point mutation (Fig. 1B). Genomic integrity was checked via karyotyping and showed a normal karyotype (Fig. 1E). Congruence to the parental fibroblasts was approved by STR analysis. Mycoplasma detection test using a Mycoplasma Test Kit Mix from Applichem was found negative for the exhibited iPSC line (Fig. 1C). Silencing of viral pluripotency factors (vir.-OCT4, vir.-SOX2, vir.-KLF4, vir.-C-MYC) to less than 0.01 fold level and upregulation of endogenous NANOG by 10.3 fold was confirmed by qRT-PCR (Fig. 1D) (Reinhardt et al., 2013). Immunofluorescence staining confirmed expression of pluripotent markers OCT3/4, TRA-1-60, SOX2 and SSEA-4 (Fig. 1F). For further validation of pluripotency, cells from HIHDNEi001-A were differentiated from embryoid-bodies into cells of all three embryonic germ layers. Immunofluorescence staining demonstrated the expression of neuron-specific class III beta-tubulin (TUJ, ectoderm), SRY-related HMG-box 17 (SOX17, endoderm) and smooth muscle actin (SMA, mesoderm) (Fig. 1G). Scale bars in all images are 100 µm. (See Table 1.)

Materials and methods

Culturing and reprogramming of fibroblast to iPSCs

The consent form for cell donation from patient's parents was approved by the Ethics Committee of the Medical Faculty of the University of Tübingen. Human dermal fibroblasts from patient skin biopsy were cultured in fibroblast culture medium (DMEM high glucose (Life Technologies) + 10% FCS (Pan BioTech)) at 37 °C, 5% CO_2 with medium change every 2–3 days. Fibroblasts were reprogrammed using four retroviral vectors expressing OCT4, SOX2, KLF4 and C-MYC (all plasmids were a gift from Shinya Yamanaka: pMXs-hOCT3/4 (Addgene plasmid # 17217), pMXs-hSOX2 (Addgene plasmid # 17218), pMXs-hKLF4 (Addgene plasmid # 17219), pMXs-hc-MYC (Addgene plasmid # 17220)) (Takahashi et al., 2007). The Multiplicity of infection (MOI) for retroviral reprogramming was 13 (calculated using QuickTiter™ Retrovirus Quantification Kit from Cell Biolabs). Fibroblast were seeded after 10 days on a mouse embryonic fibroblast (MEF) feeder layer cultured in hES medium (Knockout DMEM (Life Technologies), 20% Knockout Serum Replacement (KOSR) (Life Technologies), 0.1 mM beta-mercaptoethanol (Sigma Aldrich), 1% glutamine (Biochrom)m 1% nonessential amino acids (NEAA) (Biochrom) and 5 ng/ml human basic Fibroblast Growth Factor 2 (FGF2) (PeproTech)) until clonal selection was performed manually by picking individual clones after 14 days and placing them separate in wells. hES medium were used for the next 10 passages. Afterwards, the colonies were manually transferred on Matrigel-coated (BD Bioscience) 6-well dishes and cultivated in mTeSR (StemCell Technologies) for further characterization.

Sequencing of mutation site

The heterozygous mutation c.982T > G, p.Leu328Val in *KCNA2* was confirmed via Sanger sequencing (GATC, Konstanz, Germany) using primers flanking the mutation. The mutation was analyzed with CLC Sequence Viewer 7 (QUIAGEN Bioinformatics).

Mycoplasma detection

PCR Mycoplasma Test Kit (Product-No. A3744) from Applichem was used for the detection of mycoplasma according to the manufacturer's instructions.

qRT-PCR

To confirm silencing of the viral expression of pluripotency factors and the upregulation of NANOG as endogenous pluripotency marker, qRT-PCR with primers specific for pluripotency genes (Table 2) was performed: RNA was isolated with ISOLATE II RNA mini Kit (Bioline) and following reverse-transcribed to cDNA. QuantiTect SYBR Green Kit (Qiagen) was used for qRT-PCR (ABI7000 lightcycler from Applied Biosystems). Expression of the genes was normalized to GAPDH and compared to their expression in fibroblasts treated with reprogramming viruses for 8 days (Reinhardt et al., 2018).

Karyotyping and STR analysis

iPSCs were karyotyped according to a standard protocol. G-banding showed a normal karyotype in 26 mitoses. Cell line identity of fibroblasts and IPSCs were confirmed by STR analysis, which revealed that genomic DNA extracted from patient fibroblasts and IPSCs matched on all 21 loci tested. Analyses were performed by the Medical Genetics and Applied Genomics Department of the University of Tübingen.

Table 1
Characterization and validation.

Classification	Test	Result	Data
Morphology	Photography	Visual record of the line: normal	Fig. 1 panel A
Phenotype	Qualitative analysis (Immunocytochemistry)	Staining/expression of pluripotency markers: OCT4, TRA-1-60, SOX2 and SSEA-4	Fig. 1 panel F
	Quantitative analysis (RT-qPCR)	qRT-PCR for end-NANOG, vir-OCT4, vir-SOX2, vir-KLF4, vir-C-MYC	Fig. 1 panel D
Genotype	Karyotype (G-banding) and resolution	46,XY Resolution 300–400	Fig. 1 panel E
Identity	Microsatellite PCR (mPCR)	N/A	N/A
	STR analysis (PowerPlex®21)	21 sites were tested and fibroblasts and appendant iPSCs matched	Submitted in archive with journal
Mutation analysis	Sequencing	Heterozygous pointmutation, c.890G > A	Fig. 1 panel B
	Southern Blot OR WGS	N/A	N/A
Microbiology and virology	Mycoplasma	Mycoplasma testing by Ready-to-use PCR Mycoplasma Test Kit Mix from Applichem (#A3744), negative	Fig. 1 panel C
Differentiation potential	Directed differentiation	Expression of Neuron-specific class III beta-tubulin (TUJ1), SRY-related HMG-box 17 protein (SOX17) and smooth muscle actin (SMA).	Fig. 1 panel G
Donor screening	HIV 1 + 2 Hepatitis B, Hepatitis C	N/A	N/A
Genotype additional info	Blood group genotyping	N/A	N/A
	HLA tissue typing	N/A	N/A

Table 2
Reagents details.

Antibodies used for immunocytochemistry/flow-cytometry			
	Antibody	Dilution	Company Cat # and RRID
Pluripotency Markers	Anti-Oct4 rb antibody	1:1000	Abcam (ab19857)
	Anti-SOX2 rb antibody	1:500	Abcam (ab97959)
	Anti-SSEA4 ms antibody [MC813]	1:500	Abcam (ab16287)
	Anti-TRA-1-60 (R) ms antibody [TRA-1-60]	1:500	Abcam (ab16288)
In vitro differentiation	Anti-TUJ1 rb antibody	1:500	Covance (MRB-435P)
	Anti-SOX17 ms antibody	1:250	R&D Systems (MAB19241-SP)
	Anti-SMA ms antibody	1:100	Dako (AB_2223500)
Secondary antibodies	Alexa Fluor 488 Goat anti-Mouse IgG	1:500	Life Technologies
	Alexa Fluor 568 Goat anti-Rabbit IgG	1:500	Life Technologies

Primers		
	Target	Forward/Reverse primer (5′–3′)
Viral factors (qRT-PCR)	Vir-OCT4	CCCCAGGGCCCCATTTTGGTACC/TTATCGTCGACCACTGTGCTGCTG
	Vir-SOX2	GGCACCCCTGGCATGGCTCTTGGCTC/TTATCGTCGACCACTGTGCTGCTG
	Vir-KLF4	ACGATCGTGGCCCCGGAAAAGGACC/TTATCGTCGACCACTGTGCTGCTG
	Vir-C-MYC	CAACAACCGAAAATGCACCAGCCCCAG/TTATCGTCGACCACTGTGCTGCTG
Pluripotency markers (qRT-PCR)	End-NANOG	CCTGTATTTGTGGGCCTG/GACAGTCTCCGTGTGAGGCAT
House-keeping gene (qRT-PCR)	GAPDH	CTGGTAAAGTGGATATTGTTGCCAT/TGGAATCATATTGGAACATGTAAACC
Targeted mutation sequencing	Mutation *KCNA2* c.890G > A	GTTCTCCTTTGAATTCTTGG/CTCATTACTGTTATTTACAC

Immunocytochemical staining

iPSCs were grown on Matrigel-coated coverslips in 24-well plates and fixed with 4% paraformaldehyde solution for 20 min and then washed 3 times with PBS. Blocking and permeabilization was accomplished by incubation in blocking buffer (PBS without $CaCl_2$/$MgCl_2$, 10% normal goat serum (NGS), 0.2% Triton X-100) for 60 min. Cells were incubated over two nights at 4 °C with the primary antibody (see Table 2). After 3 times washing with PBS, the secondary antibody (see Table 2) was added and cells were incubated in the dark at room temperature for 1 h. After 3 further washing steps in PBS−/−, DAPI (1:5000) was used for nuclear staining by incubation for 2 min at room temperature. Cells were mounted using Fluoromount-G (Southern Biotech). Images were captured with an Axio Imager Z1 with ApoTome (Zeiss).

In vitro differentiation potential

To test pluripotency, the ectodermal and mesodermal differentiation was started with seeding the iPSCs on AggreWell 800 plates (Stemcell Technologies) for Embryoid Body (EB) formation. EB-medium (80% DMEM/F12, 20% KOSR, 1× NEAA, 2 mM L-Alanyl-L-Glutamine (Merck) and 0.1 mM beta-mercaptoethanol) was changed at day 2. At day 4, EBs were collected and plated on 0.1% gelatine-covered (Sigma-Aldrich) coverslips for mesodermal differentiation (Meso-Diff medium: DMEM high glucose (Life Technologies), 20% FCS, 1× NEAA, 1.5 mM beta-mercaptoethanol, 0.5 µM a-Thioglycerol (Sigma-Aldrich)) and on Matrigel-coated coverslips for ectodermal differentiation (Ecto-Diff medium: 48% DMEM/F-12, 48% Neurobasal, 1× N-2 (Capricorn Scientific), 1× B-27 (Capricorn Scientific), 1× Glutamax (Life Technologies), 1× NEAA). Differentiation medium was exchanged every other day and cells were cultivated for additional 2–3 weeks. For endodermal differentiation iPSCs were passaged in single cells on Matrigel-coated coverslips and endodermal differentiation medium was changed every day for 5 days (RPMI1640 (Merck) supplemented with 1× B27 (Life Technologies), 0.2% FCS, 2 µM CHIR-99021 (Abcam) and 50 ng/ml Activin A (Stemcell Technologies).

Acknowledgements

N.S. was in part supported from the intramural research funding program of the Faculty of Medicine Tübingen (Fortüne 2381-0-0).

References

Masnada, S., Hedrich, U.B.S., Gardella, E., Schubert, J., Kaiwar, C., Klee, E.W., ... Rubboli, G., 2017. Clinical spectrum and genotype-phenotype associations of KCNA2-related encephalopathies. Brain 140 (9), 2337–2354. https://doi.org/10.1093/brain/awx184.

Reinhardt, P., Schmid, B., Burbulla, L.F., Schondorf, D.C., Wagner, L., Glatza, M., ... Sterneckert, J., 2013. Genetic correction of a LRRK2 mutation in human iPSCs links parkinsonian neurodegeneration to ERK-dependent changes in gene expression. Cell Stem Cell 12 (3), 354–367. https://doi.org/10.1016/j.stem.2013.01.008.

Scheffer, I.E., French, J., Hirsch, E., Jain, S., Mathern, G.W., Moshe, S.L., ... Zuberi, S.M., 2016. Classification of the epilepsies: New concepts for discussion and debate-special report of the ILAE Classification Task Force of the Commission for Classification and Terminology. Epilepsia Open 1 (1–2), 37–44. https://doi.org/10.1002/epi4.5.

Syrbe, S., Hedrich, U.B.S., Riesch, E., Djemie, T., Muller, S., Moller, R.S., ... Lemke, J.R., 2015. De novo loss- or gain-of-function mutations in KCNA2 cause epileptic encephalopathy. Nat. Genet. 47 (4), 393–399. https://doi.org/10.1038/ng.3239.

Takahashi, K., Tanabe, K., Ohnuki, M., Narita, M., Ichisaka, T., Tomoda, K., Yamanaka, S., 2007. Induction of pluripotent stem cells from adult human fibroblasts by defined factors. Cell 131 (5), 861–872. https://doi.org/10.1016/j.cell.2007.11.019.

2.3 Chapter 3: Electrophysiological analysis of iPS cell-derived neurons

The established iPS cell lines described in chapter 1 and 2 from patients with *KCNA2* c.890G>A, p.R297Q or c.982T>G, p.L328V variants and two healthy control persons were differentiated into neurons for further electrophysiological analysis. Therefore, a protocol for fast and reproductive maturation was used, which is based on the overexpression of the neuronal transcription factor Neurogenin-2 (NGN2) (Busskamp et al., 2014; Y. Zhang et al., 2013). For better maturation the neurons were co-cultured on mouse astrocytes until they were analyzed via whole-cell patch-clamp technique. In the results part of chapter 3, electrical properties like resting membrane potential, input resistance and cell capacitance were compared between the patient iPS cell-derived NGN2-neurons and the control lines.

2.3.1 Methods

2.3.2 Generation of stable and inducible NGN2-iPS cell lines

For the stable and inducible integration of the transcription factor neurogenin-2 (NGN2), two lentiviruses were used. The iPS cell lines were transduced with one construct for the overexpression of NGN2 and a second construct for the transcription activator rtTA3 (Figure 7).

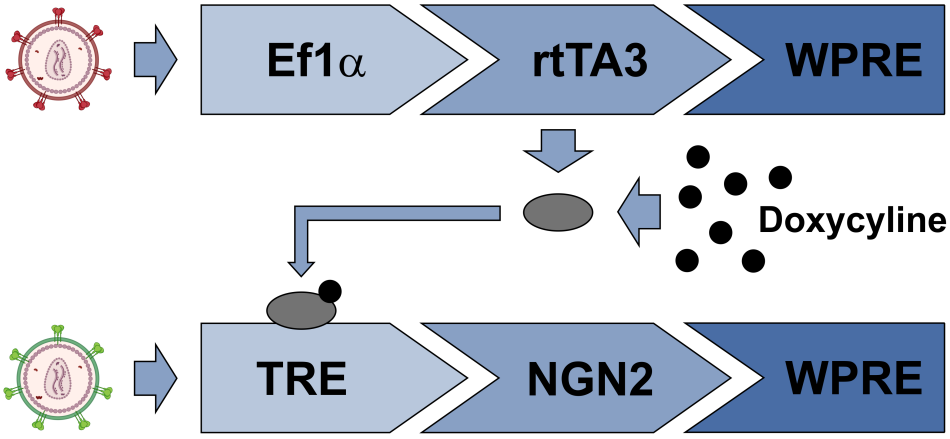


Figure 7: Lentiviral constructs for creating stable NGN2-iPS cell lines.

The upper construct contained the transcription activator rtTA3 which was constitutively expressed under a EF1α promoter. When the tetracycline transactivator (tTA) protein bound to the added doxycycline, the complex started to induce the Neurogenin-2 (NGN2) expression under the TetON promotor in the second construct (lower) and thus the neural differentiation.

2.3.3 Production of lentiviruses for neuronal differentiation

To production of lentiviruses in S2 lab was perfomed with HEK293T cells, which were seeded 24 hours before transfection. Cells were incubated at 37°C, 5% CO_2. The Co-transfection was accomplished with 4 µg of NGN2 (Addgene ID # 61474) or rtTa3 (Addgene ID # 61472), 2 µg of PLP1, 2 µg of PLP2 and 2µg of PLP-VSVG. The constructs were diluted in 100 µl Optimem (Thermo Fisher Scientific, Waltham, MA, USA) and incubated at room temperature for five minutes. In parallel, 470 µl Optimem containing 30 µl FuGENE HD transfection reagent (Promega, Madison, Wisconsin, United States) was incubated at room temperature for 5 minutes. Then, both epis were mixed and added onto HEK293T cells dropwise. The produced virus was released into the medium and collected on days 4 and 5 and centrifuged in Spin columns (Stemcell Technologies, Köln, Germany) at 4000 x g for 45 minutes. The concentrated virus was directly used for transduction of the iPS cells.

2.3.4 Generation of stable NGN2-iPS cell lines

To establish stable NGN2-iPS cell lines, iPS colonies were passaged as small colonies into 12-well plates and incubated in mTeSR medium (Stemcell Technologies, Vancouver, Canada) at 37°C, 5% CO_2. After 24 hours, the medium

was refreshed and 30 µl of NGN2 and 60 µl of rtTA3 lentivirus was added to the medium. Further, iPS colonies were cultured in mTeSR medium and passaged when they were confluent. For positive selection 0.5 µg/ml Puromycin (Invivogen, San Diego, CA, USA) was added to the medium to isolate the colonies transduced with NGN2. After selection, NGN2-iPS cells were frozen as stocks and stored in the liquid nitrogen tank at -80°C or further used for neuronal differentiation.

2.3.5 Preparation and cultivation of mouse astrocytes

Cortical glial cultures were obtained from dissection of E17.5 mouse pups (Schildge et al., 2013). The glial cultures were incubated at 37°C, 5% CO_2 in 100 µg/ml PDL-coated T75 flaks. Every 3 days the media was changed with DMEM high glucose (Thermo Fisher Scientific, Waltham, MA, USA) containing 10% FCS (Pan BioTech, Aidenbach, Germany). After 12-15 days, the flasks with mixed cultures were shaken on an orbital shaker for 1 hour at 200 rpm at 37°C to detach the microglia and then overnight at 200 rpm at 37°C to detach oligodendrocyte precursor cells. After eliminating the unwanted cells, astrocyte cultures were trypsinized with 0.02 % Trypsin (Biochrom, Berlin, Germany) and plated on new T75 flasks coated with PDL (Sigma Aldrich, St. Louis, MO, USA). The enriched astrocyte cultures were maintained in the same medium conditions and before they were co-cultured with neurons, the astrocytes were trypsinized and seeded on Matrigel-coated (BD Biosciences, Heidelberg, Germany) 13 mm coverslips with a density of $5x10^4$ cells per coverslip.

2.3.6 Differentiation of NGN2-iPS cell lines into neurons

The Matrigel coated and with mouse astrocyte seeded coverslips were prepared 3-5 days before neuronal induction. Once iPS cells have reached passage stage, the cells were treated for four hours with doxycycline (2.5 µg/ml) to induce Neurogenin-2 expression. One hour before passaging, the cells were treated with Thiazovivin (5µg/ml) (apoptosis inhibitor = AI) (Tocris Bioscience, Minneapolis, MN, USA). iPS cells were treated with Accutase (Capricorn Scientific GmbH, Ebsdorfergrund, Germany) for 20 min and triturated to get single cells for further

processing. Cells were plated with a density of 120.000 cells/coverslips on mouse astrocyte monolayers and incubated in NSC media (47% Neurobasal medium, 47% DMEM/F12, 2% B27 supplement, 1% N2 supplement, 1% Glutamax and 1% nonessential amino acids - all from Thermo Fisher Scientific, Waltham, MA, USA) containing 1 µg/ml doxycycline, Thiazovivin (2 µM) and DAPT (3 µM) (Tocris Bioscience, Minneapolis, MN, USA). 24 hours later, the media was changed to NSC media containing 1 µg/ml doxycycline, DAPT (10 µM) and PD (10 µM) (Tocris Bioscience, Minneapolis, MN, USA). After day 5, cultures were refreshed with only NSC medium by every 4-5 days for the next 8 weeks (Figure 8).

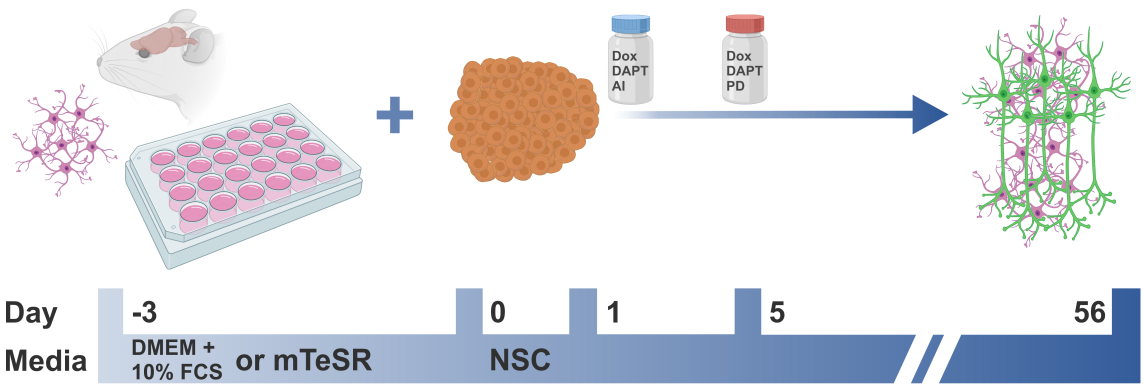


Figure 8: Timeline for the differentiation of NGN2-iPS cells into neurons.

NGN2-iPS cells were induced by doxycycline (Dox) and plated on a mouse astrocyte monolayer. Medium was switched from DMEM + 10% FCS for the astrocytes or mTeSR for iPS cells on day 0 to NSC medium with supplements for the first five days and then NSC alone for the neurons until day 56. DAPT is an inhibitor of the γ-secretase complex and promotes differentiation of neurons from human and mouse stem cells, AI = apoptosis inhibitor = Thiazovivin, PD is an inhibitor of MEK1/2 and helps to differentiate iPS cells into functional cortical neurons.

2.3.7 Immunohistochemistry

Cells were grown on glass coverslips and washed once with PBS (+/+) (Thermo Fisher Scientific, Waltham, MA, USA) containing $CaCl_2$ and $MgCl_2$ and then fixed with 4% PFA solution (Morphisto, Frankfurt Am Main, Germany) for 20 minutes at room temperature. After fixation they were washed three times with PBS (-/-) and blocked and permeabilized afterwards with PBS (-/-) containing 10% normal goat serum (NGS) (Sigma Aldrich, St. Louis, MO, USA) and 0.2% Triton X-100

(Sigma Aldrich, St. Louis, MO, USA) for 1 hour at room temperature. Fixed Cells were incubated overnight at 4°C with primary antibodies which were diluted in PBS (-/-) containing 1% NGS and 0.02% Triton X-100. After three times washing with PBS (-/-), cells were incubated with secondary antibodies diluted in PBS (-/-) containing 1% NGS and 0.02% Triton X-100 for 1 hour at room temperature in the dark. Cells were washed three times with PBS before staining with DAPI (1:5000 in PBS for 2–5 min). After three final washing steps (2x PBS, 1x Ampuwa water), cells were mounted in Fluoromount G (SouthernBiotech Birmingham, AL, USA). After three times washing with PBS (-/-), the coverslips were mounted using DAPI-fluromounting medium (Southern Biotech, Birmingham, USA). Antibodies were used at the following dilutions: chicken anti-MAP2 (1:500, Abcam, ab5392, RRID:AB_2138153); rabbit anti-GFAP (1:250, Agilent, Z0334, RRID:AB_10013382), goat anti-chicken Alexa 488 (1:500, Thermo Fisher, A-11039, RRID:AB_142924) and goat anti-rabbit IgG Alexa 568 (1:500, life technologies, A-11011, RRID:AB_143157).

2.3.8 Electrophysiology

Electrophysiological characterization of patient and control iPS cell-derived neurons was performed by whole cell voltage- and current- clamp recordings, which were accomplished eight weeks after the neuronal induction. The recordings were performed using an Axopatch 200B amplifier controlled by Clampex 10.2, filtered at 10 kHz and digitized at 10 kHz via a Digidata 1440A acquisition system (Molecular Devices, Sunnyvale, CA, USA). Ingredients for bath solution were 121 mM NaCl, 4.2 mM KCl, 29 mM $NaHCO_3$, 0.5 mM Na_2HPO4, 0.45 mM NaH_2PO_4 and 5mM HEPES. The pipette solution contained 135 mM K-Gluconate, 4 mM NaCl, 0.5 mM $CaCl_2$, 10 mM HEPES, 2 mM EGTA, 2 mM Mg-ATP and 0.4 mM GTP-Na. The Osmolarity of the solutions was adjusted to pH to 7.4 and 300 mOsm. Liquid junction potential was not subtracted from the data automatically but was calculated as -15 mV and later substracted. All data are shown with leak subtraction. After the whole-cell patch was formed on the soma of neurons, the voltage was clamped at -70 mV. Inward and outward currents were recorded via depolarization pulses from a holding potential of -70

mV to different potential levels, from -60 mV to +30 mV with 10 mV increments, for 24 seconds. The input resistance was measured for each cell as responses to 500 ms long current stimulations from -0.01 nA to -0.06 nA. The membrane potential was kept around -70 mV under current-clamp conditions for the following recordings. To assess intrinsic firing properties, responses to the stepwise current stimulations from -0.001 nA to 0.069 nA in 0.005 increments with a duration of 800 ms.

2.3.9 Data and statistical analysis

Traces were displayed off-line with the Clampfit 10.4 (Molecular Devices, Sunnyvale, CA, USA). Graphics were generated using Excel (Microsoft, Redmond, WA, USA) and Origin Software 2015 (OriginLab Inc., Massachusetts, USA). Statistical analysis was performed using SigmaPlot 12 (Systat Software GmbH, Erkrath, Germany). The data were tested for normal distribution via Shapiro-Wilk test. One Way ANOVA test was used to test significance of normally distributed data and ANOVA on Ranks test for not normally distributed data. All data are shown as mean ± SEM, n gives the number of cells. For all statistical tests, significance levels are indicated using the following symbols: *p = 0.05.

2.3.10 Results

2.3.11 Immunocytochemical confirmation of iPS cell-derived neurons

Both *KCNA2* variant carrier and control iPS cell lines were differentiated into neurons using the Neurogenin-2 overexpression differentiation protocol as described in methods (section 2.2.3 -2.2.5) (Busskamp et al., 2014; Y. Zhang et al., 2013). For confirmation of neuronal identity immunocytochemical staining against the neuron specific microtubule-associated protein 2 (MAP2) was performed. Long-term viability and maturation of the generated neurons was supported by a mouse astrocyte monolayer on the coverslips before induced iPS cells were plated. For mouse astrocytes identity the glial fibrillary acidic protein (GFAP) was stained. To examine the supporting effect of mouse astrocytes on

the viability and development of NGN2 neurons, three weeks after induction immunocytochemical analyses was performed for the neurons cultured without and with astrocytes (Figure 9).

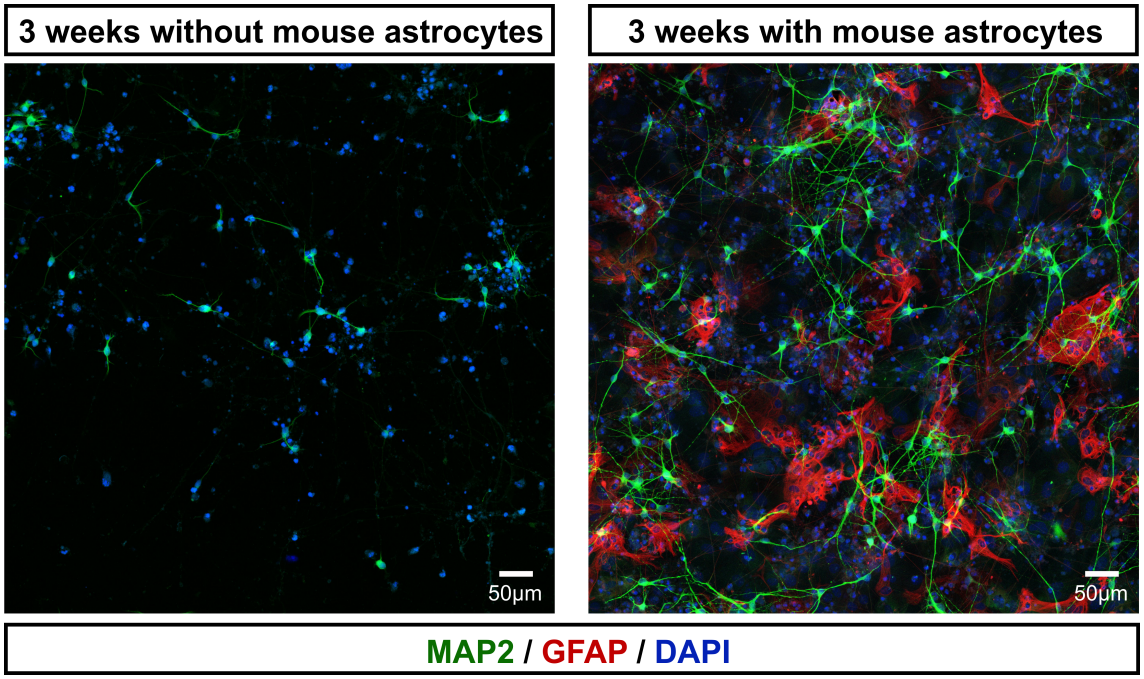


Figure 9: Supportive effect of mouse astrocytes on the maturation of NGN2 neurons.

Representative images show MAP2 positive NGN2 neurons cultured without (left) and with (right) mouse astrocytes (GFAP positive). Cultures were fixed three weeks after induction of the iPS cells.

The pure NGN2 neuronal cultures without mouse astrocytes showed many DAPI-positive nuclei but MAP2-positive neurons were relatively rare. The length and ramification of the dendrites of the neurons were very limited and most of the neurons died after the third week after induction of differentiation. In comparison, NGN2 neurons with supportive mouse astrocytes were found to have long branches extending far away from the cell bodies, intact morphology and longer lifetime. This confirmed that mouse astrocytes supported the neuronal survival in cultures for a long time, whereas the NGN2-neurons without astrocytes in culture were lost after the third week. Therefore, all differentiations for electrophysiological analysis were performed with NGN2 neurons cultured on mouse astrocytes.

Immunostainings of the neuronal cultures on mouse astrocytes were also accomplished eight weeks after induction of differentiation (Figure 10). At this time point all the electrophysiological analyses were performed because NGN2 neurons at this age were more mature and capable to fire trains of action potentials in response to current injections contrary to the neurons that could fire only one action potential in early stages of differentiation. Control and both *KCNA2* variant carrier lines showed comparable morphology for the NGN2 neurons in terms of length and ramification of the dendrites of the cells.

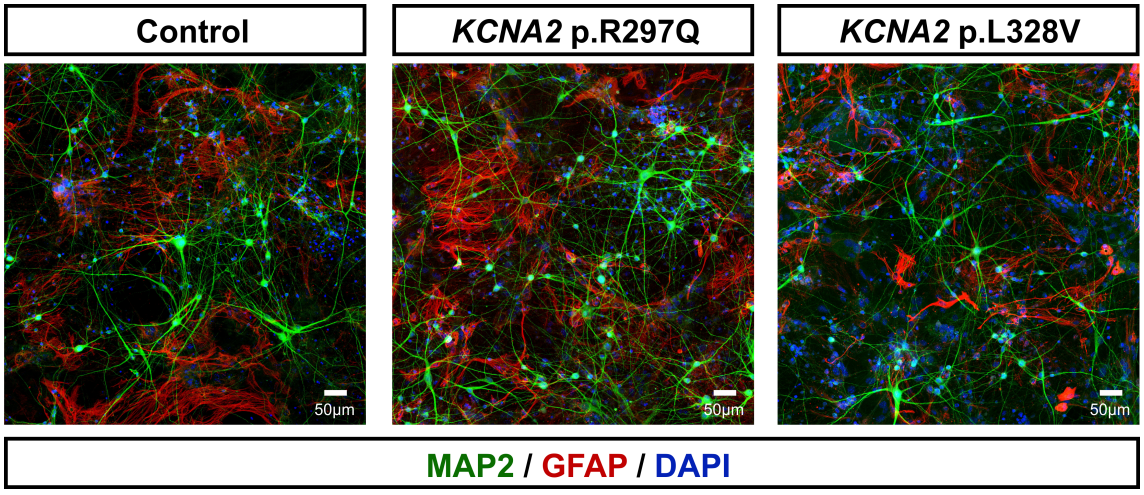


Figure 10: Immunostainings of eight weeks old NGN2 neurons.

Eight weeks old control and *KCNA2* variant carrier iPS cell-derived MAP2 positive (green) neurons differentiated on a monolayer of mouse astrocytes (GFAP = red).

2.3.12 Electrophysiological analysis of iPS cell-derived neurons

All whole-cell patch-clamp recordings of control and both *KCNA2* variant carrier iPS cell-derived neurons were performed eight weeks after the start of neuronal induction on mouse astrocytes. For the electrophysiological analyses, all neurons were included that had at least one action potential at current injections from -1 pA to 69 pA with 5 pA increments enduring 800ms. First investigations in a heterologous expression system (*Xenopus laevis* oocytes) on the two *de novo KNCA2* variants (p.R297Q and p.L328V) have already been performed by Syrbe et al., 2015 and Masnada et al., 2017. Electrophysiological analysis revealed increased current amplitudes by nine fold and a shifted voltage dependence of steady-state activation by −40 mV for the p.R297Q variant in comparison to the wild-type channel (Syrbe et al., 2015). The resting membrane potential of oocytes expressing p.R297Q channels was about 40 mV more negative than the resting membrane potential of oocytes expressing wild-type channels due to the permanently open mutant channels (Syrbe et al., 2015). The p.L328V variant resulted in a -20 mV shift of steady-state activation and a 10 mV more negative resting membrane potential in injected oocytes compared to the wild-type (Masnada et al., 2017).

2.3.13 Currents evoked in iPS cell-derived neurons

NGN2 neurons were patched in whole-cell configuration and inward and outward currents were examined via voltage-clamp recordings. The currents were evoked by depolarizing pulses from a holding potential of -70 mV, to the different potential levels in 10 mV increments from -60 mV to +30 mV (Figure 11A). Only cells with a proper inward and outward currents were recorded for further protocols. Representative inward and outward currents evoked in control and *KCNA2* variant carrier iPS cell-derived NGN2-neurons are shown in Figure 11B.

In Figure 11C, average outward current densities evoked for each membrane potential level are plotted for both control and *KCNA2* variant carrier-derived neurons. When the neuronal membranes were depolarized between -10 mV and

+20 mV, *KCNA2* p.L328V variant carrier-derived neurons created significantly smaller outward currents than the control neurons.

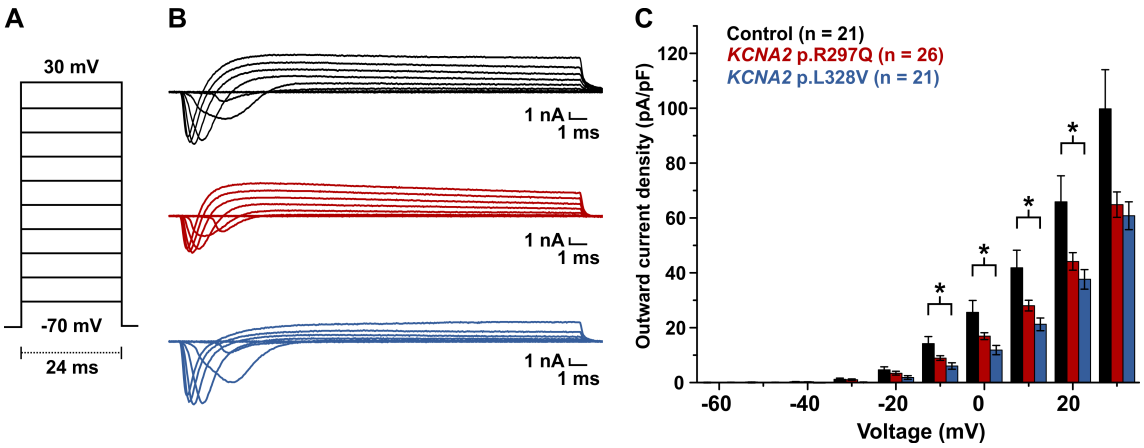


Figure 11: Currents evoked in control and *KCNA2* variant carrier iPS cell-derived neurons.

(A) The stimulus waveform of the depolarization steps used to evoke currents in neurons endured 24ms and started from a holding potential of -70 mV to different potential levels with 10 mV increments, from -60 mV to +30 mV. (B) Evoked inward and outward currents in control (black) and *KCNA2* variant carrier (red and blue) iPS cell-derived neurons. (C) Averaged outward current density was measured for all potential levels. Data were tested with ANOVA on Ranks with post-hoc Dunn's method ($P < 0.05$) (indicated by asterisks). All data are shown as mean ± SEM, n gives the number of analyzed cells.

2.3.14 Passive electrical properties of control and patient iPS cell-derived neurons

Membrane capacitance, resting membrane potential and input resistance values were analyzed for control and *KCNA2* variant carrier iPS cell-derived neurons to evaluate the passive electrical properties of the cell lines. Recordings of the neuron capacitances were performed directly after a whole-cell patch configuration was formed, without any compensation. The mean cell capacitance values for control iPS cell-derived neurons was 52.85 pF whereas it was 58.19 pF for *KCNA2* p.R297Q variant and 49.60 pF for *KCNA2* p.L328V variant, with standard error of the mean values 3.9, 3.6 and 3.6 (Figure 12A). The difference between the membrane capacitance values for control and *KCNA2* variant carrier neurons were not significant (p-value=0.223). Resting membrane potentials were obtained from the current clamp gap-free recordings which were performed

between min 7-12 after the neurons were opened. The recorded average resting membrane potential for control neurons was -47.42 mV, -52.48 mV for *KCNA2* p.R297Q variant and 51.22 pF for *KCNA2* p.L328V variant, with standard error of the mean values 1.6, 1.7 and 1.2, respectively (Figure 12B). The difference between the resting membrane potentials for control and patient neurons were not significantly different (p-value=0.451).

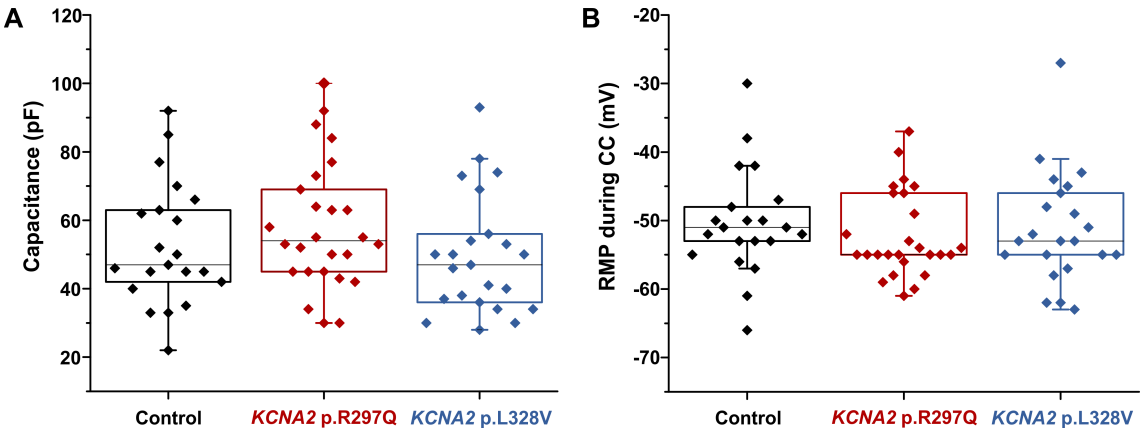


Figure 12: Resting membrane potential and cell capacitance of control and *KCNA2* variant carrier iPS cell-derived neurons.

(A) Cell capacitance values for the recorded patient and control neurons, n (control) = 21, n (*KCNA2* p.R297Q variant) = 26, n (*KCNA2* p.L328V variant) = 23. (B) Resting membrane potentials of the control and *KCNA2* variant carrier neurons 7-12 minutes after the cells were opened, n (control) = 21, n (*KCNA2* p.R297Q variant) = 26, n (*KCNA2* p.L328V variant) = 22. In (A) and (B) each symbol represents a single neuron.

The input resistance values were obtained from current-clamp recordings. Neurons were stimulated with the different current injections from -0.01 nA to -0.06 nA, as shown in Figure 13A. Exemplary current-clamp traces showing the changes in membrane potential of a control iPS cell-derived neuron in response to the current injections are shown in Figure 13B. The input resistance of the single neurons was calculated from the relationship between the injected current level and the resulting change in the membrane potential. The mean input resistance for control neurons was 576.17 MΩ, for *KCNA2* p.R297Q variant carrier it was 609.73 MΩ and for *KCNA2* p.L328V variant carrier it was 806.95 MΩ, with a standard error of the mean of 73.00, 63.03 and 123.59. The difference

between the input resistance values for control and *KCNA2* variant carrier iPS cell-derived neurons was not statistically significant (p-value=0.341).

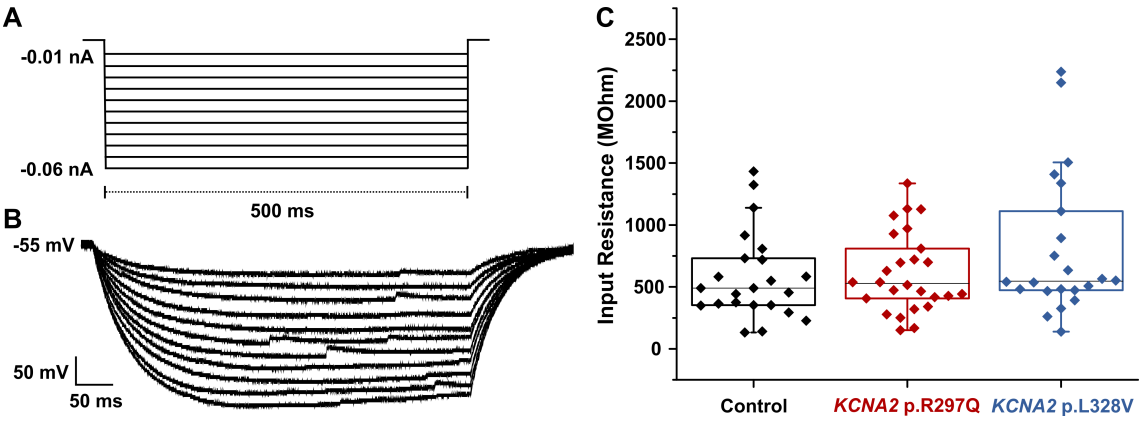


Figure 13: Input Resistance of control and *KCNA2* variant carrier iPS cell-derived neurons.

(A) Stimulus waveform of the eleven current injections steps endured 500ms and started from -0.01 nA to -0.06 nA. (B) Representative current-clamp traces of a control neuron, showing changes in membrane potential in response to the stepwise current injections. (C) Input resistance values for control and *KCNA2* variant carrier iPS cell-derived neurons, each symbol represents a single neuron, n (control) = 23, n (*KCNA2* p.R297Q variant) = 26, n (*KCNA2* p.L328V variant) = 22.

2.3.15 Firing properties of control and patient iPS cell-derived neurons

To assess the active properties of control and patient iPS cell-derived neurons in the whole-cell current-clamp mode, the cell membranes were held at -70 mV via constant current injections and stimulated for 800 ms with different levels of current injections from -1 pA to 69 pA in 5 pA increments. Exemplary current-clamp traces of a control and both *KCNA2* variant carrier neurons showing action potential trains evoked in response 69 pA to current injections are shown below in Figure 14B.

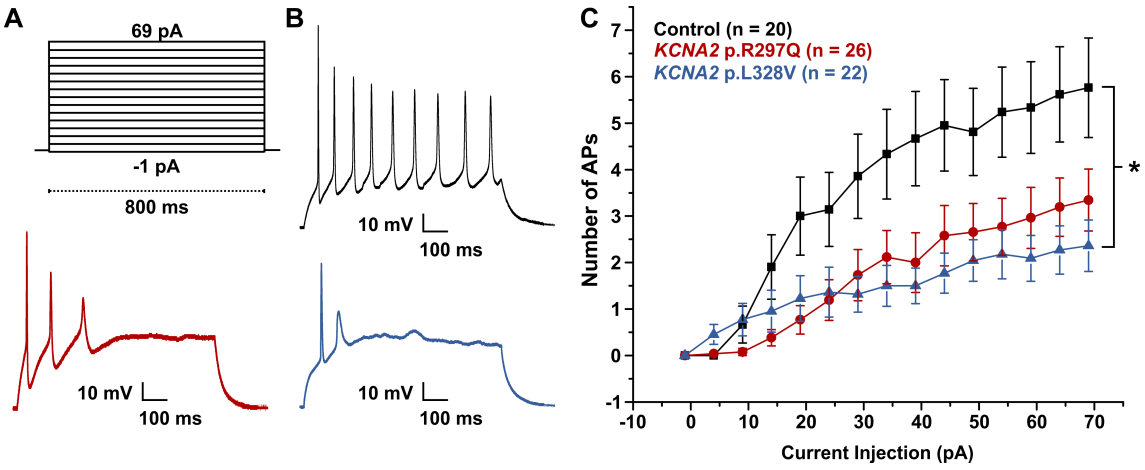


Figure 14: Action potential firing properties of control and *KCNA2* variant carrier iPS cell-derived neurons.

(A) Stimulus waveform for the current injections steps starting from -1 pA to 69 pA with 5 pA increments enduring 800ms. (B) Representative current-clamp traces of a representative control- (black), *KCNA2* p.R297Q variant (red) and *KCNA2* p.L328V variant (blue) -derived neuron showing action potential trains in response 69 pA current injections. (C) Absolute numbers of the generated action potentials of all iPS cell-derived neuron lines, in response to different current injections. Data of area under the curves were tested with ANOVA on Ranks with post-hoc Dunn's method ($P < 0.05$) (indicated by asterisks). All data are shown as mean ± SEM, n gives the number of analyzed cells.

In Figure 14C, the absolute number of action potentials generated at each current injection level is plotted for control and *KCNA2* variant carrier iPS cell-derived neurons. *KCNA2* p.L328V variant-derived neurons, generated statistically significant less action potentials than neurons derived from controls in response to the injections. A general finding was that for both control- and *KCNA2* variant carrier-derived neurons, the action potential firing behavior had a high variability from cell to cell within the cultures. Some neurons fired the highest number of action potentials in response to relatively low current infections and reached a depolarization blockade with higher amounts of injected currents, whereas some neurons fired more action potentials in response to larger current injections without reaching a depolarization block (data not shown).

2.3.16 Summary

In conclusion, it was shown that mouse astrocytes supported the neuronal survival in cultures for a long time, whereas the NGN2-neurons without astrocytes in culture were lost after three weeks in culture. The electrophysiological analyses revealed no significant differences for the iPS cell-derived neurons from the *KCNA2* p.R297Q variant carrier in comparison to the control cells. The iPS cell-derived neurons from the *KCNA2* p.L328V variant carrier, however, created significantly smaller outward currents than the control neurons, when the neuronal membranes were depolarized between -10 mV and +20 mV. Further, the *KCNA2* p.L328V variant line generated less action potentials than control neurons in response to current injections. These results suggest that the iPS cell-derived neurons from *KCNA2* p.L328V variant carrier are hypoexcitable.

2.4 Chapter 4: Establishment of human neocortical organotypic brain slice cultures

EBERHARD KARLS
UNIVERSITÄT
TÜBINGEN

Medizinische Fakultät

Declaration of contributions:

Herewith I, Niklas Schwarz declare, that I have contributed to the mayor part of the following publication:

Schwarz N, Hedrich UBS, Schwarz H, PA H, Dammeier N, Auffenberg E, Bedogni F, Honegger JB, Lerche H, Wuttke TV, Koch H, Human Cerebrospinal fluid promotes long-term neuronal viability and network function in human neocortical organotypic brain slice cultures. Sci Rep. 2017 Sep 25;7(1):12249. doi: 10.1038/s41598-017-12527-9.

The authors contributed to the publications as indicated in the following table (indicated in %):

Contribution	Niklas Schwarz	Ulrike BS Hedrich	Hannah Schwarz	Harshad P.A.	Nele Dammeier	Eva Auffenberg
Research concept	50%					
Project administration	45%					
Funding acquisition						
Selection of methods	65%					
Recruitment of patients	20%				5%	5%
Data acquisition	65%	5%	3%	3%	3%	3%
Data analysis	70%					
Visualization	70%					
Interpretation of results	60%	5%				
Preparation of Manuscript	65%	5%				

Contribution	Francesco Bedogni	Jürgen B. Honegger	Holger Lerche	Thomas V. Wuttke	Henner Koch
Research concept				10%	40%
Project administration				20%	35%
Funding acquisition				50%	50%
Selection of methods					35%
Recruitment of patients		20%	15%	20%	15%
Data acquisition	3%				20%
Data analysis					30%
Visualization					30%
Interpretation of results					35%
Preparation of Manuscript				5%	25%

EBERHARD KARLS
UNIVERSITÄT
TÜBINGEN

Medizinische Fakultät

[redacted]

Signature of the doctoral candidate:

As supervisor, I agree with the declarations by the candidate:

As corresponding author, agree with the declarations by the candidate:

As co-authors, we agree to the declarations above:

[redacted]

[Ulrike BS Hedrich] [Hannah Schwarz] [Harshad P.A.]

[redacted]

[Nele Dammeier] [Eva Auffenberg] [Francesco Bedogni]

[redacted]

[Jürgen B Honegger] [Holger Lerche] [Thomas V. Wuttke]

[redacted]

[Henner Koch]

www.nature.com/scientificreports



OPEN

Received: 5 April 2017
Accepted: 7 September 2017
Published online: 25 September 2017

Human Cerebrospinal fluid promotes long-term neuronal viability and network function in human neocortical organotypic brain slice cultures

Niklas Schwarz[1], Ulrike B. S. Hedrich[1], Hannah Schwarz[1], Harshad P.A.[1], Nele Dammeier[1], Eva Auffenberg[1], Francesco Bedogni[3], Jürgen B. Honegger[2], Holger Lerche[1], Thomas V. Wuttke[1,2] & Henner Koch[1]

Pathophysiological investigation of CNS-related diseases, such as epilepsy or neurodegenerative disorders, largely relies on histological studies on human post mortem tissue, tissue obtained by biopsy or resective surgery and on studies using disease models including animal models, heterologous expression systems or cell culture based approaches. However, in general it remains elusive to what extent results obtained in model systems can be directly translated to the human brain, calling for strategies allowing validation or even primary investigation in live human CNS tissue. In the work reported here, we prepared human organotypic slice cultures from access tissue of resective epilepsy surgery. Employing different culture conditions, we systematically compared artificial culturing media versus human cerbrospinal fluid (hCSF) obtained from patients with normal pressure hydrocephalus (NPH). Presented data demonstrates sustained cortical neuronal survival including not only maintenance of typical cellular electrophysiological properties and activity, such as robust action potential generation and synaptic connectivity, but also preservation of tonic and phasic network activity up to several weeks *in vitro*. As clearly delineated by immunocytochemistry, single cell patch clamp and extracellular recordings, we find that in contrast to artificial culturing media, hCSF significantly enhances neuron viability and maintenance of network activity.

Investigation of pathophysiological mechanisms of human neurodegenerative and other central nervous system (CNS)-related diseases as well as the development of new therapeutic avenues in first line relies on studies involving model systems that include cell culture systems and animal models. Often it is assumed that obtained data apply or can be extrapolated to human CNS but there are numerous examples given by pharmaceutical research and drug development demonstrating that there are significant differences, even posing the risk that newly developed drugs which proved to effectively target certain pathways in model systems will not show the expected effects in patients. One way of approaching this challenge is the use of embryonic stem (ES)[1] or induced pluripotent stem (iPS)[2] cell technology or cerebral organoids[3], allowing engineering and growing of "humanoid" neurons *in vitro* for investigation and analysis. While such approaches are considered a huge step forward, at the same time they are controversially discussed regarding e.g. purity, subtype-identity and maturity of generated "humanoid" neurons. Furthermore, this technology currently does not provide the tools to rebuild entire complex human CNS tissue (including entire cortical layering and columnar organization), which would be crucial when working toward a deeper understanding of physiological characteristics of human CNS circuitry or of pathophysiological mechanisms contributing to the development of human CNS-related disease. Alternative approaches to

[1]Department of Neurology and Epileptology, Hertie-Institute for Clinical Brain Research, University of Tübingen, Tübingen, Germany. [2]Department of Neurosurgery, University of Tübingen, Tübingen, Germany. [3]San Raffaele Rett Research Unit, Division of Neuroscience, San Raffaele Scientific Institute, 20132, Milan, Italy. Thomas V. Wuttke and Henner Koch jointly supervised this work. Correspondence and requests for materials should be addressed to H.K. (email: henner.koch@uni-tuebingen.de)

understand diverse aspects of highly complex connectivity and structure of the CNS down to morphological and functional properties of single cells/neurons, altogether governing the functions of the human brain, include MRI imaging technology[4] and elegant stimulation studies[5] or electrophysiological measurements in acute tissue slice preparations[6–8]. Interestingly, some of these studies were able to identify striking differences between human and rodent neurons, confirming that a direct translation from the animal model to humans might sometimes be misleading[6,9]. While – as mentioned above – electrophysiological characterizations of "static" intrinsic properties of human neurons can be successfully achieved in acute slices or potentially iPS-derived "humanoid" neurons[10,11], investigation of intermediate/long-term changes of neuronal properties/function, as for example mediated by certain neuroplasticity mechanisms or by specific gene mutations of interest, remain challenging. In studies based on rodent tissue the development of organotypic slice cultures has been successfully used to bridge the gap of *in vitro* to *in vivo* translation[12], but at the same time the challenges regarding immediate transferability of rodent data to the human organism have remained unsolved. The establishment of optimized human organotypic cortical slice cultures as an *ex vivo* system seems very tempting in this regard. Such systems could address some of the mentioned questions by enabling the investigation of dynamic properties of human neurons (such as neuroplasticity) and potentially of other cortical cells including glia over a time period of days to weeks. Furthermore, such cultures could serve as a platform to directly explore the functional impact and pathophysiological mechanisms of defined mutations (for example of ion channels) and their role in the development of CNS-related disease, which could be studied in the context of human cortical networks by help of viral-mediated overexpression. In addition, organotypic cortical slice cultures can be used for drug discovery and preclinical studies since it provides a peerless opportunity to investigate the effect of substances to human neuronal networks that developed physiologically. It also offers a possible tool for testing neuroprotective agents to networks maintaining their cellular complexity as well as their anatomical integrity[13].

While previous studies in organotypic cultures prepared from human post mortem cortical tissue demonstrated continued viability of many cells including neurons up to several weeks *in vitro*[14–16], additional neurobiological data indicated that under certain conditions cultures prepared from resected human cortical tissue may be subject to a severe injury response, involving proliferation of reactive cells as well as progressive neurodegeneration[16]. However, recent work by another group demonstrated that such processes potentially could be ameliorated using optimized complex defined artificial culturing media, enabling at least partial preservation of characteristic neuronal morphology and importantly also pathological electrophysiological activities of mainly but not exclusively subcortical limbic structures (hippocampus, subiculum) in organotypic cultures of adult human tissue[17]. Building on these data, we here demonstrate that long-term neocortical neuronal viability and robust electrophysiological single cell and network function can be preserved in human organotypic cortical slice cultures by using human cerebrospinal fluid as culturing medium. These cultures could serve as a platform enabling direct validation of data obtained in model systems including but not limited to ES-/iPS technology, rodent primary neuronal cultures, organotypic slice cultures, and *in vivo* approaches or even non-mammalian heterologous expression systems.

Results

Neuronal activity of human organotypic brain slice cultures cultured in human CSF vs. traditional media. From the initial tissue blocks, 250–300 µm thick slices (n = 57) were cut and kept in culture for 2–21 days either in human cerebrospinal fluid (hCSF) or in traditional culture media (either BrainPhys or organotypic slice culture medium (OSCM), see methods for details) before recordings were performed. To assess the viability of the slices, the electrical activity of the slices was tested with an extracellular population electrode to detect Multi-Unit-Activity (MUA). In all tested slices the concentration of potassium in the recording artificial cerebrospinal fluid (aCSF) was increased to 8 mM to facilitate spontaneous neuronal activity (Fig. 1C). In general, slices were found to either generate spontaneous rhythmic network discharges (Fig. 2A, left panel), tonic desynchronized firing (Fig. 2A, right panel) or no detectable activity at all (Fig. 2D, upper panels, 7 days *in vitro* (DIV) and 14–21 DIV).

The slices cultured in traditional media (see methods for details) showed only in a minority of cases (3/21) neuronal extracellular activity after being *in vitro* up to seven days. Strikingly, only during the first three days of culturing, the slices kept in traditional media were able to produce network driven bursting activity (n = 2/21, 3 DIV; Figs 2B and D), while 1/21 produced tonic firing after 7 days *in vitro* (DIV). In all other slices tested no activity was detected (n = 18/21, 3–21 DIV; Fig. 2C). In contrast, the majority of slices cultured in hCSF produced either tonic activity or rhythmic network discharges (n = 32/36, 3–21 DIV; Fig. 2B–D). The 4/36 slices not exhibiting any neuronal activity were at least 14 DIV or even longer.

Rhythmic network bursting in human organotypic slice cultures cultured in hCSF. From the 32 slices that showed neuronal activity, 13/32 showed rhythmic network activity in aCSF with increased potassium concentrations of 8 mM. The network activity occurred with a mean frequency of 0.245 ± 0.09 Hz and had a mean duration of 4774 ± 2251 ms. The network activity seemed to be variable in duration and frequency (Fig. 3A–C). Some slices produced long lasting (up to 30 s) synchronous discharges (Fig. 3A), while others showed a higher bursting frequency with shorter durations (under 1 s). The frequency of these slices tended to be faster in correlation to the duration *in vitro*, but this was not statistically significant (Fig. 3D, p = 0.0739). In several slices (n = 11) we also tested the effect of bath application of Muscarine 5–10 µM on the network activity in addition to raising the extracellular potassium concentration to 8 mM. 5/11 slices showed tonic activity in the presence of 8 mM potassium, which increased in the presence of Muscarine, but only induced in 1/5 rhythmic network bursting. In 4/6 slices that showed rhythmic network bursting in 3 mM or elevated levels of 8 mM extracellular potassium, the application of Muscarine increased the frequency of bursting from 0.0029 ± 0.003 to 0.16 ± 0.29, while in two slices the application of Muscarine increased the tonic activity but stopped network bursting activity. To test if

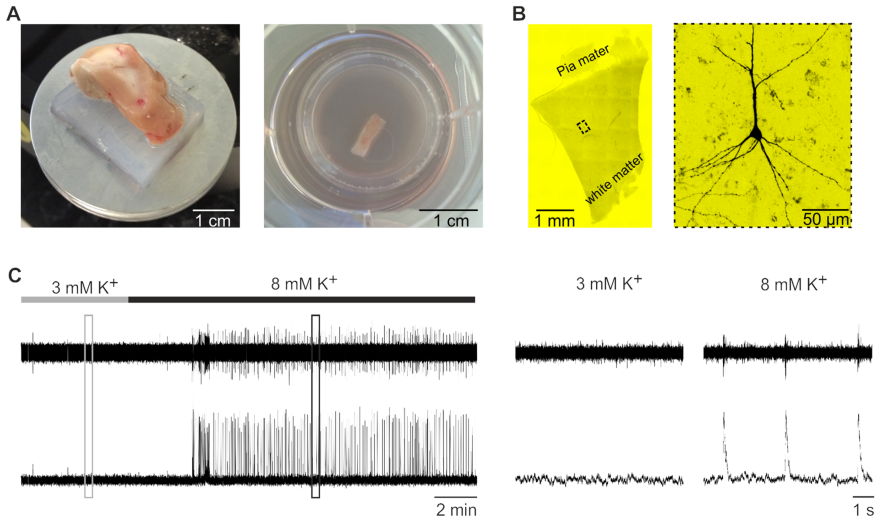


Figure 1. Human organotypic slices were cultured in six well plates for up to 21 days. (**A**) Slices were cut from tissue blocks perpendicular to the cortical surface (250–300 µm thick) and cultured in six well plates either in traditional culture media or human cerebrospinal fluid (hCSF). (**B**) Typical example of a human organotypic slice and a reconstruction of a neuron filled with biocytin after whole cell patch clamp recording revealing a pyramidal morphology (**C**) Multi-Unit extracellular population recording of a human organotypic slice culture, note the induction of rhythmic network discharges after increasing the extracellular K^+ concentration to 8 mM (4 DIV). Boxes are magnified at the right.

the network activity in human organotypic slices was driven by glutamatergic excitatory synaptic transmission we applied CNQX (20–30 µM, n = 3, Fig. 3E), which completely blocked the occurrence of network bursts in all tested slices.

Firing properties of single neurons in hCSF and traditional culture media. In a next step, we investigated in a small number of cells, if neurons cultured in human organotypic slices were still able to produce firing behavior similar to the one of acute slices reported previously[7]. We recorded a total number of 14 cortical neurons in slices cultured in hCSF or traditional media at different time points (2–14 DIV, Table 1, Fig. 4). All neurons tested had a resting membrane potential more negative than −60 mV with an average of −70.3 ± 1.9 mV. Upon positive supra-threshold current injections all neurons cultured in hCSF (n = 10, 2–14 DIV) were able to fire repetitive trains of action potentials (Fig. 4D, Fig. 5A). In slices cultured in traditional media we were able to record four cortical neurons (3 DIV-13 DIV, Fig. 5B). Repetitive supra-threshold current injections (up to 400 pA) led only to the generation of a single action potential in cells recorded in slices cultured in media for 10 to 13 DIV (Fig. 5B, n = 2), while two neurons recorded after 3 DIV cultured in media were able to produce sustained action potential firing (Fig. 5B).

The anatomy of six biocytin filled neurons recorded in hCSF-cultured slices could be reconstructed after fixation. We used biocytin filling for a better morphological reconstruction on a single cell level comparatively to Map2 staining for dendritic integrity on population level. Four of these neurons had the morphology of pyramidal cells of Layer 2/3 and showed also a typical regular spiking pattern (Fig. 4B, D). Two of the neurons we reconstructed had the morphology of non-pyramidal neurons and showed a distinct fast firing pattern typical for non-pyramidal neurons (Fig. 4A and D). Four of the cells recorded in hCSF-cultured slices could not be reconstructed. Of the four neurons recorded in slices cultured in traditional media we could recover two which had the morphology of pyramidal neurons and showed a regular spiking pattern (Fig. 5B, 3 DIV). The other two neurons showed an atypical firing behavior with only a single action potential upon supra-threshold (Fig. 5B, 10–13 DIV). In all cells recorded in hCSF-cultured slices, we recorded up to 10 min of spontaneous activity and detected in 8/10 neurons recorded in slices cultured in hCSF excitatory postsynaptic potentials (Fig. 4C, red arrow) and in 7/10 cells inhibitory postsynaptic potentials (Fig. 4C, blue arrow). Moreover, in 3/10 cells recorded in hCSF-cultured slices (3 DIV, 9 DIV, 13 DIV) phasic network driven population input was detected in elevated concentration of potassium (8 mM, Fig. 3A and B). In the cells recorded from slices cultured in media 1/4 cell received phasic population driven input (3 DIV).

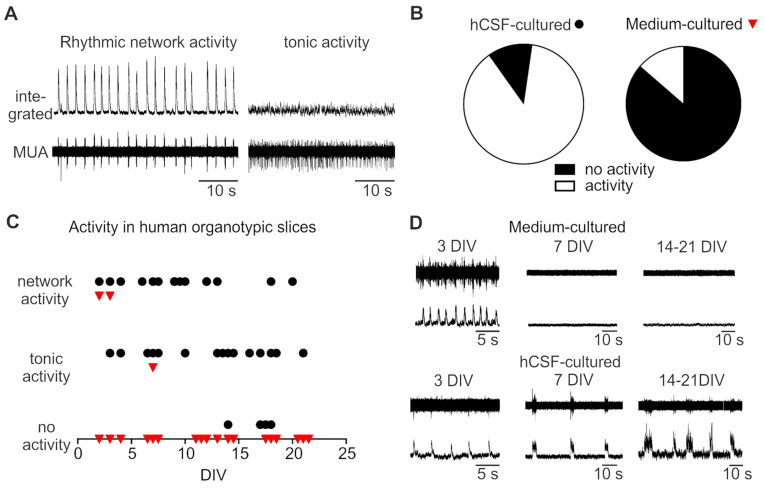


Figure 2. Electrophysiological recordings in human organotypic slice cultures. (**A**) In human organotypic slice cultures three main activity patterns were observed: Rhythmic network activity (A, left panel, 13 DIV), tonic activity (A right panel, 14 DIV) or no activity at all (D upper panels, 7 DIV and 14–21 DIV). (**B**) Overall, the number of slices being able to produce neuronal activity was much higher for slices cultured in hCSF (left pie chart) compared to slices cultured in traditional media (right pie chart). (**C**) Slices were recorded after different days *in vitro* (3–21 DIV). Slices cultured in hCSF (black circles) very frequently exhibited activity in comparison to slices cultured in traditional media (red triangles) (**C** and **D**). During the first days *in vitro* slices cultured in traditional media were still able to produce rhythmic and tonic activity, while in slices cultured for more than 7–10 days no rhythmic activity and just very rarely tonic activity could be recorded. In contrast, the majority of slices cultured in hCSF for 3–21 days showed either rhythmic or tonic activity (**B**,**C** and **D**).

Histology of slices cultured in hCSF vs. traditional media. To determine if in addition to the electrophysiological changes also differences in the structure of the slices can be detected, we conducted a set of histological assessments. We used NeuN to stain the nuclei of post-mitotic neurons and Map2 to determine the dendritic morphology of the cells (Fig. 6A–D, n = 10 for hCSF and n = 4 for traditional media). After 3, 7, 10, 13 and 18 DIV in hCSF-cultured slices we found densely populated NeuN positive cells in all layers of the cortical slice (Figs 6B, 7A and B). Furthermore, the co-labeling with Map2 revealed an intact somato-dendritic morphology of the cells with typical ramification of the apical dendrite (Fig. 6B, 18 DIV, 7A and 7B, 7 and 13 DIV). In slices cultured in traditional media we found also a similar labeling of NeuN positive cells just after a few days (3 DIV and 7 DIV, Fig. 7C), but the Map2 staining revealed already a severe loss of the dendritic structures in the neurons of these slices (Fig. 7B). To quantify this data, we analyzed a representative area of n = 4 for traditional media and n = 4 for hCSF cultured slices at the time points 3 DIV, 7 DIV, 13 DIV and 18 DIV and counted the NeuN and Map2 double positive cells within a 450 × 450 µm field taken with a confocal microscope. We found a significant higher number of double positive cells in slices treated with hCSF compared to traditional media (Fig. 7C, Mann Whitney test, *p<0.05). However, the number of cells positive for NeuN alone in slices cultured with traditional media compared to hCSF was not significantly different. In addition, in slices cultured in hCSF, we tested if we could label astrocytes (n = 6; 3 DIV, 6 DIV, 7 DIV, 14 DIV and 28 DIV). We found at all stages dense labeling of GFAP positive cells in all layers of the human slices cultured in hCSF (Fig. 6D).

Discussion

Organotypic slice cultures have been a useful tool in the last decades to study the physiology and pathology of neuronal networks[12,18,19] or mechanisms of neurodegenerative diseases[20,21]. Here, we show that hCSF can enhance the survival and improve network function in human organotypic slices of adult humans for up to three weeks, including ongoing network and cellular function compared to traditional medium strategies. The advantage of slice cultures is that they stay within an artificial, but nevertheless physiologically developed, composition of neurons[22], glia cells and even blood vessels[23]. In this, still in parts intact, original environment, the cellular and network properties of neurons can be studied in very controlled conditions. It should be noted, that in organotypic slices many artificial changes occur that lead to a different situation compared to acute slice preparations and to the situation *in vivo*. These changes include alterations in the synaptic communication between neurons[24], a change of the intrinsic properties and morphology of the cells[12,24] and an activation of the immune cells, due to the preparation of the slices and the culturing process itself. Keeping these caveats in mind, the slice cultures

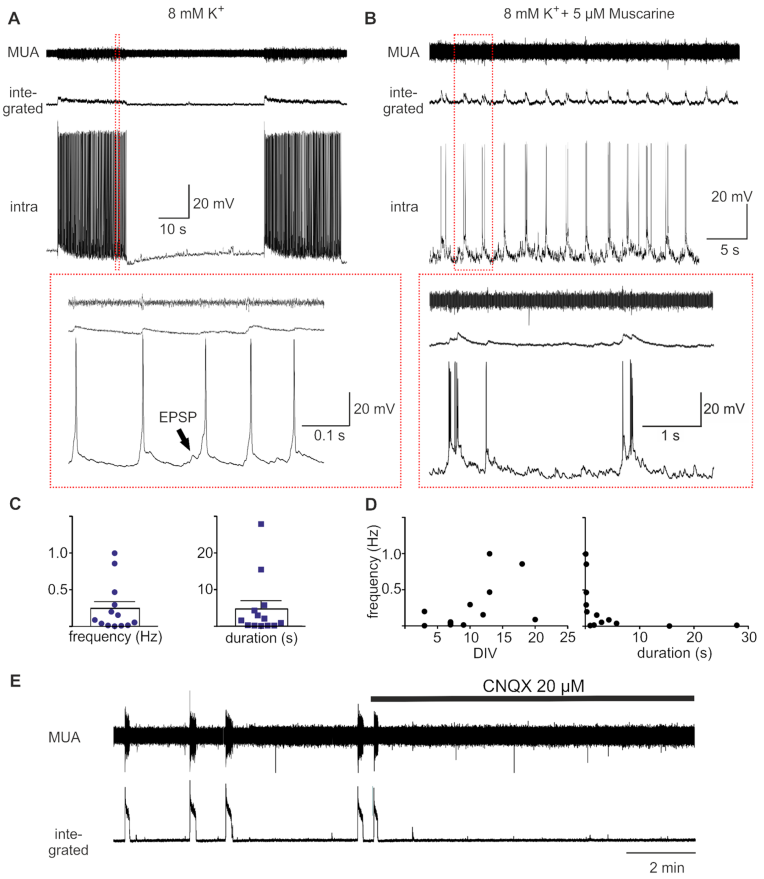


Figure 3. Rhythmic network activity of human slice cultures. The slices that produced rhythmic activity showed either long lasting network discharges (**A** and **E**) or oscillations with shorter bursts occurring with higher frequencies in the presence of 8 mM K^+ (**D**). Shown are examples of the Multi-Unit Activity (MUA) recorded with an extracellular electrode and a simultaneous intracellular recording of a cortical neuron in high potassium alone (**A**) and in high potassium and the presence of Muscarine 5 µM (**B**). The red insets in A and B show expansions of the traces above. (**A**) Note that the action potential firing is riding on a barrage of excitatory postsynaptic potential (EPSP). The neuron in (**B**) was slightly hyperpolarized with a holding current of – 50 pA to emphasize the synaptic inputs. (**C**) Plot of the frequency of the oscillation and duration of all recorded network events in high potassium. (**D**) Plot of the frequency of network discharges against the DIV (left) and duration (right). (**E**) In a subset of the experiments (n = 3) the application of CNQX abolished the network discharges.

can be used to address and study processes that require a long-term observation and might be difficult to engage *in vivo*.

The human tissue that we have received for electrophysiological measurements was taken from patients undergoing a surgery for a resection of an epileptic focus. We and other groups used tissue that needed to be removed in order to get access to the pathological area, rather than pathological tissue itself. Access tissue is not considered to be part of the epileptic focus. Nevertheless, the cells cannot be termed "normal human neurons", since they have been part of an epileptic brain for many years or may have been altered by the presence of antiepileptic drug treatment. To address this problem, Verhoog and colleagues did a careful comparison of the basic properties of human neurons of epilepsy patients and patients with a tumor[7]. No significant differences were

Number	Resting potential	Excitatory input	Inhibitory input	Morphology	DIV before recording
Cell 1	−72	No	No	PY	2
Cell 2	−72	No	No	PY	2
Cell 3	−76	Yes	Yes	PY	2
Cell 4	−63	Yes	Yes	No	3
Cell 5	−63	Yes	No	Int	9
Cell 6	−66	Yes	Yes	No	9
Cell 7	−80	Yes	Yes	No	13
Cell 8	−74	Yes	Yes	Int	13
Cell 9	−74	Yes	Yes	PY	13
Cell 10	−63	Yes	Yes	No	14

Table 1. Properties of cells cultured in hCSF. PY = pyramidal neuron, Int = Interneuron.

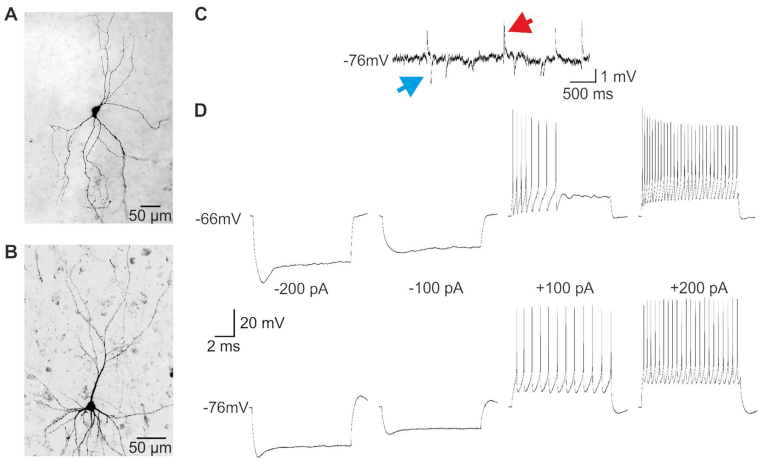


Figure 4. Representative examples of intracellular whole cell patch clamp recordings and biocytin filled morphology of human cortical neurons cultured in hCSF. In slices cultured in hCSF non-pyramidal (**A**, 9 DIV) and pyramidal neurons (**B**, 2 DIV) could be filled with biocytin and the response to hyperpolarizing and depolarizing current injections could be recorded. (**C**) The majority of cells recorded in current clamp received spontaneous inhibitory and excitatory synaptic inputs. Red arrow marks an excitatory postsynaptic potential (EPSP) and blue arrow an inhibitory IPSP in a cell recorded after 13 DIV. (**D**) All cells recorded in hCSF-cultured slices showed sustained action potential generation due to positive current injections (+50 pA to +200 pA) and showed typical firing behavior as reported before in human non – pyramidal (9 DIV, D upper trace) or pyramidal neurons (2 DIV, D lower trace).

found in the basic parameters of the cells indicating that these parameters might reflect most likely the normal properties of neurons. Another important point that has to be considered when working with human brain slices is the variability of the tissue samples (age of patients, genetic background, taken medication, part of resected tissue). To properly address such factors intra-experimental controls are needed from the experimental tissue obtained from the same patients. In our study the culture treatment of the human slices with either hCSF or traditional medium led to a significantly different outcome, when starting from the same patient tissue. As an alternative, we and also other groups have started to use iPS cells from patients to study the physiology and pathology of human neurons. Also this approach seems to have limitations that need to be considered. Adult neurons of patients have undergone development within their natural network environment within the brain up to the time point of surgical intervention and subsequent culturing. In contrast, "human neurons" that were generated from iPSCs undergo an artificial development in a rather rapid time *in vitro* and may even differentiate into neuron subtypes, resembling identities that do not even physiologically exist within the human brain[25,26]. Therefore, studying mature human neurons in organotypic slice cultures as an experimental approach seems, keeping the limitations in mind, a promising and powerful tool.

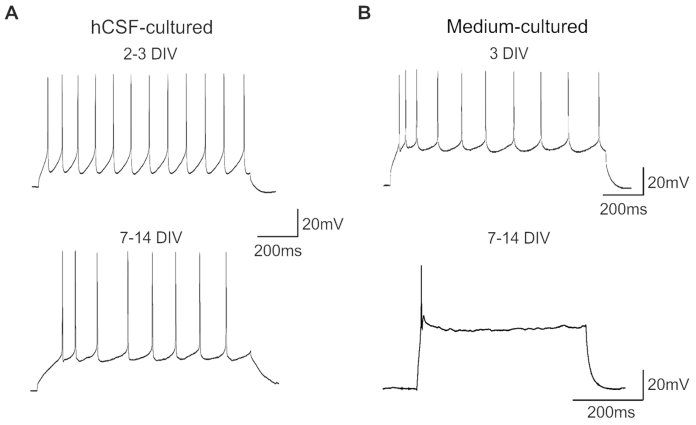


Figure 5. Effect of the culture medium on the excitability of human cortical neurons. The cortical cells recorded in slices cultured in hCSF (**A**) and after the first days in media (**B**, top) showed typical repetitive firing behavior to suprathreshold current injections (n = 10, 2–14 DIV for hCSF, n = 2, 3 DIV for media), while cells recorded from slices cultured in media for more than 7 days showed only a single action potential on suprathreshold current injections (**B**, bottom, n = 2).

However, even in the same culture conditions we observed a variability in the outcome of neuronal activity of the tissue. Most slices cultured in hCSF showed a tonic firing behavior in high potassium concentrations (8 mM), while a third of the slices showed synchronized network discharges (Figs 2 and 3) and a small number did not produce any activity. It stays uncertain what determines the outcome of the slices. Surely, not all slices prepared from the same patient have had the same starting quality, due to the position in the block or other external factors. Also the thickness and size of the slices might have varied slightly and therefore plays a role in the outcome. These differences were not studied in detail, but we plan in further experiments to test the outcome of different sizes and thicknesses of human slice cultures to optimize this tool. In addition, in a recent study by Anderson and colleagues physiological firing behavior in neurons of human organotypic slices cultured in a medium based protocol was reported[14]. However, the authors account that more than half of the neurons they recorded showed normal resting potential of approximately − 60 mV, but were not able to produce action potentials in response to depolarizing current injections[14]. Interestingly, these results are in line with our observations reported in this study, that in medium based culture protocols the neurons seem to be able to survive for up to 14 days, but show progressively reduced or abnormal firing properties (Fig. 5B). At this stage we have not performed a quantitative comparison of the firing properties between cells and cell types in acute and organotypic slices, which would exceed the scope of this study.

Taken together the data of our study provides strong evidence that human Cerebrospinal Fluid plays an indispensable role for the survival and physiological function of neurons. The main finding of this study is that human organotypic slices maintained in hCSF showed increased survival of neurons (Fig. 7) and intact network (Figs 2 and 3) and cellular function (Figs 4 and 5) compared to slices kept in media based culture methods. So far we have not directly assessed the survival of specific neuronal subpopulations (inhibitory vs. excitatory), but the occurrence of both spontaneous inhibitory and excitatory inputs suggests a substantial survival of both major cell types. It should be noted, that in this study we did not aim to detect or define the components in the used hCSF that could explain this effect. In the literature, there are numerous suggestions that various neuroactive molecules contained in hCSF could have modulatory effects on the neuronal behavior[27,28]. However, relatively little is known about the exact mechanism by which hCSF is modulating the neuronal activity and survival[29,30]. One mechanism, that could play a key role in the survival of neurons, might be the activity of the cells itself. It has been shown that inactivity of neurons can lead to apoptosis and increased cell death[19,31]. Indeed, several studies report that the presence of hCSF leads to increased activity of neurons due to an increase in the intrinsic excitability of cells, suggesting that the activity might play a role[29,32]. However, this might just be one possible mechanism. The CSF of humans is composed of a vast amount of compounds, ranging from ions, proteins, lipoproteins and metabolic products to neuropeptides and hormones[30,32]. It has been suggested that CSF even changes its composition and can act as mediator for signal transmission[33,34]. More strikingly, in states of disease, as for example during a viral or bacterial meningitis, the composition of CSF is changing dramatically and seems thereby directly influencing the function of the brain[35]. Taken together we propose that CSF of healthy individuals (or of normal pressure hydrocephalus patients) might represent a more physiological environment for human adult neurons providing these cells not only with nutrients and removing products of the neuronal metabolism, but also improving the electrophysiological function of the neuronal networks[33]. Further studies have to investigate more detailed which

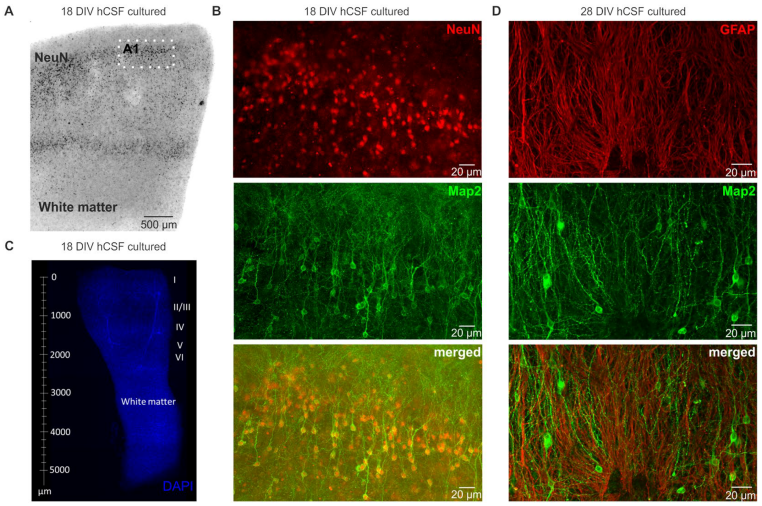


Figure 6. Morphology of human cortical slices in culture. (**A**) Example of a human organotypic slice after 18 DIV, note the dense labeling of NeuN positive cells in superficial layers and deep layers of the cortex. (A1) Inset of the superficial layers which are enlarged in (**B**) showing intact morphology of Layer 2/3 NeuN positive neurons with typical morphology of pyramidal cells revealed by Map2 staining and overlay. (**C**) Representative example of the size of a typical slice culture after 12 DIV (5 mm × 3 mm) with white matter and layers I–VI. **(D)** GFAP positive labeled astrocytes with Map2 positiv pyramidal cells cultured in hCSF after 28 DIV.

neuroprotective molecules within hCSF are responsible for the increased survival of neurons in human organotypic brain slices and if the activity is a crucial component of this process. Indeed, the fact that mature human neurons seem to depend on different components compared to rodent cells might help to discover specific neuroprotective factors, which might not be detectable in animal models. Once identified, these molecules might open up new therapeutic routes or explain failure of the predictions of animal models.

In this study, we show that human organotypic slice cultures maintained in human cerebrospinal fluid show an electrophysiological and morphological prolonged survival in comparison to slices cultured in defined culture media. This is reflected by improved single cell and network activity of these slices compared to traditional media based approaches and by an increase of the survival of adult human neurons within their original environment and with parts of the physiological network intact. Additionally, neurons of hCSF-treated organotypic slice cultures show a significantly higher number of neurons maintaining expression of the somatodendritic marker Map2 over an extended period of time (up to 18 DIV) in comparison to neurons of slices cultured in conventional media, indicating enhanced structural and morphological neuronal integrity and survival. Although the components of hCSF that are responsible for this effect are not identified yet and demand further examination, our results suggest that there might be striking differences in the components needed to culture human vs. rodent-derived CNS tissue. We propose that the human organotypic slice cultures provide a unique tool to study physiological and pathological mechanisms in mature human neurons. While clearly more work is needed to further investigate the cellular and network properties and the composition of the cells in human organotypic slices, this study provides a substantial step forward to bridge the gap between animal models and human physiology. In future studies 3D-reconstructive-confocal-microscopy based morphometric analysis (taking into account parameters such as length, number, and branches of processes, size of cell bodies and nuclei) of other cell types (e.g. astrocytes)[36] may prove as a valuable tool to study overall tissue and circuit integrity from a morphological angle and therefore also a possible difference in the activation of astrocytes (for review see ref.[37]), complementing and extending the presented network and single neuron electrophysiology data and analyses of neurons via immunocytochemistry and biocytin filling.

Human cortical slice cultures may serve as a platform enabling investigation of certain mechanisms and components of neuronal network plasticity, long-term effects of novel chemical compounds relevant to drug development, or studies involving viral mediated overexpression of proteins of interest.

Methods

Patients. Human neocortical organotypic slice cultures were prepared from access tissue obtained from patients undergoing resective epilepsy surgery. As described before, frequently removal of cortical tissue outside the epileptic focus is required in order to get access to the pathology[7]. For this study, we collected and included

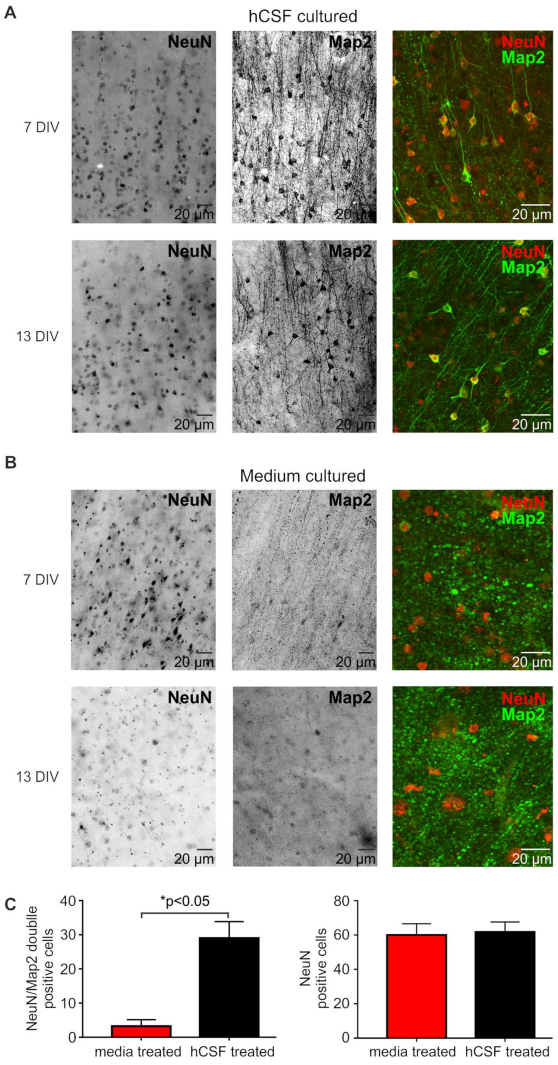


Figure 7. Morphology of human cortical neurons of slices cultured in hCSF vs. traditional media. Typical example of a NeuN and Map2 staining of human organotypic slices cultured in hCSF after 7 and 13 DIV (**A**) or traditional media after 7 and 13 DIV (**B**). Confocal images of the same slice showing co-labeling of NeuN and Map2 and intact morphology of the cells in slices cultured in hCSF (**A**) and loss of dendritic morphology in slices cultured in traditional media (**B**). Scale bars in all panels represent 20 µm. **(C)** Quantification of NeuN/Map2 double positive neurons in slices treated in traditional media compared to hCSF.

Patient	Age at surgery surgery	Gender	Resected brain area
1	38	W	parietal lobe
2	10	W	temporal lobe
3	31	M	temporal lobe
4	33	W	temporal lobe
5	24	M	temporal lobe
6	42	W	temporal lobe
7	17	M	temporal lobe

Table 2. Patients included in this study.

		unit	normal range
Appearance	Clear		
Erythrocyte	<1	thousand/µl	
Nucleated cells	<1	1/µl	0–5
Leukocytes	<1	1/µl	0–5
Polymorphnuclear cells	0	%	
Mononuclear cells	0	%	
Lactic acid	2.2	mmol/l	0–2.2
Glucose	108	mg/dl	
Proteins	47	mg/dl	0–45

Table 3. Basic chemical parameters of pooled CSF from NPH patients.

data of seven patients (Table 2). All patients were surgically treated for intractable epilepsy, in one patient the histology revealed a low grade tumor (Gangliogliom WHO Grad I).

Preparation of slices from patients. Approval of the ethics committee of the University of Tübingen as well as written informed consent was obtained from all patients, allowing spare tissue from resective surgery to be included in our study (# 338/2016A). All experiments and methods were performed in accordance with the relevant guidelines and regulations. Tissue preparation was performed according to published protocols[7]. Cortex was carefully microdissected and resected with only minimal use of bipolar forceps to ensure tissue integrity, transferred into ice-cold artificial (a)CSF (in mM: 110 choline chloride, 26 $NaHCO_3$, 10 D-glucose, 11.6 Na-ascorbate, 7 $MgCl_2$, 3.1 Na-pyruvate, 2.5 KCl, 1.25 NaH_2PO_4, und 0.5 $CaCl_2$) equilibrated with carbogene (95% O_2, 5% CO_2) and immediately transported to the laboratory. Tissue was kept submerged in cool and carbogenated aCSF at all times. After removal of the pia, tissue chunks were trimmed perpendicular to the cortical surface and 250–350 µm thick acute slices were prepared using a Microm HM 650 V vibratome (Thermo Fisher Scientific Inc).

Human organotypic slice cultures. After the cortical tissue was sliced as described above slices were cut into several evenly sized pieces (~1.0 cm × 1.0 cm, Fig. 1A). Subsequently, the slices were transferred onto culture membranes (uncoated 30 mm Millicell-CM tissue culture inserts with 0.4 µm pores, Millipore) and kept in six–well culture dishes (BD Biosciences). The plates were stored in an incubator (ThermoScientific) at 37 °C, 5% CO_2 and 100% humidity. For electrophysiological measurements slice cultures were transferred into the recording chamber of a patch clamp rig. After finishing patch clamp- or extracellular recordings, slices were fixed in 4% PFA and processed for immunocytochemistry, as detailed in the Immunocytochemistry section.

Traditional culture media. Human organotypic slice cultures were cultured in organotypic slice culture medium (OSCM) without serum as described by Eugène and colleagues[17] or BrainPhys medium according to Bardy and colleagues[27]. OSCM medium was produced by adding select components (see Eugene *et al.* for details) to commercially available DMEM/F12 and BME media. BrainPhys is a serum-free neuronal medium with adjusted concentrations of inorganic salts, neuroactive amino acids, and energetic substrates (see Bardy *et al.* 2015 for details). The media was originally developed to improve the electrical and synaptic activity of mature human neurons. Both media were found to exhibit comparable effects on human organotypic slices in our experiments and respective data were pooled and will be referred to as traditional media.

CSF collection. Human cerebrospinal fluid (hCSF) was collected from patients with normal pressure hydrocephalus (NPH). We received and pooled hCSF of several patients with NPH who needed to undergo a lumbar puncture as part of diagnostic or therapeutic procedures (up to 40 ml per patient). Approval of the ethics committee of the University of Tübingen as well as written informed consent was obtained from all patients. It is well established and known from daily clinical practice that hCSF of NPH patients exhibits physiological/normal hCSF chemistry values (lactate, glucose, cell count, protein levels – see Table 3) undistinguishable from the ones of healthy individuals[32]. The CSF was centrifuged at 4000 rpm at 4 °C for 10 minutes and the supernatant was collected and stored at −80 °C within one hour after lumbar puncture.

Extracellular Multi-Unit recording. For extracellular and intracellular recordings slices were transferred into a recording chamber and continuously superfused with artificial CSF (aCSF) containing (in mM) 118 NaCl, 3 KCl, 1.5 $CaCl_2$, 1 $MgCl_2$, 25 $NaHCO_3$, 30 D-glucose, and equilibrated with carbogen (95% NaH_2PO_4, and 30 O2–5% CO_2, pH 7.4) in a recycling system. Temperature was maintained at 30 ± 1 °C. The signal contained multiunit action potential (AP) activity. Extracellular signals were amplified 10,000-fold and filtered between 0.25 and 1.5 kHz. To facilitate detection of network-bursts, this signal was rectified and integrated by an electronic integrator with a time constant of 50–100 ms. We used an extracellular amplifier Modell 1700 (Am-Systems) or NPI (Model Ext 10–2 F) and an integrator from NPI (Model INR-011).

Whole-cell patch clamp recordings. Slices were positioned in a submerged-type recording chamber (Scientifica, United Kingdom/Warner apparatus), continuously superfused with aCSF and visualized with a BX61WI Microscope (Olympus) or a Leica stereomicroscope. Recordings were performed using recording electrodes with a resistance of 3–5 MΩ and filled with a whole-cell patch-clamp pipette solution containing the following components (in mM): 140 K-gluconic acid, 1 $CaCl_2$*$6H_2O$, 10 EGTA, 2 $MgCl_2$*$6H_2O$, 4 Na_2ATP, and 10 HEPES, pH 7.2. The intracellular pipette solution contained biocytin (5 mg/ml) to allow for posthoc identification of the location and morphology of recorded neurons. Whole cell current-clamp recordings were obtained from cortical neurons using the visual-patch or blind patch technique. Whole-cell patch-clamp recordings were obtained with a sampling rate of 10 kHz and a low-pass filter setting of 2 kHz. Recordings were performed with unpolished patch electrodes manufactured from borosilicate glass pipettes with filament (Science products). Patch-clamp experiments were performed with a patch-clamp amplifier (Multiclamp 200B) or a NPI Bridge Amplifier (Model BA-01X), a digitizing interface (Digidata 1440 A or 1550 A Digidata), and pClamp 10 software (Molecular Devices). The junction potential was calculated and subtracted offline to correct the membrane potential in current clamp mode. After recording, the slices were placed in neutral buffered 4% PFA solution at 4 °C overnight for fixation followed by three rinses in PBS and by subsequent immunocytochemical staining procedures.

Immunocytochemistry and image collection. For immunocytochemistry (ICC) slices were incubated for 60 minutes in goat block (PBS, 0.2% triton X-100, 5% normal goat serum) before primary antibodies were added in respective dilutions. Due to the thickness of the slices incubation in primary antibodies was performed overnight at 4 °C temperature and for 30 minutes at room temperature on the following morning. Slices were rinsed four times in PBS supplemented with 0.1% Triton X-100 and then incubated in Alexa-fluorophore-conjugated secondary antibodies in goat block (PBS, 0.2% triton X-100, 1% normal goat serum) for 1 hour and 15 minutes at room temperature. After four PBS rinses (2x in PBS supplemented with 0.1% Triton X-100 and 2x in PBS) the slices were stained with DAPI (1:5000 in PBS for 2–5 minutes). After four final rinses (3x PBS, 1x Ampuwa water) the slices were mounted in Fluoromount G (SouthernBiotech) on glass slides. Primary and secondary antibodies were used at the the following dilutions: mouse anti-NeuN IgG (1:100, Merck, ABN90), chicken anti-Map2 (1:500, Abcam, ab5392), rabbit anti-GFAP (1:250, Agilent, Z0334), goat anti-mouse IgG Alexa 568 (1:500, life technologies, A-11004), goat anti-rabbit IgG Alexa 568 (1:500, life technologies, A-11011) and goat anti-chicken Alexa 488 (1:500, life technologies, A-11039). Expression of tissue-specific markers was evaluated using a conventional fluorescenece microscope (Zeiss Imager.Z1) and laser confocal scanning microscopic analysis (Zeiss LSM 510 Laser Module, Zeiss Axiovert 200 M). Images were processed with Photoshop CS (Adobe Systems) and CorelDRAW (Corel Corporation).

References

1. Kriks, S. *et al.* Dopamine neurons derived from human ES cells efficiently engraft in animal models of Parkinson's disease. *Nature* **480**, 547–551, https://doi.org/10.1038/nature10648 (2011).
2. Zhang, Y. *et al.* Rapid single-step induction of functional neurons from human pluripotent stem cells. *Neuron* **78**, 785–798, https://doi.org/10.1016/j.neuron.2013.05.029 (2013).
3. Lancaster, M. A. *et al.* Cerebral organoids model human brain development and microcephaly. *Nature* **501**, 373−+, https://doi.org/10.1038/nature12517 (2013).
4. D'Esposito, M., Postle, B. R. & Rypma, B. Prefrontal cortical contributions to working memory: evidence from event-related fMRI studies. *Experimental Brain Research* **133**, 3–11, https://doi.org/10.1007/s002210000395 (2000).
5. Clark, R. E. & Squire, L. R. Classical conditioning and brain systems: the role of awareness. *Science* **280**, 77–81 (1998).
6. Molnar, G. *et al.* Human pyramidal to interneuron synapses are mediated by multi-vesicular release and multiple docked vesicles. *Elife* **5**, https://doi.org/10.7554/eLife.18167 (2016).
7. Verhoog, M. B. *et al.* Mechanisms underlying the rules for associative plasticity at adult human neocortical synapses. *J Neurosci* **33**, 17197–17208, https://doi.org/10.1523/JNEUROSCI.3158-13.2013 (2013).
8. Beck, H., Goussakov, I. V., Lie, A., Helmstaedter, C. & Elger, C. E. Synaptic plasticity in the human dentate gyrus. *J Neurosci* **20**, 7080–7086 (2000).
9. Testa-Silva, G. *et al.* High bandwidth synaptic communication and frequency tracking in human neocortex. *PLoS Biol* **12**, e1002007, https://doi.org/10.1371/journal.pbio.1002007 (2014).
10. Sareen, D. *et al.* Targeting RNA Foci in iPSC-Derived Motor Neurons from ALS Patients with a C9ORF72 Repeat Expansion. *Science Translational Medicine* **5**, doi:ARTN208ra14910.1126/scitranslmed.3007529 (2013).
11. Liu, Y. *et al.* Dravet syndrome patient-derived neurons suggest a novel epilepsy mechanism. *Ann Neurol* **74**, 128–139, https://doi.org/10.1002/ana.23897 (2013).
12. Humpel, C. Organotypic brain slice cultures: A review. *Neuroscience* **305**, 86–98, https://doi.org/10.1016/j.neuroscience.2015.07.086 (2015).
13. Dragunow, M. The adult human brain in preclinical drug development. *Nat Rev Drug Discov* **7**, 659–666, https://doi.org/10.1038/nrd2617 (2008).
14. Andersson, M. *et al.* Optogenetic control of human neurons in organotypic brain cultures. *Sci Rep* **6**, 24818, https://doi.org/10.1038/srep24818 (2016).

15. Verwer, R. W. H. *et al.* Cells in human postmortem brain tissue slices remain alive for several weeks in culture. *Faseb Journal* **16**, 54–60, https://doi.org/10.1096/fj.01-0504com (2002).
16. Verwer, R. W. H. *et al.* Altered Loyalties of Neuronal Markers in Cultured Slices of Resected Human Brain Tissue. *Brain Pathology* **26**, 523–532, https://doi.org/10.1111/bpa.12330 (2016).
17. Eugene, E. *et al.* An organotypic brain slice preparation from adult patients with temporal lobe epilepsy. *J Neurosci Methods* **235**, 234–244, https://doi.org/10.1016/j.jneumeth.2014.07.009 (2014).
18. Daviaud, N., Garbayo, E., Schiller, P. C., Perez-Pinzon, M. & Montero-Menei, C. N. Organotypic cultures as tools for optimizing central nervous system cell therapies. *Exp Neurol* **248**, 429–440, https://doi.org/10.1016/j.expneurol.2013.07.012 (2013).
19. Koch, H. *et al.* Prostaglandin E2-induced synaptic plasticity in neocortical networks of organotypic slice cultures. *J Neurosci* **30**, 11678–11687, https://doi.org/10.1523/JNEUROSCI.4665-09.2010 (2010).
20. Johansson, S., Radesater, A. C., Cowburn, R. F., Thyberg, J. & Luthman, J. Modelling of amyloid beta-peptide induced lesions using roller-drum incubation of hippocampal slice cultures from neonatal rats. *Exp Brain Res* **168**, 11–24, https://doi.org/10.1007/s00221-005-0069-z (2006).
21. Novotny, R. *et al.* Conversion of Synthetic Abeta to *In Vivo* Active Seeds and Amyloid Plaque Formation in a Hippocampal Slice Culture Model. *J Neurosci* **36**, 5084–5093, https://doi.org/10.1523/JNEUROSCI.0258-16.2016 (2016).
22. Caeser, M. & Aertsen, A. Morphological organization of rat hippocampal slice cultures. *J Comp Neurol* **307**, 87–106, https://doi.org/10.1002/cne.903070109 (1991).
23. Moser, K. V., Schmidt-Kastner, R., Hinterhuber, H. & Humpel, C. Brain capillaries and cholinergic neurons persist in organotypic brain slices in the absence of blood flow. *Eur J Neurosci* **18**, 85–94 (2003).
24. De Simoni, A., Griesinger, C. B. & Edwards, F. A. Development of rat CA1 neurones in acute versus organotypic slices: role of experience in synaptic morphology and activity. *J Physiol* **550**, 135–147, https://doi.org/10.1113/jphysiol.2003.039099 (2003).
25. Busskamp, V. *et al.* Rapid neurogenesis through transcriptional activation in human stem cells. *Molecular systems biology* **10**, 760, https://doi.org/10.15252/msb.20145508 (2014).
26. Shi, Y., Kirwan, P. & Livesey, F. J. Directed differentiation of human pluripotent stem cells to cerebral cortex neurons and neural networks. *Nat Protoc* **7**, 1836–1846, https://doi.org/10.1038/nprot.2012.116 (2012).
27. Bardy, C. *et al.* Neuronal medium that supports basic synaptic functions and activity of human neurons *in vitro*. *Proceedings of the National Academy of Sciences of the United States of America*, https://doi.org/10.1073/pnas.1504393112 (2015).
28. Veening, J. G. & Barendregt, H. P. The regulation of brain states by neuroactive substances distributed via the cerebrospinal fluid; a review. *Cerebrospinal Fluid Res* **7**, 1, https://doi.org/10.1186/1743-8454-7-1 (2010).
29. Perez-Alcazar, M. *et al.* Human Cerebrospinal Fluid Promotes Neuronal Viability and Activity of Hippocampal Neuronal Circuits *In Vitro*. *Front Cell Neurosci* **10**, 54, https://doi.org/10.3389/fncel.2016.00054 (2016).
30. Post, R. M., Rubinow, D. R., Kling, M. A., Berrettini, W. & Gold, P. W. Neuroactive substances in cerebrospinal fluid. Normal and pathological regulatory mechanisms. *Ann N Y Acad Sci* **531**, 15–28 (1988).
31. Heck, N. *et al.* Activity-dependent regulation of neuronal apoptosis in neonatal mouse cerebral cortex. *Cereb Cortex* **18**, 1335–1349, https://doi.org/10.1093/cercor/bhm165 (2008).
32. Bjorefeldt, A. *et al.* Human cerebrospinal fluid increases the excitability of pyramidal neurons in the *in vitro* brain slice. *J Physiol* **593**, 231–243, https://doi.org/10.1113/jphysiol.2014.284711 (2015).
33. Skipor, J. & Thiery, J. C. The choroid plexus–cerebrospinal fluid system: undervaluated pathway of neuroendocrine signaling into the brain. *Acta Neurobiol Exp (Wars)* **68**, 414–428 (2008).
34. Tricoire, H., Locatelli, A., Chemineau, P. & Malpaux, B. Melatonin enters the cerebrospinal fluid through the pineal recess. *Endocrinology* **143**, 84–90, https://doi.org/10.1210/en.143.1.84 (2002).
35. Otto, F. *et al.* Cerebrospinal fluid of brain trauma patients inhibits *in vitro* neuronal network function via NMDA receptors. *Ann Neurol* **66**, 546–555, https://doi.org/10.1002/ana.21808 (2009).
36. Bagheri, M., Rezakhani, A., Roghani, M., Joghataei, M. T. & Mohseni, S. Protocol for Three-dimensional Confocal Morphometric Analysis of Astrocytes. *J Vis Exp*, e53113, https://doi.org/10.3791/53113 (2015).
37. Pekny, M. & Pekna, M. Astrocyte reactivity and reactive astrogliosis: costs and benefits. *Physiol Rev* **94**, 1077–1098, https://doi.org/10.1152/physrev.00041.2013 (2014).

Acknowledgements

The authors thank all patients for participating in this study. We thank Evelyn Dubois and Elke Stransky for their assistance with collecting hCSF samples. H.K. was in part supported by the Deutsche Forschungsgemeinschaft (DFG-KO-4877/2-1) and from the intramural research funding program of the Faculty of Medicine Tübingen (Fortüne 2193-0-0). N.S. was in part supported from the intramural research funding program of the Faculty of Medicine Tübingen (Fortüne 2381-0-0).

Author Contributions

J.H. operated the patients and T.W. handled tissue directly after surgery. N.S., H.K., H.P.A., N.D. and E.A. received the tissue and prepared slices. H.K., U.H. and T.W. conducted the slice physiology study. H.L. provided institutional support. N.S., F.B. and H.S. conducted immunohistochemical stainings. N.S., U.H., T.W. and H.K. analyzed data and wrote the paper.

Additional Information

Competing Interests: The authors declare that they have no competing interests.

Publisher's note: Springer Nature remains neutral with regard to jurisdictional claims in published maps and institutional affiliations.

Open Access This article is licensed under a Creative Commons Attribution 4.0 International License, which permits use, sharing, adaptation, distribution and reproduction in any medium or format, as long as you give appropriate credit to the original author(s) and the source, provide a link to the Creative Commons license, and indicate if changes were made. The images or other third party material in this article are included in the article's Creative Commons license, unless indicated otherwise in a credit line to the material. If material is not included in the article's Creative Commons license and your intended use is not permitted by statutory regulation or exceeds the permitted use, you will need to obtain permission directly from the copyright holder. To view a copy of this license, visit http://creativecommons.org/licenses/by/4.0/.

© The Author(s) 2017

2.5 Chapter 5: Detailed characterization and genetic manipulation of long-term adult human brain slice cultures

EBERHARD KARLS
UNIVERSITÄT
TÜBINGEN

Medizinische Fakultät

Declaration of contributions:

Herewith I, Niklas Schwarz declare, that I have contributed to the mayor part of the following publication:

Schwarz N, Uysal B, Welzer M, Bahr J, Layer N, Löffler H, Stanaitis K, PA H, Weber YG, Hedrich UBS, Honegger JB, Skodras A, Becker AJ, Wuttke TV, Koch H, Long-term adult human brain slice cultures as a model system to study human CNS circuitry and disease. Elife. 2019 Sep 9;8. pii: e48417. doi: 10.7554/eLife.48417.

The authors contributed to the publications as indicated in the following table (indicated in %):

Contribution	Niklas Schwarz	Betül Uysal	Marc Welzer	Jacqueline C Bahr	Nikolas Layer	Heidi Löffler	Kornelijus Stanaitis	Harshad P.A.
Research concept	50%							
Project administration	45%							
Funding acquisition	20%							
Selection of methods	60%							
Recruitment of patients	20%							
Data acquisition	55%	5%	5%	3%	5%	3%	3%	3%
Data analysis	58%	3%	3%	3%	3%			
Visualization	70%							
Interpretation of results	60%		3%					
Preparation of Manuscript	65%							

Contribution	Yvonne G Weber	Ulrike BS Hedrich	Jürgen B Honegger	Angelos Skodras	Albert J Becker	Thomas V Wuttke	Henner Koch
Research concept						15%	35%
Project administration						15%	40%
Funding acquisition	20%	20%				20%	20%
Selection of methods							40%
Recruitment of patients	20%		25%			20%	15%
Data acquisition				3%			15%
Data analysis							30%
Visualization							30%
Interpretation of results						7%	30%
Preparation of Manuscript		3%			3%	9%	20%

EBERHARD KARLS
UNIVERSITÄT
TÜBINGEN

Medizinische Fakultät

[redacted]

Signature of the doctoral candidate:

As supervisor, I agree with the declarations by the candidate:

As corresponding author, agree with the declarations by the candidate:

As co-authors, we agree to the declarations above:

[redacted]

[Betül Uysal] [Marc Welzer] [Jacqueline C Bahr]

[redacted]

[Nikolas Layer] [Heidi Löffler] [Kornelijus Stanaitis]

[redacted]

[Harshad P.A.] [Yvonne G Weber] [Ulrike BS Hedrich]

[redacted]

[Jürgen B Honegger] [Angelos Skodras] [Albert Becker]

Institut für Neu... Bonn
der Universität Bonn
Venusberg-Campus 1
53127 Bonn

[redacted]

[Thomas V Wuttke] [Henner Koch]

eLIFE elifesciences.org

TOOLS AND RESOURCES

Long-term adult human brain slice cultures as a model system to study human CNS circuitry and disease

Niklas Schwarz[1], Betül Uysal[1], Marc Welzer[2,3], Jacqueline C Bahr[1], Nikolas Layer[1], Heidi Löffler[1], Kornelijus Stanaitis[1], Harshad PA[1], Yvonne G Weber[1,4], Ulrike BS Hedrich[1], Jürgen B Honegger[4], Angelos Skodras[2,3], Albert J Becker[5], Thomas V Wuttke[1,4†*], Henner Koch[1†*]

[1]Department of Neurology and Epileptology, Hertie-Institute for Clinical Brain Research, University of Tübingen, Tübingen, Germany; [2]Department of Cellular Neurology, Hertie-Institute for Clinical Brain Research, University of Tübingen, Tübingen, Germany; [3]German Center for Neurodegenerative Diseases (DZNE), Tübingen, Germany; [4]Department of Neurosurgery, University of Tübingen, Tübingen, Germany; [5]Department of Neuropathology, Section for Translational Epilepsy Research, University Bonn Medical Center, Bonn, Germany

Abstract Most of our knowledge on human CNS circuitry and related disorders originates from model organisms. How well such data translate to the human CNS remains largely to be determined. Human brain slice cultures derived from neurosurgical resections may offer novel avenues to approach this translational gap. We now demonstrate robust preservation of the complex neuronal cytoarchitecture and electrophysiological properties of human pyramidal neurons in long-term brain slice cultures. Further experiments delineate the optimal conditions for efficient viral transduction of cultures, enabling 'high throughput' fluorescence-mediated 3D reconstruction of genetically targeted neurons at comparable quality to state-of-the-art biocytin fillings, and demonstrate feasibility of long term live cell imaging of human cells *in vitro*. This model system has implications toward a broad spectrum of translational studies, regarding the validation of data obtained in non-human model systems, for therapeutic screening and genetic dissection of human CNS circuitry.

DOI: https://doi.org/10.7554/eLife.48417.001

***For correspondence:** Thomas.Wuttke@med.uni-tuebingen.de (TVW); henner.koch@uni-tuebingen.de (HK)

†These authors contributed equally to this work

Competing interests: The authors declare that no competing interests exist.

Funding: See page 22

Received: 13 May 2019
Accepted: 23 August 2019
Published: 09 September 2019

Reviewing editor: Inna Slutsky, Tel Aviv University, Israel

© Copyright Schwarz et al. This article is distributed under the terms of the Creative Commons Attribution License, which permits unrestricted use and redistribution provided that the original author and source are credited.

Introduction

The human brain is composed of an intricate network of diverse cell types with complex interactions and connections (***DeFelipe et al., 2002***; ***Somogyi et al., 1998***). The microstructure within the brain was already appreciated in the early pioneering work by Santiago Ramón y Cajal and has been further investigated in the last decades in post mortem human brain samples (***Elston and DeFelipe, 2002***; ***Elston et al., 2001***) and in numerous animal models (***Branco and Häusser, 2011***; ***Somogyi et al., 1998***). Neurons function as a core component of the microstructure of CNS circuits. The computation and integration of signals by these cells and the output is believed to underlie higher brain functions such as cognition and learning. Two broad classes of neurons, glutamatergic neurons (pyramidal neurons, 80%) and GABAergic interneurons (20%), populate the human neocortex. Cortical pyramidal neurons can be further categorized into four classes according to their output connectivity. Intratelencephalic pyramidal neurons are distributed throughout cortical layers 2–6 and build associative connections with other cortical areas (within one hemisphere or across the corpus callosum) or with the striatum. Pyramidal tract neurons reside in layer five and project their axons to

the brain stem and spinal cord. Corticothalamic neurons establish axonal output connectivity from layer six to area related thalamic nuclei. The fourth category comprises layer four short-axon intratelencephalic neurons, which locally relay thalamic input (**Shepherd and Rowe, 2017**). With the exception of layer four intratelencephalic neurons in sensory areas (spiny stellate cells) pyramidal neurons typically show a long apical dendrite. Overall morphology and complexity of apical and basal dendrites can substantially differ between pyramidal neurons and throughout layers. Furthermore, work by colleagues in the field provides direct evidence that there also exist marked species-specific differences of structural features and functional properties of pyramidal neurons (**Mohan et al., 2015**) as well as regarding basic cortical properties (**Eyal et al., 2016**), cell types (**Boldog et al., 2018**; **Wang et al., 2015**), morphology (**Elston et al., 2001**; **Mohan et al., 2015**), functional divergence (**Napoli and Obeid, 2016**) and plasticity mechanisms (**Verhoog et al., 2013**). Such differences underscore the challenges of modeling human disease by cellular and animal models and call for the development of new translational approaches based on human nervous tissue. Spare human CNS tissue obtained from neurosurgical procedures has proven valuable throughout the years, for example for electrophysiological studies in acute slice preparations (**Bernard et al., 2004**; **Kalmbach et al., 2018**; **Kerkhofs et al., 2017**). Unlike with rodent CNS tissue, past attempts by different groups to establish organotypic slice cultures of human CNS tissue had yet repeatedly faced pronounced limitations regarding viability and integrity (**O'Connor et al., 1997**; **Verwer et al., 2002**). However, recent efforts challenged these limitations and provided promising proof-of-concept data on electrophysiological function (**Eugène et al., 2014**) and optogenetic targeting (**Andersson et al., 2016**) in human brain slice cultures. Subsequent studies established successful neuronal labeling, optical manipulation and calcium imaging by virus-driven rapid expression of respective probes in short term cultures of several days (**Ting et al., 2018**). Recent parallel work by us in contrast focused on optimization of culture conditions and demonstrated that neuronal viability and network activity of human brain slice cultures can be significantly extended to up to three weeks under specified conditions (**Schwarz et al., 2017**). Proper function of complex CNS networks, however, critically depends on morphological and functional integrity of neurons structurally underlying circuitry. Neurons need to extend their dendritic processes to correct locations in order to receive appropriate synaptic inputs and relay them to adequate target structures. Specific functional properties are required to compute and integrate information in a meaningful way. Whether this level of morphological complexity along with inherent electrophysiological characteristics is maintained in human brain slice cultures over a period of two to three weeks or whether dendritic arbors rarefy and functional features dissipate is not known and will be investigated in this work.

In the last decades, important molecular genetic achievements and subsequent combined application of tools such as the Cre-lox system (**Song and Palmiter, 2018**), optogenetics (**Kim et al., 2017**; **Madisen et al., 2012**) and virus-mediated gene targeting/knockout/delivery (**Hendrie and Russell, 2005**; **Howard et al., 2008**; **Rao and Craig, 1997**) enabled an increasingly better understanding of how distinct cell types assemble and form functional circuitry in the rodent brain. Adapting such strategies to human brain slice cultures reflecting an environment as close as possible to the actual human brain will open new roads toward dissection of human CNS circuitry and could potentially provide an increasingly more accurate understanding of how human CNS disease develops.

Toward these aims, we now performed detailed cellular analyses of the somatodendritic and synaptic spine compartments and of characteristic electrophysiological properties of single neurons throughout the course of culturing. These features form the basis of intact network function but whether they are maintained in cortical slice cultures remained still elusive. Further experiments established the conditions for efficient viral transduction with a focus on glutamatergic pyramidal neurons within human brain slice cultures.

We find robust structural and electrophysiological stability of human pyramidal neurons and amenability of human brain slice cultures to efficient genetic manipulation, as revealed by successful transduction by GFP-encoding adeno-associated viral vectors (AAV-vectors). GFP fluorescence levels were sufficient for both post-hoc confocal microscopy- and two-photon live cell imaging-based assessment of neuronal morphology including spines emanating from the dendritic arbors. We demonstrate GFP-based cellular 3D morphological analysis with increased efficiency and compatible quality in comparison to classic intracellular biocytin fillings.

The presented data indicate feasibility of utilizing human brain slice cultures as a model system as close as possible to the actual human brain and apply them toward studies of human CNS circuitry, disease and therapeutic screening, thereby having the potential to close the translational gap to non-human model systems.

Results

Electrophysiological properties of pyramidal neurons in human brain slice cultures versus acute slices

Besides morphological and structural features intact physiology of neurons constitutes one of the hallmarks of healthy neural tissue. In a first set of experiments we determined the stability of the electrophysiological properties of pyramidal neurons performing whole cell patch clamp recordings (n = 45) from cells in acute (n = 17) or cultured (n = 28) slices (2–14 DIV). The cells recorded from cultured slices were further subdivided into early (2-3 DIV, n = 8) and late in culture (7–14 DIV, n = 20) for statistical group analysis (***Figure 1E***). Recordings of pyramidal neurons showed a typical regular spiking pattern in acute and cultured slices (***Figure 1B,C***), as described in previous studies investigating human pyramidal neurons in acute slices (***Verhoog et al., 2013***). The firing frequency in response to current injections was not significantly different between the cells recorded on the day of the surgery (acute slices = 0 DIV, with a peak firing rate of 50.84 ± 9.90 Hz in response to a current injection of 200 pA) and the cells in cultures between 2 and 3 DIV (peak firing rate: 59.4 ± 12.46) and 7–14 DIV (peak firing rate of 55.79 ± 9.34 Hz), (Kruskal-Wallis test, p=0.74, ***Figure 1C***). Similarly, mean values of AP half width, sag potential amplitude and input resistance did not differ between the tested groups (0 DIV, 2–3 DIV and 7–14 DIV, Kruskal-Wallis test, p>0.05, ***Figure 1E***). This was also reflected by no significant linear regression correlation of these parameters versus the DIV (***Figure 1D***).

For mean values of resting membrane potential we found a small significant difference (Kruskal-Wallis test, p<0.05) for the acutely measured cells (0 DIV, −77.94 ± 1.5 mV) in comparison to early cultured (2–3 DIV, −72.38 ± 0.96 mV, Dunn's multiple comparisons test, *p=0.02) and late in culture cells (7-14 DIV, 71.95 ± 1.43, Dunn's multiple comparisons test, *p=0.01). However, there was no significant difference between early (2–3 DIV) and late in culture (7–14 DIV) measured cells (Dunn's multiple comparisons test, p>0.99). This was also reflected by no significant linear regression correlation of the resting potential versus the DIV for cells of all three groups (***Figure 1D***). In summary, increasing time in culture does not impact the majority of analyzed intrinsic electrophysiological characteristics of pyramidal neurons, except for the membrane resting potential which slightly changed to more depolarized values within the first 2–3 days in culture and then stayed stable over the remaining time.

Maintenance of the glutamatergic neuron population in human brain slice cultures over time

In a further set of experiments, we determined the degree of survival of the excitatory neuronal population in human brain slice cultures over time. Satb2 is a transcription factor that is expressed exclusively in excitatory neurons in adult mouse and human cortex (***Britanova et al., 2008***; ***Huang et al., 2013***; ***Hodge et al., 2019***; http://celltypes.brain-map.org/rnaseq). Taking advantage of Map2, a neuron-specific cytoskeletal protein, in combination with Satb2 (***Figure 1—figure supplement 1A***) we found no significant changes of the absolute numbers of double-positive neurons in slice cultures between 0 DIV (3 slices), 9 DIV (3 slices) and 14 DIV (2 slices) (Dunn's multiple comparisons test, ***Figure 1—figure supplement 1B***). Double positive neurons were counted in small z-stack projections of confocal images of four to six different regions (each area 290 µm x 290 µm in size) in layers 2/3 of each slice: the absolute number of Map2 and Satb2 double positive neurons per 100 µm × 100 µm (10000 μm^2) was on average 8.57 ± 0.60 in acute slices (18 analyzed areas), 10.14 ± 3.52 (16 analyzed areas) in slices analyzed at 9 DIV and 9.49 ± 1.77 (9 analyzed areas) in slices obtained at 14 DIV (***Figure 1—figure supplement 1B***). To investigate whether the ratio of glutamatergic to GABAergic neurons remained stable we calculated the ratio of Satb2 and Map2 double-positive neurons to all Map2 positive neurons. Ratios were 0.72 ± 0.02 in acute slices, 0.59 ± 0.09 at 9 DIV and 0.65 ± 0.11 at 14 DIV and revealed a discretely lower, albeit statistically significant, ratio at 9 DIV compared to 0

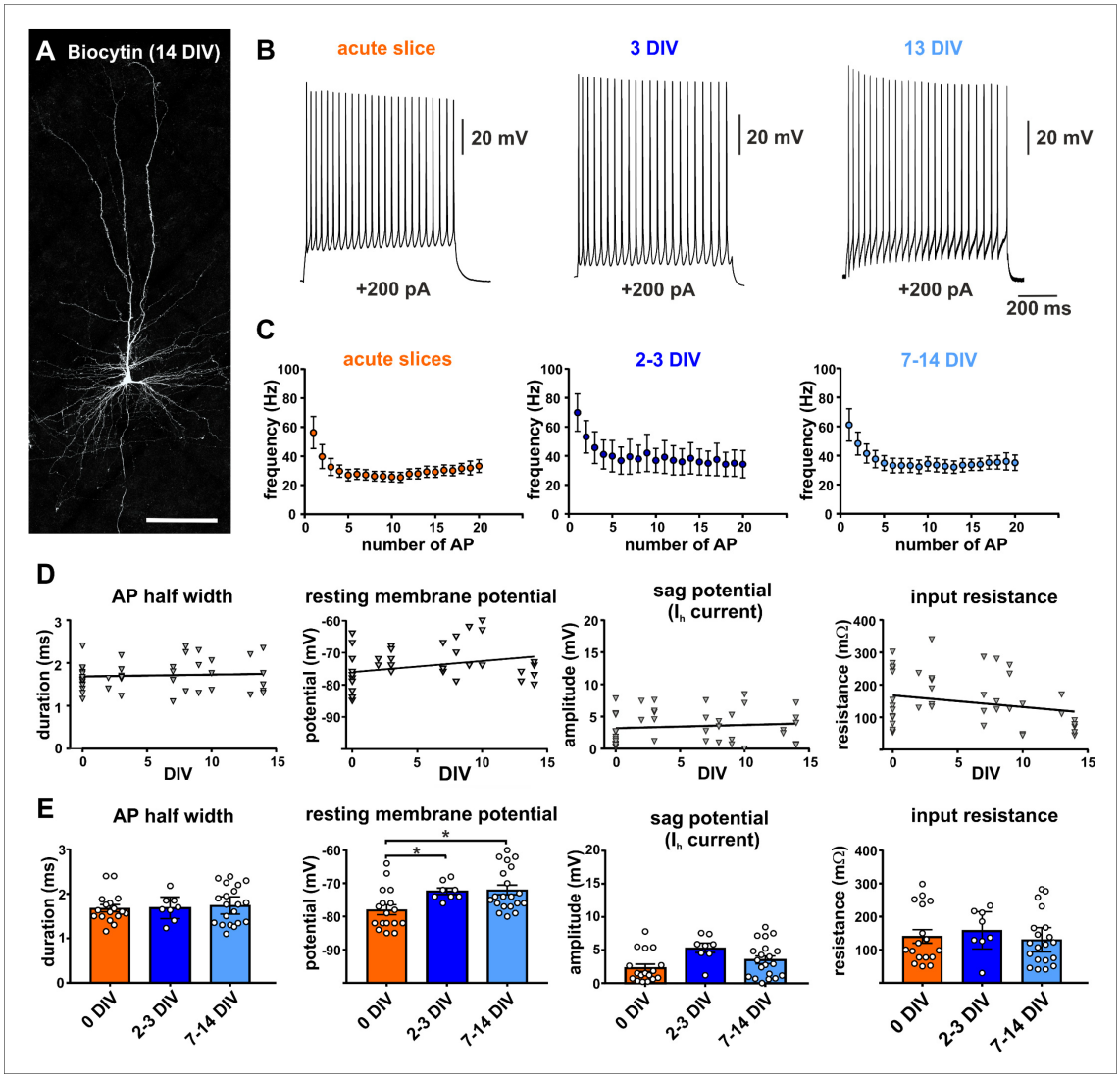


Figure 1. Electrophysiology of adult human pyramidal neurons. (**A**) Example of biocytin filled pyramidal neuron (14 DIV) after streptavidin-Cy3 counterstaining, scale bar 150 µm. (**B**) Typical regular spiking pattern of human pyramidal neurons (acute slice, 3 DIV and 13 DIV) in response to +200 pA positive current injection. (**C**) Neurons recorded in acute slices (within 12 hr after surgery) and in brain slice cultures (2–3 DIV and 7–14 DIV) showed similar action potential firing frequencies and typical spike frequency adaptation upon 200 pA current injection. (**D, E**) Quantification of (from left to right) the AP half width, resting membrane potential, sag potential amplitude and input resistance revealed no significant correlation between these values and the days *in vitro* (DIV), (**E**) except membrane resting potential which slightly changed to more depolarized values within the first 2–3 days in culture and then stayed stable over the remaining time.

DOI: https://doi.org/10.7554/eLife.48417.002

The following figure supplements are available for figure 1:

Figure supplement 1. Satb2 positive neurons in human brain slice cultures.

DOI: https://doi.org/10.7554/eLife.48417.004

Figure 1 continued on next page

Figure 1 continued

Figure supplement 2. Stability of gross structural features of cortical slices between surgeries and over time in culture.
DOI: https://doi.org/10.7554/eLife.48417.003

DIV, but no difference between 0 DIV and 14 DIV or 9 DIV compared to 14 DIV (Dunn's multiple comparisons test; ***Figure 1—figure supplement 1B***).

These data indicate robust survival of excitatory and inhibitory neurons with a sustained ratio of excitatory to inhibitory neurons throughout the culturing time.

Viral transduction of human brain slice cultures

To investigate whether neurons in human brain slice cultures can be genetically targeted with viral vectors and whether such strategies could render morphological analysis of human neurons more efficient than approaches solely relying on classic biocytin fillings, we used retrograde adeno-associated virus (AAVrg) encoding GFP under the human synapsin promoter to specifically transduce neurons. The slices were injected with the virus at 3–5 DIV using a picospritzer, cells were then recorded and imaged at 8–16 DIV (n = 20 slices). We found robust virus transduction in all injected slices with variable expression in distinct types of neurons throughout all cortical layers (***Figure 2***). The GFP expression was clearly present in somata, dendrites including spines and axons of transduced neurons (***Figure 2A1 and A2***).

GFP expression levels were found to be very robust, suggesting that several types of analyses including quantification of whole cell morphology, spine density, spine head diameter and spine length (see below) could be achieved based on GFP fluorescence. Furthermore, viral transduction of human neurons will enable direct investigation of the impact of disease causing mutations on neuronal function and morphology as well as on neuronal networks and will enable studies of human CNS circuitry involving optogenetic and chemogenetic tools.

Dendritic morphology of pyramidal neurons *in vitro*

Morphologically intact neurons are the basic framework of healthy neural brain tissue and degradation of dendritic arbors may even occur before an impairment of electrophysiological properties. Therefore, we set out to determine whether neurons are subject to morphological changes throughout their time in culture and performed 3D reconstructions of biocytin filled neurons at different time points between 0 DIV and 14 DIV. High-resolution confocal z-stack tile scans were acquired (***Figure 1A***), stitched with ImageJ and neurons were digitally reconstructed using Imaris software (see Materials and methods for details). Pyramidal neurons were filled with biocytin during electrophysiological recordings and 24 fillings were deemed to be of sufficient quality (clear presence of both apical and basal dendritic compartments, ***Figure 1A***, while incompletely filled neurons were excluded from the analysis) to enable high-resolution morphological analysis (***Figure 3***). Reconstructed neurons were classified by the distance of their soma to the pia as layers 2/3 (distance to pia: 300–1200 µm, n = 16), layer 4 (distance to pia: 1200–1500 µm, n = 3) or layers 5/6 (distance to pia: 1500–2900 µm, n = 5) pyramidal neurons (***Figure 3***) (***Mohan et al., 2015***; ***Ting et al., 2018***; ***Goriounova et al., 2018***). All neurons presented a typical pyramidal neuronal shape with distinct apical dendrites (***Figure 3***, red), extensive basal dendritic trees (***Figure 3***, blue), axons (***Figure 3***, magenta) and spines present on the apical and basal dendrites. The total length of the apical and basal dendrites as well as the combined total length of the reconstructed dendritic filaments were quantified for each analyzed neuron and correlated to the distance of the respective soma to the pia and to the DIV (Figure 5A). To investigate whether neurons undergo degenerative processes or exhibit layer-dependent morphological differences, we calculated a linear regression for the values of total basal, total apical and total combined dendritic length of all neurons to the DIV and the distance to the pia. There was no significant correlation between the total basal, apical or combined dendritic length and the number of days *in vitro* for these analyzed biocytin filled neurons (n = 24, linear regression, p=0.07). While there was also no significant correlation of all three parameters of total dendritic length with overall soma distance to the pia (n = 24), additional subgroup analysis of superficially and incrementally deeper situated layers 2/3 neurons in acute and cultured cortical

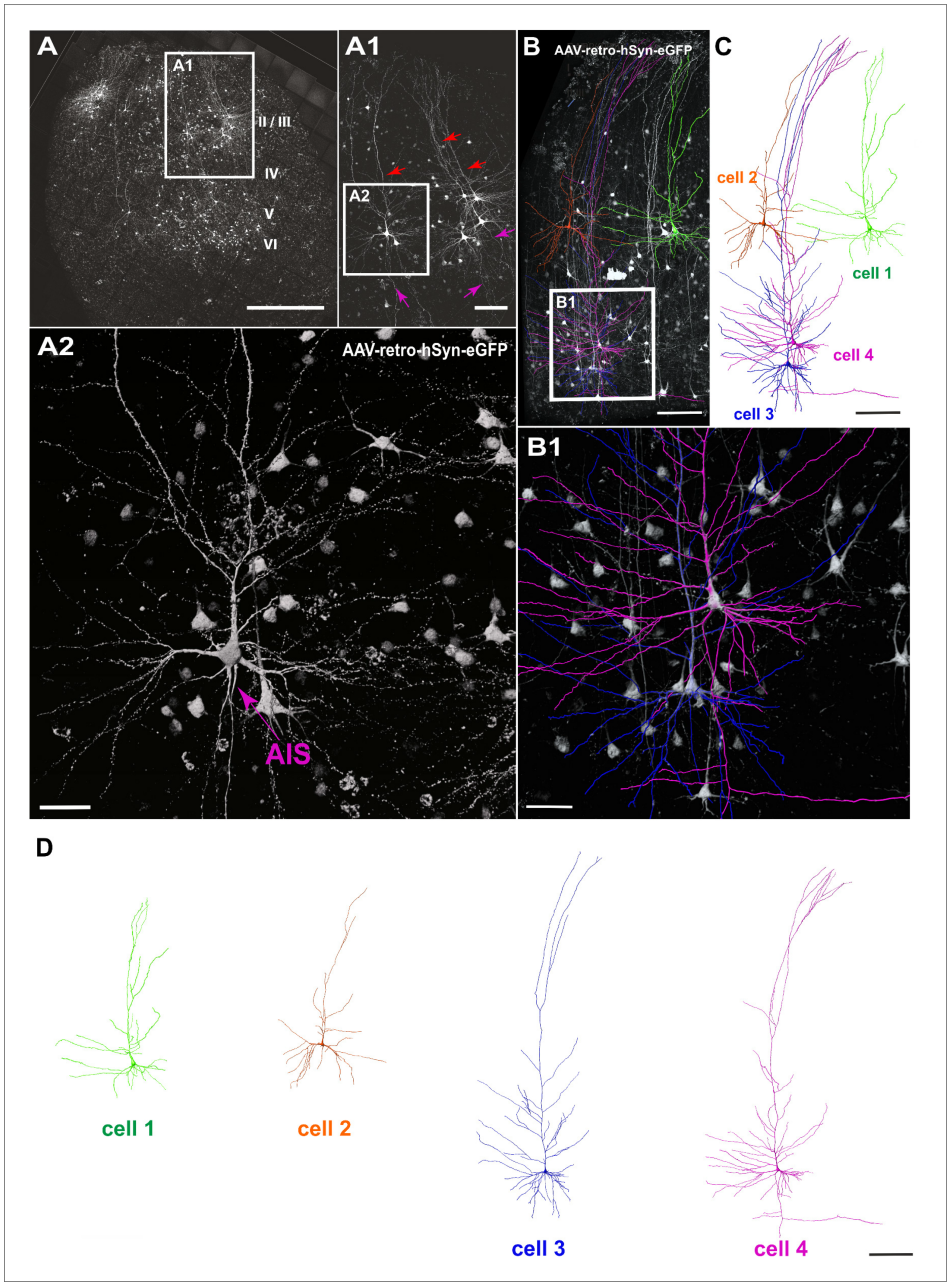


Figure 2. Viral transduction in human brain slice cultures and 3D reconstruction of GFP-labeled pyramidal neurons. (**A**) Representative example of a human brain slice after viral transduction with AAVrg-hSyn-GFP at 9 DIV, scale bar 1000 µm. (**A1**) Enlarged confocal image from A: layers 2/3 pyramidal neurons with intact apical dendrites (red arrows) and axons (magenta arrows), scale bar 200 µm. (**A2**) The soma and axon initial segment (AIS) are clearly visible in the virally transduced neurons, scale bar 50 µm. (**B**) 3D reconstructions of four GFP transduced pyramidal neurons were performed from

Figure 2 continued on next page

Figure 2 continued

confocal z-stack tile scans, scale bar 200 µm. The cells were individually traced and pseudo colored (**C**). (**B1**) Example of two neurons within close proximity of each other, which could still be clearly separated for further analysis, scale bar 50 µm. (**D**) Separation of the four distinct GFP-labeled pyramidal cells for further analysis, scale bar 200 µm.

DOI: https://doi.org/10.7554/eLife.48417.005

tissue revealed a gradually increasing total length of apical and basal dendrites (Figure 5A; n = 16), as has been described in a previous study by ***Mohan et al. (2015)*** in non-cultured CNS tissue.

Next, we asked whether the native GFP signal following viral transduction of cultures could be readily used for structural analysis of groups of neurons (***Figure 2B***). A typical example of reconstruction and separation of GFP-labeled neurons fur further analysis is shown in ***Figure 2***. We picked a total of 23 neurons from four virally transduced slices (8, 9, 10 and 14 DIV) with strong GFP expression in layers 2–6 (***Figure 2A***). Similar to biocytin filled neurons all 23 GFP positive neurons were classified by the distance of their soma to the pia as layers 2/3 (distance to pia: 300–1200 µm, n = 12), layer 4 (distance to pia: 1200–1500 µm, n = 3) or layers 5/6 (distance to pia: 1500–2900 µm, n = 8) pyramidal neurons (***Figure 4***; apical dendrites, red; basal dendrites, blue; axons, magenta). In comparison to biocytin fillings GFP-mediated tracing equally successfully detected the gradually increasing dendritic length of layers 2/3 neurons depending on their soma position (***Figure 5B***). There was no significant correlation between the combined dendritic length and the DIV, neither for GFP-based tracings (data not shown) nor for analysis after pooling all biocytin and GFP reconstructed neurons (***Figure 5C***, middle panel). Comparing combined total dendritic length of all biocytin and GFP-labeled neurons independent of the DIV revealed a slight underestimation of values by GFP (***Figure 5C***, right panel, $p<0.01$, n = 24 (biocytin), n = 23 (GFP), unpaired Mann Whitney test) – likely because very distal dendritic ramifications are being captured somewhat less reliably (due to intermingling GFP positive processes from neighboring neurons and some arising uncertainty when judging whether to assign GFP positive processes in the periphery of the neuron being reconstructed to the filament of this neuron or whether to discard them by deeming them as originating from neighboring neurons) – but overall successful reconstruction of the major parts of dendritic arbors (***Figure 2*** and ***Figure 4***).

In summary a total of 47 biocytin and GFP-labeled neurons have been analyzed (***Figures 3–5***), revealing remarkable structural preservation of pyramidal neurons without clear signs of declining morphological complexity. These data not only indicate absence of widespread progressing neuronal degeneration throughout the time in culture but also demonstrate genetic labeling as a valid alternative approach to 3D morphological analysis of adult human neurons with significantly increased efficiency in comparison to classic single cell biocytin fillings.

Electrophysiological properties of interneurons in human brain slice cultures versus acute slices

To further investigate beyond our earlier indirect assessment based on the ratio of Map2 and Satb2 double-positive neurons to all Map2 positive neurons, whether also interneurons survive in human brain slice cultures we first performed immunocytochemical stainings for calretinin. Unlike for other interneuron subtype identifiers, we were able to obtain reliable stainings for calretinin in acute and cultured human brain slice tissue. Qualitative assessment at 0 DIV and at 9 DIV demonstrated survival of at least this subset of interneurons (***Figure 6C***). Next, we performed intracellular recordings of 22 neurons that were identified morphologically or electrophysiologically as interneurons (***Figure 6A,B,D***). In comparison to pyramidal neurons interneurons represent a morphologically and electrophysiologically even more diverse class of neurons. While morphology and firing behavior are known to substantially differ between various subclasses of interneurons, there are some intrinsic properties (such as resting membrane potential, input resistance, AP half width and sag potential; ***Figure 6F–G***) which can be considered comparatively more uniform and which therefore were found suitable for an assessment over time in culture. For all these parameters we did not find significant differences between neurons measured in acute (n = 7) and in cultured slices at 7–14 DIV (n = 15) (***Figure 6D–G***). The firing behavior of the recorded interneurons showed distinct properties as

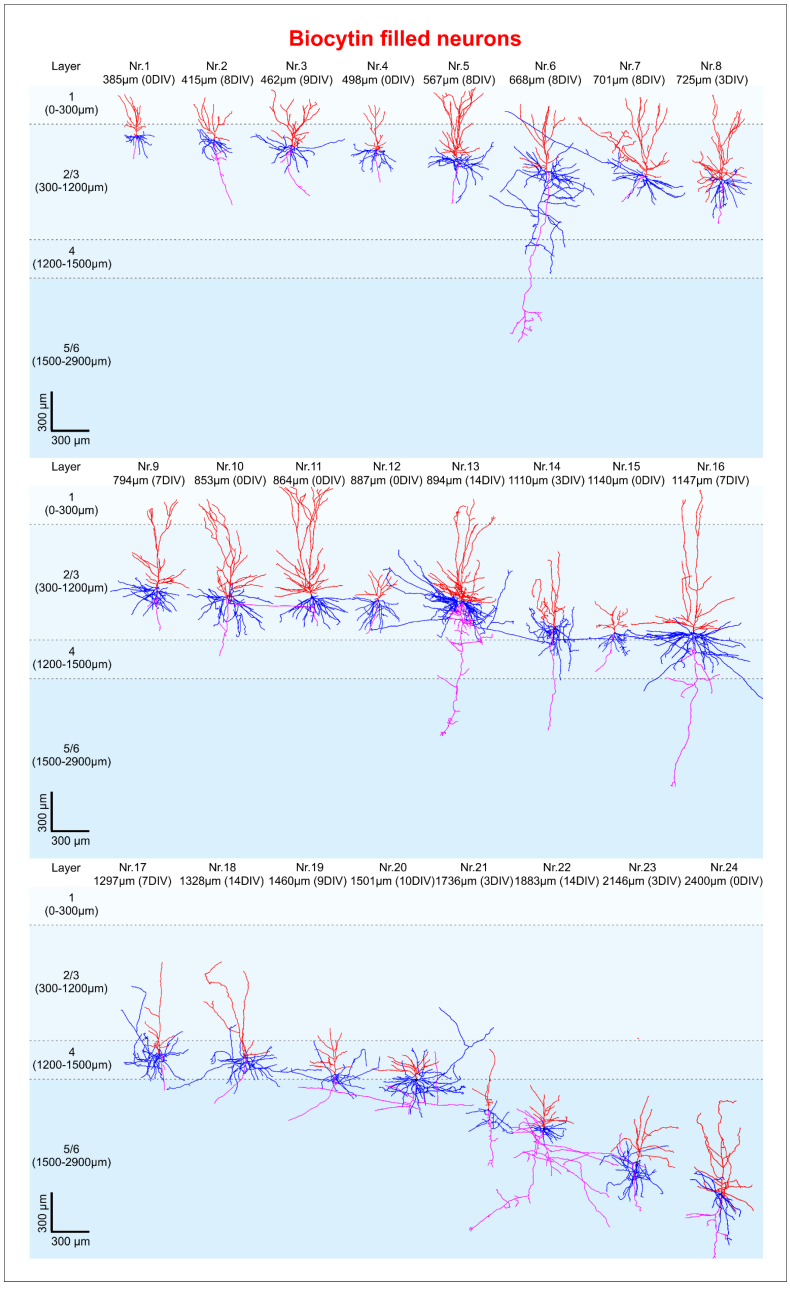


Figure 3. 3D reconstruction of biocytin filled pyramidal neurons. All 24 biocytin labeled reconstructed pyramidal neurons sorted by their soma distance to the pia ranging from 385 to 2400 µm represented in the colors red (apical dendrites), blue (basal dendrites) and magenta (axons).
DOI: https://doi.org/10.7554/eLife.48417.006

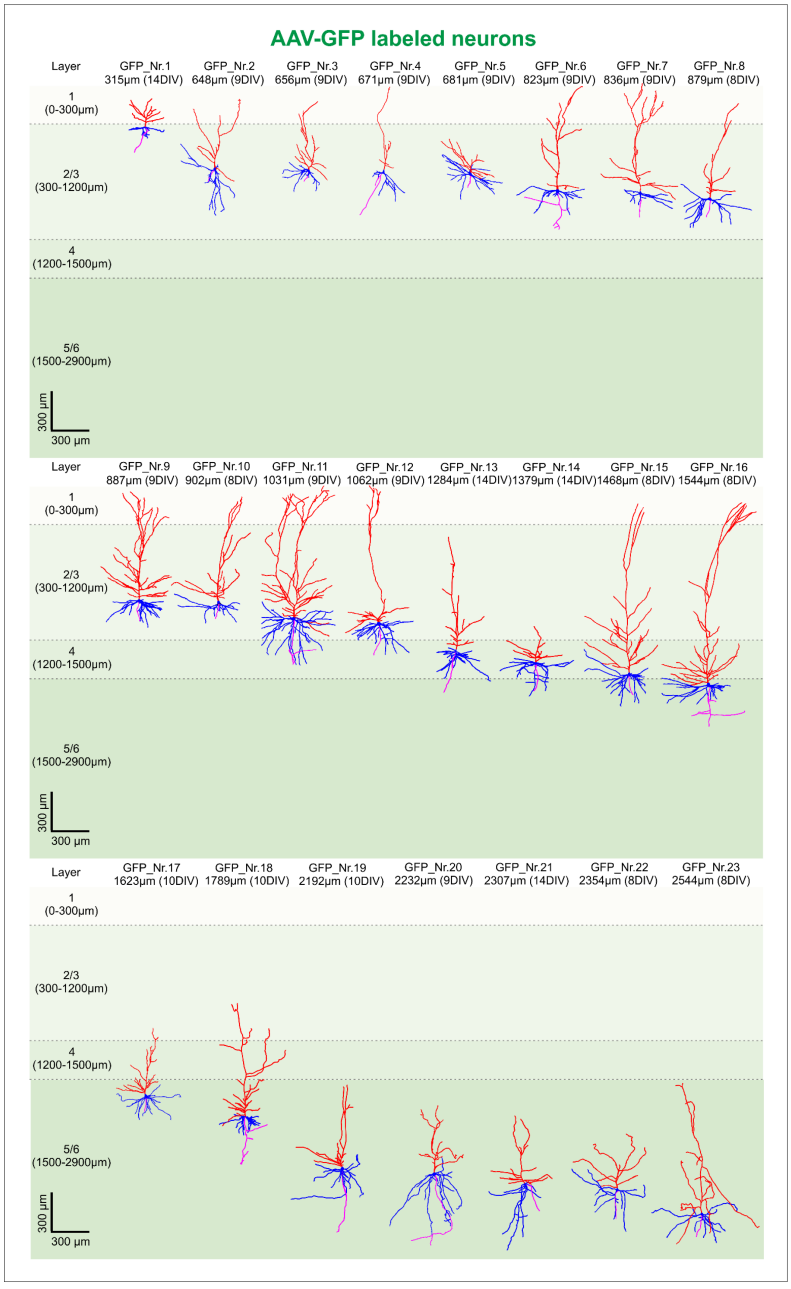


Figure 4. 3D reconstruction of GFP-labeled pyramidal neurons. All 23 GFP-labeled reconstructed pyramidal neurons sorted by their soma distance to the pia ranging from 315 to 2544 µm represented in the colors red (apical dendrites), blue (basal dendrites) and magenta (axons).
DOI: https://doi.org/10.7554/eLife.48417.007

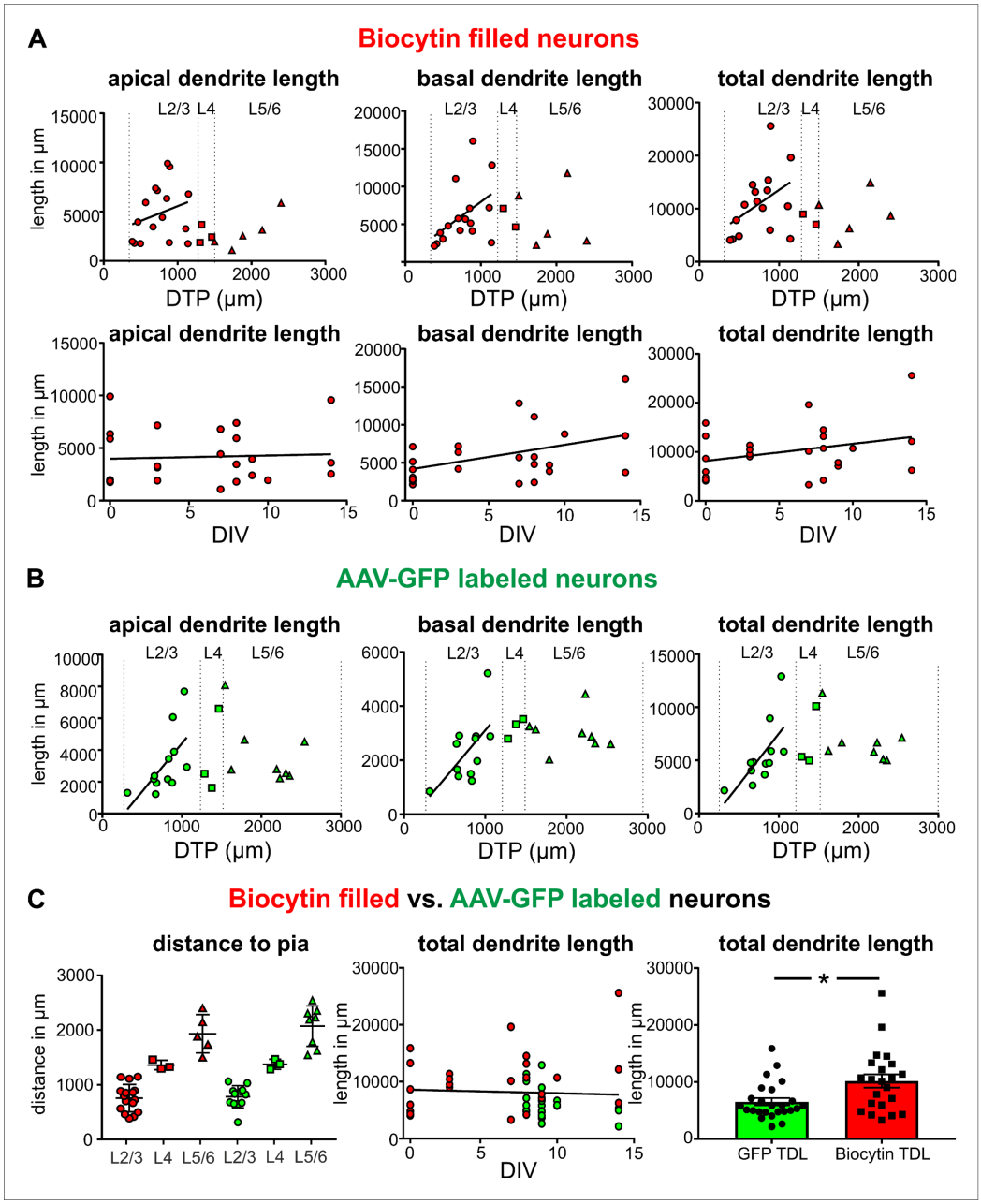


Figure 5. Quantification of the total length of apical and basal dendrites of biocytin filled and GFP-labeled neurons. (**A**) Upper panels: Neurons that were patched and filled in layers 2/3 are represented by red circles, neurons in layer four by red squares and neurons in layers 5/6 by red upward triangles. Bottom panels: Each biocytin filled neuron is represented by a red circle. (**B**) GFP-labeled layers 2/3 neurons are represented by green circles, neurons in layer four by green squares and neurons in layers 5/6 by green upward triangles. (**C**) Left: Analysis of the distribution of biocytin filled (red)

Figure 5 continued on next page

Figure 5 continued

and GFP-labeled (green) pyramidal neurons in the different layers. (**C**) Middle: Total dendritic length of biocytin filled (red) and GFP-labeled (green) pyramidal neurons plotted against DIV. (**C**) Right: Reconstructions of pyramidal neurons based on GFP expression slightly underestimated the total dendritic length compared to classic biocytin fillings (n = 22 for biocytin, n = 23 for GFP-labeled, **p<0.01).

DOI: https://doi.org/10.7554/eLife.48417.008

described before for rodents and humans and ranged from fast spiking (***Figure 6D***) to none fast spiking firing patterns (***Ascoli et al., 2008***).

Spine morphology of biocytin filled and GFP-labeled pyramidal neurons in acute and cultured slices

The spines of pyramidal neurons are the presumed site of excitatory synapses and have been shown to be a plastic part of the morphology of these cells (***Trachtenberg et al., 2002***; ***Yuste and Bonhoeffer, 2004***). To analyze morphological features of spines we acquired high-resolution confocal scans of dendritic compartments of biocytin filled (***Figure 7A,B***) or GFP positive (***Figure 7A,C***) pyramidal neurons, performed 3D reconstructions (***Figure 7A,D***) and determined spine density, spine length and spine head diameter (see Materials and methods for details). Pyramidal neurons in acute (0 DIV) and cultured slices (2 DIV - 14 DIV) revealed no significant differences on average regarding spine density (acute and filled with biocytin: 0.54 ± 0.04 spines/µm, n = 5; cultured and filled with biocytin: 0.53 ± 0.04 spines/µm, p=0.99, n = 17; cultured and GFP-labeled: 0.44 ± 0.05, p=0.19, n = 11; Kruskis Wallis Test), spine length (acute biocytin: 1.46 ± 0.04 µm, n = 5; cultured biocytin: 1.54 ± 0.08 µm, n = 17, p=0.87; cultured GFP-labeled: 1.60 ± 0.05 µm, n = 11, p=0.45; Kruskis Wallis Test) or spine head diameter (acute biocytin: 0.47 ± 0.05 µm, n = 5; cultured biocytin: 0.52 ± 0.02 µm, p=052, n = 17; cultured GFP-labeled: 0.58 ± 0.04 µm, p=0.09, n = 11; Kruskis Wallis Test) (***Figure 7—figure supplement 1***). Since we did not find significant differences between any of the groups and particularly also not for biocytin versus GFP-driven analyses, we pooled GFP- labeled and biocytin filled neurons for linear regression analysis. We found a moderate negative correlation between the spine density and the DIV (***Figure 7E***, linear regression, $r^2 = -0.21$, p<0.01) and a moderate positive correlation between the spine head diameter and the DIV (***Figure 7E***, linear regression, $r^2 = 0.15$, p<0.05), while the average spine length showed no correlation to the DIV (***Figure 7E***, linear regression, p=0.99). In addition, we found a strong positive correlation between the distance of neuronal somata to the pia and the spine length (***Figure 7F***, linear regression, $r^2 = 0.46$, p<0.001), but not to the spine head diameter (***Figure 7F***, linear regression, p=0.06) or spine density (***Figure 7F***, linear regression, p=0.05).

In summary, analyses revealed mild changes at the most on spine level without clear indication of prevalent alterations related to the culturing process, suggesting that human brain slice cultures may represent a suitable model system to study pathophysiological mechanisms of neurological and neuropsychiatric disease.

Virally transduced neurons maintain normal firing properties

To investigate whether AAV-transduction and GFP expression affected the electrophysiological properties of cortical neurons, we performed whole-cell patch clamp recordings of GFP positive neurons (n = 7) and GFP negative neurons (n = 13) at matching time points in culture (7–16 DIV) and assessed AP half width, resting membrane potential, sag potential and input resistance. All recorded neurons displayed normal AP firing upon supra-threshold current injections with either regular spiking patterns as typical for pyramidal neurons (***Figure 8C***, n = 7) or fast/adaptive spiking patterns as typical for interneurons (***Figure 8E***, n = 6) (***Ascoli et al., 2008***). Most of the parameters that we investigated in GFP positive neurons did not differ significantly from the values obtained from GFP negative control neurons (***Figure 8D and F***). We found however in the group of interneurons a significant reduction of the sag potential at hyperpolarization compared to GFP negative cells (***Figure 8F***), while all other parameters were not significantly different and while there were no significant differences found for any of the parameters in the pyramidal cell group. Taking together these results, virus transduction did not dramatically interfere with neuronal functionality.

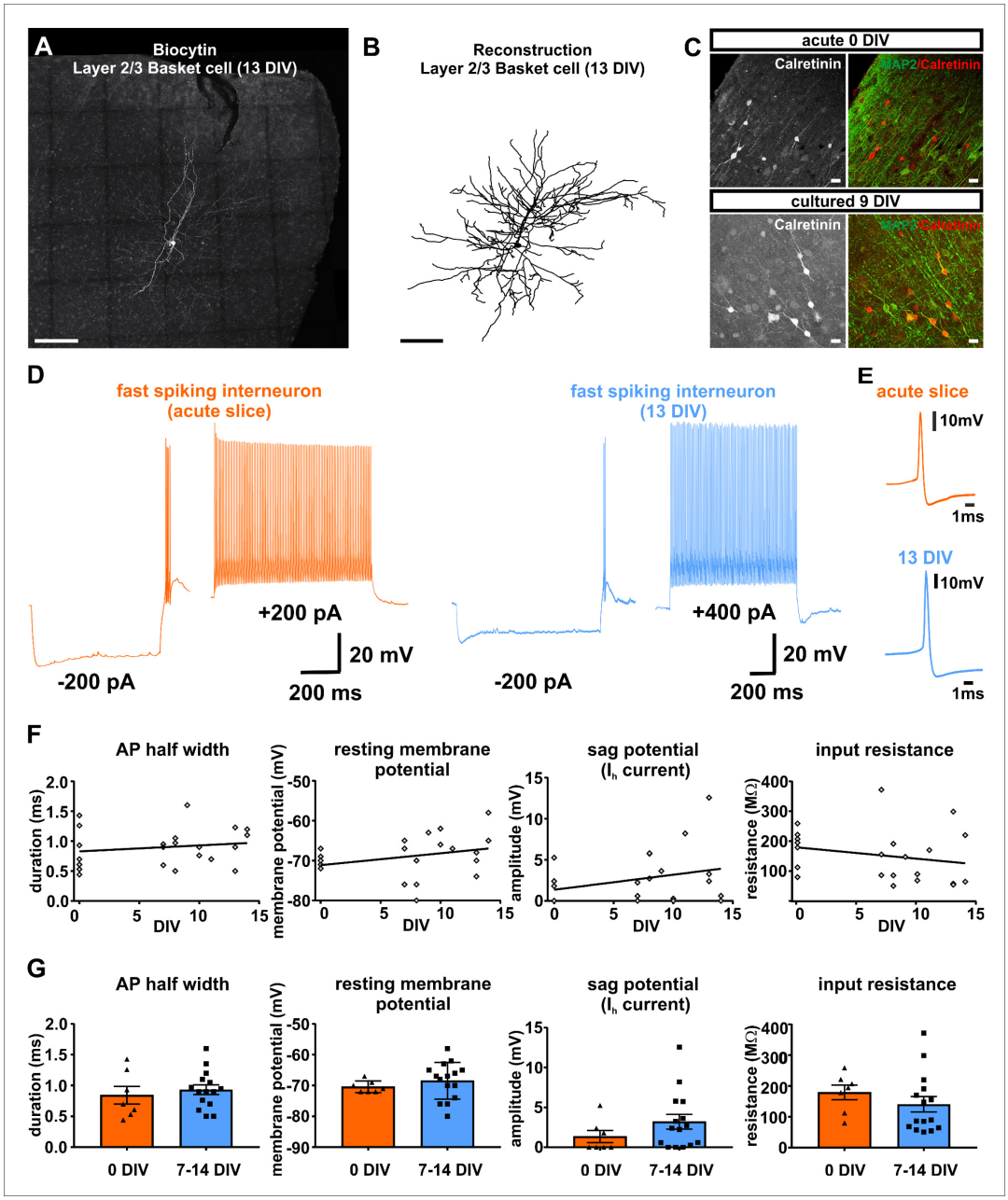


Figure 6. Presence and functionality of interneurons in human slice cultures. (**A**) Example of Layers 2/3 basket cell labled with biocytin and (**B**) after reconstruction, both scale bars 200 µm. (**C**) Staining of calretinin revealed presence of a subpopulation of inhibitory interneurons in acute (0 DIV) and late in culture (9 DIV), scale bar 20 µm. (**D**) Example of fast spiking interneuron firing in acute slices (orange) and late (blue) in culture (13 DIV). (**E**) Examples of interneuron APs in acute slice (orange) and late in culture (13 DIV, blue) reveal comparable AP half width. (**F**) Quantification and plotting of

Figure 6 continued on next page

Figure 6 continued

basic properties of IN in relation to the DIV. (**G**) Group comparison between the properties in acute slice and late in culture measured interneurons revealed no significant differences (Mann-Whitney test, p>0.05).

DOI: https://doi.org/10.7554/eLife.48417.009

Two-photon live cell imaging of human brain slice cultures

In a last step we investigated whether virus-mediated GFP expression enables two-photon live cell imaging of adult human neurons within slice cultures. Slices were transferred into a submerged aCSF chamber and large tiles scans composed of detailed high-resolution stacks were acquired with a two-photon laser microscope (water-immersion x20 Objective, Laser tuned to 920 nm). In all examined slices (n = 5, 7–15 DIV) we could successfully identify pyramidal neurons (***Figure 9A*** displays a representative example) including dendritic structures and emanating spines (***Figure 9A1***). In a second step we asked whether our system would be stable enough to enable time-lapse tracing of dendrites and spines of human pyramidal neurons over a time window of several hours. In two experiments (at 7 DIV and at 14 DIV) we imaged five distinct areas per slice for 24 hr and acquired image stacks every 30 min. While in three areas a slight shift in the z-axis resulted in an incomplete scan of the neurons and dendrites, further technical optimization allowed seven areas to be scanned successfully over the complete time course. ***Figure 9*** shows the 24 hours timepoint of the same pyramidal neuron displayed in ***Figure 9A*** at 0 hours of live cell imaging. ***Figure 9B*** and ***Figure 9B1*** show the same pyramidal neuron displayed in ***Figure 9A*** and ***Figure 9A1*** at 0 hours, now after 24 hours of live cell imaging. To further assess the stability of the system, dendrites of four imaged neurons were manually traced and reconstructed (***Figure 9—figure supplement 1A***) and total dendritic length and maximal sholl radius were semi-automatically determined for each of the four neurons at t = 0 hours and t = 24 hours. Data revealed reasonably small variability of parameters (mean ± SD: total dendritic length: −3.15 ± 10.87%; maximal sholl radius: 3.12 ± 6.50%) indicating feasibility of two-photon 24 hr life-cell imaging of human cortical slice cultures (***Figure 9—figure supplement 1B***).

After further optimization this approach will enable future studies of spine turnover of individual human neurons within brain slice cultures.

Discussion

The human cerebral cortex is composed of many distinct cell types organized in very specific arrangements according to the highly specialized function of individual cells. Thus, questions are raised whether basic anatomic and physiological knowledge as well as disease related pathophysiological data obtained in animal models can be directly translated to the human CNS. For a long time, the ability to study bona fide human cortical neurons and investigate physiologically and pathologically relevant questions was confined to post mortem studies (***Anton-Sanchez et al., 2017***; ***Elston and Fujita, 2014***; ***Huttenlocher et al., 1982***) and to acute/fresh post-surgery tissue (***Beck et al., 2000***; ***Marcuccilli et al., 2010***; ***Verhoog et al., 2013***). With standard procedures, limited viability of resected tissue restricted electrophysiological recordings to a time window of 12–72 hr following surgery (***Wickham et al., 2018***). However, in recent years several methods have been incrementally established by us and other groups to keep human CNS tissue functionally intact for extended periods of days (***Ting et al., 2018***) to weeks (***Eugène et al., 2014***; ***Andersson et al., 2016***; ***Schwarz et al., 2017***). Initial studies based on development of special culturing strategies and complex artificial media revealed feasibility and prompted further investigation and optimization (***Eugène et al., 2014***). We recently demonstrated that hCSF significantly promotes neuronal viability and long-term survival of human brain slice cultures (***Schwarz et al., 2017***), allowing robust recordings of neuronal network activity for up to 21 DIV. These results indicated that after additional thorough characterization and further optimization such a system could potentially serve as a translational tool with broad application toward studies of human disease and development of novel therapeutic strategies. The success of such a model system would be predicted to not only critically depend on the viability of neurons but also on the maintenance of their distinct morphological characteristics. While we had demonstrated general neuronal survival within cultures (***Schwarz et al.,***

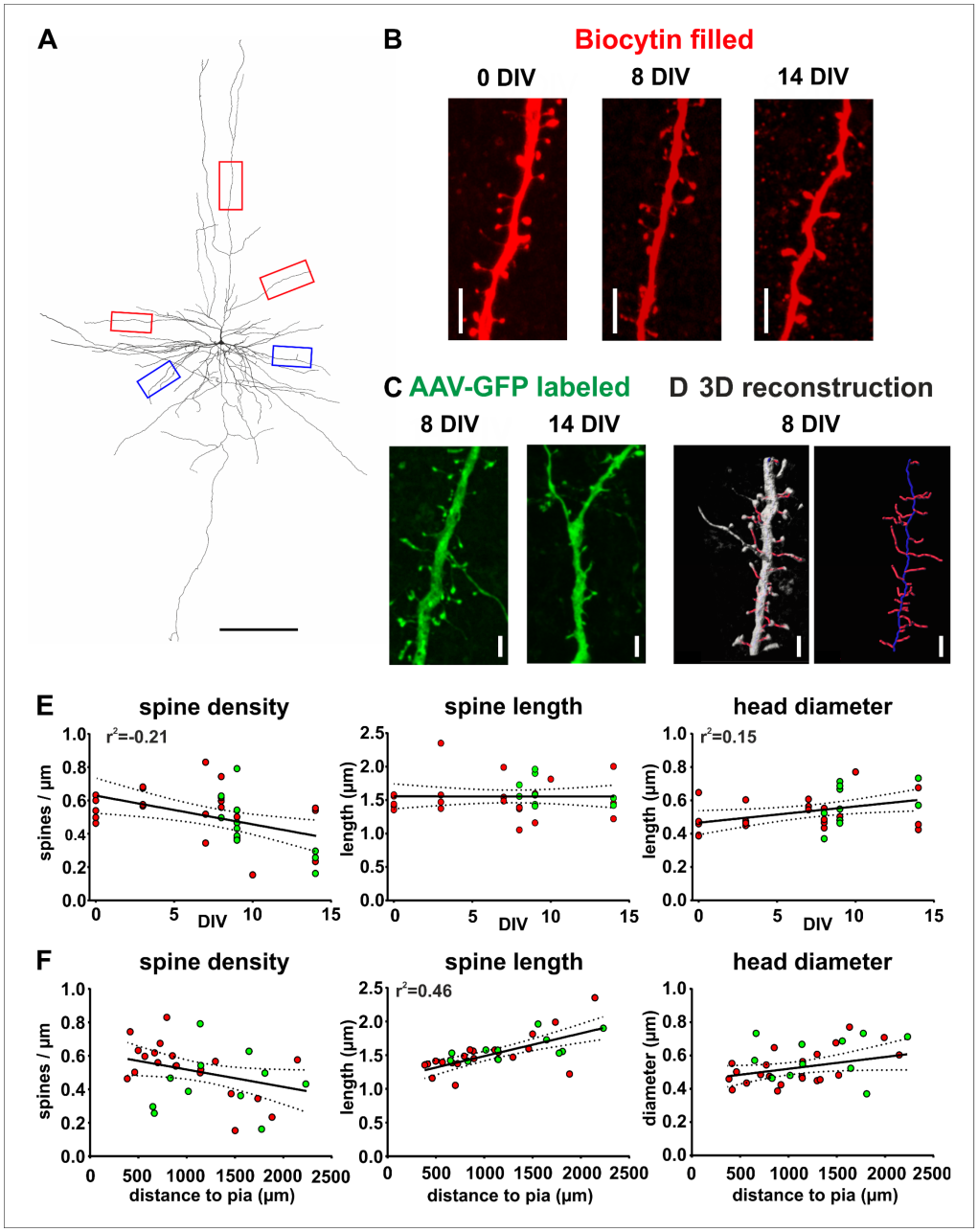


Figure 7. Spine measurements of human cortical pyramidal neurons in acute and cultured slices filled with biocytin and labeled with GFP. (**A**) 3D reconstruction of a typical layers 2/3 pyramidal neuron (biocytin filled, 7 DIV) in human brain slice cultures, scale bar 300 µm. Of each neuron five dendritic regions were chosen (three of the apical dendritic compartment, red boxes, and two of the basal dendritic tree, blue boxes). (**B**) Typical examples of spines localized on apical dendrites of representative layers 2/3 pyramidal neurons recorded and biocytin filled at 0 DIV (acute slice), at 8

Figure 7 continued on next page

Figure 7 continued

DIV and at 14 DIV, scale bar 5 µm. (**C**) Typical examples of spines of GFP-labeled neurons at 8 and 14 DIV, scale bar 5 µm. (**D**) For quantitative assessment, the z-stacks were 3D reconstructed and analyzed using NeuronStudio and Imaris software, scale bar 5 µm (see Materials and methods for details). (**E, F**) Neurons that were patched and filled with biocytin are represented by red circles and transduced GFP positive neurons by green circles. (**E**) Data reveal a moderate negative correlation of spine density with DIV and a moderate positive correlation of spine head diameter with DIV. (**F**) Plots of the same parameters versus the distance of the somata of the analyzed neurons to the pia revealed a strong positive correlation for spine length, but not the spine density or the spine head diameter.

DOI: https://doi.org/10.7554/eLife.48417.010

The following figure supplement is available for figure 7:

Figure supplement 1. Analysis of mean values of spine density, length and head diameter of biocytin filled and virally transduced GFP positive pyramidal neurons.

DOI: https://doi.org/10.7554/eLife.48417.011

2017) it remained elusive whether overall neuronal morphology, specifically dendritic complexity, spine distribution and designated structural features of spines, are preserved throughout the course of culturing. In the present study we now provide a systematic analysis of pyramidal neurons and interneurons across all cortical layers supporting overall electrophysiological and structural stability throughout the time window up to two weeks in culture. Specifically, we found that most parameters quantified in this study did not differ between neurons recorded in acute (0 DIV), early (2–3 DIV) or late stage cultures (7-14 DIV). One exception was the resting membrane potential of pyramidal neurons which was found to be slightly, but significantly lower for pyramidal neurons recorded in slices at 0 DIV. This might be interpreted as a small initial adaptation of pyramidal neurons to the new conditions in culture, particularly since we did not find continued depolarization of resting membrane potential in late stage cultures compared to early stage ones. Interestingly, interneurons did not seem to show this effect. Moreover, we measured and compared the properties of GFP positive neurons after viral transduction and found no major impairment of neuronal function in our analyzed samples of pyramidal neurons (n = 7) and interneurons (n = 6), which is in line with a previous study investigating virus transduction in human neurons (***Ting et al., 2018***). Although our data indicate no major interference of viral transduction with neuronal function we cannot rule out subtler alterations, particularly given the immense diversity of cortical neurons, which certainly cannot be represented in its entirety in our samples. This question needs to be further approached in future large-scale studies and respective investigations will benefit from community-based efforts. It has been reported before that pyramidal neurons of the human temporal cortex show a layer specific dendritic pattern with a gradual increase of the total dendritic length (both of the apical and basal compartment) of layers 2/3 pyramidal neurons correlating with the distance of the soma to the pia (***Mohan et al., 2015***). We confirmed this finding in our acute/fresh tissue samples and further demonstrate its robustness throughout the culturing period. Furthermore, we confirmed a decline in total apical dendritic length in our cultures at the intersection of layers 3 and 4, as demonstrated by ***Mohan et al. (2015)***, corresponding to the presence and survival of spiny stellate neurons which are lacking an extended apical dendrite. While the gross morphology of the apical and basal dendritic arbors of pyramidal neurons are considered fairly stable over time *in vivo* and *in vitro* in acute slices, there is strong evidence that the dendritic fine structure undergoes a constant plastic remodeling (***Trachtenberg et al., 2002***; ***Yuste and Bonhoeffer, 2004***). Especially the spines have been proven to be plastic and to appear and disappear on time scales of days in the developing (***Holtmaat and Svoboda, 2009***; ***Lendvai et al., 2000***) and adult brain (***Trachtenberg et al., 2002***). On the other hand, despite this sustained turnover overall spine density has been shown to remain generally stable in adult cortex of mice (***Trachtenberg et al., 2002***). To investigate whether anatomic features of spines change over time in human slice cultures we performed high-resolution confocal imaging of dendritic compartments and assessed spine density, spine length and spine head diameter in correlation to the DIV. We detected only small alterations of the morphological spine parameters of neurons in cultured slices compared to neurons in acute slices along with only a moderate reduction of spine density. Although this is in line with the *in vivo* data by ***Trachtenberg et al. (2002)***, this result may still seem surprising since cultured cortical tissue, disconnected from their surrounding circuitry and thus deprived from outside input, would rather be expected to significantly lose spines. However, these data are in line with ***Trachtenberg et al. (2002)***, showing plastic remodeling in mouse pyramidal

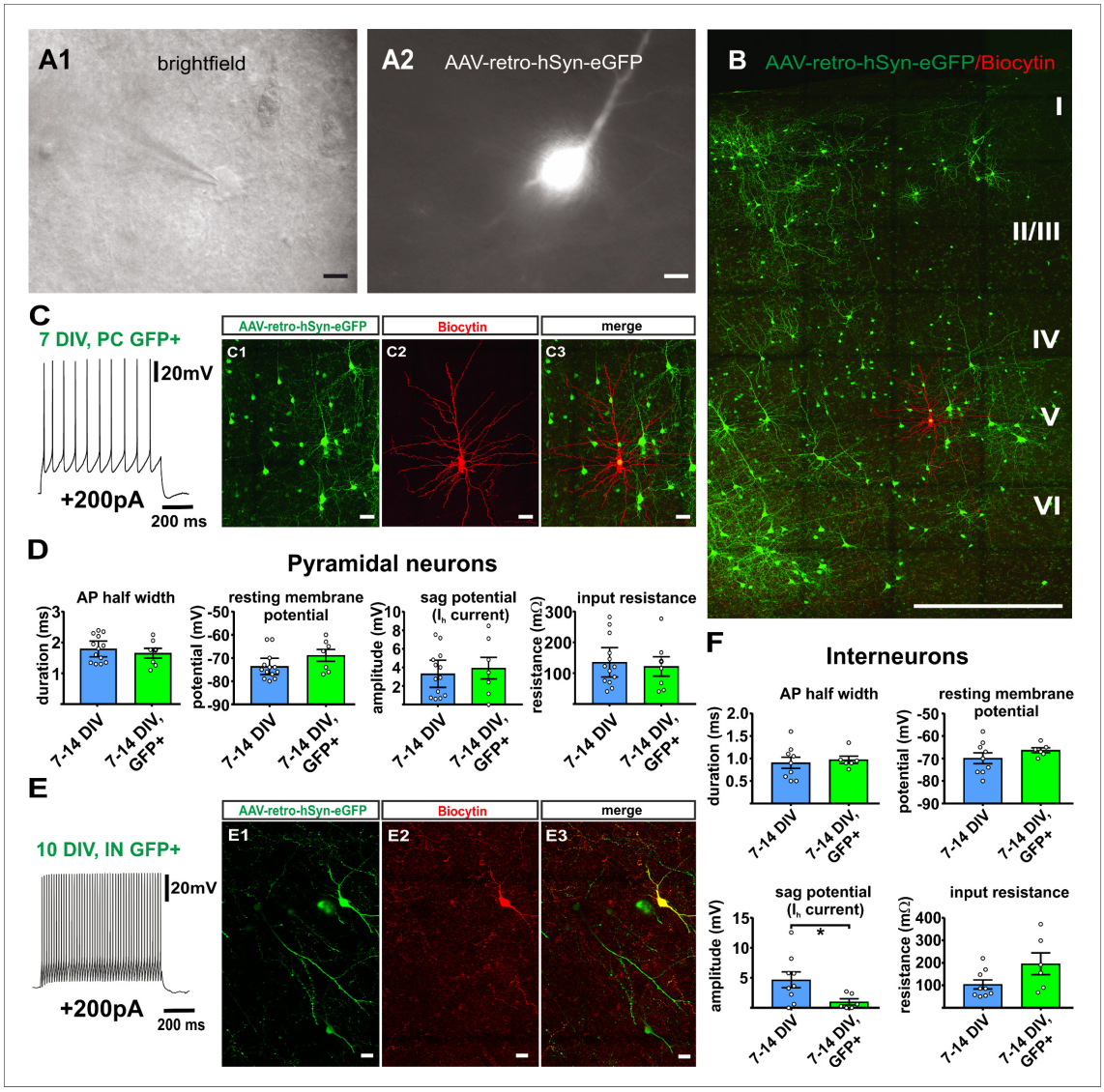


Figure 8. Virally transduced neurons show no major changes of basic properties. (**A**) GFP positive neurons were visualized according to their GFP fluorescence (**A2**) and targeted for whole-cell patch clamp recordings (**A1**), scale bars 10µm. (**B**) Overview image of a double positive pyramidal neuron (GFP and Biocytin) after whole cell recording and post-hoc staining, scale bar 500 µm; (**C1–C3**) and in detail, scale bar 20 µm. (**C**) Example of a representative regular firing pattern of a GFP positive pyramidal neuron (+200 pA). (**D**) Quantification of basic properties of GFP negative and GFP positive human pyramidal neurons. (**E**) Example of a GFP positive fast spiking interneuron. (**E1-E3**) GFP signal, biocytin filling and merge of the same neuron, scale bar 20 µm. (**F**) Quantification of basic properties of GFP negative and GFP positive human interneurons, *p<0.05, Mann Whitney test.

DOI: https://doi.org/10.7554/eLife.48417.012

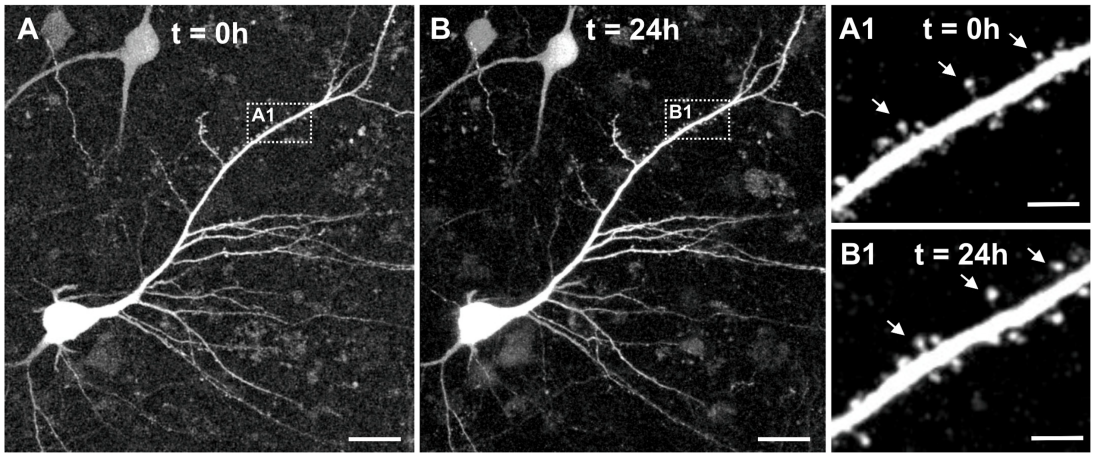


Figure 9. Two-photon live imaging of human neurons over 24 hr. (**A**) Maximum projection of a GFP positive human pyramidal neuron in slice culture at the start of the measurement and (**B**) after 24 hr life cell imaging with acquisition of image stacks every 30 min. (**A1**) and (**B1**) inserts are zoomed in images of the same branch of the apical dendrite at 0 and 24 hr of imaging. Arrows point to the same spines. Scale bars 20 µm (**A, B**) and 5 µm (**A1, B1**).

DOI: https://doi.org/10.7554/eLife.48417.013

The following figure supplement is available for figure 9:

Figure supplement 1. Filament measurements reveal stability over the time of 24 hr.

DOI: https://doi.org/10.7554/eLife.48417.014

neurons with an increased spine turnover rate and number of transient spines but overall stability of spine density in response to activity deprivation. Such a homeostatic mechanism could explain the relative stability of spine density in adult human brain slice cultures reported here. Future experiments directly determining spine turnover by two-photon live cell imaging will be needed to corroborate this hypothesis and to investigate whether alternative or additional mechanisms could have a role in maintenance of spine density in human pyramidal neurons (in slice cultures). Such studies are indeed conceivable and we provide first proof-of-concept data regarding feasibility of live cell imaging for extended time periods (up to 24 hr) of human brain slice cultures by taking advantage of virally mediated neuronal GFP expression. Furthermore, we demonstrate genetic labeling as an efficient approach toward 3D reconstruction and detailed morphological analysis of relatively large quantities of adult human neurons per tissue sample, providing a valid alternative to laborious single cell biocytin fillings. Post processing of the tissue for GFP signal amplification by standard immunocytochemistry or in combination with tyramide boosting will likely provide structural information even surpassing the one available from classic biocytin fillings. Depending on the degree of cell type specificity of the promoters used to drive the expression of fluorescent proteins this strategy may also enable screening for rare human CNS cell types or targeting of certain subpopulations like interneurons (***Dimidschstein et al., 2016***). It seems very intriguing to adopt the same set of tools to study cell autonomous and (in light of substantial viral transduction rates) potentially even cell non-autonomous effects of disease related mutated proteins on human CNS cell types of interest. Adapting state-of-the-art molecular genetic tools (such as optogenetic and chemogenetic approaches or homologous recombination-driven genetic targeting), currently available in model organisms, for application in human CNS tissue appears increasingly practical and would open completely new opportunities to study both physiological properties of human CNS circuitry and pathological conditions underlying neurological disease.

In summary, we found a remarkable stability of morphological and electrophysiological parameters of human pyramidal neurons as cortical network components of slice cultures over a time course of 14 DIV. Furthermore, we demonstrate widespread viral transduction of human brain slice cultures, enabling genetic manipulation of adult human neurons under very controlled conditions. We propose that this model system will be of great value for many investigations in viable human neuronal networks such as therapeutic screening, investigation of electrophysiological and structural properties of human CNS circuitry and direct exploration of mechanisms underlying neurological disease.

Materials and methods

Patients

Human neocortical brain slice cultures were prepared from access tissue (cortical tissue outside the epileptic focus, resected in order to gain access to the pathology) obtained from patients undergoing epilepsy surgery. For this study, we collected and included data of 15 patients (***Table 1***). All patients were surgically treated for intractable epilepsy, in two patients the histology revealed low-grade tumors (Ganglioglioma WHO Grade I; Oligodendroglioma, WHO Grade II).

Preparation of slices from resected tissue

Approval (# 338/2016A) of the ethics committee of the University of Tübingen as well as written informed consent was obtained from all patients, allowing spare tissue from resective surgery to be included in the study. Tissue preparation was performed according to published protocols (***Verhoog et al., 2013***). Cortex was carefully microdissected and resected with only minimal use of bipolar forceps to ensure tissue integrity, directly transferred into ice-cold artificial cerebrospinal fluid (aCSF) (in mM: 110 choline chloride, 26 $NaHCO_3$, 10 D-glucose, 11.6 Na-ascorbate, 7 $MgCl_2$, 3.1 Na-pyruvate, 2.5 KCl, 1.25 NaH_2PO_4, und 0.5 $CaCl_2$) equilibrated with carbogen (95% O_2, 5% CO_2) and immediately transported to the laboratory. Tissue was kept submerged in cool and carbogenated aCSF at all times. After removal of the pia, tissue chunks were trimmed perpendicular to the cortical surface and 250–350 µm thick acute slices were prepared using a Microm HM 650V vibratome (Thermo Fisher Scientific Inc) (***Figure 1—figure supplement 2A***). Afterwards the slices were kept in aCSF equilibrated with carbogen for 0.5 hr at room temperature before they were

Table 1. Tissue samples included in this study.

Age at surgery	Gender	Resected brain area	Number and type of cells included in this study
30	M	temporal lobe	3 PC
30	M	temporal lobe	2 PC
10	F	temporal lobe	3 PC + 3 IN
38	F	temporal lobe	2 IN
16	M	temporal lobe	1 PC
18	M	frontal lobe	6 PC
40	F	temporal lobe	4 PC + 3 IN
40	F	frontal lobe	1 IN
29	M	temporal lobe	5 PC
56	F	temporal lobe	3 PC
31	M	temporal lobe	3 PC + 2 IN
44	M	temporal lobe	5 PC + 3 IN
46	F	temporal lobe	2 PC + 1 IN
67	M	temporal lobe	2 PC + 1 IN
57	M	frontal lobe	6 PC + 6 IN

DOI: https://doi.org/10.7554/eLife.48417.015

transferred either to patch setups for acute electrophysiological recordings and biocytin fillings or onto culture membranes for cultivation.

Human brain slice cultures

After the cortical tissue was sliced as described above, slices were cut into several evenly sized pieces (~1.0×1.0 cm, ***Figure 1—figure supplement 2A***). Subsequently, slices were transferred onto culture membranes (uncoated 30 mm Millicell-CM tissue culture inserts with 0.4 µm pores, Millipore) and kept in sixwell culture dishes (BD Biosciences). For the first hour following the slicing procedure the slices were cultured in 1.5 ml NSC media (48% DMEM/F-12 (Life Technologies), 48% Neurobasal (Life Technologies), 1x N-2 (Capricorn Scientific), 1x B-27 (Capricorn Scientific), 1x Glutamax (Life Technologies), 1x NEAA (Life Technologies) + 20 mM HEPES before changing to 1.5 ml hCSF per well without any supplements. No antibiotics or antimycotics were used during cultivation. The plates were stored in an incubator (ThermoScientific) at 37˚C, 5% CO_2 and 100% humidity. For electrophysiological recordings slice cultures were transferred into the recording chamber of a patch clamp rig. After finishing patch clamp recordings, slices were fixed in 4% paraformaldehyde (PFA) and processed for immunocytochemistry (ICC), as described in detail in the ICC section.

Structural features of acute cortical slices and slice cultures

Mohan et al. (2015) and subsequently ***Ting et al. (2018)*** and ***Goriounova et al. (2018)*** provided a framework defining cortical layering and layer boundaries of human cortical brain slices based on distance from the pia. This system can be used to register neurons according to the distance of their soma position from the pial surface, thereby assigning neurons to cortical layers 2/3, 4 or 5/6. To confirm comparability to our acute (0 DIV) tissue and in order to assess whether this system can be also directly applied to our tissue cultures, we compared the thickness of cortical gray matter between tissue slices originating from independent surgeries and between different time points in culture. Following DAPI staining of slices (0 DIV - 15 DIV) layer four was clearly visible as delineated band (as has previously been demonstrated by ***Ting et al., 2018***)~1200 µm below the pial surface (***Figure 1—figure supplement 2E***). The distance of the outer margin (edge) of layer four from the pia was assessed for tissue slices prepared from three independent surgeries (P1-3). Mean values were plotted as bar diagrams for comparison (***Figure 1—figure supplement 2B***) and did not reveal significant differences. Furthermore, this distance did not change significantly over time in culture up to the endpoint of analysis at 20 DIV (***Figure 1—figure supplement 2C***). Importantly, results are in line with the published data referenced above. While mouse organotypic slice cultures are known to flatten out quite extensively throughout the time in culture to the point that they may even become translucent, human brain slice cultures revealed only a mild decrease of thickness of about 20% over the analyzed three-week period in culture (***Figure 1—figure supplement 2D***).

Assessment of human brain slice thickness: Slices were fixed with 4% PFA and thickness was determined by two-photon microscopy based on detection of either GFP-signal or tissue autofluorescence. Imaging was performed on an upright Zeiss LSM 880 NLO microscope, using an IR-optimized water-immersion x20 Objective (W Plan-Apochromat x20/1.0, Carl Zeiss, Jena). A MaiTai eHP DeepSee (Spectra Physics) laser was used for two-photon excitation, tuned at 920 nm for exciting GFP, YFP, hFTAA and Atto550 fluorescence. Emission was collected using Non-Descanned GaAsP detectors, separated by a 520/50 emission filter. Images were collected at a resolution of 0.208 µm x 0.208 µm x 0.640 µm per voxel. Two z-stacks at different positions of at least two slices per DIV time point were acquired and analyzed with Imaris to determine the thickness of the 3D-reconstructed image. To exclude any effects of the fixation procedure on slice thickness, late stage slice cultures (20 DIV) were first imaged unfixed via two-photon live-cell imaging and then re-imaged after fixation with 4% PFA.

Classification of neurons according to cortical layering

Mohan et al. (2015), neurons were classified by the distance of their soma to the pia as layers 2/3 (distance to pia: 300–1200 µm), layer 4 (distance to pia: 1200–1500 µm) or layers 5/6 (distance to pia: 1500–2900 µm) pyramidal neurons.

Collection of human cerebrospinal fluid (hCSF)

hCSF was collected from patients with normal pressure hydrocephalus (NPH) or idiopathic intracranial hypertension. We received and pooled hCSF of several patients who needed to undergo a CSF tap test either by lumbar puncture or lumbar drain as part of the diagnostic or therapeutic workup. Approval of the ethics committee of the University of Tübingen as well as written informed consent from all patients was obtained. It is well established and known from daily clinical practice that hCSF of NPH patients exhibits physiological/normal hCSF parameters (lactate, glucose, cell count, protein levels – see ***Schwarz et al., 2017***), undistinguishable from the ones of healthy individuals (***Bjorefeldt et al., 2015***). The hCSF was centrifuged at 4000 rpm at 4˚C for 10 min. Samples were sterile filtered using a 0.2 µm syringe filter and stored at −80˚C.

Whole-cell patch clamp recordings

Slices were positioned in a submerged-type recording chamber (Scientifica, United Kingdom/Warner apparatus), continuously superfused with 32.0 + /- 1.5˚C recording aCSF (in mM: 118 NaCl, 25 $NaHCO_3$, 30 D-glucose, 1 $MgCl_2$, 3 KCl, 1 NaH_2PO_4, und 1.5 $CaCl_2$) and visualized with a BX61WI Microscope (Olympus) or a Leica stereomicroscope. After 1 hr of equilibration in the patch setup recordings were performed using recording electrodes with a resistance of 3–5 MΩ and filled with an intracellular whole-cell patch-clamp pipette solution containing the following components (in mM): 140 K-gluconic acid, 1 $CaCl_2$*$6H_2O$, 10 EGTA, 2 $MgCl_2$*$6H_2O$, 4 Na_2ATP, and 10 HEPES, pH 7.2, 300 mOsm. The intracellular whole-cell patch-clamp pipette solution contained biocytin (5 mg/ml, Sigma, B4261) to allow for post-hoc identification of the location and morphology of recorded neurons. Resting membrane potential was recorded immediately after breaking the seal and half-witdh of the action potential was measured 5 min after breaking the seal. Whole-cell current-clamp recordings were obtained from cortical neurons using either the visual-patch or blind patch technique and sampled at 20–100 kHz with a low-pass filter of 5–30 kHz. Recordings were performed with unpolished patch electrodes manufactured from borosilicate glass pipettes with filament (Science products). Patch-clamp experiments were performed with a patch-clamp amplifier (Multiclamp 200B) or a NPI Bridge Amplifier (Model BA-01X), a digitizing interface (Digidata 1440A or 1550A Digidata), and pClamp 10 software (Molecular Devices). The junction potential was calculated and subtracted offline to correct the membrane potential in current clamp mode. After recording, the slices were placed in neutral buffered 4% PFA solution at 4˚C overnight for fixation followed by three rinses in phosphate buffered saline (PBS) and by subsequent immunocytochemical staining procedures. The patched neurons were filled with the intracellular solution for a minimum of 10 min during the electrophysiological recordings allowing full morphological reconstruction. Subsequently, the fixed slices were exposed to streptavidin-Cy3 (1:100 of 1 mg/ml, Sigma, S6402) for 3 hr at room temperature and mounted on glass coverslips for visualization of the biocytin filled neurons (***Figure 1A***).

Viral transduction

AAV-retro(AAVrg)-hSynapsin-GFP-virus was purchased from Addgene (pAAV-hSyn-GFP was a gift from Bryan Roth - Addgene viral prep # 50465-AAVrg) and had a titer of 10^{12}. The virus was injected in multiple areas of the slice using a picospritzer (PDES-O2DX/NPI electronics, Tamm, Germany) at 3–5 days *in vitro* (DIV).

3D-Reconstruction of neurons

To reconstruct the full morphology of biocytin filled (***Figure 1A***) or GFP-labeled neurons (***Figure 2***), imaging was performed on a Leica TCS SP8 confocal laser-scanning microscope (Bensheim, Germany) using a 40x/1.3NA oil-immersion objective. Z-stack tile scans of the whole culture slice were acquired. The Cy3 fluorescence was excited at 548 nm using a tunable white light laser and emission was detected between 555 nm and 615 nm. The GFP signal was excited at 488 nm and emission was detected between 493 nm and 530 nm. For a precise three-dimensional reconstruction of the dendritic segments, the slices were imaged at a voxel size of 0.2481 × 0.2481×0.7 µm. The tile scans were stitched using ImageJ and the plugin grid-stitching (***Preibisch et al., 2009***). Filament reconstruction was performed using Imaris x64 9.0.2 software (RRID:SCR_007370), enabling precise quantification of dendritic length. The number of dendrites radiating from the soma of one neuron was

thoroughly checked for misalignment and false connections using the rotating 3D fluorescence intensity image in Imaris. The apical and the basal dendrites as well as the axons were identified manually and labeled, represented in the colors red (apical dendrites), blue (basal dendrites) and magenta (axons) and then quantified separately for total length.

Spine morphology

To determine the spine morphology of the neurons we performed high-resolution scans of five selected dendritic areas of the cells. We always chose three areas of the apical dendrites (***Figure 7A***, red boxes, red boxes) and two of the basal dendrites (***Figure 7A***, blue boxes, blue boxes). The voxel size for all analyzed stacks was 0.071 × 0.071×0.1998 µm and a z-stack of 10–15 µm was taken. These stacks were further analyzed using NeuronStudio software (***Rodriguez et al., 2008***). Of each analyzed area the spines were detected using the NeuronStudio algorithm (with a minimal cutoff of 0.4 µm and maximum cutoff of 6 µm for the spine size) and subsequently manually corrected if necessary. We calculated the spine density (total number of spines/length of the analyzed dendrite), the mean value of spine length and spine head diameter of each of the five selected dendritic areas. Values of all 5 areas per neuron were averaged and plotted against the "DIV" or against the "distance to pia" such that every data point in ***Figure 7E*** and ***Figure 7F*** corresponds to the average of the 5 areas per neuron. We have chosen this method to minimize potential measuring errors for each analyzed neuron.

Immunocytochemistry

For ICC, slices were incubated for 20 min in 50% methanol with 1% H_2O_2 to quench endogenous peroxidases. The slices were rinsed with PBS supplemented with 0.2% Triton X-100 (T-PBS) and blocked for 1 hr in T-PBS, 0.4 g merthiolate and 1% normal goat serum before adding primary antibodies in respective dilutions for 2–3 days at 4˚C. Slices were rinsed three times in T-PBS and then incubated in Alexa-fluorophore-conjugated secondary antibodies in T-PBS, 0.4 g merthiolate and 1% normal goat serum overnight at 4˚C. Slices were rinsed three times with T-PBS before staining with DAPI (1:5000 in PBS for 2–5 min). After four final rinses (3x PBS, 1x Ampuwa water), slices were mounted in Fluoromount G (SouthernBiotech) on glass slides. Primary and secondary antibodies were used at the following dilutions: mouse anti-Satb2 for excitatory neurons (1:100, Abcam, ab51502, RRID:AB_882455), chicken anti-MAP2 for the somatodendritic compartment of neurons (1:500, Abcam, ab5392, RRID:AB_2138153); chicken anti-Calretinin (1:500, Merck, AB1550, RRID:AB_90764); goat anti-mouse IgG Alexa 568 (1:500, Thermo Fisher, A-11004, RRID:AB_2534072); goat anti-chicken Alexa 488 (1:500, Thermo Fisher, A-11039, RRID:AB_142924) and donkey anti-goat Alexa 568 (1:500, Thermo Fisher, A-11057, RRID:AB_142581).

Cell counts and quantification

Images for Satb2 and Map2 quantification were taken with a Leica TCS SP8 confocal laser-scanning microscope (Bensheim, Germany) using a 40x/1.3NA oil-immersion objective. We obtained images of four to six areas in layers 2/3 (each area290 µm x 290 µm in size) per slice and analyzed maximum projections of 2.1 µm stacks. The absolute number of cells per area was normalized to 100 µm X 100 µm (10000 μm^2) and plotted. The quantification was performed for the same dataset in a blinded manner by three independent researchers.

Two-photon live cell imaging and sholl analysis

Slice cultures with GFP-positive neurons were imaged on an upright Zeiss LSM 880 NLO microscope, using an IR-optimized water-immersion x20 Objective (W Plan-Apochromat x20/1.0, Carl Zeiss, Jena). A MaiTai eHP (Spectra Physics) laser was used for two-photon excitation, tuned at 920 nm for exciting the GFP fluorescence. Emission was collected using the Non-Descanned GaAsP detection path, with a 520/50 emission filter. A 3D tile scan of a larger area of the culture was setup in the ZEN black software (Carl Zeiss, Jena), collecting images at a resolution of 0.415 × 0.415×1.2 µm per voxel. The above configuration was optimized for highest light throughput, ensuring the minimum possible laser intensity, in order to avoid thermal damage to the neurons. For 24 hr time-lapse imaging stacks of images were acquired every 30 min at a resolution of 0.208 × 0.208×0.640 µm per voxel. Five areas were marked in the experiment designer of the Zen black software so that the

system could navigate to all positions and image predefined areas in an automated manner. The experiment designer was setup to repeat this chain of acquisitions every 30 min.

To guarantee a stable environment while imaging, the culture inserts were placed in a custom-made chamber, designed to securely hold the insert at the same orientation and position, submerged in aCSF. Prewarmed, carbogenated aCSF constantly perfused the chamber. The customized stage-top incubator which housed the customized culture insert holder was kept at 37˚C and was filled with humidified carbogen.

All movies acquired with two-photon live-cell imaging were deconvolved with Huygens Essential (Scientific Volume Imaging B.V., Hilversum) before further processing. After deconvolution, images and movies were analyzed using Imaris (Bitplane, Belfast, RRID:SCR_007370). The filaments tool of the Imaris software was used to semi-automatically trace the dendrites and spines of the neurons. The total length of the filaments was automatically calculated in Imaris. For the sholl analysis of the traced dendrites in Imaris, the sholl radius was set to 2 µm. The maximum radius of the sholl analysis was defined as the maximum radius in the field of view at which an intersection of the filament with one of the sholl circles could still be detected.

Analysis and statistics

Statistical analyses were performed with Graph Pad Prism seven using paired or unpaired Mann Whitney test to compare two groups and Kruskal-Wallis test with Dunn's Multiple comparisons test for three groups. Mean values ± standard error of the mean (SEM) are presented in text and Figures, unless specified differently. Linear regressions were analyzed for the correlations between properties and the days *in vitro* and the distance to the pia (DTP).

Acknowledgements

The authors thank all patients for participating in this study. We thank Evelyn Dubois, Elke Stransky and Christina Tomschitz for their assistance with collecting hCSF samples. The study was supported by the German Research Foundation (KO-4877/2–1, WE4896/3-1 and WE4896/4-1; FOR 2715) and by the ministry of rural affairs and consumer protection (award to NS supporting the replacement, refinement and reduction of animal experiments). NS was in part supported by an intramural research funding program of the Faculty of Medicine, University of Tübingen (Fortüne 2381-0-0). TVW was supported by an intramural Clinician Scientist fellowship granted by the Faculty of Medicine, University of Tübingen (419-0-0).

Additional information

Funding

Funder	Grant reference number	Author
Eberhard Karls Universität Tübingen	Fortüne 2381-0-0	Niklas Schwarz
German Research Foundation	KO-4877/2-1	Henner Koch
German Research Foundation	WE4896/3-1	Yvonne G Weber
Eberhard Karls Universität Tübingen	Clinician Scientist fellowship 419-0-0	Thomas V Wuttke
German Research Foundation	FOR 2715	Ulrike BS Hedrich Albert J Becker
German Research Foundation	WE4896/4-1	Yvonne G Weber

The funders had no role in study design, data collection and interpretation, or the decision to submit the work for publication.

Author contributions

Niklas Schwarz, Henner Koch, Conceptualization, Data curation, Formal analysis, Funding acquisition, Investigation, Methodology, Project administration, Resources, Software, Supervision,

Validation, Visualization, Writing - original draft, Writing - review and editing; Betül Uysal, Jacqueline C Bahr, Formal analysis, Investigation; Marc Welzer, Nikolas Layer, Heidi Löffler, Kornelijus Stanaitis, Harshad PA, Investigation; Yvonne G Weber, Conceptualization, Funding acquisition, Resources; Ulrike BS Hedrich, Conceptualization, Investigation, Visualization, Writing - original draft; Jürgen B Honegger, Resources; Angelos Skodras, Investigation, Software; Albert J Becker, Writing - original draft; Thomas V Wuttke, Conceptualization, Funding acquisition, Methodology, Project administration, Resources, Supervision, Validation, Writing - original draft, Writing - review & editing

Author ORCIDs
Niklas Schwarz https://orcid.org/0000-0002-4064-3073
Thomas V Wuttke https://orcid.org/0000-0001-5655-8490
Henner Koch https://orcid.org/0000-0002-6883-3071

Ethics
Human subjects: Approval (# 338/2016A) of the ethics committee of the University of Tübingen as well as written informed consent was obtained from all patients, allowing spare tissue from resective surgery to be included in the study.

Decision letter and Author response
Decision letter https://doi.org/10.7554/eLife.48417.020
Author response https://doi.org/10.7554/eLife.48417.021

Additional files

Supplementary files
- Transparent reporting form

DOI: https://doi.org/10.7554/eLife.48417.016

Data availability
Reconstructions of GFP labeled and Biocytin filled neurons and spine details of the analyzed cells have been deposited in: https://doi.org/10.5061/dryad.s5g2712.

The following dataset was generated:

Author(s)	Year	Dataset title	Dataset URL	Database and Identifier
Niklas Schwarz, Betül Uysal, Marc Welzer, Jacqueline Bahr, Nikolas Layer, Heidi Löffler, Kornelijus Stanaitis, Harshad PA, Yvonne G Weber, Ulrike BS Hedrich, Jürgen B Honegger, Angelos Skodras, Albert J Becker, Thomas V Wuttke, Henner Koch	2019	Reconstructions of GFP labeled and Biocytin filled neurons and spine details of the analyzed cells	https://doi.org/10.5061/dryad.s5g2712	Dryad Digital Repository, 10.5061/dryad.s5g2712

References

Andersson M, Avaliani N, Svensson A, Wickham J, Pinborg LH, Jespersen B, Christiansen SH, Bengzon J, Woldbye DP, Kokaia M. 2016. Optogenetic control of human neurons in organotypic brain cultures. *Scientific Reports* **6**:24818. DOI: https://doi.org/10.1038/srep24818, PMID: 27098488

Anton-Sanchez L, Larrañaga P, Benavides-Piccione R, Fernaud-Espinosa I, DeFelipe J, Bielza C. 2017. Three-dimensional spatial modeling of spines along dendritic networks in human cortical pyramidal neurons. *PLOS ONE* **12**:e0180400. DOI: https://doi.org/10.1371/journal.pone.0180400, PMID: 28662210

Ascoli GA, Alonso-Nanclares L, Anderson SA, Barrionuevo G, Benavides-Piccione R, Burkhalter A, Buzsáki G, Cauli B, Defelipe J, Fairén A, Feldmeyer D, Fishell G, Fregnac Y, Freund TF, Gardner D, Gardner EP, Goldberg

JH, Helmstaedter M, Hestrin S, Karube F, et al. 2008. Petilla terminology: nomenclature of features of GABAergic interneurons of the cerebral cortex. *Nature Reviews. Neuroscience* **9**:557–568. DOI: https://doi.org/10.1038/nrn2402, PMID: 18568015

Beck H, Goussakov IV, Lie A, Helmstaedter C, Elger CE. 2000. Synaptic plasticity in the human dentate gyrus. *The Journal of Neuroscience* **20**:7080–7086. DOI: https://doi.org/10.1523/JNEUROSCI.20-18-07080.2000, PMID: 10995855

Bernard C, Anderson A, Becker A, Poolos NP, Beck H, Johnston D. 2004. Acquired Dendritic Channelopathy in Temporal Lobe Epilepsy. *Science.* **305**:532–535. DOI: https://doi.org/10.1126/science.1097065

Bjorefeldt A, Andreasson U, Daborg J, Riebe I, Wasling P, Zetterberg H, Hanse E. 2015. Human cerebrospinal fluid increases the excitability of pyramidal neurons in the *in vitro* brain slice. *The Journal of Physiology* **593**: 231–243. DOI: https://doi.org/10.1113/jphysiol.2014.284711, PMID: 25556798

Boldog E, Bakken TE, Hodge RD, Novotny M, Aevermann BD, Baka J, Bordé S, Close JL, Diez-Fuertes F, Ding SL, Faragó N, Kocsis ÁK, Kovács B, Maltzer Z, McCorrison JM, Miller JA, Molnár G, Oláh G, Ozsvár A, Rózsa M, et al. 2018. Transcriptomic and morphophysiological evidence for a specialized human cortical GABAergic cell type. *Nature Neuroscience* **21**:1185–1195. DOI: https://doi.org/10.1038/s41593-018-0205-2, PMID: 30150662

Branco T, Häusser M. 2011. Synaptic integration gradients in single cortical pyramidal cell dendrites. *Neuron* **69**: 885–892. DOI: https://doi.org/10.1016/j.neuron.2011.02.006, PMID: 21382549

Britanova O, de Juan Romero C, Cheung A, Kwan KY, Schwark M, Gyorgy A, Vogel T, Akopov S, Mitkovski M, Agoston D, Sestan N, Molnár Z, Tarabykin V. 2008. Satb2 is a postmitotic determinant for upper-layer neuron specification in the neocortex. *Neuron* **57**:378–392. DOI: https://doi.org/10.1016/j.neuron.2007.12.028, PMID: 18255031

DeFelipe J, Alonso-Nanclares L, Arellano JI. 2002. Microstructure of the neocortex: comparative aspects. *Journal of Neurocytology* **31**:299–316. PMID: 12815249

Dimidschstein J, Chen Q, Tremblay R, Rogers SL, Saldi GA, Guo L, Xu Q, Liu R, Lu C, Chu J, Grimley JS, Krostag AR, Kaykas A, Avery MC, Rashid MS, Baek M, Jacob AL, Smith GB, Wilson DE, Kosche G, et al. 2016. A viral strategy for targeting and manipulating interneurons across vertebrate species. *Nature Neuroscience* **19**:1743–1749. DOI: https://doi.org/10.1038/nn.4430, PMID: 27798629

Elston GN, Benavides-Piccione R, DeFelipe J. 2001. The pyramidal cell in cognition: a comparative study in human and monkey. *The Journal of Neuroscience* **21**:RC163. DOI: https://doi.org/10.1523/JNEUROSCI.21-17-j0002.2001, PMID: 11511694

Elston GN, DeFelipe J. 2002. Spine distribution in cortical pyramidal cells: a common organizational principle across species. *Progress in Brain Research* **136**:109–133. PMID: 12143375

Elston GN, Fujita I. 2014. Pyramidal cell development: postnatal spinogenesis, dendritic growth, axon growth, and electrophysiology. *Frontiers in Neuroanatomy* **8**:78. DOI: https://doi.org/10.3389/fnana.2014.00078, PMID: 25161611

Eugène E, Cluzeaud F, Cifuentes-Diaz C, Fricker D, Le Duigou C, Clemenceau S, Baulac M, Poncer JC, Miles R. 2014. An organotypic brain slice preparation from adult patients with temporal lobe epilepsy. *Journal of Neuroscience Methods* **235**:234–244. DOI: https://doi.org/10.1016/j.jneumeth.2014.07.009, PMID: 25064188

Eyal G, Verhoog MB, Testa-Silva G, Deitcher Y, Lodder JC, Benavides-Piccione R, Morales J, DeFelipe J, de Kock CP, Mansvelder HD, Segev I. 2016. Unique membrane properties and enhanced signal processing in human neocortical neurons. *eLife* **5**:e16553. DOI: https://doi.org/10.7554/eLife.16553, PMID: 27710767

Goriounova NA, Heyer DB, Wilbers R, Verhoog MB, Giugliano M, Verbist C, Obermayer J, Kerkhofs A, Smeding H, Verberne M, Idema S, Baayen JC, Pieneman AW, de Kock CP, Klein M, Mansvelder HD. 2018. Large and fast human pyramidal neurons associate with intelligence. *eLife* **7**:e41714. DOI: https://doi.org/10.7554/eLife.41714, PMID: 30561325

Hendrie PC, Russell DW. 2005. Gene targeting with viral vectors. *Molecular Therapy* **12**:9–17. DOI: https://doi.org/10.1016/j.ymthe.2005.04.006, PMID: 15932801

Hodge RD, Bakken TE, Miller JA, Smith KA, Barkan ER, Graybuck LT, Close JL, Long B, Johansen N, Penn O, Yao Z, Eggermont J, Höllt T, Levi BP, Shehata SI, Aevermann B, Beller A, Bertagnolli D, Brouner K, Casper T, et al. 2019. Conserved cell types with divergent features in human versus mouse cortex. *Nature* **573**:61–68. DOI: https://doi.org/10.1038/s41586-019-1506-7, PMID: 31435019

Holtmaat A, Svoboda K. 2009. Experience-dependent structural synaptic plasticity in the mammalian brain. *Nature Reviews Neuroscience* **10**:647–658. DOI: https://doi.org/10.1038/nrn2699, PMID: 19693029

Howard DB, Powers K, Wang Y, Harvey BK. 2008. Tropism and toxicity of adeno-associated viral vector serotypes 1, 2, 5, 6, 7, 8, and 9 in rat neurons and Glia in vitro. *Virology* **372**:24–34. DOI: https://doi.org/10.1016/j.virol.2007.10.007, PMID: 18035387

Huang Y, Song N-N, Lan W, Hu L, Su C-J, Ding Y-Q, Zhang L. 2013. Expression of transcription factor Satb2 in adult mouse brain. *The Anatomical Record* **296**:452–461. DOI: https://doi.org/10.1002/ar.22656

Huttenlocher PR, de Courten C, Garey LJ, Van der Loos H. 1982. Synaptogenesis in human visual cortex–evidence for synapse elimination during normal development. *Neuroscience Letters* **33**:247–252. DOI: https://doi.org/10.1016/0304-3940(82)90379-2, PMID: 7162689

Kalmbach BE, Buchin A, Long B, Close J, Nandi A, Miller JA, Bakken TE, Hodge RD, Chong P, de Frates R, Dai K, Maltzer Z, Nicovich PR, Keene CD, Silbergeld DL, Gwinn RP, Cobbs C, Ko AL, Ojemann JG, Koch C, et al. 2018. h-Channels contribute to divergent intrinsic membrane properties of supragranular pyramidal neurons in human versus mouse cerebral cortex. *Neuron* **100**:1194–1208. DOI: https://doi.org/10.1016/j.neuron.2018.10.012, PMID: 30392798

Kerkhofs A, Xavier AC, da Silva BS, Canas PM, Idema S, Baayen JC, Ferreira SG, Cunha RA, Mansvelder HD. 2017. Caffeine controls glutamatergic synaptic transmission and pyramidal neuron excitability in human neocortex. *Frontiers in Pharmacology* **8**:899. DOI: https://doi.org/10.3389/fphar.2017.00899, PMID: 29354052

Kim CK, Adhikari A, Deisseroth K. 2017. Integration of optogenetics with complementary methodologies in systems neuroscience. *Nature Reviews Neuroscience* **18**:222–235. DOI: https://doi.org/10.1038/nrn.2017.15, PMID: 28303019

Lendvai B, Stern EA, Chen B, Svoboda K. 2000. Experience-dependent plasticity of dendritic spines in the developing rat barrel cortex in vivo. *Nature* **404**:876–881. DOI: https://doi.org/10.1038/35009107, PMID: 10786794

Madisen L, Mao T, Koch H, Zhuo JM, Berenyi A, Fujisawa S, Hsu YW, Garcia AJ, Gu X, Zanella S, Kidney J, Gu H, Mao Y, Hooks BM, Boyden ES, Buzsáki G, Ramirez JM, Jones AR, Svoboda K, Han X, et al. 2012. A toolbox of Cre-dependent optogenetic transgenic mice for light-induced activation and silencing. *Nature Neuroscience* **15**:793–802. DOI: https://doi.org/10.1038/nn.3078, PMID: 22446880

Marcuccilli CJ, Tryba AK, van Drongelen W, Koch H, Viemari JC, Peña-Ortega F, Doren EL, Pytel P, Chevalier M, Mrejeru A, Kohrman MH, Lasky RE, Lew SM, Frim DM, Ramirez JM. 2010. Neuronal bursting properties in focal and parafocal regions in pediatric neocortical epilepsy stratified by histology. *Journal of Clinical Neurophysiology* **27**:387–397. DOI: https://doi.org/10.1097/WNP.0b013e3181fe06d8, PMID: 21076335

Mohan H, Verhoog MB, Doreswamy KK, Eyal G, Aardse R, Lodder BN, Goriounova NA, Asamoah B, B Brakspear AB, Groot C, van der Sluis S, Testa-Silva G, Obermayer J, Boudewijns ZS, Narayanan RT, Baayen JC, Segev I, Mansvelder HD, de Kock CP. 2015. Dendritic and axonal architecture of individual pyramidal neurons across layers of adult human neocortex. *Cerebral Cortex* **25**:4839–4853. DOI: https://doi.org/10.1093/cercor/bhv188, PMID: 26318661

Napoli A, Obeid I. 2016. Comparative analysis of human and rodent brain primary neuronal culture spontaneous activity using Micro-Electrode array technology. *Journal of Cellular Biochemistry* **117**:559–565. DOI: https://doi.org/10.1002/jcb.25312, PMID: 26284690

O'Connor WM, Davidson BL, Kaplitt MG, Abbey MV, During MJ, Leone P, Langer D, O'Connor MJ, Freese A. 1997. Adenovirus vector-mediated gene transfer into human epileptogenic brain slices: prospects for gene therapy in epilepsy. *Experimental Neurology* **148**:167–178. DOI: https://doi.org/10.1006/exnr.1997.6658, PMID: 9398459

Preibisch S, Saalfeld S, Tomancak P. 2009. Globally optimal stitching of tiled 3D microscopic image acquisitions. *Bioinformatics* **25**:1463–1465. DOI: https://doi.org/10.1093/bioinformatics/btp184, PMID: 19346324

Rao A, Craig AM. 1997. Activity regulates the synaptic localization of the NMDA receptor in hippocampal neurons. *Neuron* **19**:801–812. DOI: https://doi.org/10.1016/S0896-6273(00)80962-9, PMID: 9354327

Rodriguez A, Ehlenberger DB, Dickstein DL, Hof PR, Wearne SL. 2008. Automated three-dimensional detection and shape classification of dendritic spines from fluorescence microscopy images. *PLOS ONE* **3**:e1997. DOI: https://doi.org/10.1371/journal.pone.0001997, PMID: 18431482

Schwarz N, Hedrich UBS, Schwarz H, PA H, Dammeier N, Auffenberg E, Bedogni F, Honegger JB, Lerche H, Wuttke TV, Koch H. 2017. Human cerebrospinal fluid promotes long-term neuronal viability and network function in human neocortical organotypic brain slice cultures. *Scientific Reports* **7**:12249. DOI: https://doi.org/10.1038/s41598-017-12527-9, PMID: 28947761

Shepherd GM, Rowe TB. 2017. Neocortical lamination: insights from neuron types and evolutionary precursors. *Frontiers in Neuroanatomy* **11**:100. DOI: https://doi.org/10.3389/fnana.2017.00100, PMID: 29163073

Somogyi P, Tamás G, Lujan R, Buhl EH. 1998. Salient features of synaptic organisation in the cerebral cortex. *Brain Research. Brain Research Reviews* **26**:113–135. PMID: 9651498

Song AJ, Palmiter RD. 2018. Detecting and avoiding problems when using the Cre-lox system. *Trends in Genetics* **34**:333–340. DOI: https://doi.org/10.1016/j.tig.2017.12.008, PMID: 29336844

Ting JT, Kalmbach B, Chong P, de Frates R, Keene CD, Gwinn RP, Cobbs C, Ko AL, Ojemann JG, Ellenbogen RG, Koch C, Lein E. 2018. A robust ex vivo experimental platform for molecular-genetic dissection of adult human neocortical cell types and circuits. *Scientific Reports* **8**:e8407. DOI: https://doi.org/10.1038/s41598-018-26803-9

Trachtenberg JT, Chen BE, Knott GW, Feng G, Sanes JR, Welker E, Svoboda K. 2002. Long-term in vivo imaging of experience-dependent synaptic plasticity in adult cortex. *Nature* **420**:788–794. DOI: https://doi.org/10.1038/nature01273, PMID: 12490942

Verhoog MB, Goriounova NA, Obermayer J, Stroeder J, Hjorth JJ, Testa-Silva G, Baayen JC, de Kock CP, Meredith RM, Mansvelder HD. 2013. Mechanisms underlying the rules for associative plasticity at adult human neocortical synapses. *The Journal of Neuroscience* **33**:17197–17208. DOI: https://doi.org/10.1523/JNEUROSCI.3158-13.2013, PMID: 24155324

Verwer RW, Dubelaar EJ, Hermens WT, Swaab DF. 2002. Tissue cultures from adult human postmortem subcortical brain Areas. *Journal of Cellular and Molecular Medicine* **6**:429–432. DOI: https://doi.org/10.1111/j.1582-4934.2002.tb00522.x, PMID: 12417060

Wang B, Yin L, Zou X, Ye M, Liu Y, He T, Deng S, Jiang Y, Zheng R, Wang Y, Yang M, Lu H, Wu S, Shu Y. 2015. A subtype of inhibitory interneuron with intrinsic persistent activity in human and monkey neocortex. *Cell Reports* **10**:1450–1458. DOI: https://doi.org/10.1016/j.celrep.2015.02.018, PMID: 25753411

Wickham J, Brödjegård NG, Vighagen R, Pinborg LH, Bengzon J, Woldbye DPD, Kokaia M, Andersson M. 2018. Prolonged life of human acute hippocampal slices from temporal lobe epilepsy surgery. *Scientific Reports* **8**:e4158. DOI: https://doi.org/10.1038/s41598-018-22554-9

Yuste R, Bonhoeffer T. 2004. Genesis of dendritic spines: insights from ultrastructural and imaging studies. *Nature Reviews Neuroscience* **5**:24–34. DOI: https://doi.org/10.1038/nrn1300, PMID: 14708001

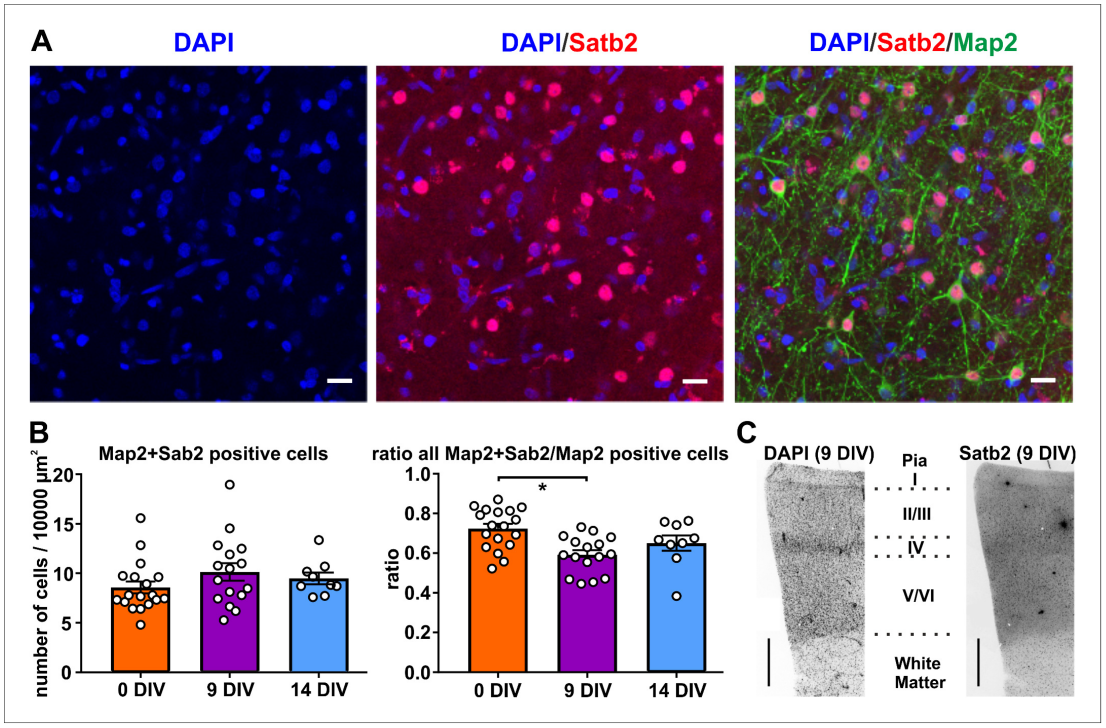


Figure 1—figure supplement 1. Satb2 positive neurons in human brain slice cultures. (**A**) High-resolution image of a confocal z-stack collapsed into one optical plane processed for ICC of the glutamatergic neuronal marker Satb2 and neuron-specific cytoskeletal protein Map2 in layers 2/3, scale bar 20 µm. (**B**) Quantification of Map2/Satb2 double positive neurons normalized to 100 µm x 100 µm areas and the plot of the ratio of Map2+Satb2/Map2 positive cells. (**C**) The slices contained all six cortical layers, shown are representative examples with staining for DAPI and Satb2, scale bar 500 µm.
DOI: https://doi.org/10.7554/eLife.48417.004

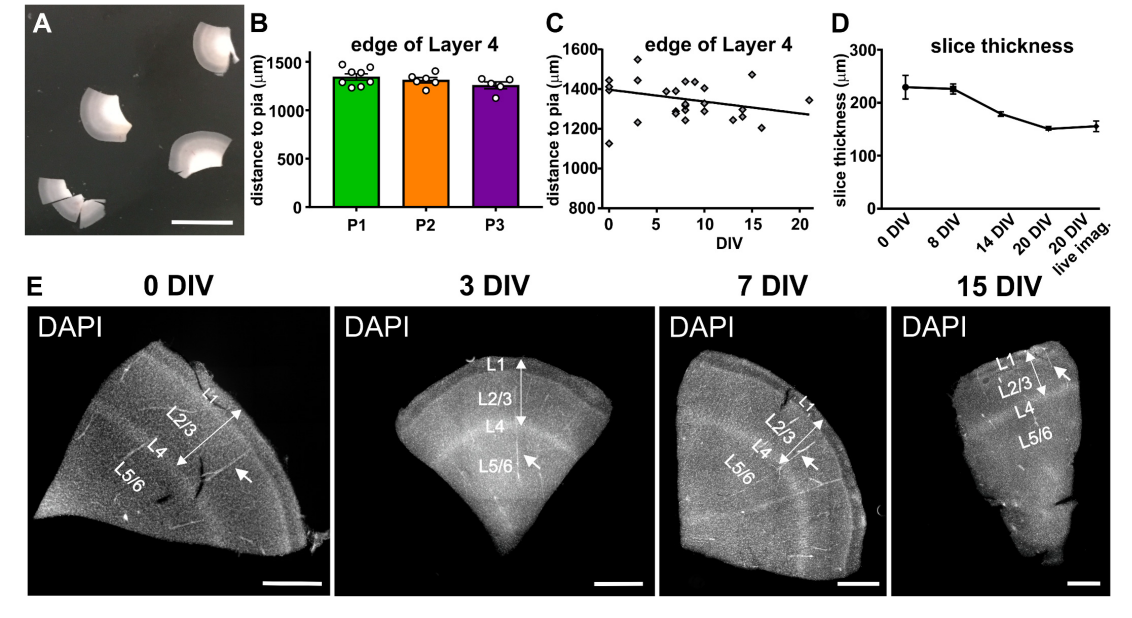


Figure 1—figure supplement 2. Stability of gross structural features of cortical slices between surgeries and over time in culture. (**A**) On the day of the surgery slices are prepared from tissue blocks and carefully cut into even slices containing all six layers, scale bar 1 cm. (**B**) Comparison of slices originating from three independent surgeries of temporal cortex (P1-3) show a comparable distance from pia to the edge of layer 4, which was clearly visible upon DAPI staining. (**C**) This distance did not change significantly over time in culture up to the endpoint of analysis at 20 DIV. (**D**) Slice thickness slightly decreased throughout the analyzed three-week period in culture. (**E**) Examples of DAPI stainings of slices of the same surgery at different time points in culture (0 DIV - 15 DIV). Cortical thickness from pia to the edge of layer 4 (double arrow). Note blood vessels (arrows) running parallel to the slicing plane, indicating that sections indeed were prepared perpendicular to the cortical surface, scale bar 1000 µm.

DOI: https://doi.org/10.7554/eLife.48417.003

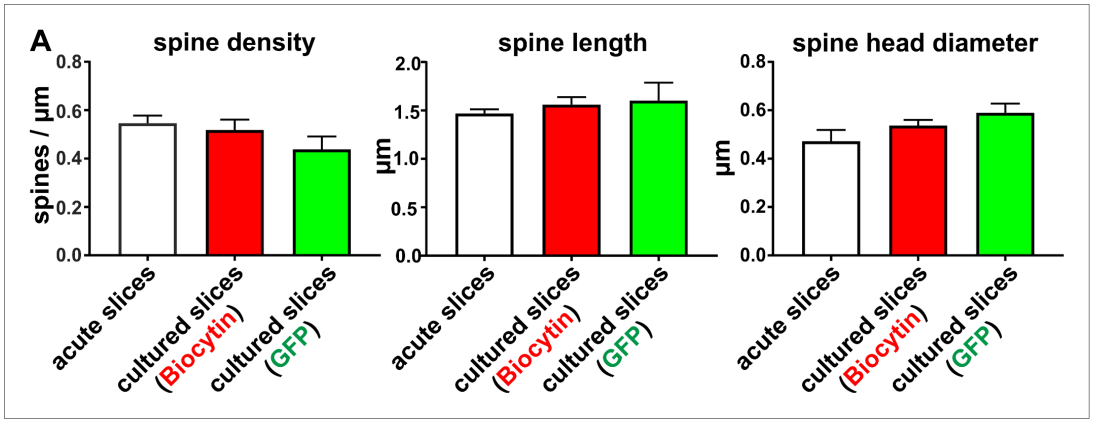


Figure 7—figure supplement 1. Analysis of mean values of spine density, length and head diameter of biocytin filled and virally transduced GFP positive pyramidal neurons. Mean values for spine density, spine length and spine head diameter of pyramidal neurons were not significantly different in acute slices (0 DIV) compared to cultured slices (2–14 DIV).

DOI: https://doi.org/10.7554/eLife.48417.011

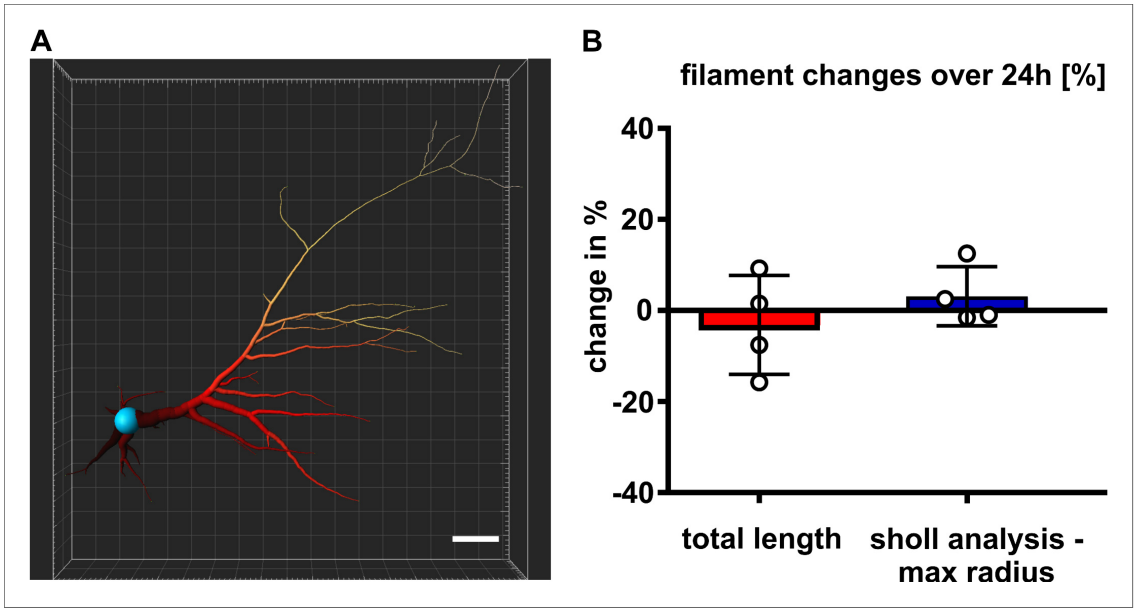


Figure 9—figure supplement 1. Filament measurements reveal stability over the time of 24 hr. (**A**) Filament reconstruction for quantification, scale bar 20 µm. (**B**) Slight changes of the filament total length and maximal sholl radius at 24 hr in % of the measurement at 0 hr. Mean values ± standard deviation (SD).

DOI: https://doi.org/10.7554/eLife.48417.014

Chapter 6: A first application example: Virotherapy using oncolytic viruses in human organotypic brain slice cultures

EBERHARD KARLS
UNIVERSITÄT
TÜBINGEN

Medizinische Fakultät

Declaration of contributions:

Herewith I, Niklas Schwarz declare, that I have contributed to the following publication as stated:

Czolk R, Schwarz N, Koch H, Schötterl S, Wuttke TV, Holm PS, Huber SM, Naumann U, In brain tumor initiating cells, irradiation enhances the therapeutic effect of the oncolytic adenovirus XVir-N-31. Int J Mol Med. 2019 Jul 31. doi: 10.3892/ijmm.2019.4296.

The authors contributed to the publications as indicated in the following table (indicated in %):

Contribution	Rebecca Czolk	Niklas Schwarz	Henner Koch	Sonja Schötterl	Thomas V. Wuttke	Per S. Holm	Stephan M. Huber	Ulrike Naumann
Research concept								100%
Project administration								100%
Funding acquisition								100%
Selection of methods	40%	20%	10%	5%		10%	10%	5%
Recruitment of patients		33%	33%		34%			
Data acquisition	40%			20%				40%
Data analysis	30%	5%	5%	10%		10%	10%	30%
Visualization	10%	30%	10%	10%		10%		30%
Interpretation of results	20%	5%	5%	5%	5%	10%	5%	45%
Preparation of Manuscript		5%	5%			5%	5%	80%

Signature of the doctoral candidate:

[redacted]

As supervisor, I agree with the declarations by the candidate:

As corresponding author, agree with the declarations by the candidate:

As co-authors, we agree to the declarations above:

[redacted]

[Rebecca Czolk] [Henner Koch] [Sonja Schötterl] [Thomas V. Wuttke]

Klinik und Poliklinik für Urologie
Klinikum rechts der Isar

[redacted]

[Per S. Holm] [Stephan M. Huber] [Ulrike Naumann]

INTERNATIONAL JOURNAL OF MOLECULAR MEDICINE 44: 1484-1494, 2019

Irradiation enhances the therapeutic effect of the oncolytic adenovirus XVir-N-31 in brain tumor initiating cells

REBECCA CZOLK[1], NIKLAS SCHWARZ[2], HENNER KOCH[2], SONJA SCHÖTTERL[1], THOMAS V. WUTTKE[3], PER S. HOLM[4,5], STEPHAN M. HUBER[6] and ULRIKE NAUMANN[1]

[1]Department of Vascular Neurology, Laboratory for Molecular Neuro-Oncology, Hertie Institute for Clinical Brain Research, Tübingen NeuroCampus, University of Tübingen; [2]Department of Neurology and Epileptology, Hertie Institute for Clinical Brain Research, Tübingen NeuroCampus, University of Tübingen; [3]Department of Neurosurgery, University Hospital Tübingen, D-72076 Tübingen; [4]Department of Urology, Hospital 'Rechts der Isar', Technical University of Munich, D-81675 Munich; [5]XVir Therapeutics GmbH, D-80331 Munich; [6]Department of Radiation Oncology, University Hospital Tübingen, D-72076 Tübingen, Germany

Received February 25, 2019; Accepted July 19, 2019

DOI: 10.3892/ijmm.2019.4296

Abstract. Virotherapy using oncolytic viruses is an upcoming therapy strategy for cancer treatment. A variety of preclinical and clinical trials have indicated that adenoviruses may be used as potent agents in the treatment of a variety of cancers, and also for the treatment of brain tumors. In these studies, it has also been shown that oncovirotherapy is safe in terms of toxicity and side effects. In addition, previous studies have presented evidence for a significant role of oncovirotherapy in the activation of anti-tumor immune responses. With regard to oncolytic adenoviruses, we have demonstrated previously that the multifunctional protein Y-box binding protein-1 (YB-1) is a potent factor that was used to develop an YB-1-dependent oncolytic adenovirus (XVir-N-31). XVir-N-31 provides the opportunity for tumor-selective replication and exhibited marked oncolytic properties in a mouse glioma tumor model using therapy-resistant brain tumor initiating cells (BTICs). In a number of, but not all, patients with glioma, YB-1 is primarily located in the nucleus; this promotes XVir-N-31-replication and subsequently tumor cell lysis. However, in certain BTICs, only a small amount of YB-1 has been identified to be nuclear, and therefore virus replication is suboptimal. YB-1 in BTICs was demonstrated to be translocated into the nucleus following irradiation, which was accompanied by an enhancement in XVir-N-31 production. R28 glioma spheres implanted in living organotypic human brain slices exhibited a significantly delayed growth rate when pre-irradiated prior to XVir-N-31-infection as compared with single treatment methods. Consistent with the *in vitro* data, R28 glioma-bearing mice exhibited a prolonged mean and median survival following single tumor irradiation prior to intratumoral XVir-N-31 injection, compared with the single treatment methods. In conclusion, the present study demonstrated that in an experimental glioma model, tumor irradiation strengthened the effect of an XVir-N-31-based oncovirotherapy.

Correspondence to: Professor Ulrike Naumann, Department of Vascular Neurology, Laboratory for Molecular Neuro-Oncology, Hertie Institute for Clinical Brain Research, Tübingen NeuroCampus, University of Tübingen, Otfried-Müller-Straße 27, D-72076 Tübingen, Germany
E-mail: ulrike.naumann@uni-tuebingen.de

Abbreviations: BTIC, brain tumor initiating cell; EGF, epithelial growth factor; bFGF, basic fibroblast growth factor; Gy, Gray; IFU, infectious unit; MOI, multiplicity of infection; TMZ, temozolomide; YB-1, Y-box binding protein-1

Key words: glioma, oncolytic adenovirus, irradiation

Introduction

Glioblastoma (GBM) is the most malignant type of brain tumor in humans, and ~3,000 incident cases are diagnosed in Germany every year. Even with the highest level of care and use of novel therapeutic strategies, including tumor treating fields, the median survival of GBM patients is <20 months (1), and survival times have only marginally improved during the previous decade. Therefore, the development of novel therapeutic strategies is necessary. The high levels of malignancy of GBM is a result of its characteristic behaviors, including immunosuppression, and high levels of resistance towards irradiation, most chemotherapeutics and hypoxia. In addition, the tumor exhibits extensive neo-angiogenesis and grows invasively into the healthy brain tissue, making complete surgical resection impossible. Brain tumor initiating cells (BTICs), also termed glioma stem cell like cells, are an extremely resistant subpopulation of GBM cells that are considered to be responsible for tumor initiation and recurrence (2). It has also been demonstrated that temozolomide (TMZ), the standard chemotherapeutic drug used to treat GBM, leads to a dedifferentiation of GBM cells towards a more stem cell like phenotype (3). Involved in this processes are signaling

cascades including the PI3K/AKT and RAS/mitogen active protein kinase pathway, which are constitutively activated in GBM cells (4,5). A downstream substrate of these pathways is Y-box binding protein-1 (YB-1), a protein that exhibits both transcriptional and translational activity (6,7). In a number of tumor types, YB-1 expression is correlated with malignancy and progression (8-10). Cellular stress, for example by DNA damage induced by irradiation or chemotherapy, induces several post-translational YB-1 modifications including phosphorylation, acetylation or SUMOylation. These modifications are suggested to promote its nuclear translocation (11-14). Subsequently, nuclear YB-1 activates the expression of multidrug resistance protein/P-glycoproteins, classical mediators of resistance towards tumor treatment (15).

YB-1 is involved in the replication of therapeutic adenoviruses. The YB-1-dependent oncolytic adenovirus XVir-N-31 developed by this study group, also termed Ad-Delo3-RGD, replicates in tumor cells harboring nuclear YB-1 (16,17). In mice bearing R28-cell-derived glioma, a single intratumoral injection of XVir-N-31 prolonged survival rates (18). In ~60% of BTICs, YB-1 is upregulated and located primarily in the nucleus, which correlates with good virus replication and virus-mediated lysis of these cells. However, in ~40% of BTICs, YB-1 is only slightly expressed and located primarily in the cytoplasm, which mitigates virus replication 100-1,000-fold (18). We demonstrated previously that irradiation of established cancer cell lines leads to the translocation of YB-1 into the nucleus (6,19). Whether this also occurs in BTICs has not yet been identified. The present study evaluated whether a therapeutically relevant irradiation dose induced the translocation of YB-1 into the nucleus, promoted XVir-N-31 replication and subsequently oncolysis of BTICs *in vitro* and in a BTIC-derived mouse glioma model, with aim of developing a clinically relevant therapeutic strategy that combines irradiation and XVir-N-31-based oncovirotherapy for patients with recurrent glioma.

Materials and methods

Cell culture. BTIC R11, R28 and R49 cell lines, kindly provided by Dr C. Beier (University Hospital Regensburg, Center for Brain Tumors, Regensburg, Germany), were obtained from patients with primary GBM, as described previously (20), and were maintained as tumor spheres in stem cell-permissive Dulbecco's modified Eagle's medium/F12 medium (Merck KGaA) supplemented with human recombinant epidermal growth factor (EGF; BD Biosciences), human recombinant basic fibroblast growth factor (bFGF; R&D Systems Europe, Ltd.), human leukemia inhibitory factor (EMD Millipore; 20 ng/ml each) and 2% B27 supplement (Thermo Fisher Scientific, Inc.) for preservation of the original molecular characteristics of the tumors and to minimize differentiation. $R28^{mCherry}$ BTIC were generated by transduction of R28 cells with Lenti-mCherry (BioCat GmbH) followed by selection with puromycin. In brief, $4x10^5$ cells were infected with pre-made lentiviral particles encoding the fluorescent protein mCherry, at multiplicity of infection (MOI) 5. At 24 h post-infection, the medium was changed to fresh growth medium. At 48 h post-infection, puromycin (2 μg/ml; Merck KGaA) was added. Selected surviving cells were monitored for mCherry fluorescence at x50 magnification using a Zeiss Axio Imager Z1 fluorescence microscope (Carl Zeiss AG). For adenoviral infection, BTIC spheres were separated into single cells by trypsinization. Irradiation of BTICs and R28-tumor-sphere containing brain slices was performed in a Gammacell GC40 device [Nordion (Canada) Inc.].

Brain tissue slices and BTIC implantation. Written informed consent was obtained from all patients, allowing spare tissue from resective surgery to be included in the present study. Ethical approval was obtained from the Ethics Commission of Tübingen (approval no. 338/2016A). Tissues from healthy cortex areas were obtained during surgery of patients with epilepsy. Tissue preparation was performed according to previously published protocols (21). The tissue was carefully micro-dissected and resected with only minimal use of bipolar forceps to ensure tissue integrity, transferred into ice-cold artificial cerebrospinal fluid (aCSF: 110 mM choline chloride, 26 mM $NaHCO_3$, 10 mM D-glucose, 11.6 mM Na-ascorbate, 7 mM $MgCl_2$, 3.1 mM Na-pyruvate, 2.5 mM KCl, 1.25 mM NaH_2PO_4, 0.5 mM $CaCl_2$) equilibrated with carbogene (95% O_2, 5% CO_2) and immediately transported to the laboratory. Tissue was kept submerged in cool and carbogenated aCSF at all times. Following removal of the pia, tissue chunks were trimmed perpendicular to the cortical surface and 250-350 μm thick slices were prepared using a Microm HM 650V vibratome (Thermo Fisher Scientific, Inc.). Following slicing of the cortical tissue, slices were cut into several evenly sized pieces (~5.0x2.0 mm). Subsequently, the slices were transferred onto culture membranes of uncoated 30 mm Millicell-CM tissue culture inserts with 0.4 μm pores (Merck KGaA) and maintained in 6-well culture dishes (BD Biosciences). For long-term culture the plates were stored in at 37˚C, 5% CO_2 and 100% humidity in human CSF isolated from non-tumor patients, as described previously (22). Neurons were stained for 1 h at 37˚C with NeuO (0.25 μM; STEMCELL Technologies, Inc.). Then, the NeuO-containing CSF was removed and fresh CSF was added. To calculate the total amount of cells in a tissue slice, nuclei were stained with DAPI (Abcam), according to the manufacturer's protocol. Z-stacks were obtained microscopically using a Zeiss Axio Imager Z1 fluorescence microscope (Carl Zeiss AG) at x50 magnification. Nuclei were counted using the ImageJ software (version win63, Fiji) (23). For BTIC implantation into the tissue slices, $R28^{mCherry}$ spheres measuring 20-50 cells in size were used. Implantation was performed manually under microscopic observation using a 10 μl pipette tip. Slices and spheres were grown in human CSF supplemented with recombinant human bFGF and EGF (20 ng/ml each) for up to 23 days. The CSF was changed every 3rd day. Images were captured using Zeiss AxioVision (version SE64 Rel. 4.8.) and ZEN2 software (version 1.0; Carl Zeiss AG) on a Zeiss Axio Imager Z1 fluorescence microscope (Carl Zeiss AG) at x50 or x100 magnification. Quantification of tumor growth was performed using Image J software (version win64, Fiji) (23). If the tumor area reached the borders of the photographically detectable area, the highest measurable value was used for quantification.

Virus preparation and infection. XVir-N-31 was prepared, purified and titrated as previously described (18). The transduction

efficacy of R11, R28 and R49 BTICs was determined using a green fluorescent protein (GFP)-expressing adenovirus (Ad-RGD-GFP) that possessed the same RGD-motif-modified capsid as XVir-N-31. Infections were performed by adding the appropriate amount of virus into the growth medium. At 48 h post-infection, the cells were separated into single cells by trypzination, and analyzed for GFP expression by flow cytometry. Analyses were performed on a Cyan ADP flow cytometer (Beckman Coulter, Inc.) using the Summit software (version 4.3; Beckman Coulter, Inc.).

The MOI of BTICs using XVir-N-31 was optimized for each *in vitro* experiment. Infections were performed, as described above. After 72 h, cells and medium were collated and freeze-thaw lysates were prepared. Viral titers in these lysates were determined in 293 cells (Microbix Biosystems, Inc.) using the Adeno-Rapid-X-Titration kit (Takara Bio Europe SAS).

Western blot analysis. Total cell lysates were prepared as described previously (18). Nuclear and cytoplasmic protein lysates were prepared according to the protocol described by Toulany *et al* (6). Western blot analysis was performed as previously described (18). The following antibodies were used: Anti-YB-1 (1:1,000, cat. no. SC-101198, Santa Cruz Biotechnology, Inc.; or cat. no. 9744, Cell Signaling Technology, Inc.), anti-Histone H3 (1:10,000; cat. no. 39163; Active Motif), anti-calreticulin (1:5,000; cat. no. C7492; Sigma-Aldrich; Merck KGaA) and GAPDH (1:1,000; cat. no. MAB374; Merck KGaA). Immunoreactive specific proteins were detected using the CLARITY Western ECL substrate on a ChemiDoc MP imaging device using the ImageLab 5.1 software (all from Bio-Rad Laboratories, Inc.). For quantification of YB-1 expression, Image J (version win64; Fiji) (23) was used.

Intracranial tumor model. A total of $1x10^5$ R28 cells were implanted under peritoneally applied anesthesia (0.05 mg/kg fentanyl, 5 mg/ml midazolam and 0.5 mg/kg medetomin) (24) in the right striatum of 5-6 week old female Rj:NMRI $Foxn1^{nu}/Foxn1^{nu}$ nude mice (Janvier Labs) using a mouse stereotactic device with automated infusion pump (Stoelting Co) and a 10 μl Hamilton syringe (Type 701SN; Medchrom Medizinischer Chromatographiebedarf GmbH). Carprofen (5 mg/kg) was injected subcutaneously as an analgesic. Following surgery, anesthesia was antagonized by a subcutaneous injection of naloxon (1.2 mg/kg), flumazenil (0.5 mg/kg) and atipamezol (2.5 mg/kg). Mice were housed in IVC cages under standard pathogen-free conditions in the animal facility of the Hertie Institute (Tübingen, Germany). Animal health and behavior was monitored 3 times per week. At day 11 after tumor cell implantation, the 30 tumor cell-injected mice were randomly split into four groups (n=5-7 animals per group). A total of two groups were tumor-irradiated with 3 Gy (6 MV photons) using a LINAC linear accelerator as described previously (25) and received an intratumoral injection of either PBS (sham) or $1.5x10^8$ infectious units (IFU) XVir-N-31 the next day. One group received only XVir-N-31 and one group received an intracranial PBS injection (sham). The mice were euthanized by lethal CO_2 inhalation (10-30 volume percentage discharge of CO_2/per minute in their homing cage) at the onset of tumor-related symptoms. Human endpoints were defined according to the score sheet of regional council approval N12/14 and include the early onset of hemi- or paraplegia, paroxism, gait disorder, or loss of body weight of >19%. Euthanasia was confirmed by the lack of respiration and faded eye color. After 150 days the experiment was terminated by euthanasia of the surviving animals. All animal research was performed in accordance with the German Animal Welfare Act and its guidelines for the care and use of laboratory animals (https://www.gesetze-im-internet.de/tierschg/BJNR012770972.html) and was approved by the regional council of Tübingen (Regierungspräsidium Tübingen, approval no. N12/14).

Statistical analysis. For the *in vitro* assays, results were calculated as means ± standard deviation (SD) and compared using the one-way analysis of variance, followed by Bonferroni post-hoc correction for multiple testing using GraphPad Prism software (version 7.04; GraphPad Software, Inc.). If not otherwise indicated, the data were from at least 3 repeat experiments. For the *in vivo* assays, survival and mean or median survival times were analysed using the Kaplan-Meier method and compared using a log-rank test with JMP v13 software (SAS Institute Inc.), followed by Bonferroni correction for multiple testing. $P<0.05$ was considered to indicate a statistically significant difference.

Results

Irradiation induces YB-1 expression, its nuclear translocation and promotes XVir-N-31 production in BTICs. For established glioma and breast cancer cell lines, it has been demonstrated that irradiation leads to the translocation of YB-1 into the nucleus (6,19). The present study examined whether this was also true in TMZ-resistant BTICs (18). Using 3 different BTIC lines, we identified an upregulation of total YB-1 in the cells 8 h after irradiation, however to a different extent (Fig. 1). Using nuclear and cytoplasmic cell extracts, an additional, higher molecular weight YB-1 band ($YB\text{-}1^{60\ kD}$) was detected in the nuclear fraction of irradiated R28 and R49 cells, but not in non-irradiated control cells. In the R11 cells, this band was present in the nuclear extracts of both irradiated and non-irradiated cells. In R49 cells, an additional YB-1 protein variant ($YB\text{-}1^{65\ kD}$) was detected at a high level at 24 h after irradiation (Fig. 2A). As it has been established that under stress stimuli, like irradiation, the YB-1 protein will be post-translationally modified, all YB-1 bands were used to quantify the amount of nuclear YB-1 (Fig. 2B). Nuclear YB-1 levels were enhanced in both irradiated R28 and R49 cells. However, doses of only 2 Gy were sufficient to relocate YB-1 into the nucleus in R28 cells whilst doses of 6 Gy were required for nuclear translocation of YB-1 in R49 cells (Fig. 2 and data not shown). Notably, in R49 cells, $YB\text{-}1^{65\ kD}$, a highly post-translationally modified YB-1, was prominent at high levels and was not observed in R11 nor in R28 cells. No relevant elevated nuclear YB-1 levels and no $YB\text{-}1^{65\ kD}$ bands were observed in R11 cells, which harbor a high basal level of nuclear YB-1 in contrast to R28 and R49 cells (Fig. 2). R11 and R28 cells were also irradiated using a dose of 6 Gy. However, this irradiation dose did not increase the level of nuclear YB-1 in R11 nor in R28 cells, and even induced cell death in R28 cells (data not shown).

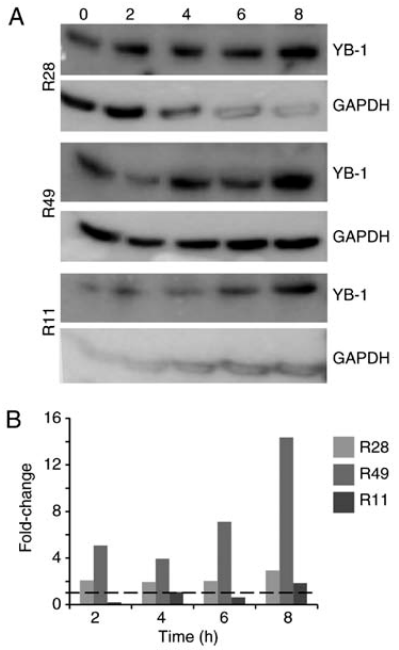


Figure 1. Irradiation induces YB-1 expression in brain tumor initiating cells. (A) R28, R11 and R49 cells were irradiated with 2 Gy. Cell lysates were prepared at the indicated time periods (2-8 h) following irradiation. YB-1 expression was determined by western blot analysis. GAPDH was used as a control. (B) Upregulation of total YB-1 following irradiation at the indicated time points. YB-1, Y-box binding protein-1.

To determine the effect of nuclear YB-1 on XVir-N-31 production, the adenoviral transduction efficacy of glioma stem cells was first examined, which was 6.55±0.1% at 1 MOI and 16.0±1.1% at 3 MOI for R11 cells, 2.5±0.1% at 1 MOI and 6.05±0.1% at 3 MOI for R28 cells and 2.3±0.1% at 1 MOI and 5.35±0.9% for R49 cells (Fig. 3A). To examine whether irradiation enhanced XVir-N-31 production, the cells were irradiated 24 h prior to XVir-N-31 infection. For infection, only the aforementioned low infection rates were used, as it has been established that XVir-N-31 replicates efficiently in glioma cells at a dose of 5 MOI (19). Although the levels were not significant due to a high variability in virus production in the independent experiments, the nuclear translocation of YB-1 in R28 and R49 cells, and in particular the level of nuclear YB-$1^{65\ kD}$, correlated well with the enhanced production of XVir-N-31 in these cells. Whilst combined irradiation and infection of R28 and R49 cells using 1 MOI of XVir-N-31 exhibited almost no enhancement in virus production, the increase of XVir-N-31 production in irradiated R49 cells infected with 3 MOI was 1.6-130-fold, depending on the irradiation dose, and was superior to that observed in R28 cells (1.2-7-fold; Fig. 3B; Table I). In R28 cells, a dose of 6 Gy of irradiation led to cell death (data not shown), paralleled by a decrease in virus production (Fig. 3). As expected, in irradiated R11 BTICs that exhibited high basal nuclear YB-1 expression but no relevant irradiated-mediated nuclear transfer of YB-1, no significant enhancement of XVir-N-31 production was detected.

Irradiation in combination with XVir-N-31 infection significantly decreases the growth of R28^{mCherry} spheres implanted in human cortical brain slices. To analyze the effect of a combined irradiation and XVir-N-31-based oncovirotherapy in therapy-resistant BTICs, an organotypic *in vitro* glioma model was established, in which R28^{mCherry} spheres were implanted in human cortical brain tissue slices. The slices were irradiated with either 3 Gy, infected with $5x10^7$ IFU of XVir-N-31 or were irradiated and infected 24 h later. Tumor sphere growth was quantified over a period of 14 days. A longer period of quantification was not possible, as most tumor sphere sizes expanded the microscopic observation area after this time point. As indicated in Figs. 4 and 5, all (6/6) untreated control R28^{mCherry} tumor spheres grew quickly, whilst irradiation or infection alone resulted in a decrease in sphere growth rate. By single infection with XVir-N-31, the growth of 3/6 spheres was almost completely inhibited, whilst 3/6 spheres continued to grow, but to a lesser extent compared with the controls. Nevertheless, in this group a number of tumor cells exhibited the typical characteristic of an oncolytic adenovirus infection, including decreased cell size and a rounded cell shape, indicating that these cells were dying (Fig. 6). When irradiation was used as a single treatment, all spheres (6/6) were delayed in growth. However, surviving tumor cells grew in a highly invasive manner into the brain tissue (Fig. 6). By contrast, combined therapy was very efficient and significantly delayed tumor sphere growth; 1/6 spheres was nearly completely eradicated upon treatment, 2/6 spheres exhibited a highly delayed growth and 3/6 grew slowly. The morphology of these slow-growing spheres was therefore assessed. As indicated in Fig. 6, in these spheres many cells exhibited the characteristics of oncolysis, however, a population of non-infected viable tumor cells that continued to proliferate was visible.

Irradiation in combination with XVir-N-31 infection prolongs the median survival of R28 tumor-bearing nude mice. The promising *in vitro* results prompted the analysis of the therapeutic effect of a combined XVir-N-31-based oncoviro-irradiation therapy in mice. For this purpose, R28 BTICs were intracranially implanted into the striatum of nude mice. The mice were treated as follows: i) Sham (no irradiation + intratumoral injection of PBS); ii) irradiation (3 Gy tumor irradiation) + intratumoral PBS injection 24 h later; iii) XVir-N-31 (no irradiation + intratumoral injection of $1.5x10^8$ IFU XVir-N-31). This virus amount represents one-half of the recently determined effective therapeutic dose (18); iv) Combi [3 Gy tumor irradiation + an intratumoral XVir-N-31 injection ($1.5x10^8$ IFU) 24 h later; Fig. 7A]. A suboptimal dose of XVir-N-31 was selected for the XVir-N-31 and Combi groups to identify any possible augmentation of the oncolytic effect of XVir-N-31 by tumor irradiation prior to infection. Large tumors were observed visually in the sham treated mice (data not shown), and these animals succumbed at around day 85. The mean survival of the single treatment groups was increased compared with that of the controls, but was almost the same for both mono-therapies (95 days for irradiation and 96 days for XVir-N-31 infection groups, respectively). The median survival of the virus-treatment group was improved (96 days) compared with that of the irradiated group (88 days), but did not reach significance. As expected, based

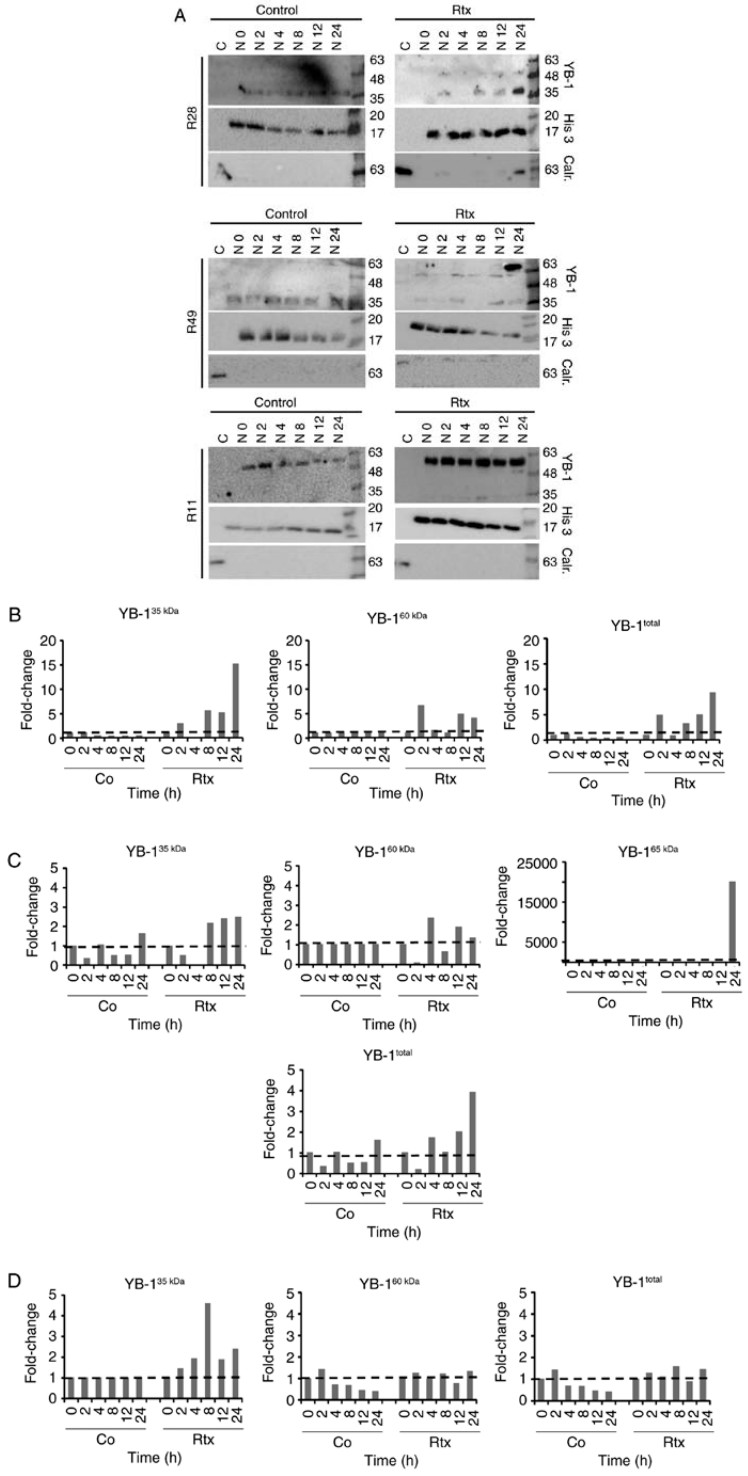


Figure 2. Irradiation induces YB-1 nuclear translocation in brain tumor initiating cells. (A) The cells were irradiated with either 2 Gy (R11 and R28 cells) or 6 Gy (R49 cells). At the indicted time periods nuclear extracts were generated. As a control, a cytoplasmic protein extract was prepared. YB-1 expression was detected by western blot analysis. To control extract purity, detection of the nuclear protein histone H3 and the cytoplasmic protein calreticulin was performed. (B-D) Upregulation of the different isoforms of nuclear YB-1 in non-irradiated and irradiated (B) R28, (C) R49 and (D) R11 cells at the indicated time points. YB-1, Y-box binding protein-1; Rtx, irradiation; C, cytoplasmic extract; N, nuclear extract.

Table I. XVir-N-31 production in irradiated brain tumor initiating cells.

	2	4	6	2	4	6	Gy
Cell lines	1	1	1	3	3	3	MOI
R28	0.4-1.4	0.8-1.4	0.5-0.9	1.2-5.0	1.6-7.0	0.5-0.9	-
R49	0.5-2.1	0.4-1.2	0.4-31.8	1.0-7.5	1.6-91.4	4.9-130.4	-
R11	1.0-1.3	0.6-1.8	1.1-2.8	1.4-2.0	0.8-1.5	0.7-3.0	-

Data are presented as fold induction compared with non-irradiated cells. MOI, multiplicity of infection.

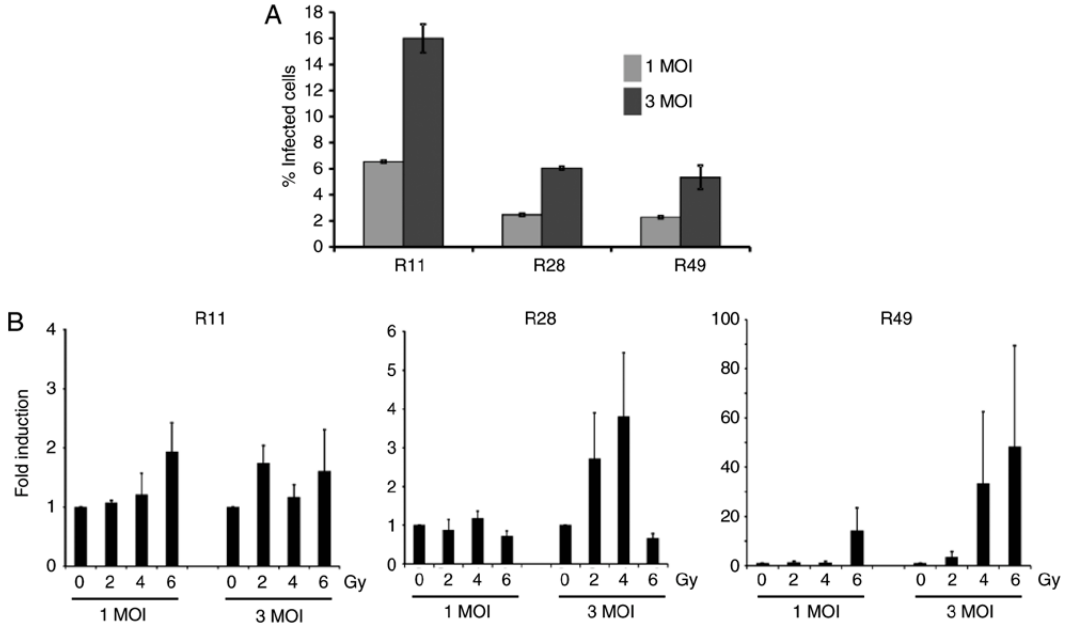


Figure 3. Irradiation of brain tumor initiating cells prior to XVir-N-31 infection potentiates the production of XVir-N-31. (A) Transduction efficacy of the adenovirus in glioma stem cells, as determined by flow cytometry analysis at 48 h post-infection, using either 1 or 3 MOI (n=2). Error bars represent standard deviation. (B) R11, R28 and R49 cells were irradiated with 2, 4 or 6 Gy and were infected with either 1 or 3 MOI of XVir-N-31 24 h later. After 72 h, cells and medium were collated and total infection units were determined (n=3). Data are presented as mean ± standard error of the mean, and analyzed by one-way analysis of variance. MOI, multiplicity of infection.

on previous data, oncovirotherapy using a suboptimal amount of infectious XVir-N-31 particles ($1.5x10^8$ IFU) did not reach the median survival of ~120 days, as was observed previously when using the double amount of XVir-N-31 ($3x10^8$ IFU) (18). Nevertheless, there was a trend towards a prolonged survival in the group of mice subjected to tumor irradiation followed by oncovirotherapy, although this did not reach significance. The median survival in this group was 101 days, and the mean survival 108 days. One mouse within this group did not exhibit any tumor-associated symptoms, even at a period of 150 days after tumor implantation. This mouse was sacrificed, but no visible tumors were detected (data not shown).

Discussion

The results of the present study demonstrated that irradiation of BTICs enhanced the lytic activity of the YB-1-dependent oncolytic adenovirus XVir-N-31. BTICs are highly therapy-resistant cells that exhibit stem cell characteristics, and have been proposed as the primordial cells responsible for disease initiation and its recurrence (2). Due to the fact that not many therapeutic options are available to efficiently treat recurrent glioma, the results of the present study may have substantial consequences on the development of future combined treatment strategies. We previously determined the effects of XVir-N-31 in BTICs and demonstrated that XVir-N-31 replicated in BTICs. In a BTIC-derived mouse glioma model, treatment of mice with a single intratumoral injection of XVir-N-31 significantly prolonged their survival (18). XVir-N-31 replication is dependent on the presence of nuclear YB-1 (19). YB-1 is primarily expressed in all high grade glioma, conveys resistance towards TMZ, the standard chemotherapeutic drug to treat GBM, and serves as a prognostic biomarker for tumor progression (18,26,27).

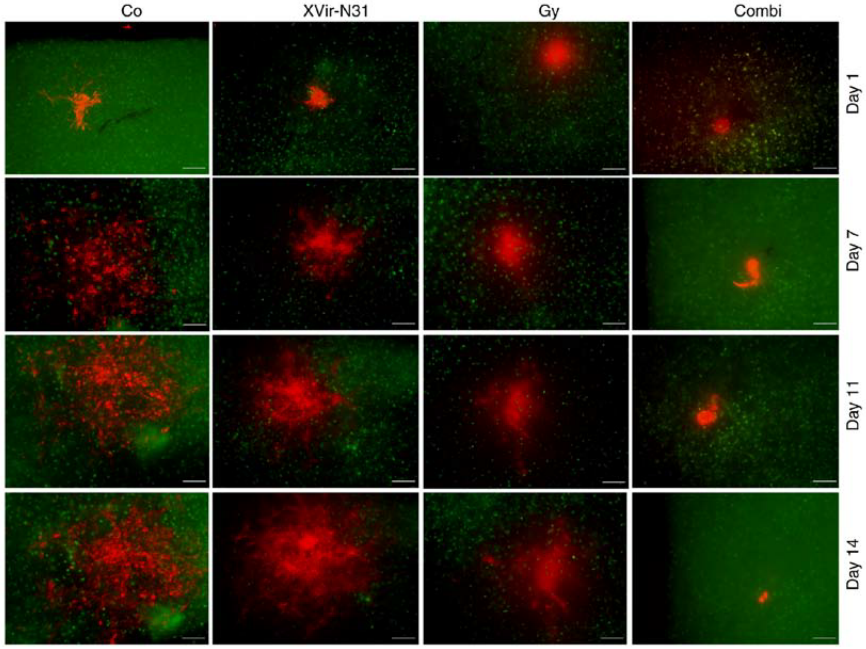


Figure 4. Irradiation prior to XVir-N-31 infection delayed the growth of R28 tumor spheroids in human cortical brain slice cultures. $R28^{mCherry}$ spheroids were implanted in human brain slices stained with NeuO. The cultures were left either untreated (Co), irradiated with 3 Gy, infected with $5x10^7$ IFU XVir-N-31, or were irradiated with 3 Gy and infected using $5x10^7$ IFU XVir-N-31 24 h later. Images were captured every second day starting at the day of XVir-N-31 infection. Green staining represents NeuO staining in the brain slices. Red staining represents $R28^{mCherry}$-expressing cells. Representative 1/6 spheres from 2 independent experiments is presented (scale bar=200 μm). IFU, infectious units; Co, control; Combi, 3 Gy tumor irradiation + an intratumoral XVir-N-31 injection ($1.5x10^8$ IFU) 24 h later.

However, in some BTICs only a small amount of YB-1 was identified to be nuclear (18), therefore virus replication is suboptimal. In previous years, several studies have demonstrated that YB-1, in response to genotoxic stress, becomes post-translationally modified and is transferred from the cytoplasm into the nucleus. This in turn enhances the replication and oncolytic effect of XVir-N-31 in established tumor cell lines and experimental glioma models (6,19,28).

Since oncovirotherapy is still not a standardized therapy option to treat glioma, it is expected to be primarily used as second line therapy for recurrent glioma. As it has been established that the irradiation of established glioma cell lines induced the translocation of YB-1 into the nucleus and supported XVir-N-31 replication, we hypothesized that irradiation prior to onco-virotherapy may augment the therapeutic effect of a XVir-N-31-based oncovirotherapy in patients with recurrent glioma. To examine this hypothesis, the effect of irradiation on the subcellular localization of YB-1 in BTICs, the primary target cells in and drivers of recurrent glioma, was investigated. Elevated nuclear YB-1 was detected in R28 and R49 BTICs, however, in R11 cells no irradiation-mediated nuclear translocation of YB-1 was observed. In the present study, in contrast to R28 and R49 BTICs, R11 cells were observed to possess a high basal level of nuclear YB-1. This observation is not concordant with previous data that revealed the presence of both cytoplasmic and nuclear YB-1 in R11 cells (18), but this may be explained by the use of different YB-1 antibodies between these studies. Nevertheless, the high basal level of nuclear YB-1 in R11 BTICs may explain why these cells possess a higher basal XVir-N-31 replication rate compared with the R28 and R49 cells, why there is no additional increase in nuclear YB-1 levels detected following irradiation of these cells, and why irradiation did not enhance XVir-N-31 production.

In the present study, R49 cells required a higher irradiation dose (6 Gy) to initiate the transfer of YB-1 into the nucleus. In concordance with the observed elevated nuclear level of YB-1 in R49 and R28 BTICs, irradiation prior to infection facilitated XVir-N-31-production in these cells up to 130-fold. However, induction of virus production was variable. As YB-1 serves as a stress protein, its posttranslational modification and nuclear translocation, and consequently its activity as a transcription factor that is necessary for XVir-N-31 replication, is very sensitive to external conditions. Additionally, virus production itself is a complex process including transcription of viral proteins, DNA replication, and the self-assembly of viral proteins and the genome to create infectious viral particles. This may explain the variability of virus production observed in the irradiated R28 and R49 cells.

Notably, in the R49 cells, which exhibited superior XVir-N-31 production following irradiation compared with the R28 cells, the presence of nuclear $YB\text{-}1^{65\ kD}$, which was suggested to represent a highly post-translationally modified version of YB-1, was detected. We hypothesized that not only the nuclear translocation of YB-1, but also its post-translational modification, is important for its function as a transcription

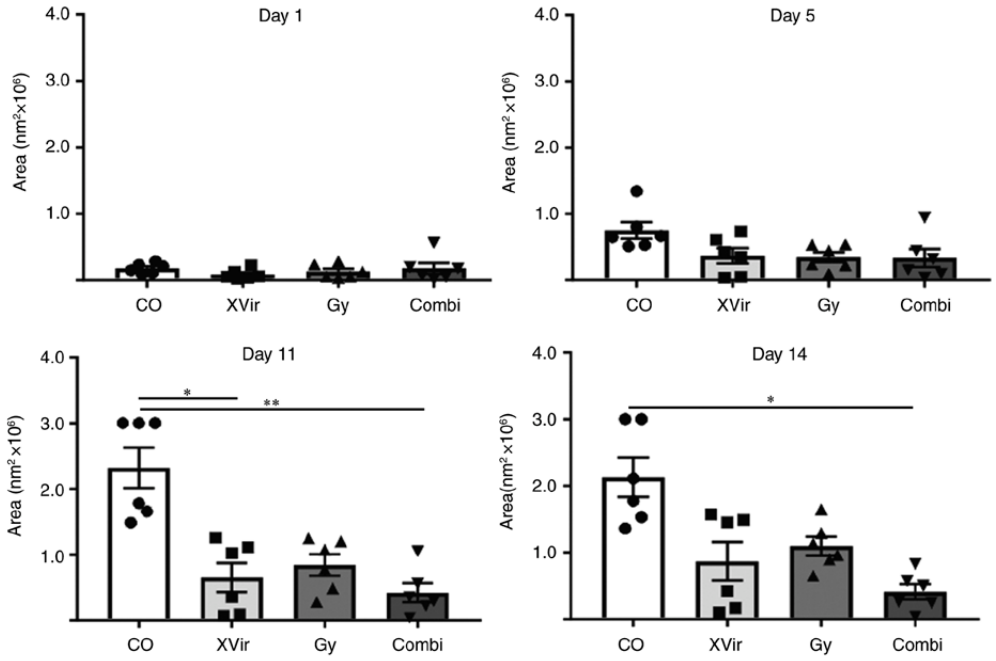


Figure 5. Irradiation prior to XVir-N-31 infection significantly decreases the growth of R28^{mCherry} spheres in human cortical brain slice cultures. Quantification of R28^{mCherry} spheroid growth in human brain slice cultures. R28^{mCherry} spheroids were implanted as described. Images were captured every second day and tumor areas were quantified (n=6 spheres). Data from 2 independent experiments are presented. Data were analyzed using one-way analysis of variance. *P<0.05 and **P<0.01. Co, control; Combi, 3 Gy tumor irradiation + an intratumoral XVir-N-31 injection (1.5x10^{8} infectious units) 24 h later.

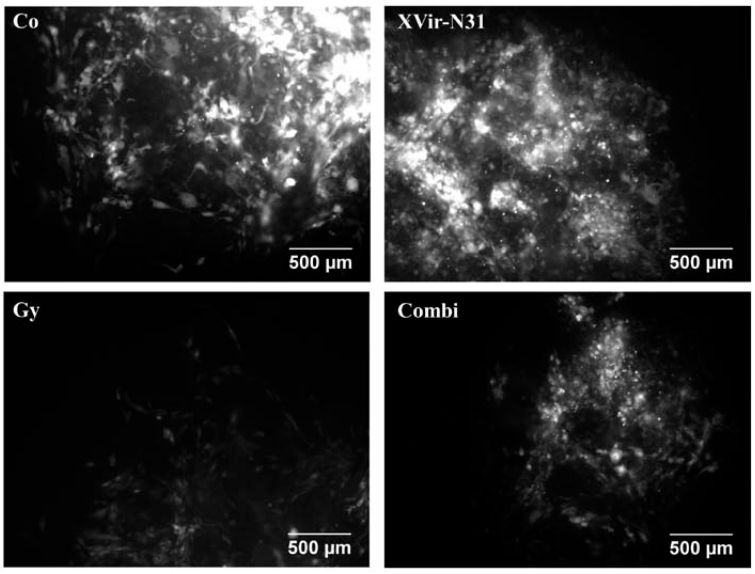
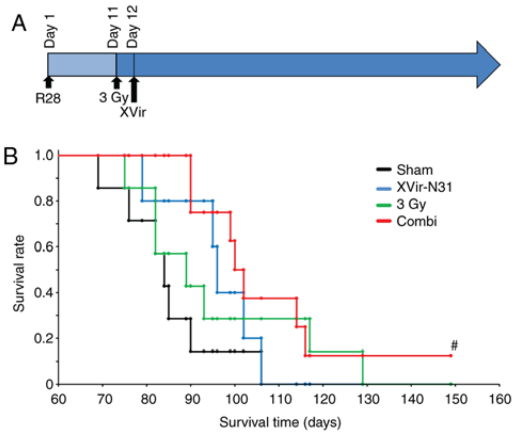


Figure 6. Morphological characteristics of R28^{mCherry} spheroids. High magnification of treated R28 spheroids growing in human brain slice cultures at day 17 after treatment. (scale bar =500 μm). Co, control; Combi, 3 Gy tumor irradiation + an intratumoral XVir-N-31 injection (1.5x10^{8} infectious units) 24 h later.

factor necessary for XVir-N-31 replication. Whether this modification includes only phosphorylation or also acetylation or SUMOylation (11-14), or even presently unknown modifications, requires additional studies. In summary, the data from the present study demonstrated a direct association between nuclear (modified) YB-1 and XVir-N-31-replication



C

	Mean survival	Median survival
Sham	85	85
XVir-N31	96	96
3 Gy	95	88
Combi	108	101

Figure 7. Irradiation prior to XVir-N-31 infection prolongs the survival of R28 tumor bearing mice. The mice (n=5-8 per group) were treated as described. (A) Treatment schema. (B) Kaplan-Meier survival analysis. (C) Mean and median survival times of the treatment groups. Combi, 3 Gy tumor irradiation + an intratumoral XVir-N-31 injection ($1.5x10^8$ infectious units) 24 h later. #No tumor visible.

and its production in established tumor cell lines, which was in concordance with our previous observations (19).

Subsequently, the therapeutic effect of a combined XVir-N31-based oncoviro-radiotherapy was assessed in human cortical brain slice cultured harboring $R28^{mCherry}$ glioma spheroids as well as in R28 glioma bearing mice. Infection of slice cultures was performed with a suboptimal dose of XVir-N-31 ($5x10^7$ IFU) to determine the synergistic effects of irradiation and virus infection. The specific time point of virus infection (24 h after irradiation) was selected as elevated levels of nuclear (post-translationally modified) YB-1 were detectable after this period. Due to the ability of XVir-N-31 to also infect neurons, glial cells and astrocytes, the virus dose selected only equated to ~0.1 IFU/cell. Therefore, the therapeutic effect of the XVir-N-31-based monotherapy was only moderate. However, a delay in $R28^{mCherry}$ tumor spheroid growth was detectable even at this concentration. A total of 3/6 analyzed spheroids exhibited a marked delay in growth, and the others a moderate delay. The variance in growth rates may not only be caused by virus infection, but also by the variable size of the implanted spheroids. When examined more closely, an oncolytic cytopathic effect and dying BTICs were observed in the XVir-N-31-infected tissues, as indicated by a rounded cell shape and the occurrence of cell debris in the spheroids (Fig. 6). Irradiation also delayed the growth of BTICs, however no dead cells were observed and the surviving cells massively invaded the surrounding brain tissue, an effect that has been described in glioma cells in the past (29). By contrast, irradiation in combination with XVir-N-31-infection significantly decreased $R28^{mCherry}$ tumor spheroid growth. Whilst 1 spheroid did not grow at all, 2 exhibited a massive and 3 a considerable decrease in growth. This effect appeared to be comparable to, or even exceed, the effect of irradiation alone. The structure of spheroids with considerable growth reduction were then microscopically examined and a number of dead cells and cell debris were detected. In addition, viable cells that had started to divide again were observed in these samples, but at a later time point following treatment (days 17-23). The outgrowth of tumor cells following combined therapy may be an effect provoked by the low amount of infectious XVir-N-31 used to treat the spheroids, and the fact that certain cells may not have been infected at all. If these cells invade the surrounding brain tissue at a faster rate compared with virus replication in the adjacent infected tumor cells occurs, the cancer cells will be protected from virus infection due to a protective wall of non-neoplastic brain cells that forms a barrier for virus distribution in which the virus is unable to replicate.

The therapeutic effects of a XVir-N-31-based oncoviro-therapy were previously determined *in vivo* in a mouse glioma model, in which it was demonstrated that ~$3x10^8$ IFU XVir-N-31 were required to significantly decrease tumor growth, leading to a significant survival prolongation (18). To confirm the therapeutic effect of a combined oncoviro-radiotherapy, as was observed in $R28^{mCherry}$ BTIC-derived glioma containing organotypic brain cultures *in vitro*, and to demonstrate the support of tumor irradiation on oncolysis-mediated tumor cell death and therefore on tumor growth and survival, only a suboptimal amount of XVir-N-31 ($1.5x10^8$ IFU) was intratumorally injected in the disease model in the present study. This virus dose was in itself not able to significantly prolong survival. Additionally, radiotherapy was administered prior to infection by a single 3 Gy tumor irradiation, a dose that is used during fractional irradiation of patients with glioma (30). Although non-significant, a prolongation of the mean survival in both monotherapy groups for 10-11 days was observed. The survival rates in the mice that received the oncoviro-irradiation therapy instead increased by 23 days. The median survival was determined in this group, and the combined treatment exhibited superior effects compared with the monotherapies. The effects achieved by the combination of tumor-irradiation and XVir-N-31-based oncovirotherapy were not statistically significant, however suboptimal total doses of irradiation and of XVir-N-31 were used in the therapeutic glioma mouse model. Therefore, we hypothesize that optimizing the therapeutic schema, for example repeated irradiation and injection of a therapeutic relevant dose of XVir-N-31, may result in improved effects of this combination on tumor growth and survival.

Although the interaction between irradiation and oncolytic adenoviruses is complex, given the diversity of cellular responses to irradiation and the diverse oncovirus-mediated antitumoral immune effects, the irradiation-mediated post-translational modifications of YB-1 and its nuclear transport, due to its central role in XVir-N-31-replication, may explain the superior effects of a combined oncoviro-radiotherapy in the glioma mouse model established in the present study using therapy-resistant BTICs. The results from the present study suggest that irradiation of patients with recurrent glioma prior to XVir-N-31 based oncovirotherapy should be performed to optimize the effect of the oncolytic virotherapy in these patients. Finally, as it is well known that both virus

infection and tumor-irradiation cause a broad-range immune cell activity against tumors (31,32), the combined radio-oncovirotherapy treatment may in turn support the therapeutic outcome of patients with recurrent GBM.

Acknowledgements

Not applicable.

Funding

The present study was supported by grants awarded to UN by the Else-Übelmesser-Foundation.

Availability of data and materials

The datasets generated during and/or analyzed during the current study are available from the corresponding author on reasonable request.

Authors' contribution

RC, NS, HK, SS, SH; TW and UN contributed to the data collection, analysis and interpretation. PH and UN contributed to the study design. UN wrote the manuscript. All authors read and approved the final manuscript.

Ethics approval and consent to participate

For patient data and material, written informed consent was obtained from all patients, allowing spare tissue from resective surgery to be included in the present study. Ethical approval was obtained from the Ethics Commission of Tübingen (approval no. 338/2016A). Animal experiments were performed according to the German Animal Welfare Act and its guidelines for the care and use of laboratory animals (approval N12/14 of the regional council Tübingen).

Patient consent for publication

Not applicable.

Competing interests

Per S. Holm is CEO and co-founder of XVir Therapeutics GmbH, 80335 Munich, Germany. All other authors declare that they have no competing interests.

References

1. Stupp R, Taillibert S, Kanner A, Read W, Steinberg D, Lhermitte B, Toms S, Idbaih A, Ahluwalia MS, Fink K, *et al*: Effect of tumor-treating fields plus maintenance temozolomide vs maintenance temozolomide alone on survival in patients with glioblastoma: A randomized clinical trial. JAMA 318: 2306-2316, 2017.
2. Auffinger B, Spencer D, Pytel P, Ahmed AU and Lesniak MS: The role of glioma stem cells in chemotherapy resistance and glioblastoma multiforme recurrence. Expert Rev Neurother 15: 741-752, 2015.
3. Auffinger B, Tobias AL, Han Y, Lee G, Guo D, Dey M, Lesniak MS and Ahmed AU: Conversion of differentiated cancer cells into cancer stem-like cells in a glioblastoma model after primary chemotherapy. Cell Death Differ 21: 1119-1131, 2014.
4. Molina JR, Hayashi Y, Stephens C and Georgescu MM: Invasive glioblastoma cells acquire stemness and increased Akt activation. Neoplasia 12: 453-463, 2010.
5. Sunayama J, Matsuda K, Sato A, Tachibana K, Suzuki K, Narita Y, Shibui S, Sakurada K, Kayama T, Tomiyama A and Kitanaka C: Crosstalk between the PI3K/mTOR and MEK/ERK pathways involved in the maintenance of self-renewal and tumorigenicity of glioblastoma stem-like cells. Stem Cells 28: 1930-1939, 2010.
6. Toulany M, Schickfluss TA, Eicheler W, Kehlbach R, Schittek B and Rodemann HP: Impact of oncogenic K-RAS on YB-1 phosphorylation induced by ionizing radiation. Breast Cancer Res 13: R28, 2011.
7. Sinnberg T, Sauer B, Holm P, Spangler B, Kuphal S, Bosserhoff A and Schittek B: MAPK and PI3K/AKT mediated YB-1 activation promotes melanoma cell proliferation which is counteracted by an autoregulatory loop. Exp Dermatol 21: 265-270, 2012.
8. Wu J, Lee C, Yokom D, Jiang H, Cheang MC, Yorida E, Turbin D, Berquin IM, Mertens PR, Iftner T, *et al*: Disruption of the Y-box binding protein-1 results in suppression of the epidermal growth factor receptor and HER-2. Cancer Res 66: 4872-4879, 2006.
9. Kosnopfel C, Sinnberg T and Schittek B: Y-box binding protein 1-a prognostic marker and target in tumour therapy. Eur J Cell Biol 93: 61-70, 2014.
10. Schittek B, Psenner K, Sauer B, Meier F, Iftner T and Garbe C: The increased expression of Y box-binding protein 1 in melanoma stimulates proliferation and tumor invasion, antagonizes apoptosis and enhances chemoresistance. Int J Cancer 120: 2110-2118, 2007.
11. Alemasova EE, Pestryakov PE, Sukhanova MV, Kretov DA, Moor NA, Curmi PA, Ovchinnikov LP and Lavrik OI: Poly(ADP-ribosyl)ation as a new posttranslational modification of YB-1. Biochimie 119: 36-44, 2015.
12. Tiwari A, Rebholz S, Maier E, Dehghan Harati M, Zips D, Sers C, Rodemann HP and Toulany M: Stress-induced phosphorylation of nuclear YB-1 depends on nuclear trafficking of p90 ribosomal S6 kinase. Int J Mol Sci 19: pii: E2441, 2018.
13. Ewert L, Fischer A, Brandt S, Scurt FG, Philipsen L, Müller AJ, Girndt M, Zenclussen AC, Lindquist JA, Gorny X and Mertens PR: Cold shock Y-box binding protein-1 acetylation status in monocytes is associated with systemic inflammation and vascular damage. Atherosclerosis 278: 156-165, 2018.
14. Pagano C, di Martino O, Ruggiero G, Maria Guarino A, Mueller N, Siauciunaite R, Reischl M, Simon Foulkes N, Vallone D and Calabrò V: The tumor-associated YB-1 protein: New player in the circadian control of cell proliferation. Oncotarget 8: 6193-6205, 2017.
15. Lage H, Surowiak P and Holm PS: YB-1 as a potential target in cancer therapy. Pathologe 2 (Suppl 2): S187-S190, 2008 (In German).
16. Holm PS, Bergmann S, Jurchott K, Lage H, Brand K, Ladhoff A, Mantwill K, Curiel DT, Dobbelstein M, Dietel M, *et al*: YB-1 relocates to the nucleus in adenovirus-infected cells and facilitates viral replication by inducing E2 gene expression through the E2 late promoter. J Biol Chem 277: 10427-10434, 2002.
17. Holm PS, Lage H, Bergmann S, Jürchott K, Glockzin G, Bernshausen A, Mantwill K, Ladhoff A, Wichert A, Mymryk JS, *et al*: Multidrug-resistant cancer cells facilitate E1-independent adenoviral replication: Impact for cancer gene therapy. Cancer Res 64: 322-328, 2004.
18. Mantwill K, Naumann U, Seznec J, Girbinger V, Lage H, Surowiak P, Beier D, Mittelbronn M, Schlegel J and Holm PS: YB-1 dependent oncolytic adenovirus efficiently inhibits tumor growth of glioma cancer stem like cells. J Transl Med 11: 216, 2013.
19. Bieler A, Mantwill K, Holzmüller R, Jürchott K, Kaszubiak A, Stärk S, Glockzin G, Lage H, Grosu AL, Gansbacher B and Holm PS: Impact of radiation therapy on the oncolytic adenovirus dl520: Implications on the treatment of glioblastoma. Radiother Oncol 86: 419-427, 2008.
20. Beier D, Hau P, Proescholdt M, Lohmeier A, Wischhusen J, Oefner PJ, Aigner L, Brawanski A, Bogdahn U and Beier CP: CD133(+) and CD133(-) glioblastoma-derived cancer stem cells show differential growth characteristics and molecular profiles. Cancer Res 67: 4010-4015, 2007.
21. Verhoog MB, Goriounova NA, Obermayer J, Stroeder J, Hjorth JJ, Testa-Silva G, Baayen JC, de Kock CP, Meredith RM and Mansvelder HD: Mechanisms underlying the rules for associative plasticity at adult human neocortical synapses. J Neurosci 33: 17197-17208, 2013.
22. Schwarz N, Hedrich UBS, Schwarz H, P A H, Dammeier N, Auffenberg E, Bedogni F, Honegger JB, Lerche H, Wuttke TV and Koch H: Human Cerebrospinal fluid promotes long-term neuronal viability and network function in human neocortical organotypic brain slice cultures. Sci Rep 7: 12249, 2017.

23. Schindelin J, Arganda-Carreras I, Frise E, Kaynig V, Longair M, Pietzsch T, Preibisch S, Rueden C, Saalfeld S, Schmid B, *et al*: Fiji: An open-source platform for biological-image analysis. Nat Methods 9: 676-682, 2012.
24. Erhardt W, Henke J and Haberstroh J (eds): Anästhesie und Analgesie beim klein-und heimtier. Schattauer Verlag, 2004.
25. Mutschelknaus L, Azimzadeh O, Heider T, Winkler K, Vetter M, Kell R, Tapio S, Merl-Pham J, Huber SM, Edalat L, *et al*: Radiation alters the cargo of exosomes released from squamous head and neck cancer cells to promote migration of recipient cells. Sci Rep 7: 12423, 2017.
26. Zheng J, Dong W, Zhang J, Li G and Gong H: YB-1, a new biomarker of glioma progression, is associated with the prognosis of glioma patients. Acta Biochim Biophys Sin (Shanghai) 48: 318-325, 2016.
27. Tong H, Zhao K, Zhang J, Zhu J and Xiao J: YB-1 modulates the drug resistance of glioma cells by activation of MDM2/p53 pathway. Drug Des Devel Ther 13: 317-326, 2019.
28. Wu J, Stratford AL, Astanehe A and Dunn SE: YB-1 is a transcription/translation factor that orchestrates the oncogenome by hardwiring signal transduction to gene expression. transl Oncogenomics 2: 49-65, 2007.
29. Wild-Bode C, Weller M, Rimner A, Dichgans J and Wick W: Sublethal irradiation promotes migration and invasiveness of glioma cells: Implications for radiotherapy of human glioblastoma. Cancer Res 61: 2744-2750, 2001.
30. Khan L, Soliman H, Sahgal A, Perry J, Xu W and Tsao MN: External beam radiation dose escalation for high grade glioma. Cochrane Database Syst Rev 19: CD011475, 2016.
31. Woller N, Gürlevik E, Fleischmann-Mundt B, Schumacher A, Knocke S, Kloos AM, Saborowski M, Geffers R, Manns MP, Wirth TC, *et al*: Viral infection of tumors overcomes resistance to PD-1-immunotherapy by broadening neoantigenome-directed T-cell responses. Mol Ther 23: 1630-1640, 2015.
32. Sahebjam S, Sharabi A, Lim M, Kesarwani P and Chinnaiyan P: Immunotherapy and radiation in glioblastoma. J Neurooncol 134: 531-539, 2017.

This work is licensed under a Creative Commons Attribution-NonCommercial-NoDerivatives 4.0 International (CC BY-NC-ND 4.0) License.

3 Discussion

The aim of this work was to investigate *in vitro* model systems to study human cortical neuronal function. The advantages and disadvantages of two human neuronal model systems (human iPS cell-derived neurons and human organotypic brain slice cultures) are discussed below. The model of human organotypic brain slice cultures in particular aims to create a physiologically developed platform for neuronal function. This new model system can contribute to the understanding of the neurological pathophysiology of various diseases and future therapeutic developments.

One of the neurological diseases that has so far been little studied in human neurons is the group of developmental and epileptic encephalopathies (DEE). Recently, variants in the voltage-gated K^+ channel $K_V1.2$, encoded by the gene *KCNA2* were identified as a new molecular entity within DEEs (Masnada et al., 2017; Syrbe et al., 2015).

Several of the DEE-triggering variants in ion channels have already been investigated in heterologous expression systems (Masnada et al., 2017; Syrbe et al., 2015), but heterologous expression systems can only give an initial insight into the consequences for a neuronal system. To truly understand the effects of the disease-causing variants in ion channels, it is important to study them in (human) neuronal models. The voltage-gated potassium channel $K_V1.2$ is expressed in both gray and white regions of the brain (Awan & Dolly, 1991) and also in different subcellular locations in different types of neuron (Inda et al., 2006; Sheng et al., 1994). In addition, the channel has not only the ability to form homotetramers, but also heterotetramers together with $K_V1.1$ and $K_V1.4$ subunits (Lambe & Aghajanian, 2001; Po et al., 1993) which makes a statement about the consequences of variants in the $K_V1.2$ channel with regard to the firing behavior of neurons very difficult. As the composition of the tetramers and the localization of $K_V1.2$-containing channels determine essentially the function and role of the channels in neurons, a model system where the other K_V subunits and also all auxiliary proteins are expressed is needed to study the effects of *KCNA2* variants.

Therefore, in the first part of this study human iPS cell-derived neurons were used to characterize the effect of the *KCNA2* variants p.R297Q and p.L328V on the intrinsic firing patterns of these neurons. The aim was to study how the variants contribute to the pathophysiology of the neurons. Therefore, in the next two sections, the reprogramming to iPS cells and the electrophysiological analyses of the neurons differentiated from the iPS cells are discussed.

3.1 Reprogramming to induced pluripotent stem cells

The induced pluripotent stem (iPS) cell technology is widely advertised as a way to improve our understanding of the pathophysiology of numerous diseases and to enable the discovery and development of new drugs and therapeutic options. Numerous advances in iPS cell culture, genome engineering, and various neural differentiation protocols have quickly made iPS cells a mainstream toolkit in cellular neuroscience (Engle et al., 2018). The results and peculiarities of this pluripotent stem cell model, which was generated in this work, will be discussed here and later compared with the model of the adult human organotypic brain slice cultures also established in this work.

Until the reprogrammability of somatic cells to iPS cells was discovered, an investigation of many neurological disease-causing variants in the target tissue, namely human cortical neurons, was not possible, or only in rare exceptional cases. Human cortical neurons, which were differentiated from embryonic stem cells, offered the possibility before, but they were and are a rare commodity and ethically much more problematic than iPS cells (S. C. Zhang et al., 2001). Therefore, the possibility of researching morally less critical and generally easily available human cortical neurons is a huge step towards a broader and better understanding of brain development and thus also broader applicability in the learning of new therapeutic options. However, there are still some challenges associated with the iPS cell method. Some of them will be shown and discussed below based on the results obtained from reprogrammed somatic skin fibroblasts from patients with developmental and epileptic encephalopathies.

The effects of the two disease-causing variants (c.890G> A, p.Arg297Gln, p.R297Q and c.982T> G, p.Leu328Val, p.L328V) in the *KCNA2* gene on the firing

behavior of cortical neurons were investigated in a first step . The characterization of the reprogrammed cells shows that there has been a complete reprogramming into a pluripotent state (Schwarz et al., 2018, 2019, Fig. 1G). The karyograms of both cell lines show no abnormalities, considering that this technique can only detect larger chromosome aberrations. A single nucleotide polymorphism (SNP) array analysis of fibroblast and generated iPS cells would reveal more precisely genomic integrity. The Pluripotency state of the cells was verified by immunofluorescence stainings of the pluripotency markers OCT3/4, TRA-1-60, SOX2 and SSEA-4. In addition, upregulation of endogenous pluripotency factor NANOG was confirmed by qRT-PCR. Both *KCNA2* variants which were identified in the affected patient via genetic analysis were confirmed in the patient-derived iPS cell lines to exclude any confusion between the used samples. For further validation, cells were differentiated from embryoid-bodies (EB) into cells of all three embryonic germ layers (ectoderm, endoderm and mesoderm). Previous characterization protocols included both *in vitro* and *in vivo* assays to verify the pluripotency and differentiation capacity (Martí et al., 2013). The earlier gold standard of the teratoma test in SCID mice is certainly no longer necessary today, since EB-based *in vitro* differentiation essays can provide sufficient information about the pluripotency of a iPS cell line (Buta et al., 2013).

In general, the reprogramming and characterization methods used in this work were fully adequate to accomplish the requirements set out here, even if they are no longer state of the art. For example, the reprogramming was performed with retroviruses, with each transcription factor being produced individually in a separate virus, which leads to a low efficiency. Furthermore, the tumorigenicity of the cells is increased by the expression of oncogenes. The low efficiency has been a problem since the method was first introduced (Takahashi & Yamanaka, 2006), but has been improved by various techniques, including the depletion of Mbd3 and can now be increased to almost 100% efficiency (Rais et al., 2013). Further problems can arise from incomplete reprogramming or genomic integration of the transcription factors and thus to unintended mutations in the genome of the target cells. This happens especially when using four different retroviruses, which all have to transduce a somatic cell for successful

reprogramming (Selvaraj et al., 2010). This can be prevented by using plasmids (Okita et al., 2008) or transposon vectors (Woltjen et al., 2009). Other methods of reprogramming are the transfection of cells with recombinant proteins of the transcription factors (Zhou et al., 2009) or by transfection of defined microRNA (Miyoshi et al., 2011). These alternative methods ensure integration-free reprogramming, but are methodologically more complicated and time-consuming. A costly alternative method that combines many advantages is reprogramming through the use of Sendai viruses (MacArthur et al., 2012). Sendai viruses are RNA viruses that express in the cytoplasm and do not integrate into the genome.

In summary, it remains to be stated that for the examinations accomplished exclusively *in vitro* in this work, the reprogramming method chosen here is certainly justifiable, since it is a fast, established and inexpensive way of generating patient-specific iPS cells. These cells were later used to study the development and function of human neurons with the genetic background of the patient. Several clones were generated for both the DEE *KCNA2* variant carrier cells and the control iPS cells. For further investigations and differentiation into neurons, however, only two clones per cell line were used, which all successfully passed the characterization steps just described before.

3.2 Electrophysiological analysis of iPS cell-derived neurons

First investigations in a heterologous expression system (*Xenopus laevis* oocytes) on the two *de novo KNCA2* variants (c.890G> A, p.Arg297Gln, p.R297Q and c.982T> G, p.Leu328Val, p.L328V) have already been performed by Syrbe et al., 2015 and Masnada et al., 2017. The patient carrying the p.R297Q variant presented with a severe phenotype consisting of moderate intellectual disability, moderate to severe ataxia and pharmacoresistant seizures. The patient with the p.L328V variant presented with severe intellectual disability, moderate ataxia, absence seizures and generalized tonic clonic seizures. Electrophysiological analysis revealed increased current amplitudes and a shifted voltage dependence of steady-state activation to more hyperpolarized values for the p.R297Q variant (Syrbe et al., 2015). In addition, the resting membrane potentials

of oocytes expressing p.R297Q channels were more negative compared to wild-type oocytes (Syrbe et al., 2015). The p.L328V variant resulted also in a shift of steady-state activation to more hyperpolarized values and more negative resting membrane potentials in injected oocytes compared to wild-type oocytes (Masnada et al., 2017). Investigations in human model systems will help to further extend these findings and to better understand the underlying pathophysiology.

For the neuronal differentiation of the previously described iPS cell lines a Neurogenin-2 (NGN2) overexpression based protocol was used, which produced pure, mainly excitatory neuronal cultures with firing neurons one week after induction. The long-term viability and maturation of generated NGN2-neurons is relatively low (Busskamp et al., 2014; Y. Zhang et al., 2013) but can be improved drastically by the co-cultivation of mouse astrocytes (Rosa et al., 2020), since astrocytes provide trophic factors to support neuronal metabolism (Vasile et al., 2017). This could be confirmed by immunocytochemical analyzes, which were performed three weeks after induction. A clearly more pronounced arborization of the neuronal dendrites can be observed and the total number of neurons is also increased compared to cultivation without mouse astrocytes. The neuronal identity of the differentiated cells was confirmed by the presence of MAP2-positive neurons eight week after the induction with doxycycline. Compared to the immunofluorescent stainings in week 3, a further morphological maturation of the neurons is observable, more precisely due to a more fanned out arborization of the dendritic tree and a longer total dendritic length. Therefore, the following electrophysiological measurements were executed at this time. Interestingly, after eight weeks, the neuronal cultures consisted of both bipolar and pyramidal neurons (results, figure 10), although in the original publication by Busskamp et al., 2014 only bibolar shaped neurons have been described. Since the morphology of only four days old neurons was examined in the original study, it could be that the neurons change their morphology during maturation and develop more processes during later stages in culture. Maybe also the astrocytes support this process which were not used by Busskamp et al., 2014.

The electrophysiological properties of both *KCNA2* variant carrier and both control iPS cell-derived neurons were examined via whole-cell patch-clamp experiments. The *KCNA2 p.L328V* variant showed a reduced outward current, when the neuronal membrane was depolarized between -10 mV and +20 mV compared to the WT values. This effect can be explained for the neurons with the variant p.L328V, since a reduced current for channels with this variant was also measured in oocytes and the current amplitude of the heterozygous variant was 0.5 compared to the WT (Masnada et al., 2017). For the variant p.R297Q, however, a five-fold increase for the current amplitude was measured in oocytes compared to the WT. Therefore, the measured, unchanged currents in neurons for the variant p.R297Q are difficult to explain (Syrbe et al., 2015). A possible explanation would be that the oocytes are an overexpression system that only expresses, in this case, homotetrameric channels. In the case of neurons in culture, there is the possibility of heterotetramer formation with multiple other K_V subunits and isoforms (Covarrubias et al., 1991; Salkoff et al., 1992). Further compensation mechanisms, such as a shift in the expression profile of K_V1.2 and other K^+ channels, can counteract the pathological behavior of the mutated K_V1.2 channel (Sánchez-Ponce et al., 2012). Another reason could be the different expression level of the channel in neurons of patients vs. controls. This should be investigated in future studies.

No significant differences in average resting membrane potential (RMP) could be revealed between WT and *KCNA2* mutated iPS cell-derived neurons. This is remarkable since the oocytes expressing the K_V1.2 channels with the p.R297Q variant had 30 mV more hyperpolarized resting membrane potentials compared to the oocytes expressing the WT (Syrbe et al., 2015). Also for oocytes expressing the K_V1.2 channels with the p.L328V variant a more than 10 mV more hyperpolarized resting membrane potential compared to the oocytes expressing the WT was recorded (Masnada et al., 2017). This shows how important measurements are in more complex model systems, since the results from the heterologous expression system of the oocytes cannot easily be transferred to human cortical neurons. The lack of transferability can, however, be explained by the fact that the resting membrane potential of neurons is not only balanced by

$K_V1.2$ channels, but it can be assumed that other potassium channels counteracted this in a compensatory manner so that the effect was not detectable (Mckeown et al., 2008).

The cellular membrane of neurons acts as a capacitor, separating the ions in the cytoplasm from the extracellular space. Since the capacity is roughly proportional to the surface area of the neuron, it is often used to determine the size of the cell (Boyle, 2008). When comparing the capacity of the WT neurons and the two *KCNA2* variants, no significant difference could be revealed. This shows that both variants, compared to WT neurons, have no greater influence on the size or formation of the cell membrane at the cell soma. The membrane capacitance determines together with the input resistance the time constant of a membrane which indicates how fast the membrane responds to current flow across the membrane. The total number of open channels in the membrane determine the membrane resistance. A high current flow results either from a high number of channels, a large surface area or a combination of both parameters. This results in an input resistance, which is used as a measure of the maturity of neurons, with lower resistance values indicating a higher degree of maturity (Boyle, 2008).

The difference between the mean input resistance values for control and *KCNA2* variant carrier iPS cell-derived neurons was in no case statistically significant. However, the absolute resistance values varied from 141 MΩ to 2237 MΩ, which suggests a substantially different degree of maturity of the neurons. Compared to rodent (64 MΩ) or human neurons (86 MΩ) there's still a difference of one order of magnitude (Verhoog et al., 2013). In general, to date, the maturity of cortically differentiated neurons *in vitro*, whether from iPS cells or in cerebral organoids, is not comparable to adult neurons, but rather in the range of the second to third trimester of human gestation (Fair et al., 2020; Rosa et al., 2020).

To evaluate the firing behavior of control and patient iPS cell-derived neurons, the cell membranes were held in current-clamp mode at -70 mV via constant current injections and stimulated with different levels of current injections. On average, the *KCNA2* p.L328V variant carrier neurons, generated less action potentials than control neurons in response to the current injections. No

significant difference could be measured for the *KCNA2* p.R297Q variant. One possible explanation is the high variability of differentiated neurons. The high variability of active electrical properties of neurons from the same line and even the same batches was clearly represented when the number of action potentials generated in response to different current injections were analyzed separately for each neuron (data not shown). This electrophysiological variability within an iPS cell line is generally a major problem with this model system and has not yet been solved satisfactorily in neuroscience, even if there are initial approaches. One example is the division of analyzed neurons of one batch into different classes, depending on the electrophysiological firing behavior (C. Bardy et al., 2016).

In conclusion, the electrophysiological analysis of the iPS cell-derived NGN2-neurons suggests a hypoexcitability of the patient-derived neurons with the variant p.L328V compared to the control neurons. This result is corroborated by the findings of Masnada et al., 2017. According to those results, the p.L328V variant would lead to permanently open channels at physiological membrane potentials. In this work the hypoexcitability could be confirmed but not due to a general electric silencing by membrane hyperpolarization, as Masnada et al. suggested. Both variants showed no altered resting membrane potential levels. The results found in this work are supported by studies on *in utero* electroporated mouse embryos, which are currently being completed here in the laboratory. These experiments also show a hypoexcitability of the neurons with normal resting membrane potentials. In contrast, other studies here in the laboratory, which are accomplished on transduced primary hippocampal mouse cultures, show that, in addition to hypoexcitability, there is also a reduced resting membrane potential. The decisive difference seems to be whether or not the neurons have a longer time to compensate for the pathological changes of the mutant channels. In the case of iPS cell-derived neurons, the cells are subject to rapid and artificial neuronal differentiation, but they nevertheless go through various early stages of maturation during their development (Busskamp et al., 2014). The same applies to neurons electroporated *in utero*, which also undergo further maturation steps in their development and thus compensation options between electroporation and electrophysiological measurements. In contrast to

this, transduced primary hippocampal cultures have no possibility for relevant compensations in the short time, which leads to a more negative resting membrane potential. However, the compensations do not seem to be sufficient for the efficient development of action potentials and thus results in a hypoexcitability. The composition of K_V channels on the axon initial segment (AIS) forms a much more balanced equilibrium with Na_V channels, so that a pathological variant of one of these channels is likely to have a greater impact here than in other neuronal compartments which are more important for the RMP (Sánchez-Ponce et al., 2012). However, it remains to be proven how accurately iPS cell-derived neurons and their expression of different channels reflect physiological, fully mature human cortical neurons.

In summary, it can be assumed that the inadequate representation of the complex pathophysiology of a disease is probably one of the reasons why translation from research to the clinic often does not work satisfactorily (Atack et al., 2011; Rice, 2012). Heterologous overexpression systems in oocytes, but also iPS cell-derived human neurons, do not adequately reflect this complexity. Therefore, new model systems that are more similar to the actual human brain are required in order to gain a better understanding of the pathophysiology of diseases (Dolmetsch & Geschwind, 2011). Experiments with human tissue has been already demonstrated very successfully in oncology by the use of tumor tissue to get a better understanding of the biology behind tumor growth and to test new therapeutic options on certain tumor types (Gillet et al., 2013). In neuroscience, several studies based on rodent brain tissue demonstrated that the development of organotypic brain slice cultures has been successfully used to bridge the gap of *in vitro* to *in vivo* translation (Humpel, 2015). The use of *in vitro* human tissue, derived from neurosurgical procedures has therefore the capability to provide an invaluable insight into the function and structure of mature human glia and neuronal cells (Mohan et al., 2015; Smith & Dragunow, 2014) and to develop and test new therapeutic prospects for neurological diseases in the future.

3.3 Human organotypic brain slice cultures

For long-term experiments, up to four weeks, living organotypic brain slices from human brain tissue is the closest representation of the *in vivo* human brain outside of a living person (Eugène et al., 2014; Le Duigou et al., 2018; Schwarz et al., 2017; Schwarz et al., 2019). Compared to brain tissue of laboratory animals, human brain tissue is a very limited and therefore a valuable resource. Several studies have already shown significant differences between rodents and human brain tissue (Herculano-Houzel, 2009). For example, human astrocytes in temporal cortex are up to three times larger and their processes are ten times more complex than their rodent counterparts (Oberheim et al., 2009). Also the quantity and diversity of interneurons is much higher (Džaja et al., 2014; Radonjić et al., 2014). Furthermore, not only is the size of the individual neurons up to three times larger (Mohan et al., 2015), but they also have a considerably more branched dendritic tree (Mansvelder et al., 2019). Finally, the total numbers of neurons, spines and synapses, as well as the synaptic strength, differ among species (Beck et al., 2000; Benavides-Piccione et al., 2002; DeFelipe, 2011; DeFelipe et al., 2002; Molnár et al., 2016). These differences are also reflected in their molecular composition (Hodge et al., 2019). In human excitatory synapses, roughly 30% of the proteins are not present in mouse synapses (Bayés et al., 2012) and there are also several differences in protein isoform expression, for example the expression of tau protein in adult mice versus adult human brains (Hernández et al., 2020). All these morphological and molecular differences in human cortical neurons, especially in layer 2 and layer 3 pyramidal neurons (Deitcher et al., 2017; Eyal et al., 2016), lead to more sophisticated computational rules when it comes to process all the neuronal signals in comparison with other mammals (Testa-Silva et al., 2010; Verhoog et al., 2013). For example, in human layers 2 and 3 pyramidal neurons a class of calcium-mediated dendritic action potentials (dCaAPs) were discovered that can modulate the neuronal output, something that has not yet been discovered in any other brain tissue (Gidon et al., 2020). All these examples emphasize the importance of directly studying human brain tissue and not just iPS cell-derived neurons, dissociated cultures or primary cell lines. Some electrophysiological questions, in particular about static

intrinsic properties of human neurons, can certainly be carried out in acute human brain slices and answered successfully. The situation is different when it comes to an investigation of medium- or long-term effects in human brain tissue, for instance in the area of neuroplasticity, the identification of new therapeutic targets, the effects of certain gene mutations or the genetic manipulation of the tissue via viral transduction. A long-term cultivation of human organotypic brain slices therefore is a very desirable goal to reduce the gap between classical *in vitro* experiments and *in vivo* experiments. These slice cultures, which consist of physiologically developed brain tissue, could not only provide new insights into the issues described above, but could also be used for pre-clinical drug development and new experimental therapy options. It is therefore particularly important to study the few tissue samples that are available as efficiently and profitably as possible. An important contribution to this is to keep the cultures physiologically intact and alive for a longer period of time. Previous studies demonstrated already a prolonged survival of human hippocampal slices by using an artificial complex defined culturing media (Eugène et al., 2014).

In Schwarz et al., 2017 we demonstrated that a long-term neuronal survival in neocortical slices is improved significantly by using human cerebrospinal fluid as culturing medium compared with other conventional culture strategies. These data were corroborated by robust electrophysiological single cell and network measurements and further from immunofluorescence staining against the neuronal marker MAP2. *In vivo*, the brain tissue is surrounded by cerebrospinal fluid (CSF) and the interstitial fluid (ISF). Together they form a continuous fluidic network, which is characterized by low protein and high salt concentrations (Agnati et al., 1986, 2010). An increase of neuronal activity has already been observed in rodent models using hCSF instead of aCSF (Bjorefeldt et al., 2015, 2018). The influence of neuroendocrine components in the hCSF was assumed to be the cause (Skipor & Thiery, 2008). Not only morphological, but also electrophysiological properties are strongly dependent on the culture or recording medium. Earlier studies showed significantly more frequent multi-unit discharges and epileptiform activities when using a serum-free medium (Eugène et al., 2014) compared to a MEM-based medium (Stoppini et al., 1991) for the cultivation of

hippocampal tissue from patients suffering from pharmacoresistant epilepsy. This was attributed to the variability of the culture medium, astrocytic proliferation, transcription factors, neurotrophic substances and high concentrations of glutamic acid and glutamine in the serum-based medium (Eugène et al., 2014). Artificial extracellular fluid (artificial liquor, aCSF) or culture media usually only consist of electrolytes, glucose, water and essential amino acids. The complex organic components of physiological CSF including proteins, peptides, lipids and other amino acids as well as a wide range of neuromodulators are missing. The relevant neuromodulators seem to have a low molecular weight (<8 kDa), as recordings with dialyzed hCSF led to a greatly reduced synaptic activity (Bjorefeldt et al., 2018). It is not yet clear which specific neuromodulators are responsible for the increase in activity, but it is likely to be a mix of classical transmitters (acetylcholine, dopamine, serotonin) (Strittmatter et al., 1997; Welch et al., 1976), neuropeptides (neuropeptide Y, somatostatin, vasopressin) (Martin et al., 2014; Nilsson et al., 2001), neurosteroids (S. B. Kim et al., 2003) and amino acids (Orhan et al., 2018; Spreux-Varoquaux et al., 2002). For further detail see chapter 2.4.

How stable the electrophysiological properties remain in culture over a longer period of time and how well the detailed cytoarchitecture of the neurons, in particular of the dendrites and spines, is preserved was subsequently examined in Schwarz et al., 2019. Remarkably, we could demonstrate that electrophysiological as well as morphological parameters of excitatory pyramidal cells and inhibitory interneurons across all cortical layers were relatively stable between the acute, an early (2-3 DIV) and a late-stage culture status (7-14 DIV). We compared spike frequency, AP half-width, resting membrane potential, sag potential and input resistance. On the spine level, spine length, spine density, and spine head diameter were included. Additionally, we demonstrated efficient viral transduction for fluorescence-mediated 3D reconstruction and unveiled that a viral mediated genetic manipulation of the neurons has no detectable influence on the morphology and the basic electrophysiological properties of the analyzed cells. Furthermore, we performed long-term live imaging on spine level, a technique that is rather difficult to accomplish *in vivo*. For further detail see

Chapter 2.5. This work creates an important basis for future studies with cultured human slices, since a relatively stable system over at least two weeks can be assumed.

Despite the obvious advantages of human long-term cultures, this method also has its disadvantages. For example, it is resection tissue of different origins from different individuals, with different ages, gender or genetic background who, for different reasons, have to undergo neurosurgical intervention. Mostly it’s about access tissue and not about the pathological focus, but still it’s not neural tissue from a healthy human brain, which may have been under the influence of drugs for years. Therefore, controls within an experimental study of a batch are essential to allow at least paired analyzes, which will add some statistical power to the experiments. The experimental approach can be further strengthened by repeated experiments in different patients with different backgrounds. A first promising indication that the patient's background does not have too much influence on the tissue properties was made by observing and comparing synaptic plasticity in tissue samples from epilepsy and tumor patients, whereby no differences between the various tissue samples could be detected (Verhoog et al., 2013). Due to the limited availability of human tissue, it would be very desirable that the tissue used, at least in its basic features (patient age, gender, co-morbidities, use of medication, tissue origin etc.), be carefully characterized and properly documented. This should best be done using a public database so that all groups working with human brain tissue can better compare their results and repeat observations.

Furthermore, the limited availability of human brain tissue does not allow high throughput experiments. Here, the advantages of iPS cell-derived neurons come into play and can serve as a complementary approach, as these can be reproduced in large numbers. Months of cultivation, including the chronic use of medication, are easy to perform and evaluate (Gunaseeli et al., 2010; Heilker et al., 2014). For instance, Roche's candidate RG7800, which is in phase II and is to be approved for the treatment of spinal muscular atrophy (SMA), was previously validated in an iPS cell model (Mullard, 2015). As already mentioned

above, despite numerous neuronal differentiation protocols (Badger et al., 2014; Bissonnette et al., 2011) it is still difficult to reproducibly differentiate the desired neuron type. Also the maturity of the neurons (Rosa et al., 2020) and the physiological microenvironment with astrocytes, microglial cells and endothelial cells of the blood vessels is not comparable to cells matured *in vivo*. The goal of the neuronal differentiation protocols is to create the most physiological structure and function of the neurons and, in the best case, the other cells in the brain. The cells from resected human brain tissue offer the best benchmark for continuously improving the protocols and thus generating cells that come as close as possible to physiologically mature neurons in the adult brain *in vivo*. Therefore, an interlocking and combination of the various models is desirable. In addition to the option of neurons differentiated in 2D from iPS cells, there is also the option of 3D cultures, especially the cortical spheroids (Pasca et al., 2015) and brain organoids (Lancaster et al., 2013), which probably offer a more physiological environment, as there are more cell types from the brain, such as glial cells. But also here the electrophysiological maturity of the cells is not yet comparable with the situation in the human brain (Fair et al., 2020). The lack of a blood-brain barrier is a significant disadvantage in 2D or 3D cultures as well as in organotypic brain slices. This means that no final drug studies can be accomplished, as this point in particular often leads to the failure of drug candidates, because the substances do not, or only insufficiently, arrive from the bloodstream in the brain tissue. So far, these studies can only be carried out *in vivo* using animal models. Likewise, studies aimed at the cognitive performance of the brain can only be performed with living animals.

In general, there is no such thing as the perfect model system in neuroscience, but that one or a combination of several models must be selected depending on the research question and application. However, many of the present systems have made little or no progress in the treatment of the aggressive brain tumor glioblastoma multiforme. Potentially long-term human organotypic brain slice cultures can make a decisive contribution to find out more about the relevant relationships between tumor cells and the surrounding tissue and thereby opening up new therapy options.

3.4 Effects of irradiation and virotherapy on brain tumor initiating cells in human organotypic brain slice cultures

A first preclinical application of the human organotypic brain slices was completed in collaboration with the working group Molecular Neurooncology of Prof. Dr. U. Naumann. The method was used to evaluate the therapeutic effect of oncolytic adenoviruses combined with irradiation in brain tumor initiating cells in their natural environment by implantation glioma spheres into cultured sections (Czolk et al., 2019). Glioblastoma multiforme (GBM - 54% of all gliomas) is one of the most malignant type of brain tumor in humans (Stupp et al., 2005), with a median survival of ≤14 months post diagnosis, even with the highest level of nursing and use of novel therapeutic strategies (Ramirez et al., 2013; Taylor et al., 2019). The survival time has increased only marginally in the last few years despite all scientific efforts. It is therefore imperative to develop new therapy options and drug candidates. One of the specific characteristics of GBM is the infiltrative growth into healthy brain tissue (Darmanis et al., 2017). However, extracranial metastases rarely occur, which is an indicator that the microenvironment in the human CNS plays a central role in the growth and progression of GBMs (Ray et al., 2015) and it is therefore of great interest to study this interaction. Many previous model systems did not present this immanent advantage of the defined human microenvironment, since they were either only 2D cell cultures of GBM cells (M. Wu & Melody, 2014) or, as a further development, 3D collagen hydrogel models (Grotzer et al., 2016). In addition, genetically modified mouse models were developed and injected with patient tumor cells (Jackson & Thomas, 2017), which also have a functioning blood-brain barrier in order to investigate the transfer of drugs from the blood to the brain tissue. Nonetheless, these experiments show significant interspecies differences, such as an altered immune response. By using human organotypic brain slice cultures, many of these disadvantages are eliminated and a microenvironment can be created for brain tumor research which is relatively close to that of the human brain. This improved setting was used to show how different treatments affect the growth of transplanted glioma spheres into human organotypic brain slice cultures. The glioma spheres were either irradiated or just treated with the YB-1-dependent

oncolytic adenovirus (XVir-N-31) or both treatment options were combined. It could be shown that the multifunctional Y-box binding protein-1 (YB-1) is more concentrated in the nucleus due to irradiation, which leads to an increase in oncolytic XVir-N-31 virus production. Therefore, the combined therapy leads to a significantly delayed invasion into surrounding brain tissue as compared with the single treatment methods (Czolk et al., 2019). With this model system, both the growth of human tumor cells and the behavior of the surrounding human brain tissue into which the glioma spheres invaded can be studied. The knowledge gained from these experiments will hopefully lead to new therapy options in the future for the still very difficult to treat glioblastoma multiforme.

3.5 Outlook

Not only in the search for new therapy options in neuro-oncology, but also in many other areas, organotypic brain slice cultures can make a significant contribution to new knowledge. In cooperation with the working group Cellular Neurology of Prof. Dr. M. Jucker, it was possible to establish a model system for the investigation of α-synucleinopathies, which has made use of the advantages of these slice cultures. In addition to other interesting findings, a successful screening of antibodies was accomplished, which prevent the spread of α-synuclein lesions in mouse slices (data are not yet published). Future studies will show whether the lesions can also be prevented from spreading in human slices. But also in the field of epileptic encephalopathies, the organotypic brain slices could provide new insights into the underlying pathophysiology. In first experiments, the disease-causing variant *KCNA2* p.R297Q was virally overexpressed in human slices and examined electrophysiologically. The analyzed cells show a similar hypoexcitability (Figure 15) as the above-mentioned transduced primary hippocampus mouse cultures, since there was also no possibility to compensate for this over a longer period of time.

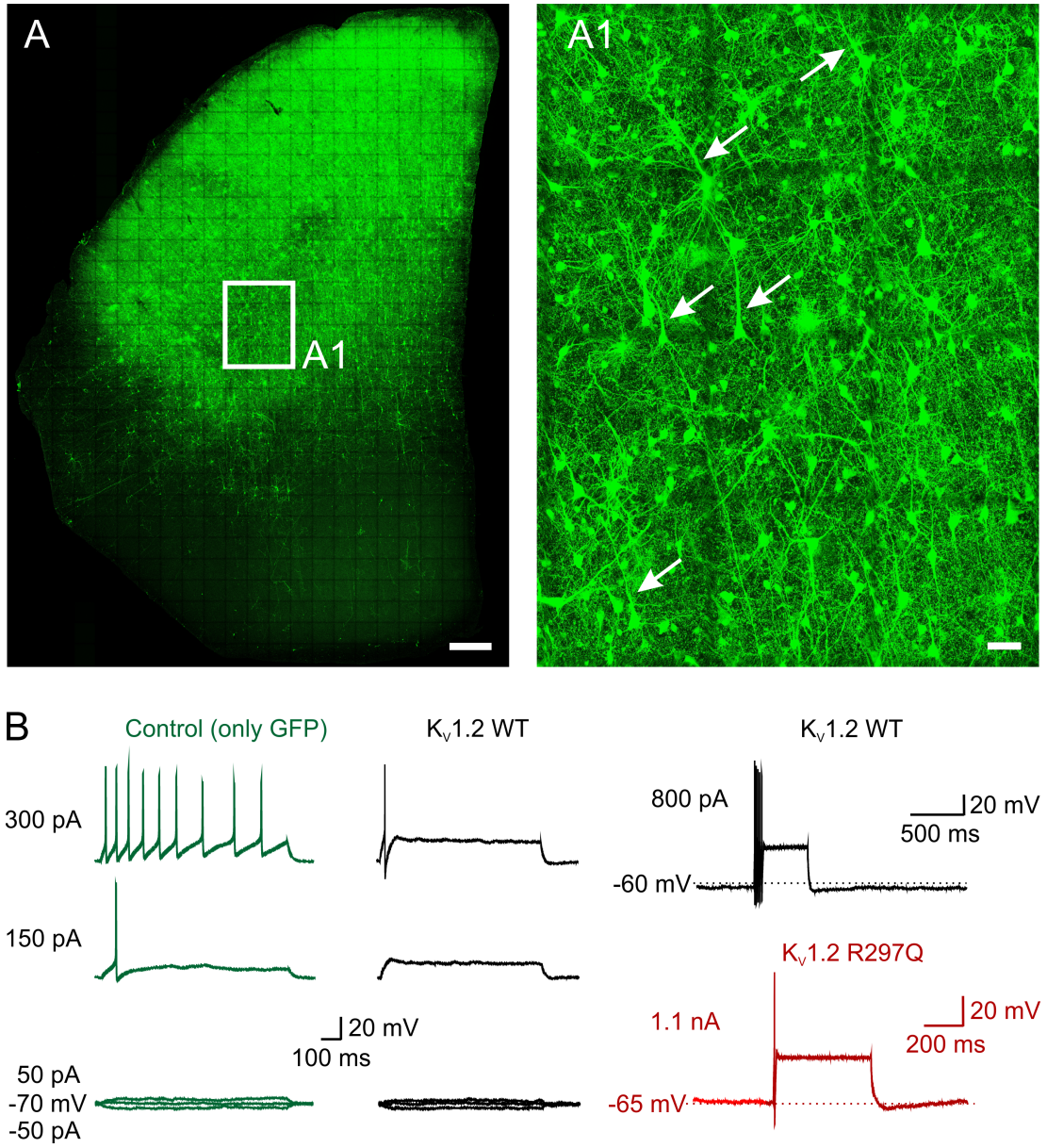


Figure 15: Transduction of cortical neurons overexpressing WT or mutant R297Q K_V1.2 channels.

(A) Overview of a representative transduction of a human organotypic brain slice with AAVrg-hSyn-*KCNA2*-WT-T2A-EGFP, scale bar 500 µm. (A1) Enlarged confocal image from A: pyramidal neurons with intact apical dendrites (white arrows), scale bar 50 µm. (B) Representative voltage traces of evoked action potentials (APs) recorded in the current clamp mode for cortical neurons transduced with either control, AAVrg-hSyn-EGFP or K_V1.2 wild-type, AAVrg-hSyn-*KCNA2*-WT-T2A-EGFP (black traces) or mutated K_V1.2 R297Q channels, AAVrg-hSyn-*KCNA2*-R297Q-T2A-EGFP (red traces).

The combination of iPS cells and organotypic brain slices will also play an important role in the future. It will be interesting to explore what happens when patient-specific cells are transplanted into human brain slices. It is not only the

behavior of the transplanted neurons that is of interest, but also their influence on the existing neuronal network of the brain slices. Both, the iPS cells and the cells in the slices can be manipulated by different tools to answer a wide variety of questions, for example CRISPR / Cas9 to edit the DNA (Jinek et al., 2012), or to regulate specific genes up or down (Konermann et al., 2015). Further possibilities are the expression of functional reporter genes like calcium sensors (Chen et al., 2013), voltage sensors (Piatkevich et al., 2018), channelrhodopsins for optogenetic experiments (Deisseroth, 2011), or designer receptors which are exclusively activated by designer drugs (DREADDs) (Roth, 2016).

Another aspect that has not yet been investigated is how human glial cells influence the physiology and pathology of human neurons and their synapses and thus ultimately also the behavior and cognitive performance of the brain. Like neurons, human astrocytes, microglia and pericytes also have specific anatomical and physiological properties that cannot be reproduced in cell culture or in non-human slice cultures (Fyfe, 2019; Oberheim et al., 2009; Rustenhoven et al., 2017). However, these cells play an essential role for normal neuronal function. Therefore, the brain slice cultures also offer an exciting opportunity to learn more about the interplay of neurons and glial cells in the brain.

During all these investigations, it is also important to keep in mind that organotypic brain slice cultures reduce the number of animal experiments and thus contribute significantly to the 3Rs (reduce, refine, replace). Another point that should not be neglected in relation to the 3R is the use of human cerebrospinal fluid as a replacement for previously used culture media. Many culture media are mixed with animal substances (e.g. fetal calf serum or growth hormones) in order to keep the cells alive in culture, which can be completely renounced with this new approach. This fact represents another exciting research area, as it is not known yet which components of the hCSF are ultimately necessary for the survival of the cultures, although there are numerous indications of neuromodulating substances in the hCSF (Veening & Barendregt, 2010).

The human iPS cells and the human organotypic brain slice cultures undoubtedly provide new and crucial information to better understand pathophysiological relationships that could not have been found in other cell culture systems or in animal experiments. This makes an important contribution to the translation of new therapy options from the laboratory to the clinic.

4 Summary

In the work presented here, two model systems for neurosciences were established in order to better examine neuronal functions. In the first and second part of the project, skin fibroblasts from patients with variants in the *KCNA2* gene (c.890G> A, p.R297Q and c.982T> G, p.L328V), which are the cause of the patients' epileptic encephalopathy (DEE), were reprogrammed into induced pluripotent stem (iPS) cells with the help of viral vectors. The characterization of the iPS cell lines was performed by karyotyping, by immunofluorescence staining against several pluripotency markers, a qRT-PCR to control the upregulation of the endogenous pluripotency markers and a differentiation of the iPS cells into cells from all three germ layers. In the third part of the project, these iPS cells were differentiated into human neurons through the virally mediated overexpression of the neuronal transcription factor NGN2. The subsequent electrophysiological characterization of the two cell lines and the comparison with healthy control lines showed no significant difference between the neurons of the *KCNA2* p.R297Q variant carrier and the control cells. The differentiated neurons of the *KCNA2* p.L328V variant carrier generated significantly smaller outward currents than the control neurons and responded to current injections with fewer action potentials than the control neurons. Because of the inadequate representation of this model system compared to the human brain, new alternatives were sought. In the fourth and fifth part of the project, it was possible for the first time to show that human cortical brain tissue outside the human body can survive for several weeks without the neurons or the entire neural network losing their basic morphological and electrophysiological properties. The decisive difference to previous approaches was the successful discovery that human brain tissue can be cultivated very well in human cerebrospinal fluid. The electrophysiological parameters compared were relatively stable between the acute, early (2-3 DIV) and a late-stage culture status (7-14 DIV). In addition, an efficient virus transduction is possible and allows fluorescence-mediated 3D reconstruction. A virally mediated GFP expression in neurons has no to date detectable influence on the morphology and the basic electrophysiological

properties of the analyzed cells. Moreover, long-term live imaging of human spines could be performed, as well as the detection of an outgrowth of human axons. Both are methods that are difficult to perform *in vivo*. The integration of human organotypic brain slices presented here into existing model systems such as that of the iPS cell-derived neurons will be of great value for studies on living human neuronal networks, as well as for the screening of new drugs, but also for direct research into neurological diseases. This new model system gives us a great opportunity to learn more about the human brain and could help us to answer the question of what makes us human after all.

5 German summary

In der hier vorgestellten Arbeit wurden zwei Modellsysteme für die Neurowissenschaften etabliert um neuronale Funktionen besser untersuchen zu können. Im ersten und zweiten Teil des Projektes wurden Hautfibroblasten von Patienten mit Varianten im *KCNA2* Gen (c.890G> A, p.R297Q und c.982T> G, p.L328V), welche ursächlich für die epileptische Enzephalopathie (DEE) der Patienten sind, zu induzierten pluripotenten Stammzellen (iPS Zellen) mit Hilfe von viralen Vektoren reprogrammiert. Die Charakterisierung der iPS Zelllinien erfolgte u.a. durch eine Karyotypisierung, durch Immunfluoreszenzfärbungen gegen mehrere Pluripotenzmarker, einer qRT-PCR zur Kontrolle der Hochregulierung der endogenen Pluripotenzmarker und einer Differenzierung in Zellen aus allen drei Keimblättern. Im dritten Teil des Projektes wurden diese iPS Zellen durch die viral vermittelte Überexpression des neuronalen Transkriptionsfaktors NGN2 zu humanen Neuronen differenziert. Die anschließende elektrophysiologische Charakterisierung der beiden Zelllinien und der Vergleich mit gesunden Kontrolllinien zeigten keinen signifikanten Unterschied der Neurone des Patienten mit der *KCNA2* p.R297Q-Variante im Vergleich zu den Kontrollzellen. Die differenzierten Neurone des Patienten mit der *KCNA2* p.L328V-Variante generierten signifikant kleinere Auswärtsströme als die Kontrollneuronen und reagierten auf Strominjektionen mit weniger Aktionspotentialen als die Kontrollneuronen. Aufgrund der unzureichenden Repräsentation dieses Modellsystems im Vergleich zum menschlichen Gehirn wurde nach neuen Alternativen gesucht. Im vierten und fünften Teil des Projektes konnte erstmals gezeigt werden, dass ein Überleben von humanem Hirngewebe außerhalb des menschlichen Körpers über mehrere Wochen möglich ist, ohne dass die Neurone bzw. das gesamte neuronale Netzwerk ihre grundlegenden morphologischen und elektrophysiologischen Eigenschaften verlieren. Der entscheidende Unterschied zu bisherigen Ansätzen liegt in der erfolgreichen Entdeckung, dass sich humanes Hirngewebe sehr gut in humanem Liquor cerebrospinalis kultivieren lässt. Die verglichenen elektrophysiolgischen Parameter waren relativ stabil zwischen dem akuten, einem frühen (2-3 DIV) und

einem späten Zeitpunkt der Kultivierung (7-14 DIV). Zusätzlich wurde gezeigt, dass eine effiziente Virustransduktion für die fluoreszenzvermittelte 3D-Rekonstruktion möglich ist und dass eine viral vermittelte genetische Manipulation der Neuronen keinen bisher nachweisbaren Einfluss auf die Morphologie und die grundlegenden elektrophysiologischen Eigenschaften der analysierten Zellen hat. Darüber hinaus konnte eine Langzeit-Live-Bildgebung der humanen Synapsen durchgeführt werden, eine Methode, die *in vivo* nur schwer durchzuführen ist. Die Integration der hier vorgestellten humanen organotypischen Hirnschnitte in bereits bestehende Modellsysteme wie das der aus iPS Zellen differenzierten Neurone wird von großem Wert für Untersuchungen an lebendigen humanen neuronalen Netzwerken, sowie beim Screening von neuen Medikamenten aber auch der direkten Erforschung neurologischer Erkrankungen sein. Dieses neue Modellsystem bietet uns eine großartige Gelegenheit, mehr über das menschliche Gehirn zu erfahren, und könnte uns helfen, die Frage zu beantworten, was uns letzten Endes zu Menschen macht.

6 List of references

Agnati, L. F., Fuxe, K., Zoli, M., Ozini, I., Toffano, G., & Ferraguti, F. (1986). A correlation analysis of the regional distribution of central enkephalin and β-endorphin immunoreactive terminals and of opiate receptors in adult and old male rats. Evidence for the existence of two main types of communication in the central nervous sys. *Acta Physiologica Scandinavica*, *128*(2), 201–207. https://doi.org/10.1111/j.1748-1716.1986.tb07967.x

Agnati, Luigi F., Guidolin, D., Guescini, M., Genedani, S., & Fuxe, K. (2010). Understanding wiring and volume transmission. In *Brain Research Reviews* (Vol. 64, Issue 1, pp. 137–159). https://doi.org/10.1016/j.brainresrev.2010.03.003

Aldape, K., Brindle, K. M., Chesler, L., Chopra, R., Gajjar, A., Gilbert, M. R., Gottardo, N., Gutmann, D. H., Hargrave, D., Holland, E. C., Jones, D. T. W., Joyce, J. A., Kearns, P., Kieran, M. W., Mellinghoff, I. K., Merchant, M., Pfister, S. M., Pollard, S. M., Ramaswamy, V., … Gilbertson, R. J. (2019). Challenges to curing primary brain tumours. *Nature Reviews Clinical Oncology*. https://doi.org/10.1038/s41571-019-0177-5

Alemasova, E. E., Pestryakov, P. E., Sukhanova, M. V., Kretov, D. A., Moor, N. A., Curmi, P. A., Ovchinnikov, L. P., & Lavrik, O. I. (2015). Poly(ADP-ribosyl)ation as a new posttranslational modification of YB-1. *Biochimie*, *119*, 36–44. https://doi.org/10.1016/j.biochi.2015.10.008

Allen Hauser, W., & Annegers, J. F. (1996). Descriptive epidemiology of epilepsy: Contributions of population-based studies from rochester, minnesota. *Mayo Clinic Proceedings*, *71*(6), 576–586. https://doi.org/10.4065/71.6.576

Andersson, M., Avaliani, N., Svensson, A., Wickham, J., Pinborg, L. H., Jespersen, B., Christiansen, S. H., Bengzon, J., Woldbye, D. P. D., & Kokaia, M. (2016). Optogenetic control of human neurons in organotypic brain cultures. *Scientific Reports*, *6*(1), 24818. https://doi.org/10.1038/srep24818

Anton-Sanchez, L., Larrañaga, P., Benavides-Piccione, R., Fernaud-Espinosa, I., Defelipe, J., & Bielza, C. (2017). Three-dimensional spatial modeling of spines along dendritic networks in human cortical pyramidal neurons. *PLoS ONE*, *12*(6), 1–14. https://doi.org/10.1371/journal.pone.0180400

Arvanitis, C. D., Ferraro, G. B., & Jain, R. K. (2020). The blood–brain barrier and blood–tumour barrier in brain tumours and metastases. In *Nature Reviews Cancer* (Vol. 20, Issue 1, pp. 26–41). https://doi.org/10.1038/s41568-019-0205-x

Ascoli, G. A., Alonso-Nanclares, L., Anderson, S. A., Barrionuevo, G., Benavides-Piccione, R., Burkhalter, A., Buzsáki, G., Cauli, B., DeFelipe, J.,

Fairén, A., Feldmeyer, D., Fishell, G., Fregnac, Y., Freund, T. F., Gardner, D., Gardner, E. P., Goldberg, J. H., Helmstaedter, M., Hestrin, S., … Yuste, R. (2008). Petilla terminology: Nomenclature of features of GABAergic interneurons of the cerebral cortex. In *Nature Reviews Neuroscience* (Vol. 9, Issue 7, pp. 557–568). https://doi.org/10.1038/nrn2402

Atack, J. R., Wafford, K. A., Street, L. J., Dawson, G. R., Tye, S., Van Laere, K., Bormans, G., Sanabria-Bohórquez, S. M., De Lepeleire, I., De Hoon, J. N., Van Hecken, A., Burns, H. D., McKernan, R. M., Murphy, M. G., & Hargreaves, R. J. (2011). MRK-409 (MK-0343), a GABAA receptor subtype-selective partial agonist, is a non-sedating anxiolytic in preclinical species but causes sedation in humans. *Journal of Psychopharmacology*, *25*(3), 314–328. https://doi.org/10.1177/0269881109354927

Auffinger, B., Tobias, A. L., Han, Y., Lee, G., Guo, D., Dey, M., Lesniak, M. S., & Ahmed, A. U. (2014). Conversion of differentiated cancer cells into cancer stem-like cells in a glioblastoma model after primary chemotherapy. *Cell Death and Differentiation*, *21*(7), 1119–1131. https://doi.org/10.1038/cdd.2014.31

Auffinger, Brenda, Spencer, D., Pytel, P., Ahmed, A. U., & Lesniak, M. S. (2015). The role of glioma stem cells in chemotherapy resistance and glioblastoma multiforme recurrence. In *Expert Review of Neurotherapeutics* (Vol. 15, Issue 7, pp. 741–752). https://doi.org/10.1586/14737175.2015.1051968

Avior, Y., Sagi, I., & Benvenisty, N. (2016). Pluripotent stem cells in disease modelling and drug discovery. In *Nature Reviews Molecular Cell Biology* (Vol. 17, Issue 3, pp. 170–182). https://doi.org/10.1038/nrm.2015.27

Awan, K. A., & Dolly, J. O. (1991). K+ channel sub-types in rat brain: Characteristic locations revealed using β-bungarotoxin, α- and δ-dendrotoxins. *Neuroscience*, *40*(1), 29–39. https://doi.org/10.1016/0306-4522(91)90172-K

Badger, J. L., Cordero-Llana, O., Hartfield, E. M., & Wade-Martins, R. (2014). Parkinson's disease in a dish - Using stem cells as a molecular tool. In *Neuropharmacology* (Vol. 76, Issue PART A, pp. 88–96). https://doi.org/10.1016/j.neuropharm.2013.08.035

Bagheri, M., Rezakhani, A., Roghani, M., Joghataei, M. T., & Mohseni, S. (2015). Protocol for three-dimensional confocal morphometric analysis of astrocytes. *Journal of Visualized Experiments*, *2015*(106). https://doi.org/10.3791/53113

Bardy, C., Van Den Hurk, M., Kakaradov, B., Erwin, J. A., Jaeger, B. N., Hernandez, R. V., Eames, T., Paucar, A. A., Gorris, M., Marchand, C., Jappelli, R., Barron, J., Bryant, A. K., Kellogg, M., Lasken, R. S., Rutten, B. P. F., Steinbusch, H. W. M., Yeo, G. W., & Gage, F. H. (2016). Predicting the functional states of human iPSC-derived neurons with single-cell RNA-

seq and electrophysiology. *Molecular Psychiatry*, *21*(11), 1573–1588. https://doi.org/10.1038/mp.2016.158

Bardy, Cedric, Van Den Hurk, M., Eames, T., Marchand, C., Hernandez, R. V., Kellogg, M., Gorris, M., Galet, B., Palomares, V., Brown, J., Bang, A. G., Mertens, J., Böhnke, L., Boyer, L., Simon, S., & Gage, F. H. (2015). Neuronal medium that supports basic synaptic functions and activity of human neurons in vitro. *Proceedings of the National Academy of Sciences of the United States of America*, *112*(20), E2725–E2734. https://doi.org/10.1073/pnas.1504393112

Bayés, À., Collins, M. O., Croning, M. D. R., van de Lagemaat, L. N., Choudhary, J. S., & Grant, S. G. N. (2012). Comparative Study of Human and Mouse Postsynaptic Proteomes Finds High Compositional Conservation and Abundance Differences for Key Synaptic Proteins. *PLoS ONE*, *7*(10). https://doi.org/10.1371/journal.pone.0046683

Beck, H., Goussakov, I. V., Lie, A., Helmstaedter, C., & Elger, C. E. (2000). Synaptic plasticity in the human dentate gyrus. *Journal of Neuroscience*, *20*(18), 7080–7086. https://doi.org/10.1523/jneurosci.20-18-07080.2000

Beier, D., Hau, P., Proescholdt, M., Lohmeier, A., Wischhusen, J., Oefner, P. J., Aigner, L., Brawanski, A., Bogdahn, U., & Beier, C. P. (2007). CD133+ and CD133- glioblastoma-derived cancer stem cells show differential growth characteristics and molecular profiles. *Cancer Research*, *67*(9), 4010–4015. https://doi.org/10.1158/0008-5472.CAN-06-4180

Benavides-Piccione, R., Ballesteros-Yáñez, I., DeFelipe, J., & Yuste, R. (2002). Cortical area and species differences in dendritic spine morphology. *Journal of Neurocytology*, *31*(3-5 SPEC. ISS.), 337–346. https://doi.org/10.1023/A:1024134312173

Bernard, C., Anderson, A., Becker, A., Poolos, N. P., Deck, H., & Johnston, D. (2004). Acquired dendritic channelopathy in temporal lobe epilepsy. *Science*, *305*(5683), 532–535. https://doi.org/10.1126/science.1097065

Bieler, A., Mantwill, K., Holzmüller, R., Jürchott, K., Kaszubiak, A., Stärk, S., Glockzin, G., Lage, H., Grosu, A. L., Gansbacher, B., & Holm, P. S. (2008). Impact of radiation therapy on the oncolytic adenovirus dl520: Implications on the treatment of glioblastoma. *Radiotherapy and Oncology*, *86*(3), 419–427. https://doi.org/10.1016/j.radonc.2007.10.009

Bissonnette, C. J., Lyass, L., Bhattacharyya, B. J., Belmadani, A., Miller, R. J., & Kessler, J. A. (2011). The controlled generation of functional basal forebrain cholinergic neurons from human embryonic stem cells. *Stem Cells*, *29*(5), 802–811. https://doi.org/10.1002/stem.626

Bjorefeldt, A., Andreasson, U., Daborg, J., Riebe, I., Wasling, P., Zetterberg, H., & Hanse, E. (2015). Human cerebrospinal fluid increases the excitability of pyramidal neurons in the in vitro brain slice. *Journal of Physiology*, *593*(1), 231–243. https://doi.org/10.1113/jphysiol.2014.284711

Bjorefeldt, A., Illes, S., Zetterberg, H., & Hanse, E. (2018). Neuromodulation via the cerebrospinal fluid: Insights from recent in vitro studies. In *Frontiers in Neural Circuits* (Vol. 12). https://doi.org/10.3389/fncir.2018.00005

Boldog, E., Bakken, T. E., Hodge, R. D., Novotny, M., Aevermann, B. D., Baka, J., Bordé, S., Close, J. L., Diez-Fuertes, F., Ding, S. L., Faragó, N., Kocsis, Á. K., Kovács, B., Maltzer, Z., McCorrison, J. M., Miller, J. A., Molnár, G., Oláh, G., Ozsvár, A., … Tamás, G. (2018). Transcriptomic and morphophysiological evidence for a specialized human cortical GABAergic cell type. *Nature Neuroscience*, *21*(9), 1185–1195. https://doi.org/10.1038/s41593-018-0205-2

Bousquet, J., & Meunier, J. M. (1962). Organotypic culture, on natural and artificial media, of fragments of the adult rat hypophysis. *Comptes Rendus Des Séances de La Société de Biologie et de Ses Filiales*, *156*, 65–67.

Boyle, J. (2008). Molecular biology of the cell, 5th edition by B. Alberts, A. Johnson, J. Lewis, M. Raff, K. Roberts, and P. Walter. *Biochemistry and Molecular Biology Education*, *36*(4), 317–318. https://doi.org/10.1002/bmb.20192

Braak, H., Del Tredici, K., Rüb, U., De Vos, R. A. I., Jansen Steur, E. N. H., & Braak, E. (2003). Staging of brain pathology related to sporadic Parkinson's disease. *Neurobiology of Aging*, *24*(2), 197–211. https://doi.org/10.1016/S0197-4580(02)00065-9

Branco, T., & Häusser, M. (2011). Synaptic Integration Gradients in Single Cortical Pyramidal Cell Dendrites. *Neuron*, *69*(5), 885–892. https://doi.org/10.1016/j.neuron.2011.02.006

Britanova, O., Akopov, S., Lukyanov, S., Gruss, P., & Tarabykin, V. (2005). Novel transcription factor Satb2 interacts with matrix attachment region DNA elements in a tissue-specific manner and demonstrates cell-type-dependent expression in the developing mouse CNS. *European Journal of Neuroscience*, *21*(3), 658–668. https://doi.org/10.1111/j.1460-9568.2005.03897.x

Busskamp, V., Lewis, N. E., Guye, P., Ng, A. H., Shipman, S. L., Byrne, S. M., Sanjana, N. E., Murn, J., Li, Y., Li, S., Stadler, M., Weiss, R., & Church, G. M. (2014). Rapid neurogenesis through transcriptional activation in human stem cells. *Molecular Systems Biology*, *10*(11), 760. https://doi.org/10.15252/msb.20145508

Buta, C., David, R., Dressel, R., Emgård, M., Fuchs, C., Gross, U., Healy, L., Hescheler, J., Kolar, R., Martin, U., Mikkers, H., Müller, F. J., Schneider, R. K., Seiler, A. E. M., Spielmann, H., & Weitzer, G. (2013). Reconsidering pluripotency tests: Do we still need teratoma assays? In *Stem Cell Research* (Vol. 11, Issue 1, pp. 552–562). https://doi.org/10.1016/j.scr.2013.03.001

Caeser, M., & Aertsen, A. (1991). Morphological organization of rat

hippocampal slice cultures. *Journal of Comparative Neurology*, *307*(1), 87–106. https://doi.org/10.1002/cne.903070109

Capovilla, G., Wolf, P., Beccaria, F., & Avanzini, G. (2013). The history of the concept of epileptic encephalopathy. In *Epilepsia* (Vol. 54, Issue SUPPL.8, pp. 2–5). https://doi.org/10.1111/epi.12416

Carroll, W. M. (2019). The global burden of neurological disorders. In *The Lancet Neurology* (Vol. 18, Issue 5, pp. 418–419). https://doi.org/10.1016/S1474-4422(19)30029-8

Catterall, W. A. (1988). Structure and function of voltage-sensitive ion channels. *Science*, *242*(4875), 50–61. https://doi.org/10.1126/science.2459775

Catterall, W. A. (2000). From ionic currents to molecular mechanisms: The structure and function of voltage-gated sodium channels. In *Neuron*. https://doi.org/10.1016/S0896-6273(00)81133-2

Chambers, S. M., Fasano, C. A., Papapetrou, E. P., Tomishima, M., Sadelain, M., & Studer, L. (2009). Highly efficient neural conversion of human ES and iPS cells by dual inhibition of SMAD signaling. *Nature Biotechnology*, *27*(3), 275–280. https://doi.org/10.1038/nbt.1529

Chen, T. W., Wardill, T. J., Sun, Y., Pulver, S. R., Renninger, S. L., Baohan, A., Schreiter, E. R., Kerr, R. A., Orger, M. B., Jayaraman, V., Looger, L. L., Svoboda, K., & Kim, D. S. (2013). Ultrasensitive fluorescent proteins for imaging neuronal activity. *Nature*, *499*(7458), 295–300. https://doi.org/10.1038/nature12354

Child, N. D., & Benarroch, E. E. (2014). Differential distribution of voltage-gated ion channels in cortical neurons: Implications for epilepsy. *Neurology*. https://doi.org/10.1212/WNL.0000000000000228

Clark, R. E., & Squire, L. R. (1998). Classical conditioning and brain systems: The role of awareness. *Science*, *280*(5360), 77–81. https://doi.org/10.1126/science.280.5360.77

Covarrubias, M., Wei, A., & Salkoff, L. (1991). Shaker, Shal, Shab, and Shaw express independent K+ current systems. *Neuron*, *7*(5), 763–773. https://doi.org/10.1016/0896-6273(91)90279-9

Crain, S. M. (1966). Development of “Organotypic” Bioelectric Activities in Central Nervous Tissues During Maturation in Culture. *International Review of Neurobiology*, *9*(C), 1–43. https://doi.org/10.1016/S0074-7742(08)60135-X

Croft, C. L., Futch, H. S., Moore, B. D., & Golde, T. E. (2019). Organotypic brain slice cultures to model neurodegenerative proteinopathies. In *Molecular Neurodegeneration* (Vol. 14, Issue 1). https://doi.org/10.1186/s13024-019-0346-0

Czolk, R., Schwarz, N., Koch, H., Schötterl, S., Wuttke, T. V., Holm, P. S., Huber, S. M., & Naumann, U. (2019). Irradiation enhances the therapeutic effect of the oncolytic adenovirus XVir-N-31 in brain tumor initiating cells. *International Journal of Molecular Medicine*, *44*(4), 1484–1494. https://doi.org/10.3892/ijmm.2019.4296

D'Esposito, M., Postle, B. R., & Rypma, B. (2000). Prefrontal cortical contributions to working memory: Evidence from event-related fMRI studies. In *Experimental Brain Research* (Vol. 133, Issue 1, pp. 3–11). https://doi.org/10.1007/s002210000395

Darmanis, S., Sloan, S. A., Croote, D., Mignardi, M., Chernikova, S., Samghababi, P., Zhang, Y., Neff, N., Kowarsky, M., Caneda, C., Li, G., Chang, S. D., Connolly, I. D., Li, Y., Barres, B. A., Gephart, M. H., & Quake, S. R. (2017). Single-Cell RNA-Seq Analysis of Infiltrating Neoplastic Cells at the Migrating Front of Human Glioblastoma. *Cell Reports*, *21*(5), 1399–1410. https://doi.org/10.1016/j.celrep.2017.10.030

Daviaud, N., Garbayo, E., Schiller, P. C., Perez-Pinzon, M., & Montero-Menei, C. N. (2013). Organotypic cultures as tools for optimizing central nervous system cell therapies. In *Experimental Neurology* (Vol. 248, pp. 429–440). https://doi.org/10.1016/j.expneurol.2013.07.012

Dawson, W. R., & Ebbell, B. (1938). The Papyrus Ebers; The Greatest Egyptian Medical Document. *The Journal of Egyptian Archaeology*, *24*(2), 250. https://doi.org/10.2307/3854804

De Lera Ruiz, M., & Kraus, R. L. (2015). Voltage-Gated Sodium Channels: Structure, Function, Pharmacology, and Clinical Indications. In *Journal of Medicinal Chemistry* (Vol. 58, Issue 18, pp. 7093–7118). https://doi.org/10.1021/jm501981g

De Simoni, A., Griesinger, C. B., & Edwards, F. A. (2003). Development of rat CA1 neurones in acute versus organotypic slices: Role of experience in synaptic morphology and activity. *Journal of Physiology*, *550*(1), 135–147. https://doi.org/10.1113/jphysiol.2003.039099

DeAngelis, L. M. (2001). Brain tumors. *New England Journal of Medicine*. https://doi.org/10.1056/NEJM200101113440207

Debanne, D., Guérineau, N. C., Gähwller, B. H., & Thompson, S. M. (1997). Action-potential propagation gated by an axonal I(A)-like K+ conductance in hippocampus. *Nature*, *389*(6648), 286–289. https://doi.org/10.1038/38502

DeFelipe, J. (2011). The evolution of the brain, the human nature of cortical circuits, and intellectual creativity. In *Frontiers in Neuroanatomy* (Issue MAY). https://doi.org/10.3389/fnana.2011.00029

DeFelipe, J., Alonso-Nanclares, L., & Arellano, J. I. (2002). Microstructure of the neocortex: Comparative aspects. *Journal of Neurocytology*, *31*(3-5 SPEC.

ISS.), 299–316. https://doi.org/10.1023/A:1024130211265

Deisseroth, K. (2011). Optogenetics. In *Nature Methods* (Vol. 8, Issue 1, pp. 26–29). https://doi.org/10.1038/nmeth.f.324

Deitcher, Y., Eyal, G., Kanari, L., Verhoog, M. B., Atenekeng Kahou, G. A., Mansvelder, H. D., De Kock, C. P. J., & Segev, I. (2017). Comprehensive Morpho-Electrotonic Analysis Shows 2 Distinct Classes of L2 and L3 Pyramidal Neurons in Human Temporal Cortex. *Cerebral Cortex*, *27*(11), 5398–5414. https://doi.org/10.1093/cercor/bhx226

del Castillo, J., & Katz, B. (1954). Quantal components of the end-plate potential. *The Journal of Physiology*, *124*(3), 560–573. https://doi.org/10.1113/jphysiol.1954.sp005129

Dimidschstein, J., Chen, Q., Tremblay, R., Rogers, S. L., Saldi, G. A., Guo, L., Xu, Q., Liu, R., Lu, C., Chu, J., Grimley, J. S., Krostag, A. R., Kaykas, A., Avery, M. C., Rashid, M. S., Baek, M., Jacob, A. L., Smith, G. B., Wilson, D. E., … Fishell, G. (2016). A viral strategy for targeting and manipulating interneurons across vertebrate species. *Nature Neuroscience*, *19*(12), 1743–1749. https://doi.org/10.1038/nn.4430

Dolmetsch, R., & Geschwind, D. H. (2011). The human brain in a dish: The promise of iPSC-derived neurons. In *Cell* (Vol. 145, Issue 6, pp. 831–834). https://doi.org/10.1016/j.cell.2011.05.034

Dragunow, M. (2008). The adult human brain in preclinical drug development. *Nature Reviews Drug Discovery*, *7*(8), 659–666. https://doi.org/10.1038/nrd2617

Džaja, D., Hladnik, A., Bičanić, I., Baković, M., & Petanjek, Z. (2014). Neocortical calretinin neurons in primates: Increase in proportion and microcircuitry structure. *Frontiers in Neuroanatomy*, *8*(SEP). https://doi.org/10.3389/fnana.2014.00103

El Kosseifi, C., Cornet, M. C., & Cilio, M. R. (2019). Neonatal Developmental and Epileptic Encephalopathies. *Seminars in Pediatric Neurology*, *32*. https://doi.org/10.1016/j.spen.2019.08.006

Elston, G. N., Benavides-Piccione, R., & DeFelipe, J. (2001). The pyramidal cell in cognition: a comparative study in human and monkey. *The Journal of Neuroscience : The Official Journal of the Society for Neuroscience*, *21*(17), RC163. https://doi.org/10.1523/jneurosci.21-17-j0002.2001

Elston, Guy N., & DeFelipe, J. (2002). Spine distribution in cortical pyramidal cells: A common organizational principle across species. *Progress in Brain Research*, *136*, 109–133. https://doi.org/10.1016/S0079-6123(02)36012-6

Elston, Guy N., & Fujita, I. (2014). Pyramidal cell development: Postnatal spinogenesis, dendritic growth, axon growth, and electrophysiology. In *Frontiers in Neuroanatomy* (Vol. 8, Issue AUG).

https://doi.org/10.3389/fnana.2014.00078

Engle, S. J., Blaha, L., & Kleiman, R. J. (2018). Best Practices for Translational Disease Modeling Using Human iPSC-Derived Neurons. In *Neuron* (Vol. 100, Issue 4, pp. 783–797). https://doi.org/10.1016/j.neuron.2018.10.033

Erhardt, W., Henke, J., Haberstroh, J., Baumgartner, C., & Tacke, S. (2018). Vorwort zur 1. Auflage. In *Anästhesie und Analgesie beim Klein- und Heimtier*. Schattauer. https://doi.org/10.1055/b-0038-158980

Eugène, E., Cluzeaud, F., Cifuentes-Diaz, C., Fricker, D., Le Duigou, C., Clemenceau, S., Baulac, M., Poncer, J. C., & Miles, R. (2014). An organotypic brain slice preparation from adult patients with temporal lobe epilepsy. *Journal of Neuroscience Methods*, *235*, 234–244. https://doi.org/10.1016/j.jneumeth.2014.07.009

Ewert, L., Fischer, A., Brandt, S., Scurt, F. G., Philipsen, L., Müller, A. J., Girndt, M., Zenclussen, A. C., Lindquist, J. A., Gorny, X., & Mertens, P. R. (2018). Cold shock Y-box binding protein-1 acetylation status in monocytes is associated with systemic inflammation and vascular damage. *Atherosclerosis*, *278*, 156–165. https://doi.org/10.1016/j.atherosclerosis.2018.09.020

Eyal, G., Verhoog, M. B., Testa-Silva, G., Deitcher, Y., Lodder, J. C., Benavides-Piccione, R., Morales, J., Defelipe, J., de Kock, C. P. J., Mansvelder, H. D., & Segev, I. (2016). Unique membrane properties and enhanced signal processing in human neocortical neurons. *ELife*, *5*(OCTOBER2016). https://doi.org/10.7554/eLife.16553

Fair, S. R., Julian, D., Hartlaub, A. M., Pusuluri, S. T., Malik, G., Summerfied, T. L., Zhao, G., Hester, A. B., Ackerman, W. E., Hollingsworth, E. W., Ali, M., McElroy, C. A., Buhimschi, I. A., Imitola, J., Maitre, N. L., Bedrosian, T. A., & Hester, M. E. (2020). Electrophysiological Maturation of Cerebral Organoids Correlates with Dynamic Morphological and Cellular Development. *Stem Cell Reports*, *15*(4), 855–868. https://doi.org/10.1016/j.stemcr.2020.08.017

Fiest, K. M., Roberts, J. I., Maxwell, C. J., Hogan, D. B., Smith, E. E., Frolkis, A., Cohen, A., Kirk, A., Pearson, D., Pringsheim, T., Venegas-Torres, A., & Jetté, N. (2016). The prevalence and incidence of dementia due to Alzheimer's disease: A systematic review and meta-analysis. In *Canadian Journal of Neurological Sciences* (Vol. 43, Issue S1, pp. S51–S82). https://doi.org/10.1017/cjn.2016.36

Fisher, R. S., Cross, J. H., French, J. A., Higurashi, N., Hirsch, E., Jansen, F. E., Lagae, L., Moshé, S. L., Peltola, J., Roulet Perez, E., Scheffer, I. E., & Zuberi, S. M. (2017). Operational classification of seizure types by the International League Against Epilepsy: Position Paper of the ILAE Commission for Classification and Terminology. *Epilepsia*, *58*(4), 522–530. https://doi.org/10.1111/epi.13670

Fyfe, I. (2019). Mouse brains, human microglia. In *Nature Reviews Neurology* (Vol. 15, Issue 10, pp. 558–559). https://doi.org/10.1038/s41582-019-0252-7

Gähwiler, B. H., Capogna, M., Debanne, D., McKinney, R. A., & Thompson, S. M. (1997). Organotypic slice cultures: A technique has come of age. *Trends in Neurosciences*, *20*(10), 471–477. https://doi.org/10.1016/S0166-2236(97)01122-3

Gangoiti, P., Granado, M. H., Alonso, A., Goñi, F. M., & Gómez-Muñoz, A. (2008). Implication of ceramide, ceramide 1-phosphate and sphingosine 1-phosphate in tumorigenesis. *Translational Oncogenomics*, *2008*(3), 81–98. https://doi.org/10.4137/TOG.S0

Gerstner, E. R., & Fine, R. L. (2007). Increased permeability of the blood-brain barrier to chemotherapy in metastatic brain tumors: Establishing a treatment paradigm. In *Journal of Clinical Oncology* (Vol. 25, Issue 16, pp. 2306–3212). https://doi.org/10.1200/JCO.2006.10.0677

Gidon, A., Zolnik, T. A., Fidzinski, P., Bolduan, F., Papoutsi, A., Poirazi, P., Holtkamp, M., Vida, I., & Larkum, M. E. (2020). Dendritic action potentials and computation in human layer 2/3 cortical neurons. *Science*, *367*(6473), 83–87. https://doi.org/10.1126/science.aax6239

Gillet, J. P., Varma, S., & Gottesman, M. M. (2013). The clinical relevance of cancer cell lines. In *Journal of the National Cancer Institute* (Vol. 105, Issue 7, pp. 452–458). https://doi.org/10.1093/jnci/djt007

Gold, M. R., Stevenson, D., & Fryback, D. G. (2002). HALYs and QALYs and DALYs, oh my: Similarities and differences in summary measures of population health. *Annual Review of Public Health*, *23*, 115–134. https://doi.org/10.1146/annurev.publhealth.23.100901.140513

Goriounova, N. A., Heyer, D. B., Wilbers, R., Verhoog, M. B., Giugliano, M., Verbist, C., Obermayer, J., Kerkhofs, A., Smeding, H., Verberne, M., Idema, S., Baayen, J. C., Pieneman, A. W., de Kock, C. P. J., Klein, M., & Mansvelder, H. D. (2018). Large and fast human pyramidal neurons associate with intelligence. *ELife*, *7*. https://doi.org/10.7554/eLife.41714

Grotzer, M. A., Neve, A., & Baumgartner, M. (2016). Dissecting brain tumor growth and metastasis in vitro and ex vivo. *Journal of Cancer Metastasis and Treatment*, *2*(5), 149. https://doi.org/10.20517/2394-4722.2016.02

Guerrini, R., & Pellock, J. M. (2012). Age-related epileptic encephalopathies. In *Handbook of Clinical Neurology* (Vol. 107, pp. 179–193). https://doi.org/10.1016/B978-0-444-52898-8.00011-2

Gunaseeli, I., Doss, M., Antzelevitch, C., Hescheler, J., & Sachinidis, A. (2010). Induced Pluripotent Stem Cells as a Model for Accelerated Patient- and Disease-specific Drug Discovery. *Current Medicinal Chemistry*, *17*(8), 759–766. https://doi.org/10.2174/092986710790514480

Gutman, G. A., Chandy, K. G., Grissmer, S., Lazdunski, M., Mckinnon, D., Pardo, L. A., Robertson, G. A., Rudy, B., Sanguinetti, M. C., Stühmer, W., & Wang, X. (2005). International Union of Pharmacology. LIII. Nomenclature and molecular relationships of voltage-gated potassium channels. In *Pharmacological Reviews* (Vol. 57, Issue 4, pp. 473–508). https://doi.org/10.1124/pr.57.4.10

Hamdan, F. F., Myers, C. T., Cossette, P., Lemay, P., Spiegelman, D., Laporte, A. D., Nassif, C., Diallo, O., Monlong, J., Cadieux-Dion, M., Dobrzeniecka, S., Meloche, C., Retterer, K., Cho, M. T., Rosenfeld, J. A., Bi, W., Massicotte, C., Miguet, M., Brunga, L., … Michaud, J. L. (2017). High Rate of Recurrent De Novo Mutations in Developmental and Epileptic Encephalopathies. *American Journal of Human Genetics*, *101*(5), 664–685. https://doi.org/10.1016/j.ajhg.2017.09.008

Heck, N., Golbs, A., Riedemann, T., Sun, J. J., Lessmann, V., & Luhmann, H. J. (2008). Activity-dependent regulation of neuronal apoptosis in neonatal mouse cerebral cortex. *Cerebral Cortex*, *18*(6), 1335–1349. https://doi.org/10.1093/cercor/bhm165

Hedrich, U., Maljevic, S., & Lerche, H. (2013). Mechanisms of genetic epilepsies. *E-Neuroforum*, *19*(2), 23–30. https://doi.org/10.1007/s13295-013-0040-6

Heilker, R., Traub, S., Reinhardt, P., Schöler, H. R., & Sterneckert, J. (2014). IPS cell derived neuronal cells for drug discovery. In *Trends in Pharmacological Sciences* (Vol. 35, Issue 10, pp. 510–519). https://doi.org/10.1016/j.tips.2014.07.003

Hendrie, P. C., & Russell, D. W. (2005). Gene targeting with viral vectors. *Molecular Therapy*, *12*(1), 9–17. https://doi.org/10.1016/j.ymthe.2005.04.006

Herculano-Houzel, S. (2009). The human brain in numbers: A linearly scaled-up primate brain. In *Frontiers in Human Neuroscience* (Vol. 3, Issue NOV). https://doi.org/10.3389/neuro.09.031.2009

Hernández, F., Merchán-Rubira, J., Vallés-Saiz, L., Rodríguez-Matellán, A., & Avila, J. (2020). Differences Between Human and Murine Tau at the N-terminal End. In *Frontiers in Aging Neuroscience* (Vol. 12). https://doi.org/10.3389/fnagi.2020.00011

Higurashi, N., Uchida, T., Lossin, C., Misumi, Y., Okada, Y., Akamatsu, W., Imaizumi, Y., Zhang, B., Nabeshima, K., Mori, M. X., Katsurabayashi, S., Shirasaka, Y., Okano, H., & Hirose, S. (2013). A human Dravet syndrome model from patient induced pluripotent stem cells. *Molecular Brain*, *6*(1). https://doi.org/10.1186/1756-6606-6-19

Hodge, R. D., Bakken, T. E., Miller, J. A., Smith, K. A., Barkan, E. R., Graybuck, L. T., Close, J. L., Long, B., Johansen, N., Penn, O., Yao, Z., Eggermont, J., Höllt, T., Levi, B. P., Shehata, S. I., Aevermann, B., Beller, A.,

Bertagnolli, D., Brouner, K., … Lein, E. S. (2019). Conserved cell types with divergent features in human versus mouse cortex. *Nature*, *573*(7772), 61–68. https://doi.org/10.1038/s41586-019-1506-7

Hodgkin, A. L., & Huxley, A. F. (1952). A quantitative description of membrane current and its application to conduction and excitation in nerve. *The Journal of Physiology*, *117*(4), 500–544. https://doi.org/10.1113/jphysiol.1952.sp004764

Holm, P. S., Bergmann, S., Jürchott, K., Lage, H., Brand, K., Ladhoff, A., Mantwill, K., Curiel, D. T., Dobbelstein, M., Dietel, M., Gänsbacher, B., & Royer, H. D. (2002). YB-1 relocates to the nucleus in adenovirus-infected cells and facilitates viral replication by inducing E2 gene expression through the E2 late promoter. *Journal of Biological Chemistry*, *277*(12), 10427–10434. https://doi.org/10.1074/jbc.M106955200

Holm, P. S., Lage, H., Bergmann, S., Jürchott, K., Glockzin, G., Bernshausen, A., Mantwill, K., Ladhoff, A., Wichert, A., Mymryk, J. S., Ritter, T., Dietel, M., Gänsbacher, B., & Royer, H. D. (2004). Multidrug-resistant Cancer Cells Facilitate E1-independent Adenoviral Replication: Impact for Cancer Gene Therapy. *Cancer Research*, *64*(1), 322–328. https://doi.org/10.1158/0008-5472.CAN-0482-2

Holtmaat, A., & Svoboda, K. (2009). Experience-dependent structural synaptic plasticity in the mammalian brain. In *Nature Reviews Neuroscience* (Vol. 10, Issue 9, pp. 647–658). https://doi.org/10.1038/nrn2699

Howard, D. B., Powers, K., Wang, Y., & Harvey, B. K. (2008). Tropism and toxicity of adeno-associated viral vector serotypes 1, 2, 5, 6, 7, 8, and 9 in rat neurons and glia in vitro. *Virology*, *372*(1), 24–34. https://doi.org/10.1016/j.virol.2007.10.007

Huang, Y., Song, N. N., Lan, W., Hu, L., Su, C. J., Ding, Y. Q., & Zhang, L. (2013). Expression of Transcription Factor Satb2 in Adult Mouse Brain. *Anatomical Record*, *296*(3), 452–461. https://doi.org/10.1002/ar.22656

Humpel, C. (2015). Neuroscience forefront review organotypic brain slice cultures: A review. *Neuroscience*, *305*, 86–98. https://doi.org/10.1016/j.neuroscience.2015.07.086

Huttenlocher, P. R., & Dabholkar, A. S. (1997). Regional differences in synaptogenesis in human cerebral cortex. *Journal of Comparative Neurology*, *387*(2), 167–178. https://doi.org/10.1002/(SICI)1096-9861(19971020)387:2<167::AID-CNE1>3.0.CO;2-Z

Inda, M. C., DeFelipe, J., & Muñoz, A. (2006). Voltage-gated ion channels in the axon initial segment of human cortical pyramidal cells and their relationship with chandelier cells. *Proceedings of the National Academy of Sciences of the United States of America*, *103*(8), 2920–2925. https://doi.org/10.1073/pnas.0511197103

Institute for Health Metrics and Evaluation (IHME). (2018). Global Burden of Disease Study 2017 Results Tool. *Seattle, United States*. http://ghdx.healthdata.org/gbd-results-tool?params=gbd-api-2017-permalink/045c4276f163ff5df0b6f485da017d26

Isom, L. L. (2001). Sodium channel β subunits: Anything but auxiliary. In *Neuroscientist* (Vol. 7, Issue 1, pp. 42–54). https://doi.org/10.1177/107385840100700108

Jackson, S. J., & Thomas, G. J. (2017). Human tissue models in cancer research: Looking beyond the mouse. In *DMM Disease Models and Mechanisms* (Vol. 10, Issue 8, pp. 939–942). https://doi.org/10.1242/dmm.031260

Jiao, J., Yang, Y., Shi, Y., Chen, J., Gao, R., Fan, Y., Yao, H., Liao, W., Sun, X. F., & Gao, S. (2013). Modeling Dravet syndrome using induced pluripotent stem cells (iPSCs) and directly converted neurons. *Human Molecular Genetics*, *22*(21), 4241–4252. https://doi.org/10.1093/hmg/ddt275

Jinek, M., Chylinski, K., Fonfara, I., Hauer, M., Doudna, J. A., & Charpentier, E. (2012). A programmable dual-RNA-guided DNA endonuclease in adaptive bacterial immunity. *Science*, *337*(6096), 816–821. https://doi.org/10.1126/science.1225829

Johansson, S., Radesäter, A. C., Cowburn, R. F., Thyberg, J., & Luthman, J. (2006). Modelling of amyloid β-peptide induced lesions using roller-drum incubation of hippocampal slice cultures from neonatal rats. *Experimental Brain Research*, *168*(1–2), 11–24. https://doi.org/10.1007/s00221-005-0069-z

Jucker, M. (2010). The benefits and limitations of animal models for translational research in neurodegenerative diseases. In *Nature Medicine* (Vol. 16, Issue 11, pp. 1210–1214). https://doi.org/10.1038/nm.2224

Kalmbach, B. E., Buchin, A., Long, B., Close, J., Nandi, A., Miller, J. A., Bakken, T. E., Hodge, R. D., Chong, P., de Frates, R., Dai, K., Maltzer, Z., Nicovich, P. R., Keene, C. D., Silbergeld, D. L., Gwinn, R. P., Cobbs, C., Ko, A. L., Ojemann, J. G., … Ting, J. T. (2018). h-Channels Contribute to Divergent Intrinsic Membrane Properties of Supragranular Pyramidal Neurons in Human versus Mouse Cerebral Cortex. *Neuron*, *100*(5), 1194-1208.e5. https://doi.org/10.1016/j.neuron.2018.10.012

Kerkhofs, A., Xavier, A. C., da Silva, B. S., Canas, P. M., Idema, S., Baayen, J. C., Ferreira, S. G., Cunha, R. A., & Mansvelder, H. D. (2018). Caffeine controls glutamatergic synaptic transmission and pyramidal neuron excitability in human neocortex. *Frontiers in Pharmacology*, *8*(JAN). https://doi.org/10.3389/fphar.2017.00899

Khan, L., Soliman, H., Sahgal, A., Perry, J., Xu, W., & Tsao, M. N. (2020). External beam radiation dose escalation for high grade glioma. In *Cochrane Database of Systematic Reviews* (Vol. 2020, Issue 5).

https://doi.org/10.1002/14651858.CD011475.pub3

Khan, S., & Al Baradie, R. (2012). Epileptic Encephalopathies: An Overview. *Epilepsy Research and Treatment*, *2012*, 1–8. https://doi.org/10.1155/2012/403592

Kim, C. K., Adhikari, A., & Deisseroth, K. (2017). Integration of optogenetics with complementary methodologies in systems neuroscience. In *Nature Reviews Neuroscience* (Vol. 18, Issue 4, pp. 222–235). https://doi.org/10.1038/nrn.2017.15

Kim, S. B., Hill, M., Kwak, Y. T., Hampl, R., Jo, D. H., & Morfin, R. (2003). Neurosteroids: Cerebrospinal Fluid Levels for Alzheimer's Disease and Vascular Dementia Diagnostics. *Journal of Clinical Endocrinology and Metabolism*, *88*(11), 5199–5206. https://doi.org/10.1210/jc.2003-030646

Kim, Y. H., Choi, S. H., D'Avanzo, C., Hebisch, M., Sliwinski, C., Bylykbashi, E., Washicosky, K. J., Klee, J. B., Brüstle, O., Tanzi, R. E., & Kim, D. Y. (2015). A 3D human neural cell culture system for modeling Alzheimer's disease. *Nature Protocols*, *10*(7), 985–1006. https://doi.org/10.1038/nprot.2015.065

Koch, H., Huh, S. E., Elsen, F. P., Carroll, M. S., Hodge, R. D., Bedogni, F., Turner, M. S., Hevner, R. F., & Ramirez, J. M. (2010). Prostaglandin E2-induced synaptic plasticity in neocortical networks of organotypic slice cultures. *Journal of Neuroscience*, *30*(35), 11678–11687. https://doi.org/10.1523/JNEUROSCI.4665-09.2010

Konermann, S., Brigham, M. D., Trevino, A. E., Joung, J., Abudayyeh, O. O., Barcena, C., Hsu, P. D., Habib, N., Gootenberg, J. S., Nishimasu, H., Nureki, O., & Zhang, F. (2015). Genome-scale transcriptional activation by an engineered CRISPR-Cas9 complex. *Nature*, *517*(7536), 583–588. https://doi.org/10.1038/nature14136

Kosnopfel, C., Sinnberg, T., & Schittek, B. (2014). Y-box binding protein 1 - A prognostic marker and target in tumour therapy. In *European Journal of Cell Biology* (Vol. 93, Issues 1–2, pp. 61–70). https://doi.org/10.1016/j.ejcb.2013.11.007

Kriks, S., Shim, J. W., Piao, J., Ganat, Y. M., Wakeman, D. R., Xie, Z., Carrillo-Reid, L., Auyeung, G., Antonacci, C., Buch, A., Yang, L., Beal, M. F., Surmeier, D. J., Kordower, J. H., Tabar, V., & Studer, L. (2011). Dopamine neurons derived from human ES cells efficiently engraft in animal models of Parkinson's disease. *Nature*, *480*(7378), 547–551. https://doi.org/10.1038/nature10648

Lage, H., Surowiak, P., & Holm, P. S. (2008). YB-1 als potenzielles ziel für die tumortherapie. *Pathologe*, *29*(SUPPL. 2), 187–190. https://doi.org/10.1007/s00292-008-1030-2

Lai, H. C., & Jan, L. Y. (2006). The distribution and targeting of neuronal

voltage-gated ion channels. In *Nature Reviews Neuroscience* (Vol. 7, Issue 7, pp. 548–562). https://doi.org/10.1038/nrn1938

Lambe, E. K., & Aghajanian, G. K. (2001). The role of Kv1.2-containing potassium channels in serotonin-induced glutamate release from thalamocortical terminals in rat frontal cortex. *Journal of Neuroscience*, *21*(24), 9955–9963. https://doi.org/10.1523/jneurosci.21-24-09955.2001

Lancaster, M. A., Renner, M., Martin, C. A., Wenzel, D., Bicknell, L. S., Hurles, M. E., Homfray, T., Penninger, J. M., Jackson, A. P., & Knoblich, J. A. (2013). Cerebral organoids model human brain development and microcephaly. *Nature*, *501*(7467), 373–379. https://doi.org/10.1038/nature12517

Lange, D., Hartline, H. K., & Ratliff, F. (1966). Inhibitory Interaction in the Retina: Techniques of Experimental and Theoretical Analysis. *Annals of the New York Academy of Sciences*, *128*(3), 955–971. https://doi.org/10.1111/j.1749-6632.1965.tb11710.x

Le Duigou, C., Savary, E., Morin-Brureau, M., Gomez-Dominguez, D., Sobczyk, A., Chali, F., Milior, G., Kraus, L., Meier, J. C., Kullmann, D. M., Mathon, B., de la Prida, L. M., Dorfmuller, G., Pallud, J., Eugène, E., Clemenceau, S., & Miles, R. (2018). Imaging pathological activities of human brain tissue in organotypic culture. *Journal of Neuroscience Methods*, *298*, 33–44. https://doi.org/10.1016/j.jneumeth.2018.02.001

Lendvai, B., Stern, E. A., Chen, B., & Svoboda, K. (2000). Experience-dependent plasticity of dendritic spines in the developing rat barrel cortex in vivo. *Nature*, *404*(6780), 876–881. https://doi.org/10.1038/35009107

Lerche, H., Shah, M., Beck, H., Noebels, J., Johnston, D., & Vincent, A. (2013). Ion channels in genetic and acquired forms of epilepsy. In *Journal of Physiology* (Vol. 591, Issue 4, pp. 753–764). https://doi.org/10.1113/jphysiol.2012.240606

Liu, Y., Lopez-Santiago, L. F., Yuan, Y., Jones, J. M., Zhang, H., O'Malley, H. A., Patino, G. A., O'Brien, J. E., Rusconi, R., Gupta, A., Thompson, R. C., Natowicz, M. R., Meisler, M. H., Isom, L. L., & Parent, J. M. (2013). Dravet syndrome patient-derived neurons suggest a novel epilepsy mechanism. *Annals of Neurology*, *74*(1), 128–139. https://doi.org/10.1002/ana.23897

Lorincz, A., & Nusser, Z. (2008). Cell-type-dependent molecular composition of the axon initial segment. *Journal of Neuroscience*, *28*(53), 14329–14340. https://doi.org/10.1523/JNEUROSCI.4833-08.2008

Louis, D. N., Perry, A., Reifenberger, G., von Deimling, A., Figarella-Branger, D., Cavenee, W. K., Ohgaki, H., Wiestler, O. D., Kleihues, P., & Ellison, D. W. (2016). The 2016 World Health Organization Classification of Tumors of the Central Nervous System: a summary. In *Acta Neuropathologica* (Vol. 131, Issue 6, pp. 803–820). https://doi.org/10.1007/s00401-016-1545-1

MacArthur, C. C., Fontes, A., Ravinder, N., Kuninger, D., Kaur, J., Bailey, M., Taliana, A., Vemuri, M. C., & Lieu, P. T. (2012). Generation of human-induced pluripotent stem cells by a nonintegrating RNA Sendai virus vector in feeder-free or xeno-free conditions. *Stem Cells International*. https://doi.org/10.1155/2012/564612

Madisen, L., Mao, T., Koch, H., Zhuo, J. M., Berenyi, A., Fujisawa, S., Hsu, Y. W. A., Garcia, A. J., Gu, X., Zanella, S., Kidney, J., Gu, H., Mao, Y., Hooks, B. M., Boyden, E. S., Buzsáki, G., Ramirez, J. M., Jones, A. R., Svoboda, K., … Zeng, H. (2012). A toolbox of Cre-dependent optogenetic transgenic mice for light-induced activation and silencing. *Nature Neuroscience*, *15*(5), 793–802. https://doi.org/10.1038/nn.3078

Mansvelder, H. D., Verhoog, M. B., & Goriounova, N. A. (2019). Synaptic plasticity in human cortical circuits: cellular mechanisms of learning and memory in the human brain? In *Current Opinion in Neurobiology* (Vol. 54, pp. 186–193). https://doi.org/10.1016/j.conb.2018.06.013

Mantwill, K., Naumann, U., Seznec, J., Girbinger, V., Lage, H., Surowiak, P., Beier, D., Mittelbronn, M., Schlegel, J., & Holm, P. S. (2013). YB-1 dependent oncolytic adenovirus efficiently inhibits tumor growth of glioma cancer stem like cells. *Journal of Translational Medicine*, *11*(1). https://doi.org/10.1186/1479-5876-11-216

Marcuccilli, C. J., Tryba, A. K., Van Drongelen, W., Koch, H., Viemari, J. C., Peña-Ortega, F., Doren, E. L., Pytel, P., Chevalier, M., Mrejeru, A., Kohrman, M. H., Lasky, R. E., Lew, S. M., Frim, D. M., & Ramirez, J. M. (2010). Neuronal bursting properties in focal and parafocal regions in pediatric neocortical epilepsy stratified by histology. In *Journal of Clinical Neurophysiology* (Vol. 27, Issue 6, pp. 387–397). https://doi.org/10.1097/WNP.0b013e3181fe06d8

Martí, M., Mulero, L., Pardo, C., Morera, C., Carrió, M., Laricchia-Robbio, L., Esteban, C. R., & Belmonte, J. C. I. (2013). Characterization of pluripotent stem cells. *Nature Protocols*, *8*(2), 223–253. https://doi.org/10.1038/nprot.2012.154

Martin, J., Kagerbauer, S. M., Schuster, T., Blobner, M., Kochs, E. F., & Landgraf, R. (2014). Vasopressin and oxytocin in CSF and plasma of patients with aneurysmal subarachnoid haemorrhage. *Neuropeptides*, *48*(2), 91–96. https://doi.org/10.1016/j.npep.2013.12.004

Masnada, S., Hedrich, U. B. S., Gardella, E., Schubert, J., Kaiwar, C., Klee, E. W., Lanpher, B. C., Gavrilova, R. H., Synofzik, M., Bast, T., Gorman, K., King, M. D., Allen, N. M., Conroy, J., Ben Zeev, B., Tzadok, M., Korff, C., Dubois, F., Ramsey, K., … Rubboli, G. (2017). Clinical spectrum and genotype-phenotype associations of KCNA2-related encephalopathies. *Brain*, *140*(9), 2337–2354. https://doi.org/10.1093/brain/awx184

Mckeown, L., Swanton, L., Robinson, P., & Jones, O. T. (2008). Surface

expression and distribution of voltage-gated potassium channels in neurons (Review). In *Molecular Membrane Biology* (Vol. 25, Issue 4, pp. 332–343). https://doi.org/10.1080/09687680801992470

McTague, A., Howell, K. B., Cross, J. H., Kurian, M. A., & Scheffer, I. E. (2016). The genetic landscape of the epileptic encephalopathies of infancy and childhood. In *The Lancet Neurology* (Vol. 15, Issue 3, pp. 304–316). https://doi.org/10.1016/S1474-4422(15)00250-1

med. Richard Kapferer, von D., & Dr. Georg Stider, von P. (1938). Die Werke des Hippokrates. *The American Journal of the Medical Sciences*, *196*(5), 723. https://doi.org/10.1097/00000441-193811000-00022

Miyoshi, N., Ishii, H., Nagano, H., Haraguchi, N., Dewi, D. L., Kano, Y., Nishikawa, S., Tanemura, M., Mimori, K., Tanaka, F., Saito, T., Nishimura, J., Takemasa, I., Mizushima, T., Ikeda, M., Yamamoto, H., Sekimoto, M., Doki, Y., & Mori, M. (2011). Reprogramming of mouse and human cells to pluripotency using mature microRNAs. *Cell Stem Cell*, *8*(6), 633–638. https://doi.org/10.1016/j.stem.2011.05.001

Mohan, H., Verhoog, M. B., Doreswamy, K. K., Eyal, G., Aardse, R., Lodder, B. N., Goriounova, N. A., Asamoah, B., B. Brakspear, A. B. C., Groot, C., Van Der Sluis, S., Testa-Silva, G., Obermayer, J., Boudewijns, Z. S. R. M., Narayanan, R. T., Baayen, J. C., Segev, I., Mansvelder, H. D., & De Kock, C. P. J. (2015). Dendritic and axonal architecture of individual pyramidal neurons across layers of adult human neocortex. *Cerebral Cortex*, *25*(12), 4839–4853. https://doi.org/10.1093/cercor/bhv188

Molina, J. R., Hayashi, Y., Stephens, C., & Georgescu, M. M. (2010). Invasive glioblastoma cells acquire stemness and increased Akt activation. *Neoplasia*, *12*(6), 453–463. https://doi.org/10.1593/neo.10126

Molnár, G., Rózsa, M., Baka, J., Holderith, N., Barzó, P., Nusser, Z., & Tamás, G. (2016). Human pyramidal to interneuron synapses are mediated by multi-vesicular release and multiple docked vesicles. *ELife*, *5*(AUGUST). https://doi.org/10.7554/eLife.18167

Mormann, F., Andrzejak, R. G., Kreuz, T., Rieke, C., David, P., Elger, C. E., & Lehnertz, K. (2003). Automated detection of a preseizure state based on a decrease in synchronization in intracranial electroencephalogram recordings from epilepsy patients. *Physical Review E - Statistical Physics, Plasmas, Fluids, and Related Interdisciplinary Topics*, *67*(2), 10. https://doi.org/10.1103/PhysRevE.67.021912

Moser, K. V., Schmidt-Kastner, R., Hinterhuber, H., & Humpel, C. (2003). Brain capillaries and cholinergic neurons persist in organotypic brain slices in the absence of blood flow. *European Journal of Neuroscience*, *18*(1), 85–94. https://doi.org/10.1046/j.1460-9568.2003.02728.x

Mullard, A. (2015). Stem-cell discovery platforms yield first clinical candidates. *Nature Reviews Drug Discovery*, *14*(9), 589–591.

https://doi.org/10.1038/nrd4708

Murray, C. J. L., Vos, T., Lozano, R., Naghavi, M., Flaxman, A. D., Michaud, C., Ezzati, M., Shibuya, K., Salomon, J. A., Abdalla, S., Aboyans, V., Abraham, J., Ackerman, I., Aggarwal, R., Ahn, S. Y., Ali, M. K., AlMazroa, M. A., Alvarado, M., Anderson, H. R., … Lopez, A. D. (2012). Disability-adjusted life years (DALYs) for 291 diseases and injuries in 21 regions, 1990-2010: A systematic analysis for the Global Burden of Disease Study 2010. *The Lancet*, *380*(9859), 2197–2223. https://doi.org/10.1016/S0140-6736(12)61689-4

Mutschelknaus, L., Azimzadeh, O., Heider, T., Winkler, K., Vetter, M., Kell, R., Tapio, S., Merl-Pham, J., Huber, S. M., Edalat, L., Radulović, V., Anastasov, N., Atkinson, M. J., & Moertl, S. (2017). Radiation alters the cargo of exosomes released from squamous head and neck cancer cells to promote migration of recipient cells. *Scientific Reports*, *7*(1). https://doi.org/10.1038/s41598-017-12403-6

Nagoshi, N., & Okano, H. (2018). iPSC-derived neural precursor cells: potential for cell transplantation therapy in spinal cord injury. In *Cellular and Molecular Life Sciences* (Vol. 75, Issue 6, pp. 989–1000). https://doi.org/10.1007/s00018-017-2676-9

Napoli, A., & Obeid, I. (2016). Comparative Analysis of Human and Rodent Brain Primary Neuronal Culture Spontaneous Activity Using Micro-Electrode Array Technology. *Journal of Cellular Biochemistry*, *117*(3), 559–565. https://doi.org/10.1002/jcb.25312

Nathan, A. J., & Scobell, A. (2012). How China sees America. In *Foreign Affairs* (Vol. 91, Issue 5). https://doi.org/10.1017/CBO9781107415324.004

Nilsson, C. L., Brinkmalm, A., Minthon, L., Blennow, K., & Ekman, R. (2001). Processing of neuropeptide Y, galanin, and somatostatin in the cerebrospinal fluid of patients with Alzheimer's disease and frontotemporal dementia. *Peptides*, *22*(12), 2105–2112. https://doi.org/10.1016/S0196-9781(01)00571-X

Novotny, R., Langer, F., Mahler, J., Skodras, A., Vlachos, A., Wegenast-Braun, B. M., Kaeser, S. A., Neher, J. J., Eisele, Y. S., Pietrowski, M. J., Nilsson, K. P. R., Deller, T., Staufenbiel, M., Heimrich, B., & Jucker, M. (2016). Conversion of synthetic Aβ to In Vivo active seeds and amyloid plaque formation in a hippocampal slice culture model. *Journal of Neuroscience*, *36*(18), 5084–5093. https://doi.org/10.1523/JNEUROSCI.0258-16.2016

O'Connor, W. M., Davidson, B. L., Kaplitt, M. G., Abbey, M. V., During, M. J., Leone, P., Langer, D., O'Connor, M. J., & Freese, A. (1997). Adenovirus Vector-Mediated Gene Transfer into Human Epileptogenic Brain Slices: Prospects for Gene Therapy in Epilepsy. *Experimental Neurology*, *148*(1), 167–178. https://doi.org/10.1006/exnr.1997.6658

Oberheim, N. A., Takano, T., Han, X., He, W., Lin, J. H. C., Wang, F., Xu, Q.,

Wyatt, J. D., Pilcher, W., Ojemann, J. G., Ransom, B. R., Goldman, S. A., & Nedergaard, M. (2009). Uniquely hominid features of adult human astrocytes. *Journal of Neuroscience*, *29*(10), 3276–3287. https://doi.org/10.1523/JNEUROSCI.4707-08.2009

Okita, K., Nakagawa, M., Hyenjong, H., Ichisaka, T., & Yamanaka, S. (2008). Generation of mouse induced pluripotent stem cells without viral vectors. *Science*, *322*(5903), 949–953. https://doi.org/10.1126/science.1164270

Orhan, F., Fatouros-Bergman, H., Goiny, M., Malmqvist, A., Piehl, F., Cervenka, S., Collste, K., Victorsson, P., Sellgren, C. M., Flyckt, L., Erhardt, S., & Engberg, G. (2018). CSF GABA is reduced in first-episode psychosis and associates to symptom severity. *Molecular Psychiatry*, *23*(5), 1244–1250. https://doi.org/10.1038/mp.2017.25

Otto, F., Illes, S., Opatz, J., Laryea, M., Theiss, S., Hartung, H. P., Schnitzler, A., Siebler, M., & Dihné, M. (2009). Cerebrospinal fluid of brain trauma patients inhibits in vitro neuronal network function via NMDA receptors. *Annals of Neurology*, *66*(4), 546–555. https://doi.org/10.1002/ana.21808

Pagano, C., Martino, O. di, Ruggiero, G., Guarino, A. M., Mueller, N., Siauciunaite, R., Reischl, M., Foulkes, N. S., Vallone, D., & Calabrò, V. (2017). The tumor-associated YB-1 protein: New player in the circadian control of cell proliferation. *Oncotarget*, *8*(4), 6193–6205. https://doi.org/10.18632/oncotarget.14051

Pasca, A. M., Sloan, S. A., Clarke, L. E., Tian, Y., Makinson, C. D., Huber, N., Kim, C. H., Park, J. Y., O'Rourke, N. A., Nguyen, K. D., Smith, S. J., Huguenard, J. R., Geschwind, D. H., Barres, B. A., & Pasca, S. P. (2015). Functional cortical neurons and astrocytes from human pluripotent stem cells in 3D culture. *Nature Methods*, *12*(7), 671–678. https://doi.org/10.1038/nmeth.3415

Patel, V., Chisholm, D., Parikh, R., Charlson, F. J., Degenhardt, L., Dua, T., Ferrari, A. J., Hyman, S., Laxminarayan, R., Levin, C., Lund, C., Medina Mora, M. E., Petersen, I., Scott, J., Shidhaye, R., Vijayakumar, L., Thornicroft, G., & Whiteford, H. (2016). Addressing the burden of mental, neurological, and substance use disorders: Key messages from Disease Control Priorities, 3rd edition. In *The Lancet* (Vol. 387, Issue 10028, pp. 1672–1685). https://doi.org/10.1016/S0140-6736(15)00390-6

Pekny, M., & Pekna, M. (2014). Astrocyte reactivity and reactive astrogliosis: Costs and benefits. *Physiological Reviews*, *94*(4), 1077–1098. https://doi.org/10.1152/physrev.00041.2013

Pena, S. D. J., & Coimbra, R. L. M. (2015). Ataxia and myoclonic epilepsy due to a heterozygous new mutation in KCNA2: Proposal for a new channelopathy. *Clinical Genetics*, *87*(2), 1–3. https://doi.org/10.1111/cge.12542

Perez-Alcazar, M., Culley, G., Lyckenvik, T., Mobarrez, K., Bjorefeldt, A.,

Wasling, P., Seth, H., Asztely, F., Harrer, A., Iglseder, B., Aigner, L., Hanse, E., & Illes, S. (2016). Human cerebrospinal fluid promotes neuronal viability and activity of hippocampal neuronal circuits in vitro. *Frontiers in Cellular Neuroscience*, *10*(MAR2016). https://doi.org/10.3389/fncel.2016.00054

Piatkevich, K. D., Jung, E. E., Straub, C., Linghu, C., Park, D., Suk, H. J., Hochbaum, D. R., Goodwin, D., Pnevmatikakis, E., Pak, N., Kawashima, T., Yang, C. T., Rhoades, J. L., Shemesh, O., Asano, S., Yoon, Y. G., Freifeld, L., Saulnier, J. L., Riegler, C., … Boyden, E. S. (2018). A robotic multidimensional directed evolution approach applied to fluorescent voltage reporters article. *Nature Chemical Biology*, *14*(4), 352–360. https://doi.org/10.1038/s41589-018-0004-9

Po, S., Roberds, S., Snyders, D. J., Tamkun, M. M., & Bennett, P. B. (1993). Heteromultimeric assembly of human potassium channels: Molecular basis of a transient outward current? *Circulation Research*, *72*(6), 1326–1336. https://doi.org/10.1161/01.RES.72.6.1326

Post, R. M., Rubinow, D. R., Kling, M. A., Berrettini, W., & Gold, P. W. (1988). Neuroactive Substances in Cerebrospinal Fluid: Normal and Pathological Regulatory Mechanisms. *Annals of the New York Academy of Sciences*, *531*(1), 15–28. https://doi.org/10.1111/j.1749-6632.1988.tb31808.x

Preibisch, S., Saalfeld, S., & Tomancak, P. (2009). Globally optimal stitching of tiled 3D microscopic image acquisitions. *Bioinformatics*, *25*(11), 1463–1465. https://doi.org/10.1093/bioinformatics/btp184

Radonjić, N. V., Ayoub, A. E., Memi, F., Yu, X., Maroof, A., Jakovcevski, I., Anderson, S. A., Rakic, P., & Zecevic, N. (2014). Diversity of Cortical Interneurons in Primates: The Role of the Dorsal Proliferative Niche. *Cell Reports*, *9*(6), 2139–2151. https://doi.org/10.1016/j.celrep.2014.11.026

Rais, Y., Zviran, A., Geula, S., Gafni, O., Chomsky, E., Viukov, S., Mansour, A. A., Caspi, I., Krupalnik, V., Zerbib, M., Maza, I., Mor, N., Baran, D., Weinberger, L., Jaitin, D. A., Lara-Astiaso, D., Blecher-Gonen, R., Shipony, Z., Mukamel, Z., … Hanna, J. H. (2013). Deterministic direct reprogramming of somatic cells to pluripotency. *Nature*, *502*(7469), 65–70. https://doi.org/10.1038/nature12587

Ramirez, Y. P., Weatherbee, J. L., Wheelhouse, R. T., & Ross, A. H. (2013). Glioblastoma multiforme therapy and mechanisms of resistance. In *Pharmaceuticals* (Vol. 6, Issue 12, pp. 1475–1506). https://doi.org/10.3390/ph6121475

Rao, A., & Craig, A. M. (1997). Activity regulates the synaptic localization of the NMDA receptor in hippocampal neurons. *Neuron*, *19*(4), 801–812. https://doi.org/10.1016/S0896-6273(00)80962-9

Ray, A., Manjila, S., Hdeib, A. M., Radhakrishnan, A., Nock, C. J., Cohen, M. L., & Sloan, A. E. (2015). Extracranial metastasis of gliobastoma: Three

illustrative cases and current review of the molecular pathology and management strategies. *Molecular and Clinical Oncology*, *3*(3), 479–486. https://doi.org/10.3892/mco.2015.494

Reinhardt, P., Schmid, B., Burbulla, L. F., Schöndorf, D. C., Wagner, L., Glatza, M., Höing, S., Hargus, G., Heck, S. A., Dhingra, A., Wu, G., Müller, S., Brockmann, K., Kluba, T., Maisel, M., Krüger, R., Berg, D., Tsytsyura, Y., Thiel, C. S., … Sterneckert, J. (2013). Genetic correction of a lrrk2 mutation in human iPSCs links parkinsonian neurodegeneration to ERK-dependent changes in gene expression. *Cell Stem Cell*, *12*(3), 354–367. https://doi.org/10.1016/j.stem.2013.01.008

Rice, J. (2012). Animal models: Not close enough. In *Nature* (Vol. 484, Issue 7393 SUPPL.). https://doi.org/10.1038/nature11102

Rich, J. N., & Bigner, D. D. (2004). Development of novel targeted therapies in the treatment of malignant glioma. In *Nature Reviews Drug Discovery* (Vol. 3, Issue 5, pp. 430–446). https://doi.org/10.1038/nrd1380

Rodriguez, A., Ehlenberger, D. B., Dickstein, D. L., Hof, P. R., & Wearne, S. L. (2008). Automated three-dimensional detection and shape classification of dendritic spines from fluorescence microscopy images. *PLoS ONE*, *3*(4), e1997. https://doi.org/10.1371/journal.pone.0001997

Rosa, F., Dhingra, A., Uysal, B., Mendis, G. D. C., Loeffler, H., Elsen, G., Mueller, S., Schwarz, N., Castillo-Lizardo, M., Cuddy, C., Becker, F., Heutink, P., Reid, C. A., Petrou, S., Lerche, H., & Maljevic, S. (2020). In Vitro Differentiated Human Stem Cell-Derived Neurons Reproduce Synaptic Synchronicity Arising during Neurodevelopment. *Stem Cell Reports*, *15*(1), 22–37. https://doi.org/10.1016/j.stemcr.2020.05.015

Roth, B. L. (2016). DREADDs for Neuroscientists. In *Neuron* (Vol. 89, Issue 4, pp. 683–694). https://doi.org/10.1016/j.neuron.2016.01.040

Russell, S. N., Publicover, N. G., Hart, P. J., Carl, A., Hume, J. R., Sanders, K. M., & Horowitz, B. (1994). Block by 4-aminopyridine of a Kv1.2 delayed rectifier K+ current expressed in Xenopus oocytes. *The Journal of Physiology*. https://doi.org/10.1113/jphysiol.1994.sp020464

Rustenhoven, J., Jansson, D., Smyth, L. C., & Dragunow, M. (2017). Brain Pericytes As Mediators of Neuroinflammation. In *Trends in Pharmacological Sciences* (Vol. 38, Issue 3, pp. 291–304). https://doi.org/10.1016/j.tips.2016.12.001

Sahebjam, S., Sharabi, A., Lim, M., Kesarwani, P., & Chinnaiyan, P. (2017). Immunotherapy and radiation in glioblastoma. In *Journal of Neuro-Oncology* (Vol. 134, Issue 3, pp. 531–539). https://doi.org/10.1007/s11060-017-2413-0

Salkoff, L., Baker, K., Butler, A., Covarrubias, M., Pak, M. D., & Wei, A. (1992). An essential “set” of K+ channels conserved in flies, mice and humans.

Trends in Neurosciences, *15*(5), 161–166. https://doi.org/10.1016/0166-2236(92)90165-5

Salkoff, L., & Wyman, R. (1981). Genetic modification of potassium channels in Drosophila Shaker mutants. *Nature*, *293*(5829), 228–230. https://doi.org/10.1038/293228a0

Sánchez-Ponce, D., DeFelipe, J., Garrido, J. J., & Muñoz, A. (2012). Developmental Expression of Kv Potassium Channels at the Axon Initial Segment of Cultured Hippocampal Neurons. *PLoS ONE*, *7*(10). https://doi.org/10.1371/journal.pone.0048557

Sareen, D., O'Rourke, J. G., Meera, P., Muhammad, A. K. M. G., Grant, S., Simpkinson, M., Bell, S., Carmona, S., Ornelas, L., Sahabian, A., Gendron, T., Petrucelli, L., Baughn, M., Ravits, J., Harms, M. B., Rigo, F., Frank Bennett, C., Otis, T. S., Svendsen, C. N., & Baloh, R. H. (2013). Targeting RNA foci in iPSC-derived motor neurons from ALS patients with a C9ORF72 repeat expansion. *Science Translational Medicine*, *5*(208). https://doi.org/10.1126/scitranslmed.3007529

Scheffer, I. E., Berkovic, S., Capovilla, G., Connolly, M. B., French, J., Guilhoto, L., Hirsch, E., Jain, S., Mathern, G. W., Moshé, S. L., Nordli, D. R., Perucca, E., Tomson, T., Wiebe, S., Zhang, Y. H., & Zuberi, S. M. (2017). ILAE classification of the epilepsies: Position paper of the ILAE Commission for Classification and Terminology. *Epilepsia*, *58*(4), 512–521. https://doi.org/10.1111/epi.13709

Scheffer, I. E., French, J., Hirsch, E., Jain, S., Mathern, G. W., Moshé, S. L., Perucca, E., Tomson, T., Wiebe, S., Zhang, Y. H., & Zuberi, S. M. (2016). Classification of the epilepsies: New concepts for discussion and debate—Special report of the ILAE Classification Task Force of the Commission for Classification and Terminology. *Epilepsia Open*, *1*(1–2), 37–44. https://doi.org/10.1002/epi4.5

Schildge, S., Bohrer, C., Beck, K., & Schachtrup, C. (2013). Isolation and culture of mouse cortical astrocytes. *Journal of Visualized Experiments : JoVE*, *71*. https://doi.org/10.3791/50079

Schindelin, J., Arganda-Carreras, I., Frise, E., Kaynig, V., Longair, M., Pietzsch, T., Preibisch, S., Rueden, C., Saalfeld, S., Schmid, B., Tinevez, J. Y., White, D. J., Hartenstein, V., Eliceiri, K., Tomancak, P., & Cardona, A. (2012). Fiji: An open-source platform for biological-image analysis. In *Nature Methods* (Vol. 9, Issue 7, pp. 676–682). https://doi.org/10.1038/nmeth.2019

Schittek, B., Psenner, K., Sauer, B., Meier, F., Iftner, T., & Garbe, C. (2007). The increased expression of Y box-binding protein 1 in melanoma stimulates proliferation and tumor invasion, antagonizes apoptosis and enhances chemoresistance. *International Journal of Cancer*, *120*(10), 2110–2118. https://doi.org/10.1002/ijc.22512

Schwarz, N., Hedrich, U. B. S., Schwarz, H., Harshad, P. A., Dammeier, N., Auffenberg, E., Bedogni, F., Honegger, J. B., Lerche, H., Wuttke, T. V., & Koch, H. (2017). Human Cerebrospinal fluid promotes long-term neuronal viability and network function in human neocortical organotypic brain slice cultures. *Scientific Reports*, *7*(1). https://doi.org/10.1038/s41598-017-12527-9

Schwarz, N., Uysal, B., Rosa, F., Löffler, H., Mau-Holzmann, U. A., Liebau, S., & Lerche, H. (2018). Generation of an induced pluripotent stem cell (iPSC) line from a patient with developmental and epileptic encephalopathy carrying a KCNA2 (p.Leu328Val) mutation. *Stem Cell Research*, *33*, 6–9. https://doi.org/10.1016/j.scr.2018.08.019

Schwarz, N., Uysal, B., Rosa, F., Löffler, H., Mau-Holzmann, U. A., Liebau, S., & Lerche, H. (2019). Establishment of a human induced pluripotent stem cell (iPSC)line (HIHDNEi002-A)from a patient with developmental and epileptic encephalopathy carrying a KCNA2 (p.Arg297Gln)mutation. *Stem Cell Research*, *37*. https://doi.org/10.1016/j.scr.2019.101445

Schwarz, N., Uysal, B., Welzer, M., Bahr, J. C., Layer, N., Löffler, H., Stanaitis, K., Harshad, P. A., Weber, Y. G., Hedrich, U. B. S., Honegger, J. B., Skodras, A., Becker, A. J., Wuttke, T. V., & Koch, H. (2019). Long-term adult human brain slice cultures as a model system to study human CNS circuitry and disease. *ELife*, *8*. https://doi.org/10.7554/eLife.48417

Selvaraj, V., Plane, J. M., Williams, A. J., & Deng, W. (2010). Switching cell fate: The remarkable rise of induced pluripotent stem cells and lineage reprogramming technologies. In *Trends in Biotechnology* (Vol. 28, Issue 4, pp. 214–223). https://doi.org/10.1016/j.tibtech.2010.01.002

Sheng, M., Tsaur, M. L., Yuh Nung Jan, & Lily Yeh Jan. (1994). Contrasting subcellular localization of the Kv1.2 K+ channel subunit in different neurons of rat brain. *Journal of Neuroscience*, *14*(4), 2408–2417. https://doi.org/10.1523/jneurosci.14-04-02408.1994

Shepherd, G. M., & Rowe, T. B. (2017). Neocortical lamination: Insights from neuron types and evolutionary precursors. *Frontiers in Neuroanatomy*, *11*. https://doi.org/10.3389/fnana.2017.00100

Shi, Y., Kirwan, P., & Livesey, F. J. (2012). Directed differentiation of human pluripotent stem cells to cerebral cortex neurons and neural networks. *Nature Protocols*, *7*(10), 1836–1846. https://doi.org/10.1038/nprot.2012.116

Shi, Y., Kirwan, P., Smith, J., Robinson, H. P. C., & Livesey, F. J. (2012). Human cerebral cortex development from pluripotent stem cells to functional excitatory synapses. *Nature Neuroscience*, *15*(3), 477–486. https://doi.org/10.1038/nn.3041

Sinnberg, T., Sauer, B., Holm, P., Spangler, B., Kuphal, S., Bosserhoff, A., & Schittek, B. (2012). MAPK and PI3K/AKT mediated YB-1 activation promotes melanoma cell proliferation which is counteracted by an

autoregulatory loop. *Experimental Dermatology*, *21*(4), 265–270. https://doi.org/10.1111/j.1600-0625.2012.01448.x

Sison-Young, R. L. C., Kia, R., Heslop, J., Kelly, L., Rowe, C., Cross, M. J., Kitteringham, N. R., Hanley, N., Park, B. K., & Goldring, C. E. P. (2012). Human Pluripotent Stem Cells for Modeling Toxicity. In *Advances in Pharmacology* (Vol. 63, pp. 207–256). https://doi.org/10.1016/B978-0-12-398339-8.00006-9

Skipor, J., & Thiery, J. C. (2008). The choroid plexus - cerebrospinal fluid system: Undervaluated pathway of neuroendocrine signaling into the brain. In *Acta Neurobiologiae Experimentalis* (Vol. 68, Issue 3, pp. 414–428).

Smith, A. M., & Dragunow, M. (2014). The human side of microglia. In *Trends in Neurosciences* (Vol. 37, Issue 3, pp. 125–135). https://doi.org/10.1016/j.tins.2013.12.001

Somogyi, P., Tamás, G., Lujan, R., & Buhl, E. H. (1998). Salient features of synaptic organisation in the cerebral cortex. *Brain Research Reviews*, *26*(2–3), 113–135. https://doi.org/10.1016/S0165-0173(97)00061-1

Song, A. J., & Palmiter, R. D. (2018). Detecting and Avoiding Problems When Using the Cre–lox System. In *Trends in Genetics* (Vol. 34, Issue 5, pp. 333–340). https://doi.org/10.1016/j.tig.2017.12.008

Spreux-Varoquaux, O., Bensimon, G., Lacomblez, L., Salachas, F., Pradat, P. F., Le Forestier, N., Marouan, A., Dib, M., & Meininger, V. (2002). Glutamate levels in cerebrospinal fluid in amyotrophic lateral sclerosis: A reappraisal using a new HPLC method with coulometric detection in a large cohort of patients. *Journal of the Neurological Sciences*, *193*(2), 73–78. https://doi.org/10.1016/S0022-510X(01)00661-X

Stoppini, L., Buchs, P. A., & Muller, D. (1991). A simple method for organotypic cultures of nervous tissue. *Journal of Neuroscience Methods*, *37*(2), 173–182. https://doi.org/10.1016/0165-0270(91)90128-M

Strittmatter, M., Grauer, M., Isenberg, E., Hamann, G., Fischer, C., Hoffmann, K. H., Blaes, F., & Schimrigk, K. (1997). Cerebrospinal fluid neuropeptides and monoaminergic transmitters in patients with trigeminal neuralgia. *Headache*, *37*(4), 211–216. https://doi.org/10.1046/j.1526-4610.1997.3704211.x

Stupp, R., Mason, W. P., van den Bent, M. J., Weller, M., Fisher, B., Taphoorn, M. J. B., Belanger, K., Brandes, A. A., Marosi, C., Bogdahn, U., Curschmann, J., Janzer, R. C., Ludwin, S. K., Gorlia, T., Allgeier, A., Lacombe, D., Cairncross, J. G., Eisenhauer, E., & Mirimanoff, R. O. (2005). Radiotherapy plus Concomitant and Adjuvant Temozolomide for Glioblastoma. *New England Journal of Medicine*, *352*(10), 987–996. https://doi.org/10.1056/nejmoa043330

Stupp, R., Taillibert, S., Kanner, A., Read, W., Steinberg, D. M., Lhermitte, B.,

Toms, S., Idbaih, A., Ahluwalia, M. S., Fink, K., Di Meco, F., Lieberman, F., Zhu, J. J., Stragliotto, G., Tran, D. D., Brem, S., Hottinger, A. F., Kirson, E. D., Lavy-Shahaf, G., … Ram, Z. (2017). Effect of tumor-treating fields plus maintenance temozolomide vs maintenance temozolomide alone on survival in patients with glioblastoma a randomized clinical trial. *JAMA - Journal of the American Medical Association*, *318*(23), 2306–2316. https://doi.org/10.1001/jama.2017.18718

Sunayama, J., Matsuda, K. I., Sato, A., Tachibana, K., Suzuki, K., Narita, Y., Shibui, S., Sakurada, K., Kayama, T., Tomiyama, A., & Kitanaka, C. (2010). Crosstalk between the PI3K/mTOR and MEK/ERK pathways involved in the maintenance of self-renewal and tumorigenicity of glioblastoma stem-like cells. *Stem Cells*, *28*(11), 1930–1939. https://doi.org/10.1002/stem.521

Syrbe, S., Hedrich, U. B. S., Riesch, E., Djémié, T., Müller, S., Møller, R. S., Maher, B., Hernandez-Hernandez, L., Synofzik, M., Caglayan, H. S., Arslan, M., Serratosa, J. M., Nothnagel, M., May, P., Krause, R., Löffler, H., Detert, K., Dorn, T., Vogt, H., … Lemke, J. R. (2015). De novo loss-or gain-of-function mutations in KCNA2 cause epileptic encephalopathy. *Nature Genetics*. https://doi.org/10.1038/ng.3239

Takahashi, K., Tanabe, K., Ohnuki, M., Narita, M., Ichisaka, T., Tomoda, K., & Yamanaka, S. (2007). Induction of Pluripotent Stem Cells from Adult Human Fibroblasts by Defined Factors. *Cell*. https://doi.org/10.1016/j.cell.2007.11.019

Takahashi, K., & Yamanaka, S. (2006). Induction of Pluripotent Stem Cells from Mouse Embryonic and Adult Fibroblast Cultures by Defined Factors. *Cell*, *126*(4), 663–676. https://doi.org/10.1016/j.cell.2006.07.024

Tao, Y., & Zhang, S. C. (2016). Neural Subtype Specification from Human Pluripotent Stem Cells. In *Cell Stem Cell* (Vol. 19, Issue 5, pp. 573–586). https://doi.org/10.1016/j.stem.2016.10.015

Taylor, O. G., Brzozowski, J. S., & Skelding, K. A. (2019). Glioblastoma multiforme: An overview of emerging therapeutic targets. In *Frontiers in Oncology* (Vol. 9, Issue SEP). https://doi.org/10.3389/fonc.2019.00963

Tempel, B. L., Papazian, D. M., Schwarz, T. L., Jan, Y. N., & Jan, L. Y. (1987). Sequence of a probable potassium channel component encoded at Shaker locus of Drosophila. *Science*, *237*(4816), 770–775. https://doi.org/10.1126/science.2441471

Testa-Silva, G., Verhoog, M. B., Goriounova, N. A., Loebel, A., Hjorth, J. J. J., Baayen, J. C., de Kock, C. P. J., & Mansvelder, H. D. (2010). Human synapses show a wide temporal window for spike-timing-dependent plasticity. *Frontiers in Synaptic Neuroscience*, *JUL*. https://doi.org/10.3389/fnsyn.2010.00012

Testa-Silva, G., Verhoog, M. B., Linaro, D., de Kock, C. P. J., Baayen, J. C., Meredith, R. M., De Zeeuw, C. I., Giugliano, M., & Mansvelder, H. D.

(2014). High Bandwidth Synaptic Communication and Frequency Tracking in Human Neocortex. *PLoS Biology*, *12*(11). https://doi.org/10.1371/journal.pbio.1002007

Tidball, A. M., Lopez-Santiago, L. F., Yuan, Y., Glenn, T. W., Margolis, J. L., Clayton Walker, J., Kilbane, E. G., Miller, C. A., Martina Bebin, E., Scott Perry, M., Isom, L. L., & Parent, J. M. (2020). Variant-specific changes in persistent or resurgent sodium current in SCN8A-related epilepsy patient-derived neurons. *Brain*, *143*(10), 3025–3040. https://doi.org/10.1093/brain/awaa247

Ting, J. T., Kalmbach, B., Chong, P., De Frates, R., Keene, C. Di., Gwinn, R. P., Cobbs, C., Ko, A. L., Ojemann, J. G., Ellenbogen, R. G., Koch, C., & Lein, E. (2018). A robust ex vivo experimental platform for molecular-genetic dissection of adult human neocortical cell types and circuits. *Scientific Reports*, *8*(1). https://doi.org/10.1038/s41598-018-26803-9

Tiwari, A., Rebholz, S., Maier, E., Harati, M. D., Zips, D., Sers, C., Rodemann, H. P., & Toulany, M. (2018). Stress-induced phosphorylation of nuclear YB-1 depends on nuclear trafficking of p90 ribosomal S6 kinase. *International Journal of Molecular Sciences*, *19*(8). https://doi.org/10.3390/ijms19082441

Tong, H., Zhao, K., Zhang, J., Zhu, J., & Xiao, J. (2019). YB-1 modulates the drug resistance of glioma cells by activation of MDM2/p53 pathway. *Drug Design, Development and Therapy*, *13*, 317–326. https://doi.org/10.2147/DDDT.S185514

Toulany, M., Schickfluß, T. A., Eicheler, W., Kehlbach, R., Schittek, B., & Rodemann, H. P. (2011). Impact of oncogenic K-RAS on YB-1 phosphorylation induced by ionizing radiation. *Breast Cancer Research*, *13*(2). https://doi.org/10.1186/bcr2845

Trachtenberg, J. T., Chen, B. E., Knott, G. W., Feng, G., Sanes, J. R., Welker, E., & Svoboda, K. (2002). Long-term in vivo imaging of experience-dependent synaptic plasticity in adult cortex. *Nature*, *420*(6917), 788–794. https://doi.org/10.1038/nature01273

Tricoire, H., Locatelli, A., Chemineau, P., & Malpaux, B. (2002). Melatonin enters the cerebrospinal fluid through the pineal recess. *Endocrinology*, *143*(1), 84–90. https://doi.org/10.1210/endo.143.1.8585

Trimmer, J. S., & Rhodes, K. J. (2004). Localization of Voltage-Gated Ion Channels IN Mammalian Brain. *Annual Review of Physiology*. https://doi.org/10.1146/annurev.physiol.66.032102.113328

Vasile, F., Dossi, E., & Rouach, N. (2017). Human astrocytes: structure and functions in the healthy brain. In *Brain Structure and Function* (Vol. 222, Issue 5, pp. 2017–2029). https://doi.org/10.1007/s00429-017-1383-5

Veening, J. G., & Barendregt, H. P. (2010). The regulation of brain states by neuroactive substances distributed via the cerebrospinal fluid; a review. In

Cerebrospinal Fluid Research (Vol. 7). https://doi.org/10.1186/1743-8454-7-1

Verhoog, M. B., Goriounova, N. A., Obermayer, J., Stroeder, J., Johannes Hjorth, J. J., Testa-Silva, G., Baayen, J. C., de Kock, C. P. J., Meredith, R. M., & Mansvelder, H. D. (2013). Mechanisms underlying the rules for associative plasticity at adult human neocortical synapses. *Journal of Neuroscience*, *33*(43), 17197–17208. https://doi.org/10.1523/JNEUROSCI.3158-13.2013

Verwer, R. W. H., Dubelaar, E. J. G., Hermens, W. T. J. M. C., & Swaab, D. F. (2002). Tissue cultures from adult human postmortem subcortical brain areas. *Journal of Cellular and Molecular Medicine*, *6*(3), 429–432. https://doi.org/10.1111/j.1582-4934.2002.tb00522.x

Verwer, R. W. H., Hermens, W. T. J. M. C., Dijkhuizen, P. A., Brake, O. Ter, Baker, R. E., Salehi, A., Sluiter, A. A., Kok, M. J. M., Müller, L. J., Verhaagen, J., & Swaab, D. F. (2002). Cells in human postmortem brain tissue slices remain alive for several weeks in culture. *The FASEB Journal*, *16*(1), 54–60. https://doi.org/10.1096/fj.01-0504com

Verwer, R. W. H., Sluiter, A. A., Balesar, R. A., Baayen, J. C., Speijer, D., Idema, S., & Swaab, D. F. (2016). Altered Loyalties of Neuronal Markers in Cultured Slices of Resected Human Brain Tissue. *Brain Pathology*, *26*(4), 523–532. https://doi.org/10.1111/bpa.12330

Wang, B., Yin, L., Zou, X., Ye, M., Liu, Y., He, T., Deng, S., Jiang, Y., Zheng, R., Wang, Y., Yang, M., Lu, H., Wu, S., & Shu, Y. (2015). A subtype of inhibitory interneuron with intrinsic persistent activity in human and monkey neocortex. *Cell Reports*, *10*(9), 1450–1458. https://doi.org/10.1016/j.celrep.2015.02.018

Welch, M. J., Markham, C. H., & Jenden, D. J. (1976). Acetylcholine and choline in cerebrospinal fluid of patients with Parkinson's disease and Huntington's chorea. *Journal of Neurology Neurosurgery and Psychiatry*, *39*(4), 367–374. https://doi.org/10.1136/jnnp.39.4.367

Wickham, J., Brödjegård, N. G., Vighagen, R., Pinborg, L. H., Bengzon, J., Woldbye, D. P. D., Kokaia, M., & Andersson, M. (2018). Prolonged life of human acute hippocampal slices from temporal lobe epilepsy surgery. *Scientific Reports*, *8*(1). https://doi.org/10.1038/s41598-018-22554-9

Wild-Bode, C., Weller, M., Rimner, A., Dichgans, J., & Wick, W. (2001). Sublethal irradiation promotes migration and invasiveness of glioma cells: Implications for radiotherapy of human glioblastoma. *Cancer Research*, *61*(6), 2744–2750.

Wolf, M. K. (1970). Anatomy of cultured mouse cerebellum. II. Organotypic migration of granule cells demonstrated by silver impregnation of normal and mutant cultures. *Journal of Comparative Neurology*, *140*(3), 281–297. https://doi.org/10.1002/cne.901400304

Woller, N., Gürlevik, E., Fleischmann-Mundt, B., Schumacher, A., Knocke, S., Kloos, A. M., Saborowski, M., Geffers, R., Manns, M. P., Wirth, T. C., Kubicka, S., & Kühnel, F. (2015). Viral Infection of Tumors Overcomes Resistance to PD-1-immunotherapy by Broadening Neoantigenome-directed T-cell Responses. *Molecular Therapy*, *23*(10), 1630–1640. https://doi.org/10.1038/mt.2015.115

Woltjen, K., Michael, I. P., Mohseni, P., Desai, R., Mileikovsky, M., Hämäläinen, R., Cowling, R., Wang, W., Liu, P., Gertsenstein, M., Kaji, K., Sung, H. K., & Nagy, A. (2009). PiggyBac transposition reprograms fibroblasts to induced pluripotent stem cells. *Nature*, *458*(7239), 766–770. https://doi.org/10.1038/nature07863

Wu, J., Lee, C., Yokom, D., Jiang, H., Cheang, M. C. U., Yorida, E., Turbin, D., Berquin, I. M., Mertens, P. R., Iftner, T., Gilks, C. B., & Dunn, S. E. (2006). Disruption of the Y-box binding protein-1 results in suppression of the epidermal growth factor receptor and HER-2. *Cancer Research*, *66*(9), 4872–4879. https://doi.org/10.1158/0008-5472.CAN-05-3561

Wu, M., & Melody, A. S. (2014). Modeling tumor microenvironments in Vitro. *Journal of Biomechanical Engineering*, *136*(2). https://doi.org/10.1115/1.4026447

Yu, J., Vodyanik, M. A., Smuga-Otto, K., Antosiewicz-Bourget, J., Frane, J. L., Tian, S., Nie, J., Jonsdottir, G. A., Ruotti, V., Stewart, R., Slukvin, I. I., & Thomson, J. A. (2007). Induced pluripotent stem cell lines derived from human somatic cells. *Science*, *318*(5858), 1917–1920. https://doi.org/10.1126/science.1151526

Yuste, R., & Bonhoeffer, T. (2004). Genesis of dendritic spines: Insights from ultrastructural and imaging studies. *Nature Reviews Neuroscience*, *5*(1), 24–34. https://doi.org/10.1038/nrn1300

Zhang, S. C., Wernig, M., Duncan, I. D., Brüstle, O., & Thomson, J. A. (2001). In vitro differentiation of transplantable neural precursors from human embryonic stem cells. *Nature Biotechnology*, *19*(12), 1129–1133. https://doi.org/10.1038/nbt1201-1129

Zhang, Y., Pak, C. H., Han, Y., Ahlenius, H., Zhang, Z., Chanda, S., Marro, S., Patzke, C., Acuna, C., Covy, J., Xu, W., Yang, N., Danko, T., Chen, L., Wernig, M., & Südhof, T. C. (2013). Rapid single-step induction of functional neurons from human pluripotent stem cells. *Neuron*, *78*(5), 785–798. https://doi.org/10.1016/j.neuron.2013.05.029

Zheng, J., Dong, W., Zhang, J., Li, G., & Gong, H. (2016). YB-1, a new biomarker of glioma progression, is associated with the prognosis of glioma patients. *Acta Biochimica et Biophysica Sinica*, *48*(4), 318–325. https://doi.org/10.1093/abbs/gmw012

Zhou, H., Wu, S., Joo, J. Y., Zhu, S., Han, D. W., Lin, T., Trauger, S., Bien, G., Yao, S., Zhu, Y., Siuzdak, G., Schöler, H. R., Duan, L., & Ding, S. (2009).

Generation of Induced Pluripotent Stem Cells Using Recombinant Proteins. In *Cell Stem Cell* (Vol. 4, Issue 5, pp. 381–384). https://doi.org/10.1016/j.stem.2009.04.005

Figures 3, 5, 6 and parts of figures 8 and 9 were created with BioRender.com.